Extension of radiolytic procedure to the preparation of conducting polymers in organic solvents : synthesis, characterization and applications

Teseer Bahry

université PARIS-SACLAY

NNT : 2019SACLS328

Thèse de doctorat

UNIVERSITÉ PARIS SUD
Comprendre le monde, construire l'avenir

Extension of radiolytic procedure to the preparation of conducting polymers in organic solvents: synthesis, characterization and applications

Thèse de doctorat de l'Université Paris-Saclay
préparée à l'Université Paris Sud

ECOLE DOCTORALE N° 571
Sciences chimiques : molécules, matériaux, instrumentation et biosystèmes (2MIB)
Spécialité de doctorat: Chimie

Thèse présentée et soutenue à Orsay, le 18 Octobre 2019, par

Teseer Bahry

Composition du Jury :

Mr Fabien Miomandre Professeur, ENS Saclay	Président du jury
Mr Jean-Marc Jung Professeur, Université de Strasbourg	Rapporteur
Mme Ngono-Ravache Yvette Cadre scientifique des EPIC, CEA GANIL	Rapporteur
Mme Rachel Méallet-Renault Professeur, Université Paris-Saclay	Examinatrice
Mme Muriel Ferry Cadre scientifique des EPIC, CEA Saclay	Examinatrice
Mme Najla Fourati-Ennouri Maître de Conférences, CNAM et SATIE	Examinatrice
Mr Thanh-Tuän Bui Maître de Conférences, Université de Cergy-Pontoise	Examinateur
Mr Samy Remita Professeur, Université Paris-Saclay et CNAM	Directeur de thèse

Université Paris-Saclay
Espace Technologique / Immeuble Discovery
Route de l'Orme aux Merisiers RD 128 / 91190 Saint-Aubin, France

Acknowledgment

This thesis would not have been possible without the inspiration and support of a number of wonderful individuals in Laboratoire de Chimie Physique (LCP) in Université Paris-Sud- my thanks and appreciation to all of them for being part of this journey and making this thesis possible.

First and foremost, I owe my deepest gratitude to my supervisor Prof. Samy Remita. Without his enthusiasm, encouragement, support and continuous optimism this thesis would hardly have been completed. His meticulous and precious guidance were an enormous help to me. I am profoundly honored to work with him.

I take pride in acknowledging the insightful guidance of my external supervisors Prof. Thanh-Tuân BUI and Prof. Laure Catala who followed up the advancement of this thesis. Their guidance and precious comments has been a valuable input for this thesis.

I am thankful to Prof. Philippe Maître as the director of LCP for his kind help. My deepest heartfelt appreciation goes to Prof. Mehran Mostafavi for support and encouragement.

I am particularly grateful for the assistance given by Mireille Benoit and Alexandre Demarque during the experiments.

Many thanks to Prof. Fabrice G oubard, and Prof. Pierre Henri Aubert for the warm welcoming and for allowing me to perform the photovoltaics experiments in Laboratoire de Physicochimie des Polymères et des Interfaces (LPPI) of University of Cergy Pontoise.

My sincere thanks also go to all the cooperators Alexandre Dazzi, Ariane Deniset-Besseau for, Matthieu Gervais, Cyrille Sollogoub, Jean-Michel Guigner. I have greatly benefited from them.

I express my warmest gratitude to Prof. Nabil JOUDIEH at Damascus University. I am deeply indebted and grateful to his help, support and encouragement.

I would also like to express my gratitude to Ministry of Higher Education, Research and Innovation for their financial support.

Finally, my deep and sincere gratitude to my family for their continuous and unparalleled love, help and support. I am forever indebted to my parents for giving me the opportunities and experiences that have made me who I am. They selflessly encouraged me to explore new

directions in life and seek my own destiny. This journey would not have been possible if not for them, and I dedicate this milestone to them.

I am forever thankful to my colleagues at LCP for their friendship and support, and for creating a cordial working environment. I would never forget all the beautiful moments I shared with them: my dearest friends Iyad, Iskander, Zhenpeng, Sarah, Vjona, Ali, Shiraz and also my lab mates also Slava, Xiaojiao, Cong, Benazir.

Abbreviations and Acronyms

3HT	3-hxylthiophene
ATR-FTIR	attenuated total reflection fourier transform infrared spectroscopy
CPs	conducting polymers
Cryo-TEM	cryogenic-transmission electron microscopy
CV	cyclic voltammetry
D	dose
DCM	dichloromethane
EDOT	3,4-ethylenedioxythiophene
EDX	energy dispersive X-Ray spectroscopy
G	radiolytic yield
Gy	gray
IPV	Inorganic photovoltaic cells
OPV	organic photovoltaic cells
P3HT	poly (3-hxylthiophene)
PEDOT	poly(3,4-ethylenedioxythiophene)
PPy	polypyrrole
PSC	perovskite solar cells
PTAA	poly (3-thiophene acetic acid)
PV	photovoltaic cells
Py	pyrrole
SEC	size exclusion chromatography
SEM	scanning electron microscopy
SHE	standard hydrogen electrode
TAA	3-thiophene acetic acid
TGA	thermogravimetric analysis
UV-vis	ultraviolet-visible
XRD	x-ray powder diffraction
ε	molar extinction coefficient

Table of Contents

Résumé en Français

Dans le présent travail, nous avons étendu aux solvants organiques notre méthodologie radiolytique de synthèse de polymères conducteurs (PCs), initialement développée en solutions aqueuses. Dans ce contexte, la polymérisation des PCs a été étudiée par radiolyse gamma dans différents solvants organiques et sous différentes conditions expérimentales. La synthèse radio-induite a, en particulier, été optimisée dans le dichlorométhane grâce à la variation et à l'ajustement de différents paramètres : atmosphère, dose, débit de dose, concentration des monomères, etc. Cette synthèse a ainsi pu mener à la préparation de différents types de polymères conducteurs : poly (3,4-éthylènedioxythiophène) (PEDOT), poly (3-thiophène acétique acide) (PTAA) et poly (3-hexylthiophène) (P3HT). Ces derniers ont été totalement caractérises en solutions ou après dépôt par des techniques analytiques, spectroscopiques et microscopiques complémentaires. Nous avons en particulier démontré la simplicité et la versatilité de la polymérisation radio-induite de TAA que ce soit dans le dichlorométhane ou dans l'eau, et avons mis en évidence quelques différences notables entre ces deux voies de synthèse. Nous avons, par ailleurs, évalué l'influence de la nature des espèces radiolytiques oxydantes générées dans le dichlorométhane, via la variation de l'atmosphère de travail (N_2, air ou O_2), sur les propriétés des polymères conducteurs radio-synthétises, en particulier dans le cas de P3HT. Parmi les nombreuses propriétés physiques chimiques que nous avons sondées dans le cas de tous nos polymères conducteurs radio-synthétises les propriétés électroniques et électrochimiques ont fait l'objet d'une attention particulière. Nos matériaux ont alors été incorporés au sien de cellules solaires à pérovskite hybrides organiques-inorganique (PSCs) et y ont été utilisés comme matériaux de transport de trous (HTMs). Notre nouvelle stratégie radiolytique de synthèse décrite et étende dans le présent manuscrit, ouvre sans aucun doute la voie à la préparation de nouveaux PCs nanostructurés, de morphologie contrôlée et aux propriétés augmentées : par exemple grâce à l'utilisation d'une polymérisation en microémulsions ou par le développement d'une copolymérisation raisonnée.

Introduction to the research interest

1 Conducting polymers (CPs)

1.1 Brief background

Conducting polymers (CPs) by definition are organic polymers that are characterized by their electrical conductance.[1] The ancestry of (CPs) discovery backs to 19th century when Fritzche reported the synthesis of polyaniline (PANI).[1-3] In the same time period, Henry Letheby worked on the investigation of the electrochemical behavior of PANI.[4] The merit of that work evinces the electrochromic behavior of CPs through showing that PANI is colorless in reduced state while in oxidized state, it is deep blue. [4] Since then, there were many research which works studied and investigated relevant materials. In 1958, Giulio Natta elaborated for the first time linear polyacetylene. The produced polyacetylene as dark powder was not stimulating to scientific community due to its low processability, insolubility, air sensitivity and instability.[5] Not far from that date, exactly in 1963, Weiss and coworkers described the preparation of polypyrrole (Ppy) at high conductivity degree.[6] Perhaps, the most paramount research in the end of 20th century is the 2000 Nobel Prize in Chemistry "for the discovery and development of conductive polymers».[7-9] The prize was awarded to three scientists, Alan J. Heeger, Alan G. MacDiarmid and Hideki Shirakawa. In 1977, the trio figured out that the doping of polyacetylene can change its behavior from insulating to metallic.[7-9] Although, polyacetylene was not usable for practical applications, the discovery of conducting polymers drew the attention to these types of materials.[1] On top of that, such incident is an important milestone because it called attention to new fields of researches in chemistry and condensed matter physics.[7] Accordingly, CP induced the progression to understanding fundamental chemistry and physics of π-bonded macromolecules.[7] Admittedly, the extraordinary features of these materials have made their development growing rapidly in short time period. Today CPs are major of importance and offer great profits in a wide range of areas.[10-13] No doubts, the world intensively accelerated the commercialization of these materials due to their promising practical use in daily life.

1.2 Types of CPs

Unlike saturated polymers, CPs are characterized by a backbone chain of alternating double-bond and single-bonds. The duplication of π-bonds along the polymer chain gives CPs an intrinsic electrical conductivity.[7] Essentially, the π-conjugation in CPs is similar to the spine column whatever the side groups or functional groups. This unique chemical structure led up to investigate and explore a large variety of this sort of conducting material.[7, 9] What's more interesting that modifying or changing the side chains and functional groups on building blocks of CPs can enhance their physical and chemical properties. In another word, by judiciously choosing the molecular combinations, CPs can be easily customized and tailored for almost any specific purposes.[7, 14-16] Thus, CPs can be categorized into a long list according to their chemical compositions. For instance, polypyrrole (PPy) and polyaniline (PANI) are nitrogen-containing conducting polymers while polythiophenes (PTs) and their derivatives are sulfur-containing conducting polymers. The table below shows some examples of the most investigated CPs (**Figure 1**):[17]

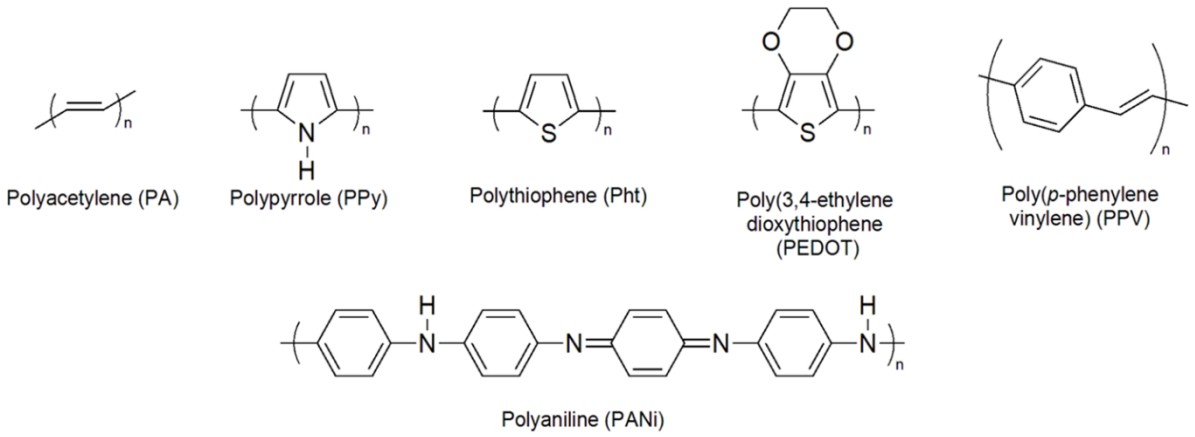

Figure 1 Chemical structures of some conducting polymers

One of the most important CPs are poly (3,4-ethylenedioxythiophene) (PEDOT), Poly 3-hexylthiophene (P3HT), polypyrrole (PPy) and polyaniline (PANI). They are well known as being easy to synthesize, possessing good processability and presenting excellent properties.[18-22] Due to the appropriate characters of these CPs, synthesis and processing of these materials besides their derivatives are of great interests as they are promising candidates for interesting applications such as organic photovoltaics (OPVs). Therefore, investigations on the mechanism and principles of the electrical conductivity of CPs are of great importance.

1.3 The Principle of electrical conductivity

In saturated polymers, such as polyethylene, the hybridization of each carbon atoms is sp^3. In another word, the four valence electrons of carbon atom are used up in sigma covalent bonds. These sigma-bonding electrons are not free to move throughout the structure and therefore do not contribute to the electrical conductivity. The case of CPs is substantially different and the electrical conductance of CPs is driven by several processes. CPs have backbones of contiguous sp^2p_z hybridized carbon centers (**Figure 2**).[23, 24] Each carbon atom supplies a p_z orbital perpendicular to the plane of the molecule. If the conjugated system is planar, the p_z orbitals overlap with another adjacent p_z orbital across an intervening σ bond along the backbone of polymer chain[7]. The conjugated p_z orbitals form a one-dimensional electronic band, and the electrons within this band become mobile when it is partially emptied. This possible when CPs are doped by oxidation leading to removal of some of delocalized electrons.[7] In such a case, the p_z orbitals are available for electrons delocalization along the backbone of polymer (**Figure 2, 1**). These electrons have high charge mobility and are free to move throughout the polymer structure, and consequently give rise to properties such as electrical conductivity.[7, 8] Since there are no partially filled orbital, CPs are typically semiconductors.[8] Thus, the electronic structure of CPs determines their electrical conductance. This is represented by chain symmetry the number and kind of atoms within the repeat unit and besides the more conjugated the π-system is, the better conductivity and properties are expected (**Figure 2, 2**). With all these features, such polymers can have metallic conductivity or can be semiconductors.[25, 26]

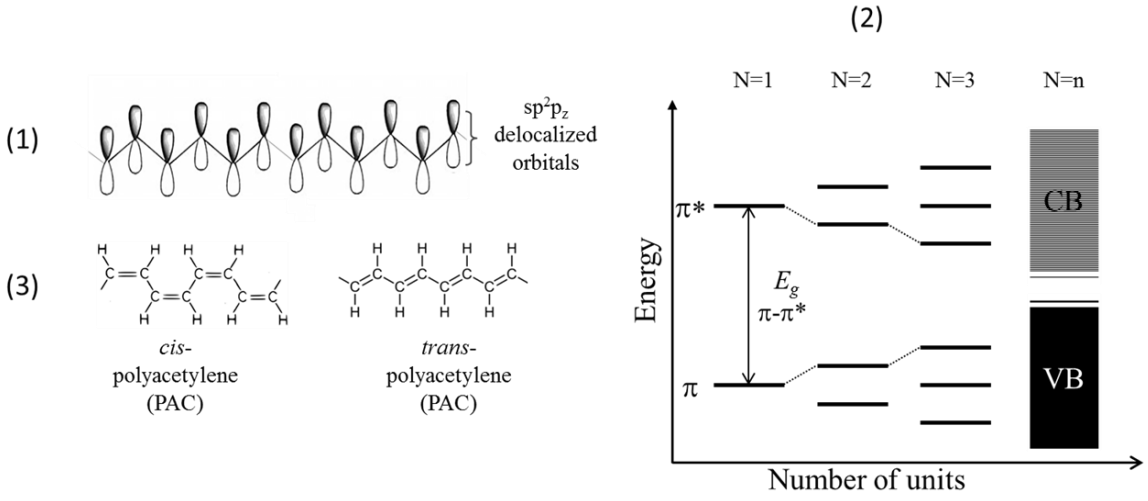

Figure 2 Delocalized set of p_z orbitals (1), cis-isomer and trans-isomer of polyacetylene, PAC (2), illustration energy diagram showing the decrease in energy band gap when number of π-conjugation in conducting polymers increases (3)

If we look at the chemical structure of polyacetylene ,-$(CH)_x$, it is possible to differentiate two configurations: *cis* and *trans* (**Figure 2, 3**).[27] The *cis*-isomer is considered as insulator since its electrical conductivity is extremely low ($1.7 \times 10^{-9}\ \mathrm{S.cm^{-1}}$), whereas the *trans*-form is semiconductor due to its higher electrical conductivity ($4.4 \times 10^{-5}\ \mathrm{S.cm^{-1}}$). However, the electrical conductivity can be easily tuned by doping upon oxidation.[27, 28] This process can drastically increase the electrical conductivity (**Figure 3**). That was evident when the electrical conductivity of -$(CH)_x$ films increased by many orders of magnitude upon treatment with halogen vapor (i.e. I_2, Cl_2 or Br_2).[7, 9, 27, 29] After doping process, the resulted -$(CH)_x$ possesses at room temperature electrical conductivity not far from metal one ($10^5\ \mathrm{S.cm^{-1}}$).[30, 31] Such an expansive degree of adjustability of CPs, to be varied from insulators to conductors, was indeed revolutionary. Therefore, CPs are called as "synthetic metals".[8]

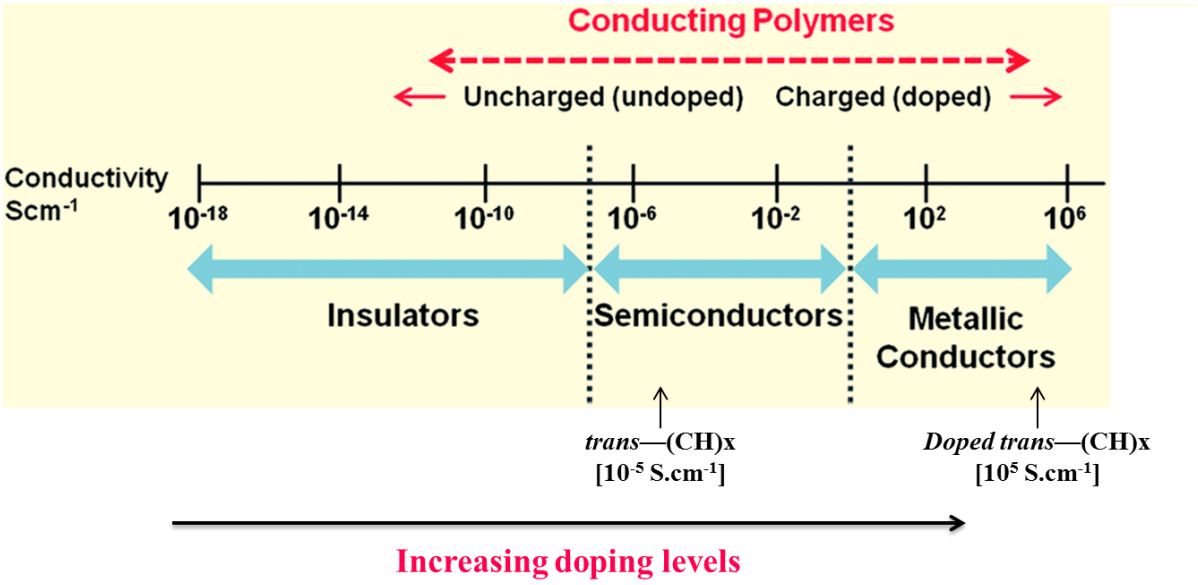

Figure 3 The electrical conductivity scale of conducting polymers compared with insulators and metals

1.3.1 Energy band gap theory

To better understand the molecular basis of electrical conductivity, it is a must to introduce the band gap theory. As mentioned, the overlapping of π-conjugated orbitals along the backbone of polymer form electronic band. In band theory, two bands can be identified: π- and π*- band.[32] Knowing that each band complies with two electrons of different spin, π-band is filled and π*-band is empty.[7] The first band (π-band) represents the valence band (VB) corresponding to the *Highest Occupied Molecular Orbital* (HOMO). The second band (π*-

band) represents the conduction band (CB) corresponding to the *Lowest Unoccupied Molecular Orbital* (LUMO). The difference between the two energy levels is called π-π* energy band gap, E_g and it is given in electron volts (eV) (**Figure 4**). The level in-between VB and CB is defined as Fermi's level that indicates the work required to move an electron between different electronic states. The position of the Fermi level with the relation to the band energy levels is a crucial factor in determining electrical properties. Thus, Electrons feasibility to move between valence band and conduction band defines the electrical conductivity and hence three groups of materials are recognized: metals, insulators and semiconductors.[25]

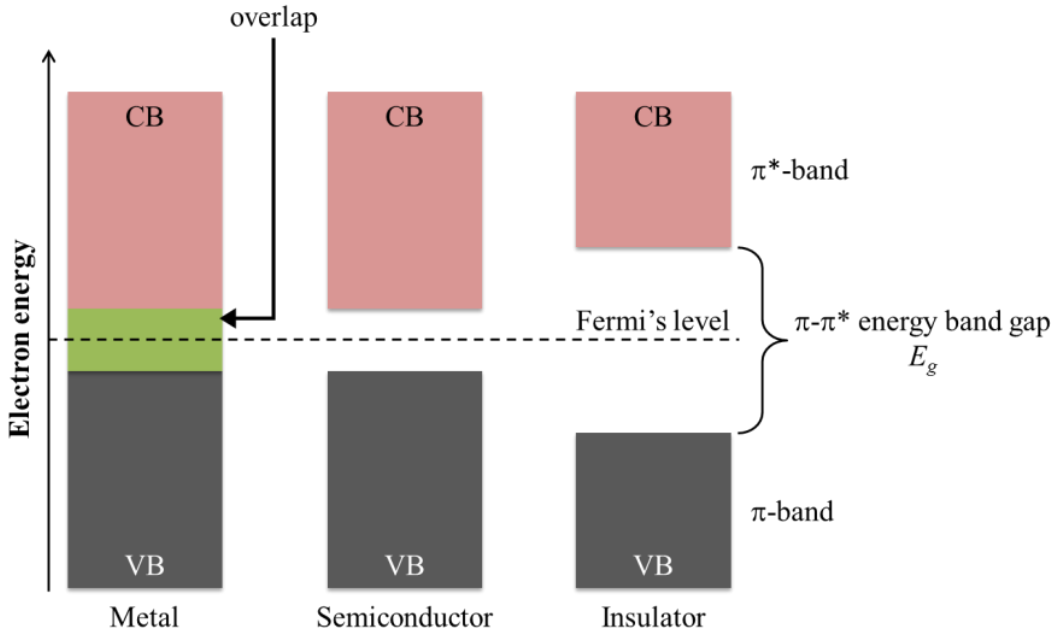

Figure 4 Energy band structure of conductors, semiconductors and insulators.

In case of metals, the E_g is null because VB and CB are overlapped and subsequently the electrons are fully free to mobilize between them. On the contrary, the E_g for insulators is quite immense and the transition of electrons from VB to CB is impossible. In semiconductors, the energy difference between the π-band and π*-band is relatively small. What makes the semiconductors electrically conductive is that upon excitation the occupied electrons in the VB can be mobilized to CB. Subsequently, this electronic mobility forms the electrical conductivity. The excitation requires a specific minimum amount of energy for the electronic transition. The required energy differs with different materials. The electrons can be excited by absorbing either a phonon (heat) or a photon (light). This electron mobility can be adjusted according to the applied conditions (i.e. doping by oxidation) and hence

controlling the band gap of conductive material. Controlling the band gap allows us to design material for specific applications [33], such as laser diodes and solar cells. It is worth mentioning that, the band gap in semiconductors can be either direct or indirect, depending on the electronic band structure. Moreover, in semiconductors, there is a distinction difference between "optical band gap" and "electrical band gap". The difference between them can be significantly large especially in some systems such as organic solar cells or organic light emitting diodes (OLEDs).

1.3.2 Direct and *indirect band gap*

In direct band gap, the maximum energy level of the valence band aligns with the minimum energy level of the conduction band with respect to momentum. By contrast, in an indirect band gap semiconductor, the maximum energy of the valence band occurs at a different value of momentum to the minimum in the conduction band energy (**Figure 5**). The difference between the two is most important in optical devices. For example, direct bandgap materials are used for manufacturing light emitting and laser diodes, while photovoltaics are always made of indirect band gap materials.

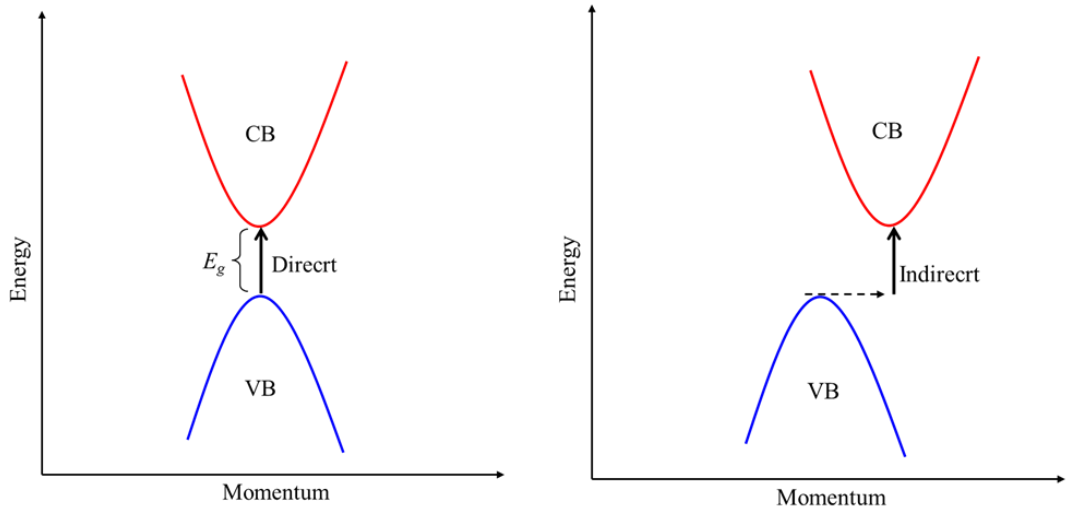

Figure 5 Direct band-gap semiconductor and indirect band-gap semiconductor

1.3.3 Optical and electronic band gap

The optical bandgap is the threshold for photons to be absorbed, while the transport gap is the threshold for creating an electron-hole pair that is not bound together. The electronic band gap is larger than the optical band gap, as well known that the measurement by electrochemistry requires additional energy because of Coulomb interactions and hence, the electronic band gap is slightly higher when compared to optical band gap.[34] In a solar cell, the

only important value is the optical gap, because the excitation is induced by photons. In a light emitting diode, however, applying a potential that corresponds to the optical gap will not be enough and therefore a potential corresponding to the electronic gap must be applied.

1.3.4 Determination of energy band gap

Generally the optical band gap (E_{gap}) in an amorphous semiconductor is determined by Tauc's polt .[35] A Tauc plot is used to determine the optical band gap in semiconductors. From Tauc's equation (1), $(\alpha h\upsilon)^{1/n}$ is principally plotted as function of photon energy ($h\upsilon$):

$$(\alpha h\upsilon)^{1/n} = A(h\upsilon - E_{gap}) \qquad (1)$$

Where α, h, υ and E_{gap} are respectively the absorption coefficient, Planck constant, light frequency, oprical band gap energy and A is a constant. The value of the exponent n denotes the nature of the transition.[35, 36] The exponent n is 0.5 for direct allowed transitions, 1.5 for direct forbidden transitions, 2 for indirect allowed transitions, and 3 for indirect forbidden transitions.

Another possible way to estimate the optical band gap is directly from the UV-Vis absorption spectrum of the material. By determining the absorption edge wavelength, λ_{edge}, (see **Figure 6**)[37] the E_{gap} values can be calculated according to the equation (2):

$$E_{gap} = \frac{1240}{\lambda_{edge}(nm)}\ (eV) \qquad (2)$$

The E_g value of insulators is normally larger than 6 eV and the E_{gap} value of semiconductors is around 1 eV.[33] The E_g value of doped CPs is generally detected within the bounds of semiconductors scale between 1.0~3.0 eV.[25, 26]

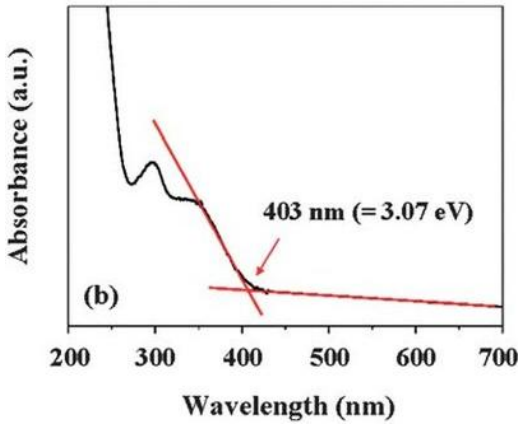

Figure 6 UV-vis absorption spectrum in which shows the onset of absorption band (λ_{edge}) and the way for determining its value.[37]

Cyclic voltammetry (CV) enables the determination of the electronic band gap. The CV profile gives information about the oxidation E_{ox} and reduction E_{red} potentials of the materials. **Figure 7** shows an example of CV profile of poly (3-thiophene acetic acid) (PTAA) as well as a CV profile of ferrocene that were obtained in this work. In the **Figure 7** we can clearly see where E_{ox} and E_{red} occur and also the way of determination of ferrocene ionization potential (E_{Fc}) from cathodic (E_{pc}) and anodic (E_{pa}) potentials. Knowing these potential values, the energy levels of the highest occupied molecular orbital (HOMO) and the energy of lowest unoccupied molecular orbital (LUMO) can be calculated according to the empirical equations(3) and (4)[38], using the ferrocene ionization potential value as the standard (E_{Fc}):

$$\text{from ionization potential, } E_{HOMO}(eV) = -4.8 - e(E_{ox} - E_{Fc}) \quad (3)$$

$$\text{from electronic affinity, } E_{LUMO}(eV) = -4.8 - e(E_{red} - E_{Fc}) \quad (4)$$

Where e is the elementary charge and where 4.8 eV is the corrected value of ferrocene potential vs. vacuum which is widely adopted and this value is based on the calculations obtained by Pommerehne et al.[39]

The energy difference between the calculated E_{HOME} and E_{LUMO} enables the determination of electronic band gap.

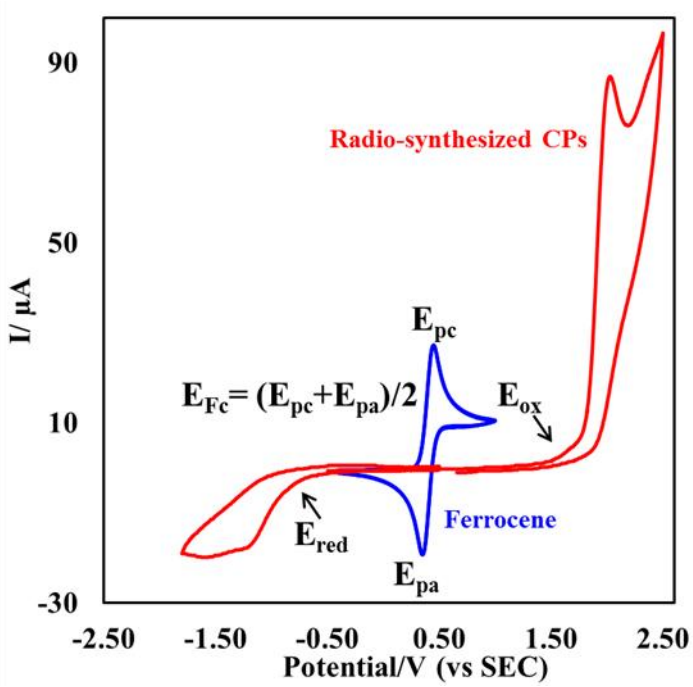

Figure 7 Cyclic voltammetry (CV) profiles of poly (3-thiophene acetic acid) (PTAA) and ferrocene that have been analyzed in this work showing the way of determination of their oxidation and reduction potentials

1.4 Doping of CPs

Doping is defined as the injection of charge onto conjugated semiconducting macromolecular chains.[40] Accordingly, there are several ways which result in doping, such as, chemical doping, electrochemical doping , photodoping, etc.[7]

As mentioned before, upon doping treatment with halogen, the conductivity of polyacetylene $(C_2H_2)_x$ drastically increase. Based on the final conducting mode of the CPs, the doping treatment can be divided into two kinds: *p*-doping and *n*-doping. For example, the *p*-doping and *n*-doping of $(C_2H_2)_x$ can be expressed as follows:

Oxidation with Iodine (*p*-doping): $(C_2H_2)_x + \frac{3n}{2} I_2 \rightarrow (C_2H_2)_x^{n+} + nI_3^-$ (5)

Reduction with sodium metal (*n*-doping): $(C_2H_2)_x + nNa \rightarrow (C_2H_2)_x^{n-} + nNa^+$ (6)

In the case of *p*-doping, oxidation of the CPs occurs forming cations by extracting electrons from polymer backbones. The oxidant becomes anions by reduction and works as the counter ions. The *p*-doping process forms *p*-type CPs. Inversely, reduction of the CPs happens during the *n*-doping injecting electrons to the polymer backbones, forming negatively charged CPs while reductant is oxidized into cations. The *n*-doping by reduction makes CPs *n*-type conductors. CPs can be doped by many different means: chemical doping, electrochemical doping, protonation by acid-base chemistry, photo-doping and charge injection have been successfully performed.

Evidently, upon doping process the polymer chains of CPs are charged. In the electronic structure of conjugated polymers, charge carriers (electrons or holes), appearing on polymer chains, are energetically favorable to be localized and coupled to the distortions in the backbone. This process causes the presence of localized electronic states in the band gap due to the shift of the valence band and conduction band.[41] In *p*-doping, the removal of one electron from the CPs chain leads to the formation to what is called polarons (**Figure 8**). When two polarons are close enough, their energy decreases by sharing the same distortions, which leads to an effective attraction between the polarons. Subsequently, formation of bipolaron is favorable and thermodynamically more stable than two polaron (**Figure 8**).[7, 41, 42] As a consequence of formation of polarons and bipolarons in the chain, two new optical transitions are emerged below the band gap.[41]

As the doping level increases, the population of polaron and bipolaron increases and thus the energy band gap is becoming sufficiently small to ensure high electrons mobility (**Figure 8**).[43]

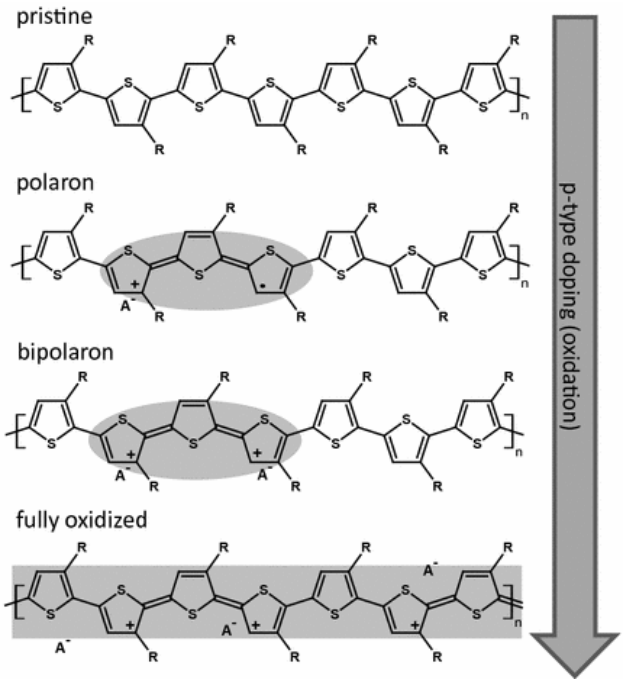

Figure 8 Schematic structure of poly (3-alkylthiophene) showing the formation of polaron and bipolaron along a polymer chain.[43]

The high electrical conductivity of conducting polymers at high doping levels is thus reasonable. Therefore, the electrical conductivity of conjugated polymer can be well controlled by the doping process.[31]

1.5 Applications

There is no doubt that what makes CPs unique among the other materials is their innumerable of applications.[7, 10] The most attracting properties of CPs are their tunable electrical conductivity and excellent optical properties which enable CPs to possess unique electrical conductivity and good transparency.

Among the CPs, PEDOT and P3HT polymers are the most known used materials in the field of organic photovoltaics (OPVs).[44-47] OPVs based on semiconductor polymers have attracted a great attention as a potential and promising source of renewable energy due to their low cost production, flexibility and easy to commercialize. Generally, P3HT is incorporated in OPVs as electron donor (p-type semiconductor) and accompanied with electron acceptor (n-type semiconductor) such as [6,6]-phenyl-C61-butyric acid methyl ester (PCBM). Conducting polymer blends of poly (3,4-ethylenedioxythiophene) (PEDOT) and poly(styrene

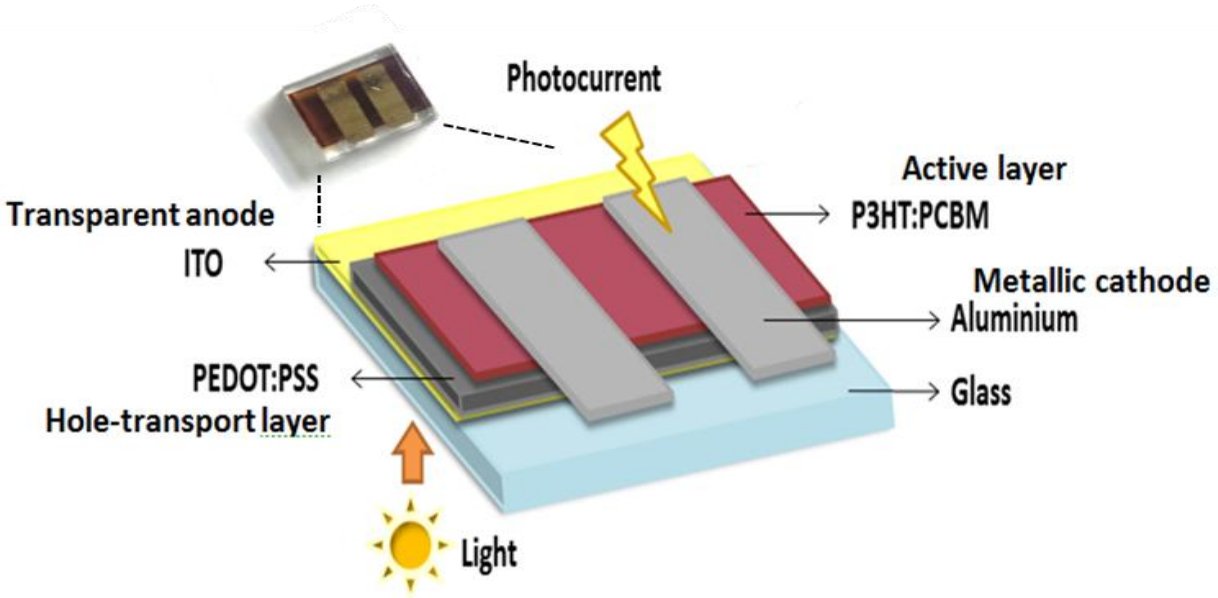

Figure 9 Organic photovoltaic device fabricated in this work. It shows the main components which are involved in its structure.

sulfonate) (PEDOT/PSS), are commonly used in OPVs as hole transport material (**Figure 9**). OPVs based on the blend system of P3HT:PCBM and PEDOT:PSS shows, relatively, good performance and high power conversion efficiencies (PCEs). Liang et al. studied the whole simulation of a traditional bulk-heterojunction apparatus based on P3HT. The power conversion efficiency of state of the art PSCs has been reported more than 9% for single cells, 10% for tandem cells and 11% for the PSC based on P3HT.[48]

Another remarkable field of use of CPs is electrochromism. Electrochromic polymers (EC) are a phenomenal class of CPs.[49] Their specialness is the capability to change color upon an application of a voltage or current. PEDOT and PANI are mainly used due to their exceptional electrical conductivity and optoelectronic properties.[50] This property has led to the development of flat panel displays.

The list of CPs application is endless but it is possible to mention some of the most prominent applications such as organic transistors, data storage, batteries, super capacitors chemical sensors, gas sensors, biosensors, etc.[51-55]

1.6 Potential synthesis methods

The great interest on CP instituted tremendous efforts towards their development and upgrading their synthesis methodologies which all aim the easy preparation of new and novel CP structures, stable in different solvents such as water. An important and possible synthesis method of conducting polymers is the chemical synthesis. The synthesis can be carried out

through Ni-catalyzed polymerization of Grignard reagents and in presence of brominated monomers (e.g. 2,5-dihalothiophenes).[56, 57] The advantages of this method are the ability to select diversely wide range of organic monomers and to synthesize perfectly regioregular substituted PTs. In contrast to chemical synthesis that requires brominated monomers, oxidation induced polymerization is another way to obtain conducting polymers.[58] CPs are commonly synthesized by chemical polymerization through adding oxidizing reagents or electrochemical polymerization by applying a potential across a solution containing the monomers.[59-62] Based on these two methods, intensive researches are performed to develop these methods, optimize the preparation conditions and control the polymers morphology in order to obtain better optical and electrical properties, and subsequently, good performances and higher efficiency in their applications.[63]

CPs are chemically synthesized, through the oxidation of monomers typically by using oxidizing species (i.e. $FeCl_3$, $K_2S_2O_8$)[60, 61] or reduction of monomers by chemical reductants (i.e. N_2H_4, $LiAlH_4$)[64, 65] which in turn induces polymerization of corresponding monomers. The chemical oxidants have higher redox potential than that of monomers and oxidize the monomers into cations which undergo further polymerization into polymers. The chemical method induced polymerization has been proposed to proceed according to a step-by step growth procedure and not according to chain reaction.[66] One of the advantages of chemical polymerization is producing CPs with high molar masses.[67]

Electrochemical polymerization is one of the most important methods to produce CPs due to its simplicity, cost-effective, reproducibility, etc. CPs are mostly prepared by anodic oxidation and much less often by cathodic reduction.[67] In general, the initiation of monomers polymerization is achieved by applying an oxidation potential on the working electrode. The monomers are oxidized into radical cations which dimerize by eliminating two H atoms. Then, dimers are oxidized and react with dimer cations producing the oligomers. Elongation of oligomers through the same procedure finally results in the polymers on the surface of working electrode.[10] By adjusting the oxidation potential, the oxidation of different monomers can be successfully realized. Therefore, both traditional chemical and electrochemical methods more generally involve the oxidation of monomers to initiate the polymerization and a step-by-step mechanism is often proposed. Nevertheless, chain reaction mechanism is alternatively proposed as it is suggested that radical cations can directly react with monomers forming a dimer cation.[68]

Even though these previously mentioned methods are well understood and their mechanism is relatively well understood, still remain some problems such as chemical contamination, purification steps and sometime need to use a catalyst. However, there are other potential synthesis methods that are rarely proposed in literature such as, photochemical method[69], methathesis method[70, 71], plasma polymerization[72], concentrated emulsion method[73], etc.[67] Radiation induced polymerization via the interaction of high energetic rays with the matter is narrowly used to prepare CPs.[74] Karim *et al.* synthesized PPy using γ-radiation induced oxidative polymerization with ammonium peroxy-disulfate (APS) as chemical oxidant.[75] And besides, he prepared buckyball shaped conducting polythiophene by gamma induced polymerization method in presence of $FeCl_3$ as chemical oxidant.[76] The same approach was attained by Pillalamarri *et al.* to synthesize PANI nanofibers in the presence of APS.[77] Radiation method based on radiation chemistry in the absence of any additional oxidizing agents with γ-irradiation or pulse radiolysis for the synthesis of CPs has recently been reported. Using water soluble monomers, Samy Remita's team used an original synthetic method to polymerize EDOT and Py by γ radiolysis of water.[74, 78] Lattach *et al.* produced PEDOT polymers with different morphologies using γ irradiation by varying the reactive species.[79] Coletta *et al.* studied the growth mechanism of PEDOT polymers initiated by accelerated electrons.[80] Koizumi *et al*. endeavored to use γ-radiolysis method to polymerize water insoluble monomer, 3-octylthiophene, in several organic solvents.[81]

As it appears, radiation method, can be performed under various experimental conditions, and is free from the metal contaminations. Moreover, this method leads to formation of nano-structured CPs. Research reports showed that nanostructured conducting polymers in the form of nanofibers and nanosponges, showed significantly improved capacitance values as compared to their non-nanostructured counterparts.[82, 83] Therefore, radiation method based on γ-irradiation may offer a useful method for the synthesis of CPs possible in the bulk of a solution and even on a solid substrate (conductive or not). In order to expand the development of this method and to reach better level of reliability, processability and applicability, new materials were synthesized in the present work via an original radiolysis route.

2 Objective of the work

In this research work, the main aim is to extend the radiolysis methodology based on radiation chemistry to synthesize different kinds of conducting polymers in organic solvents and besides to investigate their application opportunities. Contrarily to the previous radiolytic

route that based on γ-radiolysis of water, in which relies on the generation of hydroxyl radicals to initiate the oxidation induced polymerization, nevertheless this approach no longer valid. That is due to low processability and solubility or sometimes insolubility of some of organic monomers. Thus, the restrictions on use of aqueous solutions for radiation induced synthesis of CPs stimulated us to investigate γ-induced polymerization in more processable media.

The use of organic solvents to synthesize CPs was came into view when Koizumi *et al*. studied the mechanism of oxidative polymerization of conducting polymers in several organic solvents by γ-irradiation.[81] The study was performed on 3-octylthiophene, 3OT, and the oxidative polymerization initiated by γ-radiolysis of chloroform, hexane and neat monomer solution. The polymerization was successfully induced in chloroform. The study showed that, the products contain large amount of small oligomers, and the yield of polymers with high molecular weight is low. Furthermore, high irradiation dose and removal of the oligomers is necessary to obtain usable polymers for any potential applications. Actually, halo-methanes, in particular chloroform and dichloromethane, are wieldy used as solvent to carry out polymerization reactions of CPs either chemically or electrochemically. Furthermore, γ-irradiation of halo-methanes is generating several oxidizing species and they are defined as strong oxidizing agents towards organic materials.[84] Among halo-methanes solvents, dichloromethane has been used to carry out electrochemical or radiolytic one-electron oxidation of solutes.[85-87] Moreover, it has been proved that irradiated CH_2Cl_2 is a good oxidizing system.[84] The oxidative polymerization of CPs induced directly by γ-irradiation of dichloromethane has not been reported in literature. In these studies, in order to develop a new synthetic method and to study mechanism of oxidative polymerization of CPs in organic solvent, polymerization of 3-hexylthiophene, 3HT, and 3, 4-ethylenedioxythiophene, EDOT and 3-thiophene acetic acid, TAA, in dichloromethane were examined by γ-irradiation. The work was mainly addressed to investigate the appropriate synthesis conditions of different kind of CPs by γ-radiolysis of dichloromethane. The discussion for application opportunities was opened for OPVs and electrochromism. Hence, the research work can be stated as follows:

In the first chapter, all the chemical agents and radiolysis methodologies are reported and explained. In addition, all the techniques applied for detecting and characterizing radio-synthesized CPs are briefly introduced. Ultimately, the fabrication steps of OPVs are viewed.

In the second chapter, the use of radiolysis route as original and alternative method to synthesize CPs in aqueous media by Samy Remita‘s team (that I was in as a member) is discussed. The state of art of the potential synthesis of CPs via radiolysis route in organic solvent is summarized.

Chapter 3 studies in details the polymerization of EDOT by γ-radiolysis of dichloromethane. The polymerization is examined under different atmospheres: N_2, O_2 and air. The chapter also reviews the optimized conditions that guarantee the successful formation of PEDOTs. The work includes the potential attempts to enhance the properties and to increase the molecular weights of radio-synthesized PEDOTs in dichloromethane. The ultimate product was eventually characterized and its optical and electrical properties were checked

Chapter 4 is allocated to synthesize a new derivative of polythiophene, namely poly (3-thiophene acetic acid), PTAA that the monomers of which are soluble in water and dichloromethane. In this particular study, two radiolysis routes are considered: water radiolysis and dichloromethane radiolysis. The merit of this work is that 3-thiophene acetic acid is directly polymerized in one step without using oxidizing agents or any prior esterification. This chapter reviews detailed comparative study, in term of the electrical and optical properties for radio-produced materials.

In chapter 5, the polymerization of a monomer insoluble in water, namely 3-hexylthiophene is described in details, in dichloromethane under different atmospheres relying on the use of dichloromethyl, chloromethyl and their corresponding peroxyl radicals.

Applications possibilities, in particular, photovoltaics (PVs), are previewed in chapter 6 including fabrication of different types of PVs and their photo-activity performance.

Finally, the highlighted parts and achievements realized in my work are summarized to draw general conclusions. The synthesis of CPs with new radiolytic methodologies as well as the possible improvement suggestions of radio-synthesized CPs, are mentioned in perspectives.

References

1. Inzelt, G., *Conducting Polymers: A New Era in Electrochemistry*. 2008.

2. Fritsche, J., Ueber das Anilin, ein neues Zersetzungsproduct des Indigo. *Journal für Praktische Chemie* **1840,** *20* (1), 453-459.

3. Wudl, F.; Angus, R. O.; Lu, F. L.; Allemand, P. M.; Vachon, D.; Nowak, M.; Liu, Z. X.; Schaffer, H.; Heeger, A. J., Poly-p-phenyleneamineimine: synthesis and comparison to polyaniline. *Journal of the American Chemical Society* **1987,** *109* (12), 3677-3684.

4. Letheby, H., XXIX.—On the production of a blue substance by the electrolysis of sulphate of aniline. *Journal of the Chemical Society* **1862,** *15* (0), 161-163.

5. Saxman, A. M.; Liepins, R.; Aldissi, M., Polyacetylene: Its synthesis, doping and structure. *Progress in Polymer Science* **1985,** *11* (1), 57-89.

6. Bolto, B.; McNeill, R.; Weiss, D., Electronic Conduction in Polymers. III. Electronic Properties of Polypyrrole. *Australian Journal of Chemistry* **1963,** *16* (6), 1090-1103.

7. Heeger, A. J., Semiconducting and Metallic Polymers: The Fourth Generation of Polymeric Materials. *The Journal of Physical Chemistry B* **2001,** *105* (36), 8475-8491.

8. MacDiarmid, A. G., "Synthetic Metals": A Novel Role for Organic Polymers (Nobel Lecture). *Angewandte Chemie International Edition* **2001,** *40* (14), 2581-2590.

9. Shirakawa, H., The Discovery of Polyacetylene Film: The Dawning of an Era of Conducting Polymers (Nobel Lecture). *Angewandte Chemie International Edition* **2001,** *40* (14), 2574-2580.

10. Li, C.; Bai, H.; Shi, G., Conducting polymer nanomaterials: electrosynthesis and applications. *Chemical Society Reviews* **2009,** *38* (8), 2397-2409.

11. Balint, R.; Cassidy, N. J.; Cartmell, S. H., Conductive polymers: Towards a smart biomaterial for tissue engineering. *Acta Biomaterialia* **2014,** *10* (6), 2341-2353.

12. Zhou, Q.; Shi, G., Conducting Polymer-Based Catalysts. *Journal of the American Chemical Society* **2016,** *138* (9), 2868-2876.

13. Guo, X.; Baumgarten, M.; Müllen, K., Designing π-conjugated polymers for organic electronics. *Progress in Polymer Science* **2013,** *38* (12), 1832-1908.

14. Ates, M.; Karazehira, T.; Sarac, A., Conducting Polymers and their Applications. *Current Physical Chemistry* **2012,** *2*, 224-240.

15. Gedde, U. W., A Brief Introduction to Polymer Science. In *Polymer Physics*, Springer Netherlands: Dordrecht, 1999; pp 1-18.

16. Heeger, A. J., Semiconducting polymers: the Third Generation. *Chemical Society Reviews* **2010,** *39* (7), 2354-2371.

17. Llorens, E.; Armelin, E.; Del Mar Pérez-Madrigal, M.; Del Valle, L. J.; Alemán, C.; Puiggalí, J., Nanomembranes and Nanofibers from Biodegradable Conducting Polymers. *Polymers* **2013,** *5* (3), 1115-1157.

18. Syed, A. A.; Dinesan, M. K., Review: Polyaniline—A novel polymeric material. *Talanta* **1991,** *38* (8), 815-837.

19. De Jesus, M. C.; Fu, Y.; Weiss, R. A., Conductive polymer blends prepared by in situ polymerization of pyrrole: A review. *Polymer Engineering & Science* **1997,** *37* (12), 1936-1943.

20. Kirchmeyer, S.; Reuter, K., Scientific importance, properties and growing applications of poly(3,4-ethylenedioxythiophene). *Journal of Materials Chemistry* **2005,** *15* (21), 2077-2088.

21. Roncali, J.; Blanchard, P.; Frère, P., 3,4-Ethylenedioxythiophene (EDOT) as a versatile building block for advanced functional π-conjugated systems. *Journal of Materials Chemistry* **2005,** *15* (16), 1589-1610.

22. Groenendaal, L.; Jonas, F.; Freitag, D.; Pielartzik, H.; Reynolds, J. R., Poly(3,4-ethylenedioxythiophene) and Its Derivatives: Past, Present, and Future. *Advanced Materials* **2000,** *12* (7), 481-494.

23. Cochran, J. C., Advanced organic chemistry: Reactions, mechanisms, and structure (March, Jerry). *Journal of Chemical Education* **1969,** *46* (8), 537.

24. Muller, P., Glossary of terms used in physical organic chemistry (IUPAC Recommendations 1994). In *Pure and Applied Chemistry*, 1994; Vol. 66, p 1077.

25. Wan, M., *Conducting Polymers with Micro or Nanometer Structure*. 2008.

26. Furukawa, Y., Electronic Absorption and Vibrational Spectroscopies of Conjugated Conducting Polymers. *The Journal of Physical Chemistry* **1996,** *100* (39), 15644-15653.

27. Shirakawa, H.; Louis, E. J.; MacDiarmid, A. G.; Chiang, C. K.; Heeger, A. J., Synthesis of electrically conducting organic polymers: halogen derivatives of polyacetylene, (CH). *Journal of the Chemical Society, Chemical Communications* **1977,** (16), 578-580.

28. Chiang, C. K.; Fincher, C. R.; Park, Y. W.; Heeger, A. J.; Shirakawa, H.; Louis, E. J.; Gau, S. C.; MacDiarmid, A. G., Electrical Conductivity in Doped Polyacetylene. *Physical Review Letters* **1977,** *39* (17), 1098-1101.

29. Natta, G.; Mazzanti, G.; Corradini, P., 81 - STEREOSPECIFIC POLYMERIZATION OF ACETYLENE. In *Stereoregular Polymers and Stereospecific Polymerizations*, Natta, G.; Danusso, F., Eds. Pergamon: 1967; pp 463-465.

30. Burroughes, J. H.; Bradley, D. D. C.; Brown, A. R.; Marks, R. N.; Mackay, K.; Friend, R. H.; Burns, P. L.; Holmes, A. B., Light-emitting diodes based on conjugated polymers. *Nature* **1990,** *347* (6293), 539-541.

31. Heeger, A. J.; Kivelson, S.; Schrieffer, J. R.; Su, W. P., Solitons in conducting polymers. *Reviews of Modern Physics* **1988,** *60* (3), 781-850.

32. Salzner, U.; Lagowski, J. B.; Pickup, P. G.; Poirier, R. A., Design of low band gap polymers employing density functional theory—hybrid functionals ameliorate band gap problem. *Journal of Computational Chemistry* **1997,** *18* (15), 1943-1953.

33. Millman, J.; Halkias, C., *Integrated Electronics : Analog and Digital Circuits and Systems / J. Millman, C.C. Halkias*. 2019.

34. Bredas, J.-L., Mind the gap! *Materials Horizons* **2014,** *1* (1), 17-19.

35. Tauc, J., Optical properties and electronic structure of amorphous Ge and Si. *Materials Research Bulletin* **1968,** *3* (1), 37-46.

36. Davis, E. A.; Mott, N. F., Conduction in non-crystalline systems V. Conductivity, optical absorption and photoconductivity in amorphous semiconductors. *The Philosophical Magazine: A Journal of Theoretical Experimental and Applied Physics* **1970,** *22* (179), 0903-0922.

37. Lee, T. J.; Ko, Y.-G.; Yen, H.-J.; Kim, K.; Kim, D. M.; Kwon, W.; Hahm, S. G.; Liou, G.-S.; Ree, M., Programmable digital nonvolatile memory behaviors of donor–acceptor

polyimides bearing triphenylamine derivatives: effects of substituents. *Polymer Chemistry* **2012,** *3* (5), 1276-1283.

38. Alcácer, L., Electronic Structure of Organic Semiconductors. In *Polymers and small molecules* [Online] Morgan & Claypool Publishers: 2018.

39. Pommerehne, J.; Vestweber, H.; Guss, W.; Mahrt, R. F.; Bässler, H.; Porsch, M.; Daub, J., Efficient two layer leds on a polymer blend basis. *Advanced Materials* **1995,** *7* (6), 551-554.

40. MacDiarmid, A. G.; Mammone, R. J.; Kaner, R. B.; Porter, L.; Pethig, R.; Heeger, A. J.; Rosseinsky, D. R.; Gillespie, R. J.; Day, P., The concept of doping of conducting polymers: the role of reduction potentials. *Philosophical Transactions of the Royal Society of London. Series A, Mathematical and Physical Sciences* **1985,** *314* (1528), 3-15.

41. Bredas, J. L.; Street, G. B., Polarons, bipolarons, and solitons in conducting polymers. *Accounts of Chemical Research* **1985,** *18* (10), 309-315.

42. G. Kiess, H., *Conjugated Conducting Polymers*. 1992.

43. Cobet, C.; Gasiorowski, J.; Farka, D.; Stadler, P., Polarons in Conjugated Polymers. *Ellipsometry of Functional Organic Surfaces and Films* **2018**, 355-387.

44. Vanlaeke, P.; Swinnen, A.; Haeldermans, I.; Vanhoyland, G.; Aernouts, T.; Cheyns, D.; Deibel, C.; D'Haen, J.; Heremans, P.; Poortmans, J.; Manca, J. V., P3HT/PCBM bulk heterojunction solar cells: Relation between morphology and electro-optical characteristics. *Solar Energy Materials and Solar Cells* **2006,** *90* (14), 2150-2158.

45. Tremel, K.; Ludwigs, S., Morphology of P3HT in Thin Films in Relation to Optical and Electrical Properties. 2014; Vol. 265, pp 39-82.

46. Lee, S. J.; Pil Kim, H.; Mohd Yusoff, A. R. b.; Jang, J., Organic photovoltaic with PEDOT:PSS and V2O5 mixture as hole transport layer. *Solar Energy Materials and Solar Cells* **2014,** *120*, 238-243.

47. Yan, H.; Kagata, T.; Okuzaki, H., Micrometer-scaled OFET channel patterns fabricated by using PEDOT/PSS microfibers. *Synthetic Metals* **2009,** *159* (21), 2229-2232.

48. Liang, C.; Wang, Y.; Li, D.; Ji, X.; Zhang, F.; He, Z., Modeling and simulation of bulk heterojunction polymer solar cells. *Solar Energy Materials and Solar Cells* **2014,** *127*, 67-86.

49. Abidin, T.; Zhang, Q.; Wang, K.-L.; Liaw, D.-J., Recent advances in electrochromic polymers. *Polymer* **2014,** *55* (21), 5293-5304.

50. Xia, Y.; Sun, K.; Ouyang, J., Solution-Processed Metallic Conducting Polymer Films as Transparent Electrode of Optoelectronic Devices. *Advanced Materials* **2012,** *24* (18), 2436-2440.

51. Heuer, H. W.; Wehrmann, R.; Kirchmeyer, S., Electrochromic Window Based on Conducting Poly(3,4-ethylenedioxythiophene)–Poly(styrene sulfonate). *Advanced Functional Materials* **2002,** *12* (2), 89-94.

52. Laforgue, A., Electrically controlled colour-changing textiles using the resistive heating properties of PEDOT nanofibers. *Journal of Materials Chemistry* **2010,** *20* (38), 8233-8235.

53. Ramanavičius, A.; Ramanavičienė, A.; Malinauskas, A., Electrochemical sensors based on conducting polymer—polypyrrole. *Electrochimica Acta* **2006,** *51* (27), 6025-6037.

54. Saranya, K.; Rameez, M.; Subramania, A., Developments in conducting polymer based counter electrodes for dye-sensitized solar cells – An overview. *European Polymer Journal* **2015,** *66*, 207-227.

55. Ameen, S.; Akhtar, M. S.; Seo, H.-K.; Shin, H. S., Distinctive polypyrrole nanobelts as prospective electrode for the direct detection of aliphatic alcohols: Electrocatalytic properties. *Applied Catalysis B: Environmental* **2014,** *144*, 665-673.

56. Chen, T. A.; Rieke, R. D., The first regioregular head-to-tail poly(3-hexylthiophene-2,5-diyl) and a regiorandom isopolymer: nickel versus palladium catalysis of 2(5)-bromo-5(2)-(bromozincio)-3-hexylthiophene polymerization. *Journal of the American Chemical Society* **1992,** *114* (25), 10087-10088.

57. Chen, T. A.; O'Brien, R. A.; Rieke, R. D., Use of highly reactive zinc leads to a new, facile synthesis for polyarylenes. *Macromolecules* **1993,** *26* (13), 3462-3463.

58. Jiang, C.; Chen, G.; Wang, X., High-conversion synthesis of poly(3,4-ethylenedioxythiophene) by chemical oxidative polymerization. *Synthetic Metals* **2012,** *162* (21), 1968-1971.

59. Gospodinova, N.; Terlemezyan, L., Conducting polymers prepared by oxidative polymerization: polyaniline. *Progress in Polymer Science* **1998,** *23* (8), 1443-1484.

60. Paradee, N.; Sirivat, A., Synthesis of poly(3,4-ethylenedioxythiophene) nanoparticles via chemical oxidation polymerization. *Polymer International* **2014,** *63* (1), 106-113.

61. Zhang, X.; Manohar, S. K., Bulk Synthesis of Polypyrrole Nanofibers by a Seeding Approach. *Journal of the American Chemical Society* **2004,** *126* (40), 12714-12715.

62. Baik, W.; Luan, W.; Zhao, R. H.; Koo, S.; Kim, K.-S., Synthesis of highly conductive poly(3,4-ethylenedioxythiophene) fiber by simple chemical polymerization. *Synthetic Metals* **2009,** *159* (13), 1244-1246.

63. Yin, Z.; Zheng, Q., Controlled Synthesis and Energy Applications of One-Dimensional Conducting Polymer Nanostructures: An Overview. *Advanced Energy Materials* **2012,** *2* (2), 179-218.

64. Kitada, K.; Ozaki, S., Reductive Polymerization of Halothiophene. *Polymer Journal* **1995,** *27*, 1161.

65. Snyder, H. R.; Putnam, R. E., Reductive Polymerization of α,β-Unsaturated Amides. I. N,N-Diethylcrotonamide. *Journal of the American Chemical Society* **1954,** *76* (1), 33-35.

66. Ha, Y.-H.; Nikolov, N.; Pollack, S. K.; Mastrangelo, J.; Martin, B. D.; Shashidhar, R., Towards a Transparent, Highly Conductive Poly(3,4-ethylenedioxythiophene). *Advanced Functional Materials* **2004,** *14* (6), 615-622.

67. Ravindra Kumar; Satyendra Singh; B C Yadav, Conducting Polymers: Synthesis, Properties and Applications. *International Advanced Research Journal in Science, Engineering and Technology* **2015,** *2* (11), 110-124.

68. Sadki, S.; Schottland, P.; Brodie, N.; Sabouraud, G., The mechanisms of pyrrole electropolymerization. *Chemical Society Reviews* **2000,** *29* (5), 283-293.

69. Ghosh, S.; Kouamé, N.; Ramos, L.; Remita, S.; Dazzi, A.; Deniset-Besseau, A.; Beaunier, P.; Goubard, F.; Aubert, P.-H.; Remita, H., Conducting polymer nanostructures for photocatalysis under visible light. **2015,** *14*.

70. Masuda, T.; Abdul Karim, S. M.; Nomura, R., Synthesis of acetylene-based widely conjugated polymers by metathesis polymerization and polymer properties. *Journal of Molecular Catalysis A: Chemical* **2000,** *160* (1), 125-131.

71. Evans, P.; Grigg, R.; Monteith, M., Metathesis of aniline and 1,2-dihydroquinoline derivatives. *Tetrahedron Letters* **1999,** *40* (28), 5247-5250.

72. Arefi, F.; Andre, V.; Montazer-Rahmati, P.; Amouroux, J., Plasma polymerization and surface treatment of polymers. *Pure and Applied Chemistry* **1992,** *64* (5), 715.

73. Pan, C.-y.; Chen, Z.-h.; Huang, Y.-l.; Huang, K.-l., Effects of water phase concentration on the emulsion polymerization of polyaniline. **2001,** *8*, 140-142.

74. Lattach, Y.; Deniset-Besseau, A.; Guigner, J.-M.; Remita, S., Radiation chemistry as an alternative way for the synthesis of PEDOT conducting Polymers under "soft" Conditions. *Radiation Physics and Chemistry* **2013,** *82*, 44-53.

75. Karim, M. R.; Lee, C. J.; Lee, M. S., Synthesis of conducting polypyrrole by radiolysis polymerization method. *Polymers for Advanced Technologies* **2007,** *18* (11), 916-920.

76. Karim, M.; Jae Lee, C.; Jin Kim, H.; Tauhidul Islam Bhuiyan, M.; Sang Lee, M., Preparation of Buckyball-Shaped Conducting Polythiophene by the Gamma Radiation-Induced Polymerization Method. *Macromolecular Symposia* **2007,** *249-250*, 234-240.

77. Pillalamarri, S. K.; Blum, F. D.; Tokuhiro, A. T.; Story, J. G.; Bertino, M. F., Radiolytic Synthesis of Polyaniline Nanofibers: A New Templateless Pathway. *Chemistry of Materials* **2005,** *17* (2), 227-229.

78. Cui, Z.; Coletta, C.; Dazzi, A.; Lefrançois, P.; Gervais, M.; Néron, S.; Remita, S., Radiolytic Method as a Novel Approach for the Synthesis of Nanostructured Conducting Polypyrrole. *Langmuir* **2014,** *30* (46), 14086-14094.

79. Lattach, Y.; Coletta, C.; Ghosh, S.; Remita, S., Radiation-Induced Synthesis of Nanostructured Conjugated Polymers in Aqueous Solution: Fundamental Effect of Oxidizing Species. *ChemPhysChem* **2014,** *15* (1), 208-218.

80. Coletta, C.; Cui, Z.; Archirel, P.; Pernot, P.; Marignier, J.-L.; Remita, S., Electron-Induced Growth Mechanism of Conducting Polymers: A Coupled Experimental and Computational Investigation. *The Journal of Physical Chemistry B* **2015,** *119* (16), 5282-5298.

81. Ishigaki, A.; Koizumi, H., Radiation-induced polymerization of 3-octylthiophene. *Radiation Physics and Chemistry* **2012,** *81* (7), 803-806.

82. Tebyetekerwa, M.; Wang, X.; Wu, Y.; Yang, S.; Zhu, M.; Ramakrishna, S., Controlled synergistic strategy to fabricate 3D-skeletal hetero-nanosponges with high performance for flexible energy storage applications. *Journal of Materials Chemistry A* **2017,** *5* (40), 21114-21121.

83. Tebyetekerwa, M.; Yang, S.; Peng, S.; Xu, Z.; Shao, W.; Pan, D.; Ramakrishna, S.; Zhu, M., Unveiling Polyindole: Freestanding As-electrospun Polyindole Nanofibers and Polyindole/Carbon Nanotubes Composites as Enhanced Electrodes for Flexible All-solid-state Supercapacitors. *Electrochimica Acta* **2017,** *247*, 400-409.

84. Emmi, S. S.; Beggiato, G.; Casalbore-Miceli, G., Transient species in the pulse radiolysis of methylene chloride and the self-reaction of chloromethyl radicals. *International Journal of Radiation Applications and Instrumentation. Part C. Radiation Physics and Chemistry* **1989,** *33* (1), 29-37.

85. Alfassi, Z. B.; Mosseri, S.; Neta, P., Reactivities of chlorine atoms and peroxyl radicals formed in the radiolysis of dichloromethane. *The Journal of Physical Chemistry* **1989,** *93* (4), 1380-1385.

86. Emmi, S. S.; Poggi, G.; D'Angelantonio, M.; Russo, M.; Favaretto, L., The solvatochromic effect on some oligothiophene radical cations: a pulse radiolysis and semiempirical investigation. *Radiation Physics and Chemistry* **2003,** *67* (3), 251-256.

87. Guldi, D. M.; Field, J.; Grodkowski, J.; Neta, P.; Vogel, E., One-Electron Oxidation of Metalloporphycenes As Studied by Radiolytic Methods. *The Journal of Physical Chemistry* **1996,** *100* (32), 13609-13614.

Chapter 1 Materials, instruments and synthesis methodologies

The use of radiolysis seems to be a good approach to understand the mechanism of conducting polymers growth and eventually to improve the synthesis procedure. The polymerization by irradiation is based on the interaction of ionizing radiation with solvent molecules which produces reactive species, like radicals, which can initiate the polymerization. As will be discussed in the next chapters, the aim of this work is to develop a new method of synthesis of conductive polymers in an organic solvent based on radiation chemistry which is in one hand, easy and efficient comparing to chemical and electrochemical polymerization routes, and on the other hand processable towards the variety of corresponding monomers of CPs.

In this chapter, all the chemicals that have been used for synthesis and post treatment of CPs will be presented and also all the instruments that have been used during this work for CPs characterization will be described. Furthermore, you will be acquainted with all the radiation methods used for the preparation of CPs will be discussed in details. The final part of this thesis is dedicated to the elaboration of OPVs and testing their photoactivities. This part was done in collaboration with Laboratoire de Physicochimie des Polymères et des Interfaces (LPPI) of University of Cergy Pontoise. Most of the experiments were performed by me in LPPI laboratory. Thus, the present chapter will also include the fabrication process of photovoltaic devices with all their concomitant characterizations and tests.

1.1. Chemicals

In the following section, all chemical products used during preparation of solution are described. The choice of products are explained and discussed. Finally the procedure of solution preparation is detailed.

1.1.1. Monomers

3,4-Ethylenedioxythiophene (EDOT). EDOT ($C_6H_6O_2S$) monomer (molecular weight of 142.18 $g.mol^{-1}$) in **Figure 1. 1** was purchased from Sigma-Aldrich with purity of 97% and used as received. The derived polymer (PEDOT) in **Figure 1.1** is known for its high conductivity and good optical trasparency in the visible spectral region.[1] EDOT is not very soluble in water (2.1 $g.L^{-1}$ at 20 ° C or 15 mM at 25 ° C).[2-3] Due to its low solubility in water only relatively low concentrations in EDOT were used. By contrast, EDOT is highly soluble in dichloromethane. By taking the variation of the absorption as a function of the

concentration, the solubility of EDOT in dichlormethane was found in this work to be more than 50 mM.

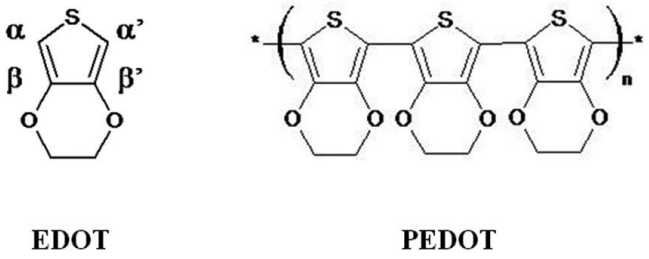

Figure 1.1 Chemical structures of 3,4-ethylenedioxythiophene (EDOT) and poly(3,4-ethylenedioxythiophene) (PEDOT). EDOT structure displays the free α, α' positions where polymerization could occur.

The concentrations 10 mM in EDOT in aqueous solutions and up to 50 mM in dichloromethane were used for solutions preparation. All the solutions were prepared at room temperature. The monomers concentrations of prepared aqueous and dichloromethane solutions were always checked by recording UV-Vis absorption spectra before and after irradiation. In both aqueous and dichloromethane solutions, EDOT has two characteristic bands that are observed at 235 nm and 255 nm in aqueous solution and at 242 nm and 259 nm in dichloromethane (**Figure 1.2**).

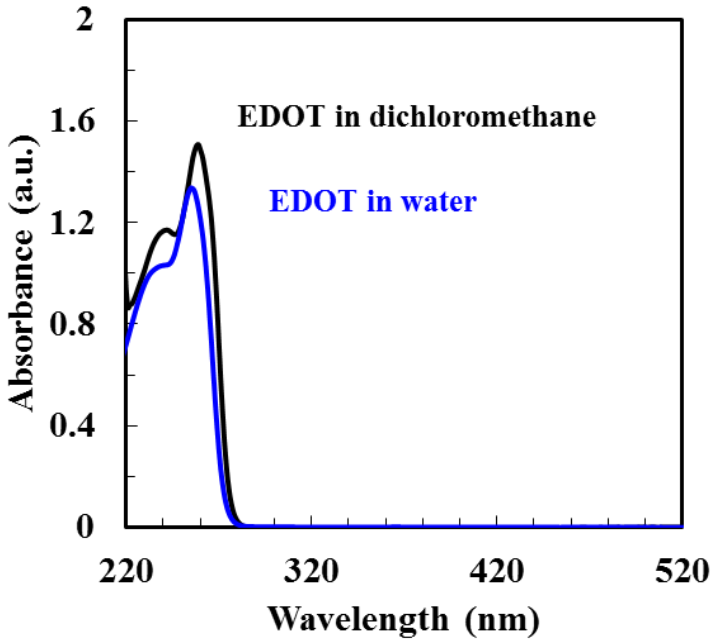

Figure 1.2 UV-Vis absorption spectra of aqueous and dichloromethane solutions containing 10 mM in EDOT diluted 10 times before irradiation. The path length is 0.2 cm and the reference is the pure solvent.

By recording the variation of the absorbance as a function the concentration thanks to Beer Lambert law, we were able to deduce the values of the extinction coefficients at the maximal absorbances.

Table 1.1 shows the extinction coefficients that were estimated in aqueous solution in a previous work[4] as well as in dichloromethane that were estimated in present work[5]:

Extinction coefficients in water (ε) ($L.mol^{-1}.cm^{-1}$)		Extinction coefficients in dichloromethane (ε) ($L.mol^{-1}.cm^{-1}$)	
ε_{235}	ε_{255}	ε_{242}	ε_{259}
5650	7048	4747	6020

Table 1.1 The estimated extinction coefficients values of EDOT in water[4] and dichloromethane[5]

3-thiopheneacetic acid (TAA). TAA ($C_6H_6O_2S$) monomer (molecular weight of 142.18 $g.mol^{-1}$) in **Figure 1.3** was purchased from Sigma-Aldrich with purity of 98% and used as received. TAA has limited solubility in aqueous media.[6] In fact, the solubility of TAA in aqueous solution was found after heating up to 60 ° C higher than 20 mM. However, TAA exhibits good solubility in dichloromethane, which has been shown to be higher than 50 mM in this work. In this work, we chose to work with concentrations of 10 mM in TAA both in aqueous solutions and in dichloromethane. These concentrations were then used for solutions preparation.

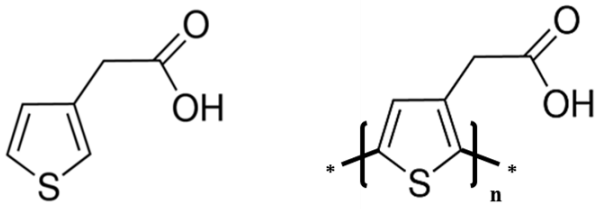

Figure 1.3 Chemical structures of 3-thiopheneacetic acid (TAA) and poly (3-Thiopheneacetic acid) (PTAA)

The monomers concentration of prepared aqueous and dichloromethane solutions were always checked by recording UV-Vis absorption spectra before and after irradiation. The UV-Vis spectra of TAA molecules in water and dichloromethane (**Figure 1.4**), show maximum absorptions at 235 nm with a molar extinction coefficient: ε_{235} (H_2O) = 7304 and ε_{235} (CH_2Cl_2) = 6896 $L.mol^{-1}.cm^{-1}$.

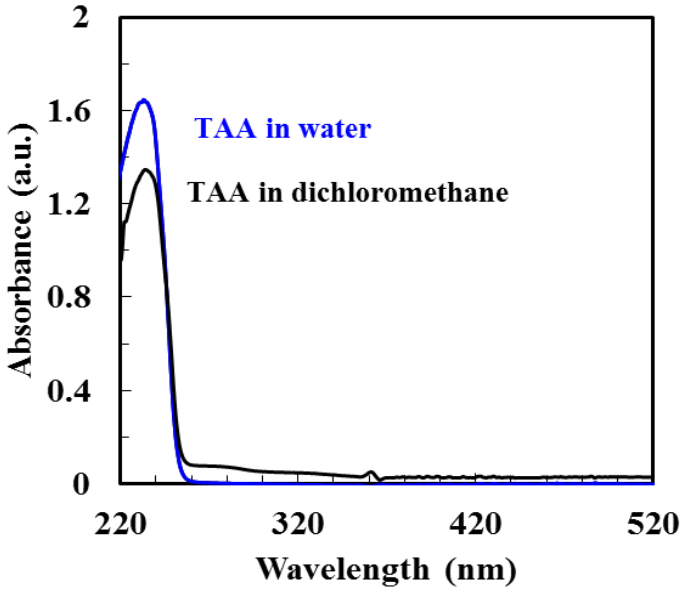

Figure 1.4 UV-Vis absorption spectra of aqueous and dichloromethane solutions containing 10 mM in TAA diluted 10 times before irradiation. The path length is 0.2 cm and the reference is the pure solvent.

3-hexylthiophene (3HT). 3HT ($C_{10}H_{16}S$) monomer (molecular weight of 168.30 $g.mol^{-1}$) in **Figure 1.5** was purchased from Sigma-Aldrich with purity higher than 99% and used as received. 3HT is used as starting reagent in the synthesis of P3HT (**Figure 1.5**).

Contrarily to PEDOT and TAA 3HT is water insoluble monomer due to its hydrophobic substituent (Hexyl group). However, 3HT has very good solubility in common organic solvents including dichloromethane. The absorption spectrum of 10 mM in 3HT in dichloromethane is displayed in **Figure 1.6**. 3HT has absorption maximum at 238 nm and also shows very good solubility in dichloromethane higher than 50 mM as found in this work. Thus, concentrations up to 50 mM in 3HT were used in DCM for solutions preparation.

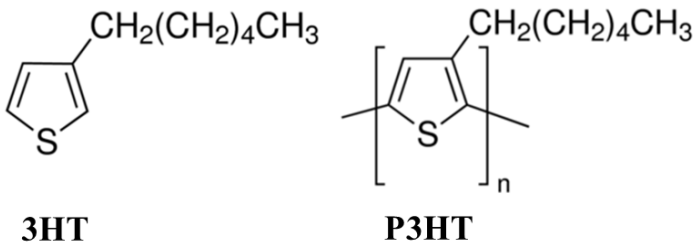

Figure 1.5 Chemical structures of 3-hexylthiophene (3HT) and poly(3-hexylthiophene) (P3HT)

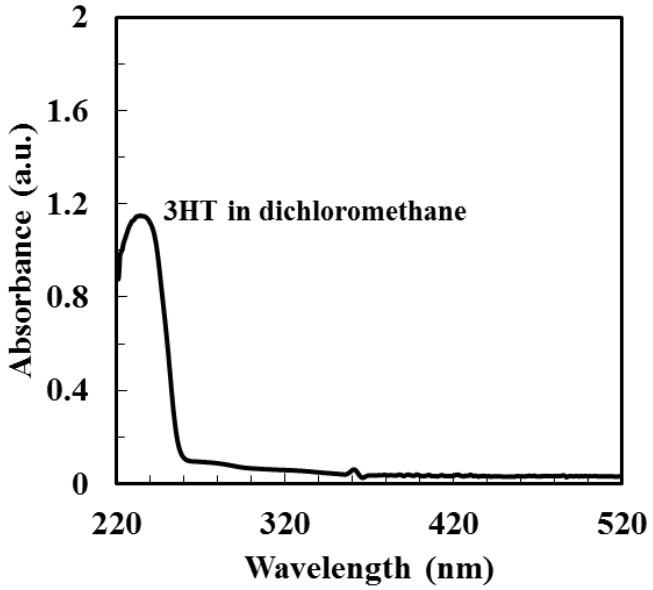

Figure 1.6 UV-Vis absorption spectrum of dichloromethane solutions containing 10 mM in 3HT diluted 10 times before irradiation. The length path is 0.2 cm and the reference is the solvent.

The extinction coefficient has been calculated and it was found to be ε_{238}= 5570 $L.mol^{-1}cm^{-1}$. The monomers concentration of prepared dichloromethane solutions were always checked by recording UV-Vis absorption spectra before and after irradiation.

1.1.2. Solvents and reagents

Distilled water (Millipore system 18.2 $\Omega.cm^{-1}$) was used for preparation of aqueous solutions of EDOT and TAA and also for washing. Sodium dodecyl sulfate, SDS ($C_{12}H_{25}NaO_4S$) was bought from Sigma-Aldrich with purity ≥98.5 %) and was used as surfactant. Sodium azide (NaN_3, ≥ 99%) was purchased from Sigma Aldrich. It was used radiolytically to produce azide radicals $N_3^{\bullet}$ as oxidants to initiate the polymerization of EDOT in aqueous solutions. Isopropanol (from Sigma-Aldrich, with purity ≥ 95 %) was used as $HO^{\bullet}$ scavenger.

Hydrochloric acid (HCl) (VWR International S.A.S., 37 %) and perchloric acid ($HClO_4$) (Sigma-Aldrich, ACS grade) were used as hydrated electrons e_{aq}^- scavenger during radiolysis of acidic solution solution scavenger and to adjust the pH of the aqueous medium.

Isopropanol (from Sigma-Aldrich, purity ≥ 95 %) was also used as e_{aq}^- scavenger.

Anhydrous dichloromethane, DCM (CH_2Cl_2) with purity ≥99.80 %, chloroform ($CHCl_3$) with purity ≥99.50 %Anhydrous carbon tetrachloride, (CCl_4) with purity ≥99.50 % were purchased from Sigma- Aldrich and were used for preparation of solutions of EDOT, TAA and 3HT and study of their oxidative polymerization.

Nitrogen (N_2), nitrous oxide (N_2O) and oxygen (O_2) (from Air Liquid Co. with purity 99.99 %) were used for solutions degassing and for the selection of reacting radicals upon radiolysis.

Anhydrous tetrahydrofuran, THF (C_4H_8O) with purity ≥ 99.9 % was used purchased from Sigma-Aldrich and was used for size exclusion chromatography analysis and some of cyclic voltammetry measurements. Acetonitrile (bought from Sigma-Aldrich, 99.8%) was also used as solvent to perform some cyclic voltammetry measurements. Tetrabutylammonium hexafluorophosphate ($(CH_3CH_2CH_2CH_2)_4N(PF_6)$, $TBAPF_6$, was bought from Sigma-Aldrich, with purity ≥99 %) which was used as electrolyte during electrochemistry measurement. Ferrocene (bis(cyclopentadienyl)iron, di(cyclopentadienyl)iron), $Fe(C_5H_5)_2$, with purity of 98 %) was used as standard during cyclic voltammetry measurements to estimate the electronic band gaps of radio-synthesized conducting polymers.

Pure water, Ethanol absolute (from VWR) and acetone (from Sigma-Aldrich) were used for washing the samples.

Chlorobenzene, 1,2-dichlorobenzene, chloroform and DMSO (bought from Sigma-Aldrich) were used to test the solubility of radio-synthesized conducting polymers for organic solar cells application.

Also hydrochloric acid and ammonium hydroxide solution (NH_4OH) (VWR, 25%) were used to undope and redope the radio-synthesized conducting polymers.

Nitrosyl tetrafluoroborate 95% ($NOBF_4$) was bought from Sigma-Aldrich and used as dopant for electrical conductivity measurements.

1.2. Gamma-irradiation and radiolytic routes

In the Laboratoire de Chimie Physique d'Orsay, there are two sources of ionizing radiations: ^{60}Co source and ELYSE electron accelerator. These two facilities allow the study of the polymerization by steady-state radiolysis and by pulsed radiolysis respectively. I would like to mention that during my thesis I only worked and performed experiments using ^{60}Co gamma source.

1.2.1. The irradiation platform: Cobalt 60 (^{60}Co) as source of γ-rays

As an important ionizing radiation source, γ-rays released by radioactive cobalt (^{60}Co) have been widely applied in both industry and research. The decay of ^{60}Co isotopes produces γ-rays with high energy and the half-life period of ^{60}Co is 5.27 years (**Figure 1.7**).[7] It is well

known that γ-rays are highly energetic waves and the penetration ability of gamma photons is strong which needs protection by the way of lead walls.

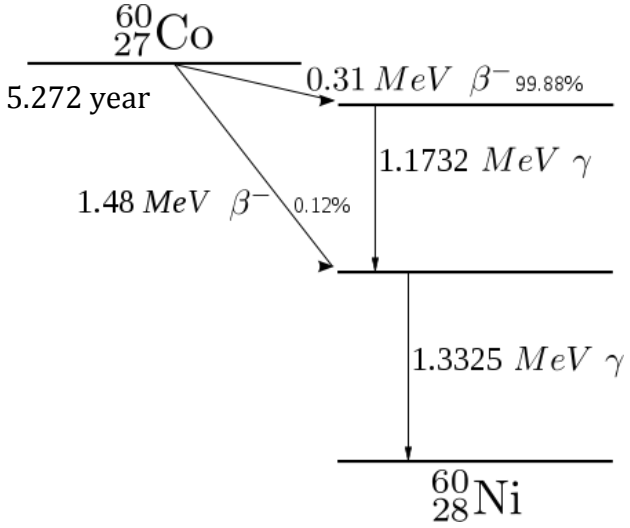

Figure 1.7 Decay scheme of ^{60}Co isotopes

In order to describe the energy absorbed during a γ-irradiation, the concept of dose (D) is introduced to quantify the amount of energy deposited in the irradiated media (aqueous solutions or DCM solutions in this work). Normally, D is counted with the unit of gray (Gy) which is defined as the energy of 1 J absorbed by 1 kg of irradiated medium or 1 L in case of aqueous solutions since water density is 1 g.mL^{-1}. Therefore, the dose of 1 Gy corresponds to 1 J.kg^{-1} or 1 J.L^{-1} for water solution.[8] In addition, within a per unit time (min or h), the amount of energy deposited is termed as the dose rate (Gy.min^{-1} or Gy.h^{-1}). Thus, the energy absorbed during the γ radiation of water can be calculated as follows:

$$D\ (Gy) = \text{Dose rate}\ (Gy.min^{-1}\ \text{or}\ G.h^{-1}) \times \text{Time (min or h)} \qquad (1.1)$$

In the gamma source (LCP, University Paris-Sud), the ^{60}Co is stored in a lead jar and mechanically lifted up for irradiation which is controlled by the operator (**Figure 1.8** left). To irradiate the samples by γ-rays, all the glass vials containing aqueous solutions are put on the plat inside the irradiation room at fixed positions (**Figure 1.8** right). The dose rates at different positions depend on the distance to the source and are determined with Fricke‘s dosimetry.[9]

As a result, when the dose rate is determined, the dose, D, deposited by γ-irradiation can be calculated according to equation (2.1).

Knowing the radiolytic yield (G) (which will be defined in the next paragraph) values of the different radiolytic species, their produced concentrations can be determined according to the following equation:

$$C\ (mol \cdot L^{-1}) = D\ (Gy) \times G\ (mol \cdot J^{-1}) \times d\ (kg.\ L^{-1}) \qquad (1.2)$$

Where *d* is the density of the irradiated solution

In the same way, the dose which is necessary to quantitatively oxidize or reduce a solute in the solution can be deduced from this equation knowing the yield of its disappearance.

Figure 1.8 Photographs of ^{60}Co gamma source installation (LCP, Paris-Sud University). Control panel (left) and irradiation plate (right)

1.2.2. Water radiolysis

Upon γ-irradiation γ-rays interact with all molecules of the irradiated medium. But since the molecules of the solvent are in large excess, only we neglect the effect of g-rays onto the solutes (direct effect). We only consider the effect on the solvent which generates reactive species which will react on the solutes (indirect effect). Thus, in this work radiation method is based on the radiolysis of solvent which produces various oxidizing and reducing species.[4] The initiators produced using radiation method can induce as we will see the oxidation of organic monomers making it a new method for the synthesis of CPs and reduction of metal ions into metal nanoparticles. Compared with traditional chemical method, radiation method avoids the addition of chemical oxidants or reducing species while just needs the common solvent making the polymerization process clean and environment friendly. Furthermore, radiation method can realize the production of large quantity of CPs or CPs nanocomposites

which overcomes the limitation of electrochemical method.[10] The history of radiation chemistry is long and investigations on radiation chemistry of different solvents have already been carried out.[11-13] However, both complex physical processes and chemical reactions happen during the radiation process. For the moment, the mechanism of radiolysis of water is relatively well understood.[12]

As the most commonly used and abundant solvent, water (H_2O) is of great importance and the radiolysis of water is meaningful. Ionizing radiation can be initiated by gamma (γ)-rays, X-rays and accelerated particles (electrons, α-particles) which possess high energy. When water is exposed to ionizing radiation, both physical and chemical stages undergo as a function of the time (**Figure 1.9**).[14-15]

After the physico-chemical stage, complex reactions occur and stable species are produced at the ns time scale. At the chemical stage, the kinds and amounts of produced species can be known. Therefore, the radiolysis of water under N_2 atmosphere at neutral pH can be summarized as follows:[13]

$$H_2O \rightsquigarrow e_{aq}^-, HO^\bullet, H^\bullet, H_3O^+, H_2O_2, H_2 \qquad (1.3)$$

In order to quantify the amounts of the different species produced by water radiolysis, the concept of radiolytic yield (G-value) is used to express and quantify the production or consumption of the evolved different species. G value is defined as the amount of species

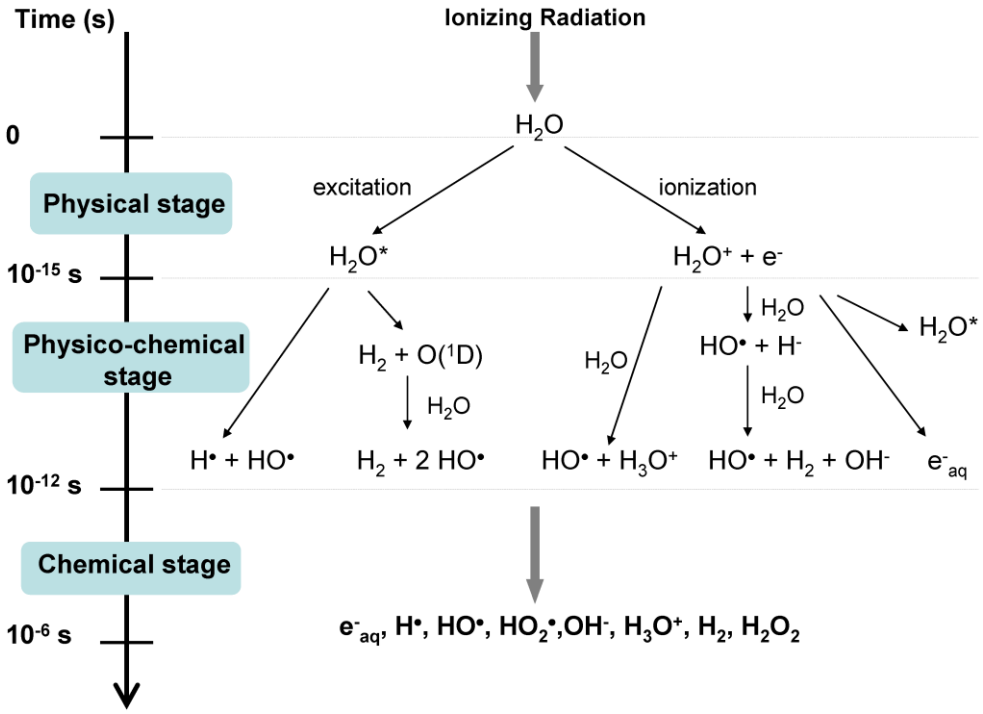

Figure 1.9 Time scale of events of the primary products that are generated during water radiolysis [14-15]

(mol) formed or disappeared in the medium when one joule (J) is absorbed and the commonly used unit of radiolytic yield is mol J^{-1}.[16] In the early literature, G value is termed as the number of molecules produced when the energy of 100 eV is absorbed.[13] These two definations could be transferred into each other by

$$1 \text{ molecule } (100 \text{ eV})^{-1} = 1.036 \times 10^{-7} \text{mol.J}^{-1} \quad (1.4)$$

The G-values of the different radiolytic species involved in water radiolysis which evidently depend on the experimental conditions are summarized and listed for different radiation types and pH values under N_2 atmosphere (**Table 1.2**).[14]

Radiation	$\mathbf{e_{aq}^-}$	$\mathbf{HO^\bullet}$	$\mathbf{H^\bullet}$	$\mathbf{H_2}$	$\mathbf{H_2O_2}$	$\mathbf{HO_2^\bullet}$
γ Electrons (0.1-10 MeV) pH=3-11	0.28	0.28	0.06	0.047	0.073	0.0027
γ Electrons (0.1-10 MeV) pH=0.5	0	0.301	0.378	0.041	0.081	0.0008
5.3 MeV α particles pH=0.5	0	0.052	0.062	0.163	0.150	0.011

Table 1.2 Radiolytic yields (μmol.J^{-1}) as a function of the type of radiation and the pH of water under N_2 atmosphere.[14]

According to **Table 1.2**, γ-radiolysis of water under N_2 atmosphere in neutral medium produces in our experimental conditions (Co source in LCP laboratory) different species the G- values of which are:[13]

$$G_{HO^\bullet} = 2.8 \times 10^{-7} \text{mol.J}^{-1} \quad (1.5)$$

$$G_{e_{aq}^-} = 2.8 \times 10^{-7} \text{mol.J}^{-1} \quad (1.6)$$

$$G_{H^\bullet} = 0.6 \times 10^{-7} \text{mol.J}^{-1} \quad (1.7)$$

$$G_{H_2} = 0.46 \times 10^{-7} \text{mol.J}^{-1} \quad (1.8)$$

$$G_{H_2O_2} = 0.73 \times 10^{-7} \text{mol.J}^{-1} \qquad (1.9)$$

$$G_{HO_2^{\bullet}} = 0.027 \times 10^{-7} \text{mol.J}^{-1} \qquad (1.10)$$

It is clear that among the various species produced by the γ-radiolysis of water under N_2 atmosphere in neutral medium, $HO^{\bullet}$ and e_{aq}^{-} are the major species. The effect of pH on the G- values of the different species produced during the radiolysis of water by γ-rays and accelerated electrons has to be taken into account. Also the variation of the yields with the pH is shown (**Figure 1.10**).[17-18]

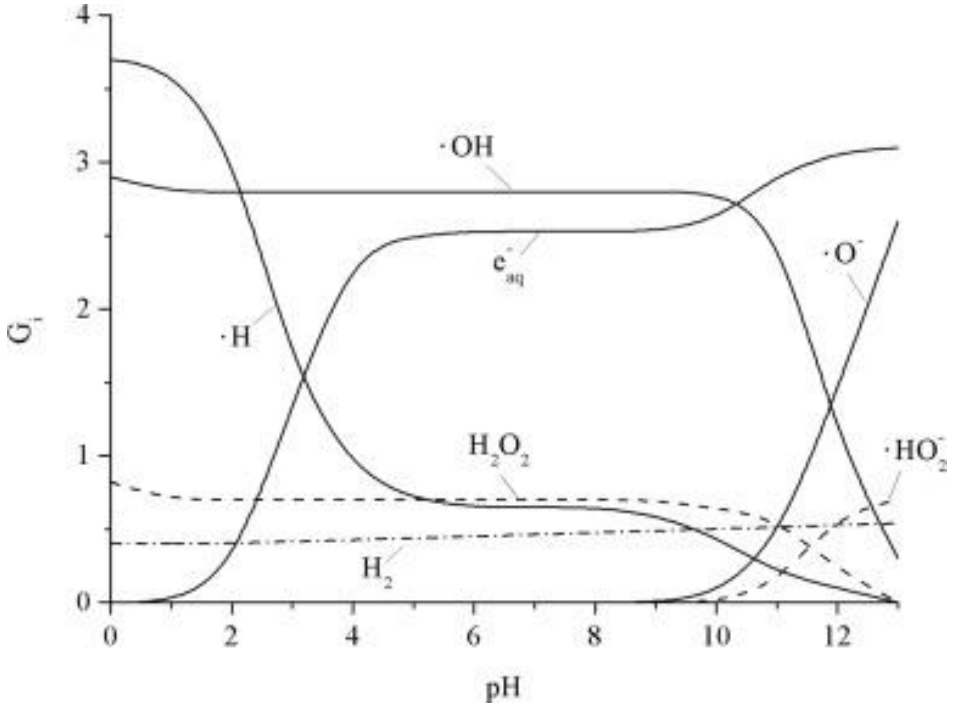

Figure 1.10 Effect of pH on the yields of primary products of water radiolysis. Yields are for γ-rays and fast electrons under N_2 atmosphere with energies of the of the order of 1 to 20 MeV [17-18]

Therefore, the production of different species can be adjusted by controlling the pH. In particular, one can observe that hydrated electrons are scavenged by H+ leading to H. atoms according to:

$$e_{aq}^{-} + H^{+} \rightarrow H^{\bullet} \qquad (1.11)$$

In addition, the G values of different species can be tuned by adding scavengers during the radiolysis. Under different conditions, by changing the atmosphere, by adding specific scavengers or changing the pH values, the amount of different species can be varied and both reducing species and oxidizing species can be obtained. Therefore, the species produced can be adjusted by changing the radiolytic conditions.[19-21]

1.2.2.1. Radiolysis of aqueous solutions under different atmospheres and environmental conditions

As mentioned before, the radiolysis of water with γ rays produces a wide variety of species and the G-values of the different species depend on the radiolytic conditions. During the radiolysis of water, oxidizing and reducing species are formed. As a result, both produced species may work as initiators of oxidation radicals to induce monomers polymerization or of reduction reactions to lead to metal nanoparticles and have the potential application for the synthesis of CPs and their metal composites. Under the oxidative conditions, reducing species (such as e_{aq}^-) should be scavenged and converted into secondary radicals to optimize and to increase the yield of oxidation. In order to quantify the polymerization of monomers with the oxidizing species produced by γ-radiolysis of water, it is necessary to know the kinds and amounts of all oxidizing species produced under the given experimental conditions.

a. Radiolysis of aerated aqueous solutions

When the radiolysis of water undergoes in presence of oxygen (O_2), $H^\bullet$ atoms and e_{aq}^- are scavenged by O_2 to produce respectively perhydroxyl radicals ($HO_2^\bullet$) and superoxide radicals ($O_2^{\bullet-}$) which are the two acid-basic forms of the couple $HO_2^\bullet$/ $O_2^{\bullet-}$ (pKa ($HO_2^\bullet/O_2^{\bullet-}$) = 4.8 at 298 K).[12] As a consequence, when irradiating aerated aqueous solutions at neutral pH, only two short lived transient species are formed: $HO^\bullet$ and $O_2^{\bullet-}$ with the following radiolytic yields: [22]

$$G_{HO^\bullet} = 2.8 \times 10^{-7} \text{mol.J}^{-1} \qquad (1.12)$$

$$G(O_2^{\bullet-}) = G_{H^\bullet} + G_{e_{aq}^-} = 3.4 \times 10^{-7} \text{mol.J}^{-1} \qquad (1.13)$$

It is well known that $HO^\bullet$ is a strong oxidizing species since its apparent standard redox potential at pH = 7 amounts to $E°'(HO^\bullet/H_2O)$ = 2.2 V_{SHE}[22] enabling the oxidation of organic

monomers. These $HO^{\bullet}$ radical can add onto organic molecules to afford radical adducts.[23]Nevertheless, $O_2^{\bullet-}$ is also oxidizing species with a redox potential $E°'(O_2^{\bullet-}/H_2O_2)$ = 0.9 V_{SHE}.[12] However, its redox potential is relatively low and its oxidizing power is poor. Thus, the presence of latter species can be neglected at neutral pH.

b. Radiolysis under N_2O

When irradiating nitrous oxide (N_2O, 25 mM) saturated aqueous solutions at neutral pH, e_{aq}^- is quantitatively converted into $HO^{\bullet}$ according to the following reaction: [24]

$$e_{aq}^- + N_2O + H_2O \rightarrow HO^{\bullet} + HO^- + N_2 \qquad (1.14)$$

Therefore, the main oxidizing species produced under N_2O atmosphere is $HO^{\bullet}$ radicals with the radiolytic yield of:

$$G(HO^{\bullet}) = G_{HO^{\bullet}} + G_{e_{aq}^-} = 5.6 \times 10^{-7} \text{mol.J}^{-1} \qquad (1.15)$$

Note that $H^{\bullet}$ atoms are still present in such conditions ($G_{H^{\bullet}} = 0.6 \times 10^{-7} \text{mol.J}^{-1}$). Nevertheless, due to its relatively small amount and unknown reactivity, the presence of $H^{\bullet}$ atoms is often neglected.[25]

c. Radiolysis under N_2O in presence of NaN_3

When the radiolysis of water occurs under N_2O atmosphere and in the presence of sodium azide (NaN_3) (100 mM), $HO^{\bullet}$ radicals are very quickly scavenged by N_3^- ions leading to the quantitative formation of azide radicals ($N_3^{\bullet}$) according to: [26-27]

$$HO^{\bullet} + N_3^- \rightarrow HO^- + N_3^{\bullet} \qquad (1.16)$$

It is well known that $N_3^{\bullet}$ radicals are an alternative oxidizing system more selective than $HO^{\bullet}$. It is a soft one-electron oxidant $E°'(N_3^{\bullet}/N_3^-)$ = 1.33 V_{SHE} at pH=7 leading to radical cations of organic molecules. [26-28] Thus, when irradiating N_2O saturated aqueous solutions at neutral pH in the presence of NaN_3, the main oxidizing species produced is $N_3^{\bullet}$ radicals with a radiolytic yield of formation which amounts to:[29]

$$G(N_3^{\bullet}) = G_{HO^{\bullet}} + G_{e_{aq}^-} = 5.6 \times 10^{-7} \text{mol.J}^{-1} \qquad (1.17)$$

$H^{\bullet}$ atoms also remains in these conditions with ($G_{H^{\bullet}} = 0.6 \times 10^{-7} mol.J^{-1}$) and its presence is neglected.

d. Radiolysis under N_2O at pH 0

When the radiolysis of water happens under N_2O atmosphere in acidic medium such as under N_2 (Figure 2.10), e_{aq}^{-} can quickly be transformed into $H^{\bullet}$ atoms by reacting with hydronium ions (H^+):[20]

$$e_{aq}^{-} + H^{+} \rightarrow H^{\bullet} \qquad (1.1)$$

As can be seen in equations (1.14) and (1.1) in such expected conditions (presence of N_2O and H^+), the hydrated electrons are quickly scavenged according to these two competitive reactions leading to additional amounts of $HO^{\bullet}$ with a yield of production noted $G'_{HO^{\bullet}}$ and to additional amounts of $H^{\bullet}$ with a yield noted $G'_{H^{\bullet}}$. Evidently, as illustrated in equation (1.18)

$$G'_{HO^{\bullet}} + G'_{H^{\bullet}} = G_{e_{aq}^{-}} = 2.8 \times 10^{-7} mol.J^{-1} \qquad (1.18)$$

Knowing the concentrations in H^+ and N_2O in the solution and knowing the rate constants of reactions (1.11) and (1.14), one can calculate the ratios between $G'_{HO^{\bullet}}$ and $G'_{H^{\bullet}}$. Then considering equation (1.18), it is possible to calculate the yields $G'_{HO^{\bullet}}$ and $G'_{H^{\bullet}}$ whatever the pH.[30] In particular in our previous work [25], it was found that only one hundred percent of hydrated electrons are converted, under N_2O at pH 0, into $HO^{\bullet}$ ($G'_{HO^{\bullet}} \sim 0$). In turn, our calculations highlighted that nearly all e_{aq}^{-} are converted into $H^{\bullet}$ atoms ($G'_{H^{\bullet}} \sim G_{e_{aq}^{-}} = 2.8 \times 10^{-7} mol.J^{-1}$). Under such conditions (under N_2O at pH =0), the yield of production of $HO^{\bullet}$ and $H^{\bullet}$ can be calculated as follows:

$$G(HO^{\bullet}) = G_{HO^{\bullet}} + G'_{HO^{\bullet}} = 2.8 \times 10^{-7} mol.J^{-1} \qquad (1.19)$$

$$G(H^{\bullet}) = G_{H^{\bullet}} + G'_{H^{\bullet}} = 3.4 \times 10^{-7} mol.J^{-1} \qquad (1.20)$$

Thus, at pH 0, two reactive species can be considered in the irradiated medium: $HO^{\bullet}$ and $H^{\bullet}$. This is the case when perchloric acid ($HClO_4$) is used to adjust the pH of the

aqueous solution since (ClO_4^-) remains unreactive upon irradiation (R). Therefore $HO^\bullet$ is the only oxidative species in the medium. Nevertheless, as highlighted thanks to equations (1.19) and (1.20), $H^\bullet$ becomes predominant at pH 0 and thus its reactivity onto organic monomers should not be omitted as demonstrated in some cases in literature [31].

In the case of the use of hydrochloride acid (HCl) instead of $HClO_4$ to adjust the pH under N_2O, $HO^\bullet$ radicals are quantitatively transformed into dichloride radical anions ($Cl_2^{\bullet-}$) [21] and therefore its radiolytic yield is equivalent to that of $HO^\bullet$:

$$G(Cl_2^{\bullet-}) = 2.8 \times 10^{-7} \text{mol. J}^{-1} \qquad (1.21)$$

Such as $HO^\bullet$, $Cl_2^{\bullet-}$ is a strong oxidizing species with a very high standard redox potential: $E^\circ(Cl_2^{\bullet-}/Cl^-)$ = 2.1 V_{SHE}.[19] This should enable, as in the case of hydroxyl radicals and azide radicals, the oxidation of organic monomers (EDOT, TAA) by $Cl_2^{\bullet-}$ and as we will their polymerization into CPs.

Here also, $H^\bullet$ remains with a yield of $G_{H^\bullet} = 3.4 \times 10^{-7} \text{mol. J}^{-1}$ (1.20).

e. Radiolysis under N_2 in presence of isopropanol

When radiolysis of water takes place under N_2 atmosphere with isopropanol (0.2 M), while $G_{e_{aq}^-}$ remains stable $HO^\bullet$ radicals and $H^\bullet$ atoms quantitatively react with isopropanol leading to isopropanol radical ($(CH_3)_2C^\bullet OH$) is generated according to: [32]

$$(CH_3)_2CHOH + HO^\bullet \rightarrow (CH_3)_2C^\bullet OH + H_2O \qquad (1.22)$$

$$(CH_3)_2CHOH + H^\bullet \rightarrow (CH_3)_2C^\bullet OH + H_2 \qquad (1.13)$$

The redox potential of this alcohol radical $(CH3)2C^\bullet OH$ which is also a reducing species amounts to -1.8 V_{SHE} at pH=7.40 Although $H^\bullet$ atoms are also powerful reducing species with a redox potential of -2.3 V_{SHE}, both the $HO^\bullet$ radicals and $H^\bullet$ atoms are tranformed into $(CH3)_2C^\bullet OH$.[17] Therefore, radiolysis of water under N_2 atmosphere with isopropanol produces two main reducing species e_{aq}^- and $(CH_3)_2C^\bullet OH$ with the radiolytic yields:

$$G_{e_{aq-}} = 2.8 \times 10^{-7} \text{mol. J}^{-1} \qquad (1.24)$$

$$G((CH_3)_2C^{\bullet}OH) = G_{HO^{\bullet}} + G_{H^{\bullet}} = 3.4 \times 10^{-7} mol.J^{-1} \quad (1.25)$$

Both e_{aq}^- and $(CH_3)_2C^{\bullet}OH$ are reducing species which are usually employed in metal ions reduction and should be used, as we will see, for the reduction of organic monomers.

1.2.2.2. Radiation induced polymerization

As demonstrated in paragraph (1.2.2.1b) concerning radiolysis of water under N_2O, $HO^{\bullet}$ radical is produced with radiolytic yield which amounts to $G(HO^{\bullet}) = 5.6 \times 10^{-7} mol.J^{-1}$. $HO^{\bullet}$ radicals are strong oxidizing species and its standard redox potential at pH = 7 amounts to $E°'(HO^{\bullet}/H_2O)$ = +2.2 V_{SHE} [22], and thus significantly, hydroxyl radical ($HO^{\bullet}$) under these experimental conditions, are the most abundant species with very high reactivity. These radicals are definitely able to initiate the oxidative polymerization and leads to production of conducting polymers as demonstrated in case PEDOT and Polypyrrole.[4, 33-34]

In addition, other oxidizing species can alternatively to $HO^{\bullet}$ be generated in the aqueous and efficiently enable the oxidative polymerization of CPs. These radicals can be simply generated by changing the environmental conditions of the irradiated aqueous solutions in the presence of certain substances. As said in paragraph 1.2.2.1d, when irradiating a very acidic aqueous solution containing organic monomers under N_2O atmosphere in the presence of HCl, a very strong oxidizing species, namely $Cl_2^{\bullet -}$, are produced instead of $HO^{\bullet}$. Also, the presence of NaN_3 in the irradiated aqueous solution under N_2O leads to formation oxidizing species, namely $N_3^{\bullet}$, which enables the oxidation of organic molecules and leads to production of conducting polymers. In addition, when irradiating aqueous solution at 0 °C containing organic monomers under Ar atmosphere in the presence of *tert*-butanol (as $HO^{\bullet}$ radicals scavenger) and in the presence of potassium persulfate ($K_2S_2O_8$), hydrated electrons reacts quickly with $S_2O_8^{2-}$ anions under these conditions, producing sulfate radicals ($SO4^{\bullet -}$).[35] These radical are very strong oxidizing species with a redox potential estimated to be 2.6 $V_{SHE.}$[36]

Subsequently, taking the radiation induced polymerization of organic monomers, oxidizing radicals first react with the organic monomers such as EDOT or Py, then with dimers, then with oligomers. The quantitative synthesis of CPs polymers throughout such a step-by-step mechanism necessarily implies the use of two oxidizing radicals for the oxidation of one monomer (as in the case of EDOT and Py polymerization). Noting that all the produced radicals ($HO^{\bullet}$, $N_3^{\bullet}$, $SO4^{\bullet -}$, $Cl_2^{\bullet -}$) by different radiolytic route are quantitatively able

to oxidize the organic monomers and thus the yield of organic monomers oxidation equals to yield of the oxidizing species present in the medium [G_{ox} (mol J^{-1}) = G (oxidizing species production)]. Thus, in order to initiate the oxidation of organic monomers and realize complete polymerization, the amount of oxidizing species should be twice that of the amount of organic monomers as already demonstrated.[4, 29, 34] Therefore, the total dose needed for quantitative polymerization is

$$D\ (Gy) = \frac{2[monomers]_0\ (mol\ L^{-1})}{G_{ox}\ (mol\ J^{-1})\ d\ (kg\ L^{-1})} \qquad (1.26)$$

Where $[monomers]_0$ is the initial concentration and where G_{ox} is the effective yield of monomers oxidation by all the oxidizing species present in the medium ($HO^{\bullet}$, $N_3^{\bullet}$, $SO4^{\bullet-}$, $Cl_2^{\bullet-}$) and where d is the density of the aqueous solution (d = 1 $kg.L^{-1}$).

1.2.3. Radiolysis of some organic solvents

The extension of original radiolytic methodology to the use of organic solvents is a need since radiation-induced polymerization in aqueous solution cannot always be used. In fact, there are several obstructions that have been faced with γ-radiolysis of aqueous solutions, such as the poor processability, low solubility and even sometimes the insolubility of some of organic monomers, namely 3-alkylthiophenes. Thus, the γ-radiolysis of many organic solvents was investigated in this work in presence of 3HT and other monomers such as EDOT and TAA in order to produce some conducting polymers.

1.2.3.1. Ethanol radiolysis under N_2O atmosphere

γ-irradiation of ethanol induced polymerization was used in literature to synthesize some polymers such as poly-butadiene [37] and poly-acrylamide [38]. In fact gamma radiolysis of liquid ethanol at 25 °C in presence of nitrous oxide (N_2O) yields to various oxidizing species according to the following reactions [39]:

$$CH_3CH_2OH \rightsquigarrow [CH_3CH_2OH]^{\bullet+}, e^-, H^{\bullet}, H_2 \qquad (1.27)$$

In the presence of N_2O, solvated electrons yield to N_2 and $O^{\bullet-}$ the alkaline from of $HO^{\bullet}$:

$$e_{solv}^- + N_2O \rightarrow O^{\bullet-} + N_2 \qquad (1.28)$$

At high concentration in N_2O, N_2O reacts again with $O^{\bullet-}$ producing superoxide $O_2^{\bullet-}$:

$$O^{\bullet-} + N_2O \rightarrow O_2^{\bullet-} + N_2 \qquad (1.29)$$

In summary, the main reactive products are $[CH_3CH_2OH]^{\bullet+}$ and $O_2^{\bullet-}$. Thus, we want to use these radicals as oxidizing species in order to initiate the oxidative polymerization of organic molecules.

1.2.3.2. Radiolysis of halo-methanes (Carbon tetrachloride (CCl_4), Chloroform ($CHCl_3$) and Dichloromethane (CH_2Cl_2))

Halo-methanes are very good solvents for many organic compounds and their gamma-radiolysis has been studied in literature in different conditions. Moreover, γ-irradiation of halo-methane solvents yields to several oxidizing radicals which could be employed to induce polymerization of organic monomers.

In chloroform and in an oxygen free atmosphere (under N_2 for instance), the radiolysis of chloroform leads to the production of many primary species: $Cl^{\bullet}$, $CHCl_2^{\bullet}$, $CCl_3^{\bullet}$ and $Cl^{\bullet}$ [40]. In case of dichloromethane and under inert atmosphere, γ-radiolysis generates basically $CH_2Cl^{\bullet}$, $CHCl_2^{\bullet}$ and $Cl^{\bullet}$ radicals [41-43] whereas carbon tetrachloride irradiation by γ-rays or X-rays yields under inert atmosphere to primary radicals: $Cl^{\bullet}$ and $CCl_3^{\bullet}$.[44] **Table 1.3** exhibits the primary action of γ -radiation on these three halo-methane solvents.

Carbon tetrachloride CCl_4	**Chloroform $CHCl_3$**	**Dichloromethane CH_2Cl_2**
$CCl_4 \rightarrow [CCl_4]^{\bullet+} + e^-$ $e^- + CCl_4 \rightarrow {}^{\bullet}CCl_3 + Cl^-$ $CCl_4 \rightarrow {}^{\bullet}CCl_3 + Cl^{\bullet}$ $Cl^{\bullet} + CCl_4 \rightarrow {}^{\bullet}CCl_3 + Cl_2$	$CHCl_3 \rightsquigarrow [CHCl_3]^+ + e^-$ $[CHCl_3]^+ \rightarrow {}^{\bullet}CCl_3 + H^+$ $CHCl_3 + e^- \rightarrow CHCl_3^{\bullet-}$ $CHCl_3^{\bullet-} \rightarrow {}^{\bullet}CHCl_2 + Cl^-$ The net reactions: $2CHCl_3 \rightarrow {}^{\bullet}CCl_3 + {}^{\bullet}CHCl_2 + HCl$	$CH_2Cl_2 \rightarrow [CH_2Cl_2]^{\bullet+} + e^-$ or $CH_2Cl_2 \rightarrow {}^{\bullet}CH_2Cl + Cl^{\bullet}$ $e^- + CH_2Cl_2 \rightarrow {}^{\bullet}CH_2Cl + Cl^-$ $Cl^{\bullet} + CH_2Cl_2 \rightarrow {}^{\bullet}CHCl_2 + HCl$ $[CH_2Cl_2]^{\bullet+} \rightarrow {}^{\bullet}CHCl_2 + H^+$ The net reaction: $2CH_2Cl_2 \rightarrow {}^{\bullet}CH_2Cl + {}^{\bullet}CHCl_2 + HCl$

Table 1.3 The primary action of γ-irradation on CCl_4, $CHCl_3$ and CH_2Cl_2 solvents under N_2 atmosphere

In all cases, the generated radicals are known as strong oxidants. For instance, chlorine radicals $Cl^{\bullet}$ have an ionization potential of 11,48 (eV) [45], while the halo-methane radical cations have an ionization potential between 11,35 and 11,47 (eV).[41] **Table 1.4** shows the ionizing potentials of these produced species.[41] It is also worth to mention that it has been

proved the possibility of oxidation of aromatic hydrocarbons by neutral chloromethyl ($^{\bullet}CH_2Cl$) and dichloromethyl ($^{\bullet}CHCl_2$) radicals in spite of their relatively lower redox potentials. In general halo-methane radicals can efficiently oxidize aromatic hydrocarbon molecules.[42, 46]

In this thesis, the polymerization of 3HT in CCl_4 did not proceed for further investigation due to the toxicity of this solvent. Also, the results and data that came out from CH_2Cl_2 were more encouraging and promising than those obtained with $CHCl_3$. Thus, I only proceeded my investigations with dichloromethane due to the fact that dichloromethane is being used to carry out electrochemical or radiolytic one-electron oxidation of solutes.[42, 47] Additionally the oxidative polymerization of conducting polymers (CPs) induced by gamma irradiation of dichloromethane has never been studied in literature. During my thesis I focused my investigations on radiolysis of aerated, deaerated and O_2-saturated solutions of dichloromethane.

Solvent	**$S^{\bullet+}/S$**	**I.P., eV**	**$R^+/R^{\bullet}$**	**I.P., eV**
CCl_4	$CCl_4^{\bullet+}/CCl_4$	11.47	$CCl_3^+/^{\bullet}CCl_3$	8.78
$CHCl_3$	$CHCl_3^{\bullet+}/CHCl_3$	11.42	$CHCl_2^+/^{\bullet}CHCl_2$	9.30
CH_2Cl_2	$CH_2Cl_2^{\bullet+}/CH_2Cl_2$	11.35	$CH_2Cl^+/^{\bullet}CH_2Cl$	9.32
CH_3Cl	$CH_3Cl^{\bullet+}/CH_3Cl$	11.30	$CH_3^+/^{\bullet}CH_3$	9.83

Table 1.4 Ionizing potentials of generated species during halo-methane radiolysis[41]

a. Radiolysis of N_2-saturated solutions of dichloromethane

It is well established that γ-irradiation of deoxygenated solutions of dichloromethane (under N_2 for instance) leads, within short nanosecond time scale, to the formation of solvated electrons in addition to neutral radicals and solvent radical cations which quickly lead to dichloromethyl ($^{\bullet}CHCl_2$) and chloromethyl ($^{\bullet}CH_2Cl$) radicals[41-43]

$$CH_2Cl_2 \rightarrow [e^- + Cl^{\bullet} + CH_2Cl_2^{\bullet+}] \rightarrow {}^{\bullet}CHCl_2 + {}^{\bullet}CH_2Cl + HCl \quad (1.30)$$

The yield of production of these radicals has not been determined in literature. As a consequence, since the yield of monomers oxidation is not known the dose which should be necessary for quantitative polymerization cannot be calculated. Nevertheless, as it will be shown later in the manuscript, radiation-induced oxidation of organic monomers by generated radicals upon DCM radiolysis is possible under N_2 atmosphere. As demonstrated in this thesis

and as highlighted in chapter 3, the radiolytic yield, G_{ox}, of solutes oxidation by these radicals under N_2 atmosphere amounts to: [5]

$$G_{ox} = 4.12 \times 10^{-7} \text{mol.J}^{-1} \quad (1.31)$$

b. Radiolysis of aerated and *O_2-saturated solutions of dichloromethane*

In fact introduction of oxygen into the sample has practically no effect on production of the organic monomer radical cations. In aerated and O_2-saturated solutions of dichloromethane, the produced dichloromethyl and chloromethyl radicals are rapidly scavenged by the molecular oxygen (O_2) to produce the corresponding peroxyl radicals: $CH_2ClO_2^{\bullet}$ and $CHCl_2O_2^{\bullet}$:[42-43]

$$^{\bullet}\text{RCl} + \text{O}_2 \rightarrow \text{RClOO}^{\bullet} \quad (1.32)$$

It is worth noting that, the oxidizing power of $CH_2ClO_2^{\bullet}$ and $CHCl_2O_2^{\bullet}$ is higher with respect to the original carbon centered radicals.

Contrarily to the case of N_2 atmosphere, under air the total yield of oxidation of organic compounds in dichloromethane solutions containing various solutes has already been calculated in literature by way of pulse radiolysis.[42] The total yield of oxidation by the primary radicals and the peroxyl radicals in these conditions amounts to:

$$\text{G}_{\text{ox}} = 7.77 \times 10^{-7} \text{mol.J}^{-1} \quad (1.33)$$

In this thesis, the total yield of monomers oxidation (in DCM under N2, under air or under saturated with O_2) will be verified and evaluated in order to quantitatively synthesized CPs.

1.2.3.3. Radiation induced polymerization in dichloromethane

The oxidative polymerization of the three different derivatives of thiophenes, namely EDOT, TAA and 3HT has been studied in this work. In case of EDOT and TAA, the oxidation by neutral radicals and solvent radical cations is possible since their ionization potential is high enough (see table 2.4) in comparison to ionization potential of EDOT and TAA monomers that have relatively low ionization energies.[48] By contrast, 3-alkylthiophene derivatives possess higher ionizing potential and in particular when the length of the alkyl side chain increases.[49] Therefore, the oxidative polymerization of 3-hexylthiophene in deaerated solution of dichloromethane will supposedly be to a lesser degree than those of

EDOT and TAA. Thus, oxygen was introduced to increase the oxidizing power of the generated species and make the oxidation of 3-hexylthiophen (i.e. 3HT) feasible.

As demonstrated in our previous works conducted in water[4, 29, 34], the mechanism of CPs is not a chain reaction but proceeds through a step-by-step oxidation mechanism and thus if we consider that the growth mechanism is similar in organic solvents, the theoretical irradiation dose which should lead to the quantitative formation of CPs is twice the dose necessary for the total oxidation of organic monomers. As a consequence, the dose D_{max} needed for a quantitative polymerization can be once again calculated according to equation:

$$D(Gy) = \frac{2[monmer]_0(mol.L^{-1})}{G_{ox}\,(mol.J^{-1}) \times d\,(kg.L^{-1})} \qquad (1.26)$$

where $[monomer]_0$ is the initial concentration of the organic monomer and where G_{ox} is the radiolytic yield of the generated oxidizing species from dichloromethane radiolysis and where d is dichloromethane density (d = 1.35 $kg.L^{-1}$).

1.2.3.4. pH adjustment of the prepared solutions

pH meter was used to measure the pH values of prepared aqueous solutions before and after irradiation. The pH-meter was also used to adjust then pH values before gamma irradiation by adding acids. For this purpose a Radiometer pH/Ionmeter PHM 250 (Laboratoire de Chimie Physique, LCP, Paris-Sud University) (**Figure 1.11**) was used.

Figure 1.11 Radiometer pH/Ionmeter PHM 250 available at (Laboratoire de Chimie Physique, LCP, Paris-Sud University)

1.3. Post-processing treatment of radio-synthesized CPs

In case of aqueous solutions, after irradiation the solutions or suspensions obtained as well as the materials dispersed in the liquid phase were characterized without any treatment. In order to carry out analyses and characterizations in solid state, material powders were obtained by treating aqueous solutions or suspensions with drying process centrifugation or lyophilization.

In case of irradiated dichloromethane solutions, the irradiated solutions were to remove the solvents and the produced organochlorides were removed either by using a rotary evaporator or by using centrifuge machine at a speed of $13\times10^{+3}$ rpm.s^{-1} for 20 min. In all cases the obtained powders were placed in the oven for desiccation at 50 °C for 24 h and lastly the powders were used for further characterizations and spectral analysis.

1.3.1. Drying tools

After gamma irradiation some of the aqueous solutions are dried by lyophilization with a Heto PowerDry® LL1500 (Thermo Electron Co., France) to obtain dehydrated powders (**Figure 1.12**). The drying procedures are done as follows: first, all the solutions are transfered to culture dishes and frozen into ices; then, the frozen samples are moved to the drying chamber and lyophilized at -110 ^{o}C for 48 h.

Figure 1.12 Heto PowerDry® LL1500 lyophilizer (Équipe Industries Agroalimentaires, Département Chimie Vivant Santé, Conservatoire National des Arts et Métiers).

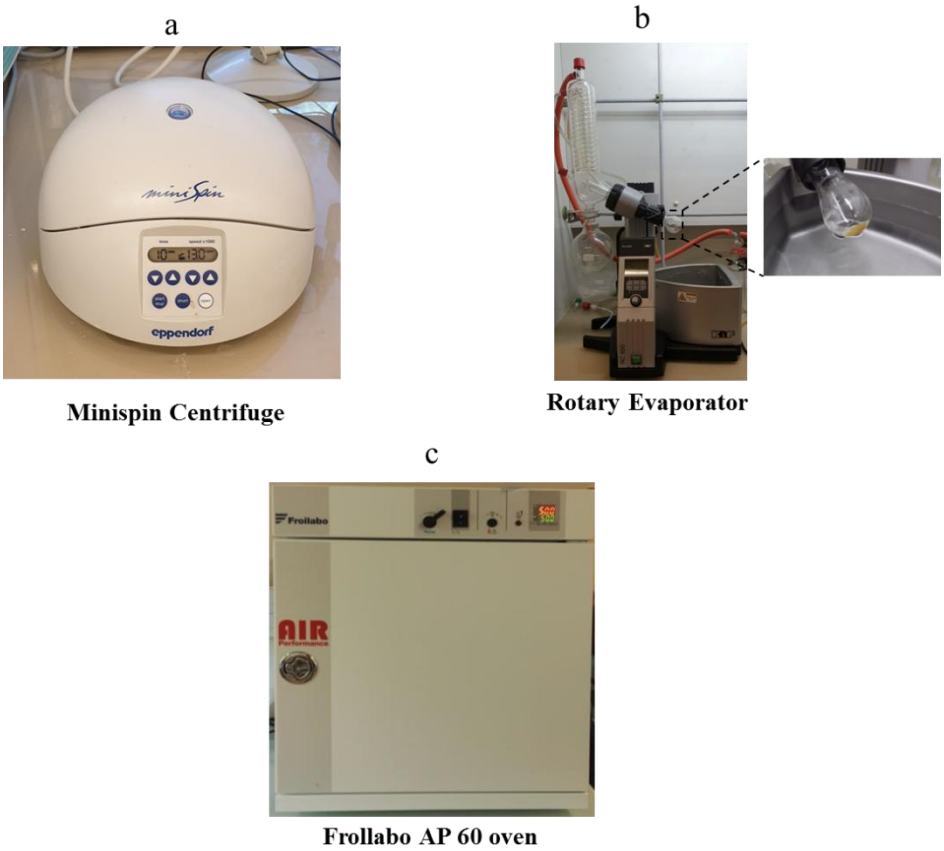

Figure 1.13 Drying tools that were used to dry irradiated aqueous and DCM in order to isolate radio-synthesized conducting polymers. These apparatus are available at Laboratoire de Chimie Physique, LCP, Paris-Sud University: a) Eppendorf 5452 Minispin Centrifuge machine, b) RC 600 Rotary Evaporator and c) Frollabo AP 60 oven.

After irradiation most of , the aqueous and dichloromethane solutions containing suspended polymers were centrifuged with Eppendorf 5452 Minispin Centrifuge machine (Marshall scientific LLC) (**Figure 1.13a**) and washed with water or dichloromethane. Before further centrifugation, also for dichloromethane solutions a RC 600 Rotary Evaporator was used to extract the radio-synthesized polymers (**Figure 1.13b**). The obtained materials are then dried in the Frollabo AP 60 oven at 50 o C for 24 h (**Figure 1.13c**).

1.3.2. Films preparation by spin coating for electrical conductivity measurements and photovoltaics devices elaboration

After irradiation, the radio-synthesized polymers in aqueous or dichloromethane solutions were dried as seen before and were dissolved in an adequate solvent at a concentration of 5 or 10 mg.mL^{-1}. Later, for electrical conductivity measurement a drop of the polymeric solution was deposited onto a glass substrate by spin coating with a SCC-200 spin coater with a speed of 100 rpm for 60 s leading to the formation of a film (**Figure 1.14a left**). During the spin

coating, the glass substrates were held by the vacuum formed by the pump (**Figure 1.14a right**).

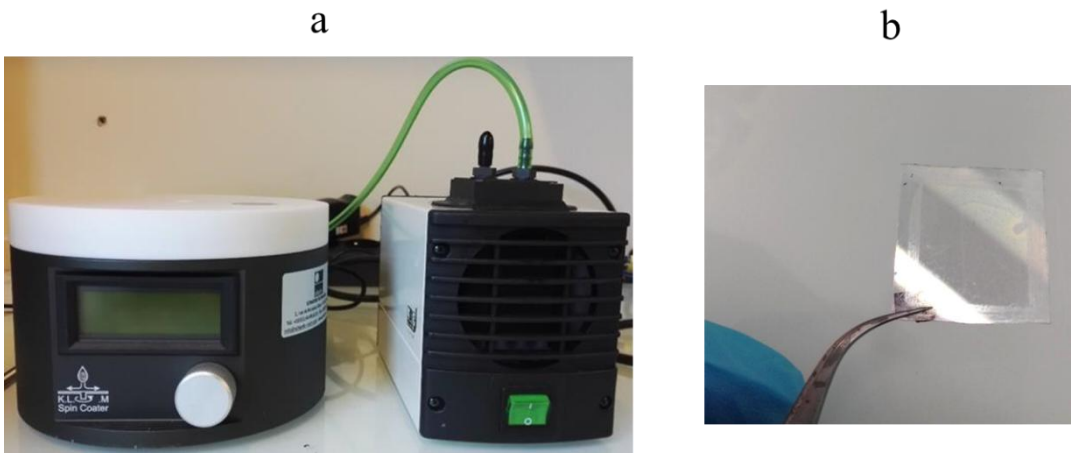

Figure 1.14 Thin film preparation by spin coating: a) SCC-200 spin coater (left) and coupled pump for vacuum (right) available at Laboratoire de Chimie Physique, LCP, Paris-Sud University b) PEDOT thin film prepared by spin coating. PEDOT polymers were synthesized by dichloromethane radiolysis under N_2 atmosphere at absorbed dose 36 kGy.

The formed films were then doped with $NOBF_4$ (20 mM in acetonitrile). After the films got dried, the thickness was determined by surface profiler (see later). The doping process of electrically conducting polymers is realized by the oxidative nitrosonium cation (NO^+) with a redox potential of 0.87 V_{SHE}.[50] **Figure 1.14b** shows the obtained film made of PEDOT polymers that were synthesized by dichloromethane radiolysis under N_2 atmosphere at absorbed dose 36 kGy.

The spin coating for photovoltaics devices elaboration was carried out at Laboratoire de Physicochimie des polymères et Interfaces, LPPI, Cergy-Pontoise University.

1.4. Material characterizations

After irradiation and post-treatment processes, the obtained materials were characterized by using different spectroscopic, microscopic and electrochemical techniques.

1.4.1. UV-Vis absorption spectroscopy

UV-Vis absorption spectroscopy was used to check the optical properties of EDOT, TAA and 3HT monomers and those of PEDOT, PTAA and P3HT polymers prepared using different radiolytic routes (in aqueous solution under and in organic solvents under different

atmospheres). A HP 8543 spectrophotometer was used to measure the absorbance of solutions before and after irradiation (**Figure 1.15**). The apparatus covers wide range of wavelengths, starting from 200 nm in the UV region till 1200 nm in the near-infrared region. A quartz cell with an optical pathlength of 2 mm was generally used to perform all the measurements. The reference was in all cases pure solvents.

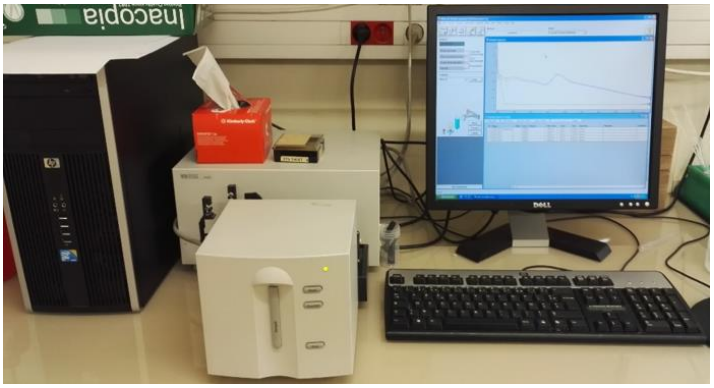

Figure 1.15 UV-Vis absorption spectrophotometer available at Laboratoire de Chimie Physique, LCP, Paris-Sud University.

1.4.2. Size exclusion chromatography (SEC)

SEC was used in order to check the average molecular weight of radiosyntheszied polymers. SEC analysis for PEDOT polymers has been performed as follows: the injection of PEDOT polymers into SEC injector was done by using DCM solution right after γ-irradiation. To do so, 100 mL of a DCM solution containing radio-synthesized PEDOT polymers were mixed with 300 mL of THF solvent and then 100 µL of the resulting mixture was injected into SEC apparatus. While in case of PTAA and P3HT polymers, after post-treatment procedure, 3 $mg.L^{-1}$ of polymer powder were directly dissolved in THF, then 100 µL of the prepared solution was injected into SEC apparatus.

THF was used as eluent and SEC was performed at 40 °C on a Malvern Viscotek TDA apparatus equipped with two columns, Malvern T3000 and T6000, with a Malvern refractive index detector at an elution rate of 1 $mL.min^{-1}$. Polystyrene polymers were used as standards. (**Figure 1.16**) This apparatus is available at Laboratoire Procédés et Ingénierie en Mécanique et Matériaux, PIMM, Conservatoire National des Arts et Métiers, CNAM, Paris. SEC experiments enabled to record chromatograms which give different molecular weights

Indeed, in this method we can recognize four definitions that describe the commonly used molecular weight averages that can be determined by size exclusion chromatography (SEC),

also called gel permeation chromatography (GPC). Molecular weight average can be described using several definitions (**Figure 1.17**). The most commonly used average is number average molecular weight Mn (The number average molecular weight is the statistical average molecular weight of all the polymer chains in the sample). There are other ways of describing molecular weight average weight such as, average molecular weight Mw (this values takes into account the molecular weight of a chain in determining contributions to the molecular weight average), higher average molecular weight Mz (it is sensitive to high molecular weight polymers) and the peak molecular weight Mp (the molecular weight at the position of the top of the peak in SEC chromatogram.

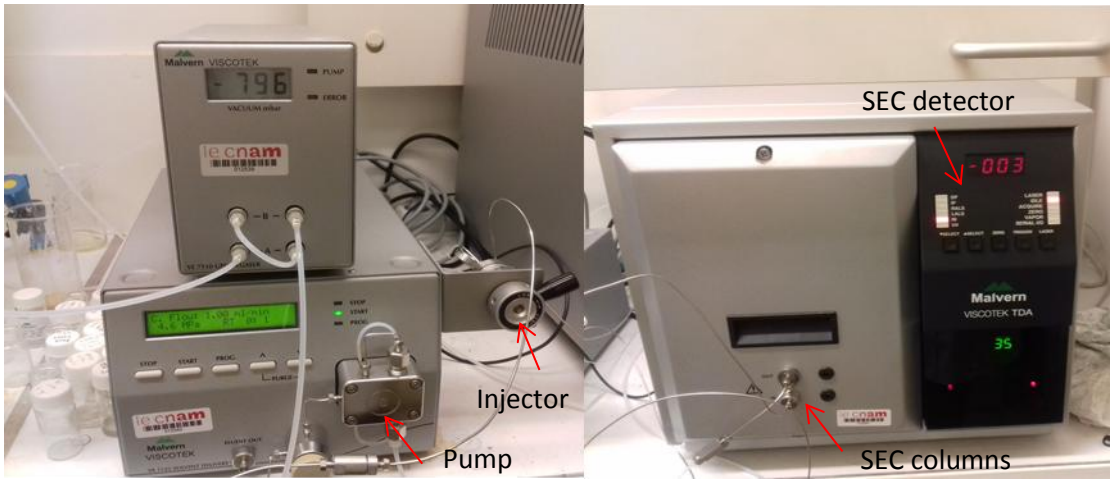

Figure 1.16 SEC apparatus Malvern Viscotek TDA (Laboratoire Procédés et Ingénierie en Mécanique et Matériaux, PIMM, Conservatoire National des Arts et Métiers, CNAM, Paris). The lmage on the left shows the pump and samples injector and the image on the right shows SEC columns and Malvern refractive index detector.

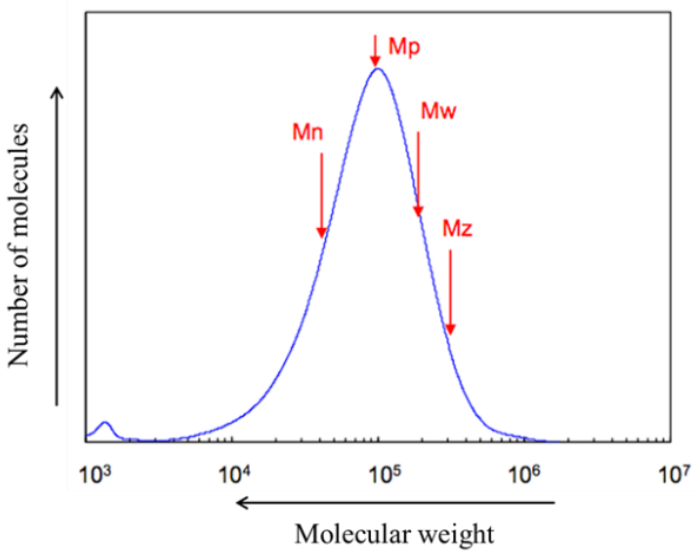

Figure 1.17 SEC chromatogram showing the commonly used molecular weight averages that can be determined by size exclusion chromatography (SEC)

1.4.3. Maldi-TOF (Matrix Assisted Laser Desorption/Ionization Time of Flight) mass spectrometry

Maldi-TOF (Matrix Assisted Laser Desorption/Ionization Time of Flight) mass spectrometry was used to measure the degree of conducting polymerization of conducting polymers (in particular PTAA polymers synthesized in dichloromethane under N_2 atmosphere at irradiation dose of 36 kGy).

The tetrahydrofurane (THF) solution of the sodium salt of PTAA ($PTAA^-Na^+$) was first prepared and then mixed with a matrix solution (THF-trans-2-[3-(4-t-butyl-phenyl)-2-methyl-2-propenylidene] malononitrile (DCTB)). The matrix-sample solution was then placed on a stainless steel plate. The spectra were obtained in the reflection mode and in the positive ion mode. The experiment was done at Institut de Chimie des Substances Naturelles, CNRS, in Gif-Sur-Yvette by using MALDI TOF UltrafleXtreme, Bruker daltonic (**Figure 1.18**).

Figure 1.18 MALDI TOF TOF UltrafleXtreme, Bruker daltonic (Institut de Chimie des Substances Naturelles, CNRS, in Gif-Sur-Yvette)

1.4.4. Cryo-transmission electron microscopy and EDX analysis

To observe the original morphology of the as-prepared conducting polymers in dichloromethane and in aqueous solutions, *in situ* observation of the morphology is carried out on a transmission electron microscope in a cryogenic environment (Cryo-TEM), known to be adapted to low density contrasts (Institut de Minéralogie et de Physique des Milieux Condensés, IMPMC, Pierre and Marie Curie University). A drop of each irradiated solution is deposited on a “quantifoil”® (Quantifoil Micro Tools Gmbh, Germany) 200 mesh holey-carbon-coated grid. After being blotted with filter paper, the grid is quenchfrozen by being

rapidly plunged into liquid ethane in order to form a thin (amorphous frozen solid film avoiding any crystallization. The grids are then transferred into the microscope using a side entry Gatan 626 cryoholder cooled at -180 ^{o} C with liquid nitrogen. Images are taken with an Ultrascan 2k CCD camera (Gatan, USA) by using a LaB6 JEOL JEM 2100 (JEOL, Japan) (**Figure 1.19**). Advantages of Cryo-TEM are not only ensuring the observation of soft nanostructures directly in solution but also avoiding the phase transition and aggregation which should result from the drying procedures when SEM, TEM or AFM observations are conducted after deposition on solid substrates. Energy dispersive X-Ray (EDX) analysis is carried out to identify the chemical composition of the materials during the characterizations by Cryo-TEM (Institut de Minéralogie et de Physique des Milieux Condensés, IMPMC, Pierre and Marie Curie University). During Cryo-TEM observations, in situ EDX spectroscopy is used to check the chemical composition and to perform the elemental analysis within a selected area of the samples. An EDX JEOL Si(Li) detector mounted on the cryo-microscope is used with a resolution of 140 eV.

Figure 1.19 JEOL 2100 Cryo-TEM microscope (Institut de Minéralogie et de Physique des Milieux Condensés, IMPMC, Pierre and Marie Curie University).

1.4.5. Attenuated Total Reflectance Fourier Transform Infrared (ATR-FTIR) spectroscopy

To identify the obtained conducting polymers and to check their chemical composition and to prove the quantitative polymerization, Fourier transform infrared (FTIR) spectra of dried polymer powder are recorded using a FTIR spectrometer (Bruker Vertex 70) with diamond attenuated total reflection (ATR) attachment (PIKEMIRACLE crystal plate diamond/ZnSe) and MCT detector with a liquid nitrogen cooling system (**Figure 1.20**). The dried powders are deposited onto the ZnSe diamond and scanning is conducted from 4000 to 600 cm^{-1} with a 4 cm^{-1} spectral resolution for 100 times and averaged for each spectrum.

Figure 1.20 ATR-FTIR spectrometer available at (Laboratoire de Chimie Physique, LCP, Paris-Sud University).

1.4.6. Atomic Force Microscopy coupled with infrared nanospectroscopy (AFM-IR)

Three setups of AFM (coupled or not with IR spectroscopy) microscopes have been used to characterize the radiosynthesized polymers. First AFM-IR is a commercial version called nanoIRTM (@Anasys Instruments) (**Figure 1.21a**). It combines an atomic force microscope (AFM) with an infrared pulse source. This system is used in contact mode and the pulsed infrared laser setup covers the IR range from 4000 cm^{-1} to 1000 cm^{-1} with a repetition rate of 1 kHz and a pulse width of 10 ns. This AFM-IR was used to characterize PEDOT polymers synthesized at 36 kGy in DCM and to check whether PEDOT polymers in DCM solution maintain their original morphology during the drying process. In this context, polymers powders were solubilized in ethanol and then a small drop of ethanolic solution was deposited

onto the upper surface of ZnSe prism (transparent in the mid-IR) and dried naturally at air. The dried deposit was observed by IR nanospectroscopy.

The Second AFM-IR (nanoIR, Anasys Instruments Corp, Bruker NANO Group, California, USA) (**Figure 1. 21b**) is used in tapping mode with a 40 $N.m^{-1}$ silicon cantilever (PPP-NCLR-50, nanosensors, Neuchâtel, Switzerland). This system was used to check the topography of PTAA polymers that were obtained by gamma radiolysis of CH_2Cl_2 under N_2 atmosphere or of water under N_2O atmosphere at irradiation doses of 36 kGy. The polymers powders were first solubilized in ethanol and then a small drop of ethanolic solution was deposited onto the upper surface CaF_2 disk and dried under He.

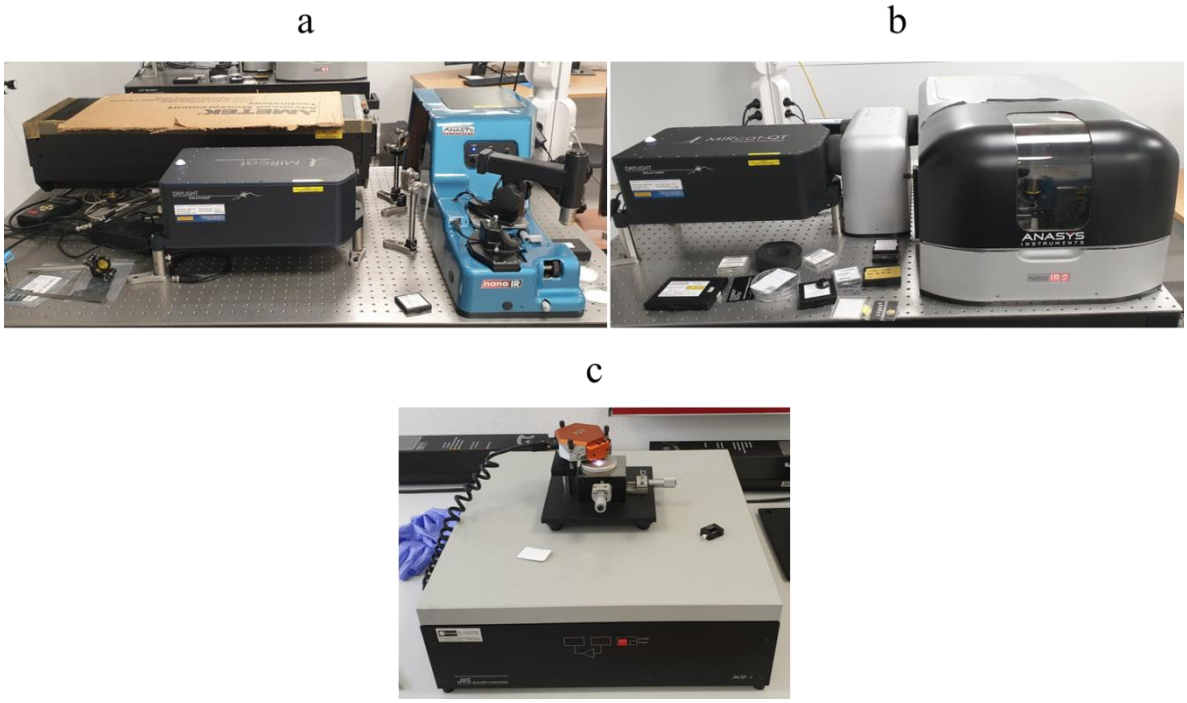

Figure 1.21 AFM and AFM-IR microscopes available in Laboratoire de Chimie Physique, LCP, Paris-Sud University ; a) nanoIRTM (@Anasys Instruments), b) nanoIR, Anasys Instruments Corp, Bruker NANO Group, c) Nanosurf Easyscan 2 AFM.

The third system is a typical AFM microscope (Nanosurf Easyscan 2 AFM) (**Figure 1. 21c**). This AFM was used to check the topographical morphology of $P3HT_{N_2}$ and $P3HT_{O_2}$ that were obtained by gamma radiolysis of CH_2Cl_2 under N_2 or O_2 atmospheres at irradiation doses of 36 kGy. The polymers powders were first solubilized in ethanol and then a small drop of ethanolic solution was deposited on a mica sheet and dried naturally at air.

While the typical AFM microscope gives only a topographical analysis, AFM-IR enables recording topographical image and chemical mapping at a given wavenumber. Thus, in order

to check the morphology and the chemical nature of radio-synthesized conducting polymers AFM-IR was used.

During all AFM-IR the measurements, the tip of the AFM remained in contact with the surface. The IR source highlights the sample from the bottom in total internal reflexion configuration. When the sample absorbs IR laser pulse, the absorbing region warms up and a thermal expansion occurs. This rapid thermal expansion is detected by the tip in contact and causes the cantilever oscillation. As the amplitude of oscillations is proportional to the absorption, scanning the surface at a given wavenumber enables the acquisition of a chemical map of the sample, while changing the wavenumber of the IR source at a fixed position of the tip gives a local infrared spectrum (**Figure 1.22**).

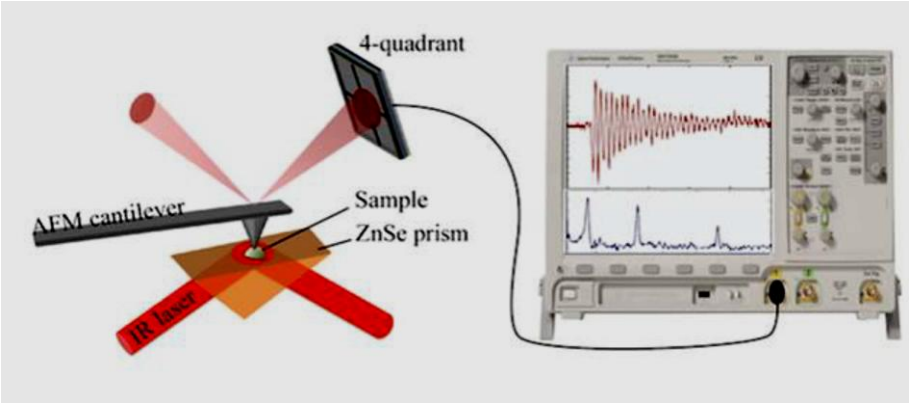

Figure 1.22 Schematic representation of AFM-IR principle which enables at the same time to record a topographical image of the surface and its chemical mapping.

1.4.7. SEM microscopy and EDX analysis

In order to check the morphology of the samples after deposition, powders obtained after drying procedures were sprinkled onto carbon tape adhered to aluminum mounts and the resulting images were obtained with EVO MA10 scanning electron microscope (SEM) (Laboratoire Procédés et Ingénierie en Mécanique et Matériaux, PIMM, Conservatoire National des Arts et Métiers, CNAM, Paris). (**Figure 1.23, left**). In order to obtain better observation of the morphology, the deposited powders were coated with gold in some cases (**Figure 1.23, right**). The Magnification, accelerating voltage and scale bar were adjusted to obtain the SEM images of the samples

During the observations by SEM, *in situ* EDX analysis was also carried out to identify the chemical composition of the materials. EDX spectroscopy was used to check the chemical composition the powders obtained after irradiation and solvent removing of and to perform

their elemental analysis within a selected area of the samples. All the EDX spectra were recorded with a beam energy of 15.0 keV.

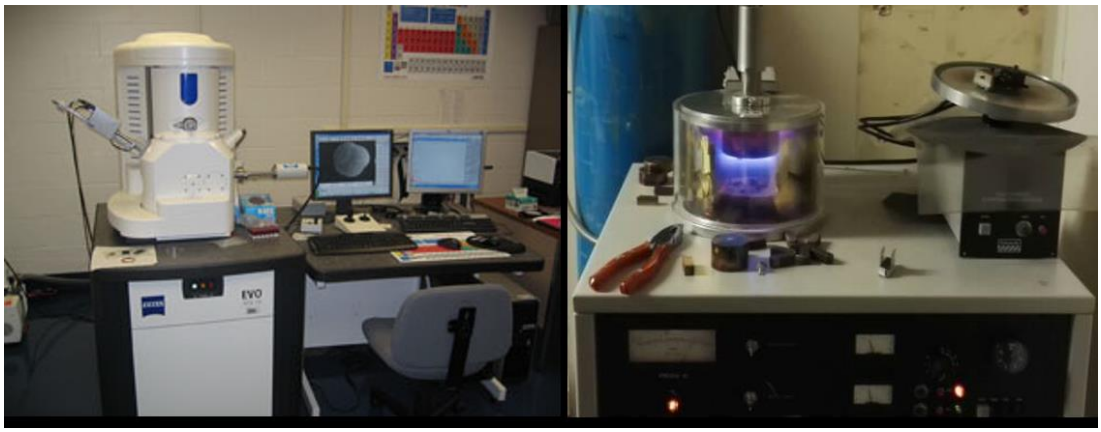

Figure 1.23 EVO MA10 SEM (left) and SC-6 Pelco Sputter Coater (Laboratoire Procédés et Ingénierie en Mécanique et Matériaux, PIMM, Conservatoire National des Arts et Métierss, CNAM, Paris).

1.4.8. TGA analysis

The thermal stability and composition analysis of the obtained polymers after radiolysis were performed on a thermogravimetric analysis instrument TGA Q500 (TA instruments, USA) (Laboratoire Procédés et Ingénierie en Mécanique et Matériaux, PIMM, Conservatoire National des Arts et Métiers, CNAM, Paris) (**Figure 1.24**).

Figure 1.24 Thermogravimetric analysis (TGA) instrument (Laboratoire Procédés et Ingénierie en Mécanique et Matériaux, PIMM, ENSAM, Conservatoire National des Arts et Métiers, CNAM, Paris).

The thermal degradation of the solid samples obtained after irradiation and solvent removal was carried out under a nitrogen flow of 50 $mL.min^{-1}$ within the temperature range of 40 to 800 °C at a heating rate of 20 $°C.min^{-1}$.

1.4.9. X-Ray Diffraction (XRD) analysis

XRD analysis was used to check the crystallinity of radiosynthesized polymers. The polymers powders obtained after solvent removal were crushed and hand-milled in order to obtain fine powders which were then used for XRD characterization (PANalytical X'pert pro MPD with X'celerator acquisition system) **(**Institut de Chimie Moléculaire et des Matériaux d'Orsay**,** ICMMO**)** (**Figure 1.25**). The Cu Ka1 (λ = 1.54059 Å) radiation was used as the X-ray source. A scanning rate of 0.0015° s^{-1} was employed to perform θ–2θ scans from 10° to 80°.

Figure 1.25 PANalytical X'pert pro MPD with X'celerator acquisition system (Institut de Chimie Moléculaire et des Matériaux d'Orsay, ICMMO)

1.4.10. Cyclic voltammetry measurements (CV)

CV was used to investigate the electronic properties of radio-synthesized conducting polymers. The CV analysis enabled us to measure highest occupied molecular orbital (HOMO) and lowest unoccupied molecular orbital (LUMO) energy levels of these polymers and also to calculate the electronic energy band gaps (E_{gap}). Experiments were carried out either in our laboratory in (Laboratoire de Chimie Physique, LCP) or in Laboratoire de Physicochimie des Polymères et Interfaces, LPPI (Université de Cergy Pontoise). The CV analysis for PEDOT and P3HT polymers was done at LPPI while that for PTAA polymers was performed at LCP. Therefore, two setups were realized and used.

The first setup at LPPI was a three-electrode cell, with a Pt disc as working electrode, an Au wire as counter-electrode and a Pt/silver wire as the pseudo-reference electrode. This latter was calibrated as recommended by the IUPAC by probing ferrocenium/ferrocene (Fc^{+}/Fc)

redox potential measured at the end of each experiment. The polymers powders obtained after γ-irradiation and after solvent evaporation (in case of PEDOT and P3HT polymers) were dissolved in DCM at a concentration of 1 $mg.mL^{-1}$. Then, 1 mL of this solution was mixed into the electrochemical cell with 5 mL of acetonitrile solution containing tetrabutylammonium hexafluorophosphate ($TBAPF_6$) used as electrolyte at a concentration of 0.1 M. The three electrodes were then immersed into the electrochemical cell and the cyclic voltammograms were recorded at a scan rate of 20 $mV\ s^{-1}$ between -2.5 V and +2.5 V.

The second setup at LCP was a three-electrodes cell, with a Pt disk of 1 mm diameter as working electrode, a Pt wire in separated compartment as counter electrode and saturated calomel electrode (SCE) in separated compartment is reference electrode. This latter was calibrated as recommended by IUPAC by probing ferrocenium/ferrocene (Fc^+/Fc) redox potential measured at the end of each experiment. PTAA polymers (dissolved at a concentration of 3 $mg.mL^{-1}$ in THF) were used. Later the electrodes were immersed into the electrochemical cell containing acetonitrile with 0.1 M tetrabutylammonium hexafluorophosphate ($TBAPF_6$) and the as prepared PTAAs in THF solutions. The cyclic voltammetry of the compounds were recorded at a scan rate of 100 $mV.s^{-1}$ between −2.5 V and +2.5 V.

Figure 1.26 Electrochemistry setup available in Laboratoire de Chimie Physique, LCP, Paris-Sud University. The setup exhibits the electrochemical cell as well as the electrodes that were used during the electrochemistry experiments

1.4.11. Electrical conductivity measurements

The electrical conductivity of spin coated films on glass substrates prepared after radiolysis was measured by the traditional four-point probe method.[51] The resistances of the samples were measured using a Keithley 2420 system (**Figure 1.26**) (Laboratoire de

Physicochimie des Polymères et Interfaces, LPPI, Cergy-Pontoise University). Each sample was checked at three different positions and the resistance values were averaged.

The thickness of the spin coated samples was measured on a 3 Veeco Dektak 150 surface profiler (**Figure 1.27**). The thickness of each sample was also measured three times and averaged.

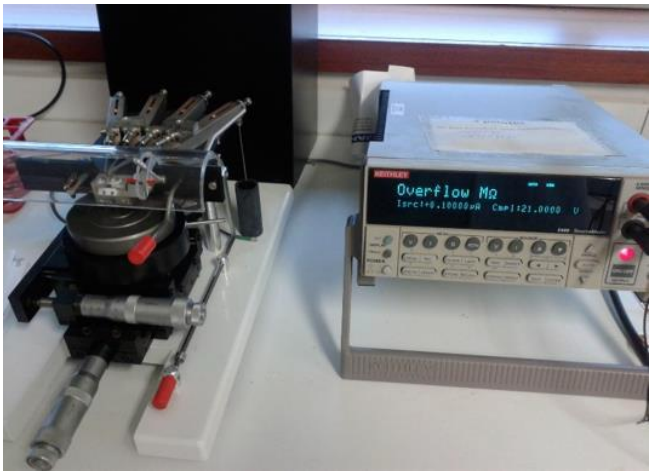

Figure 1.26 Kelvin four-point probe setup coupled with a Keithley 2420 system (Laboratoire de Physicochimie des Polymères et Interfaces, LPPI, Cergy-Pontoise University).

The conductivity, ρ ($S \cdot cm^{-1}$) was then determined thanks to the following equation:[52]

$$\rho = \left(\frac{\pi}{\ln 2} \times \frac{V}{I} \times t\right) \qquad (2.36)$$

where V is the voltage difference (V), t the film thickness (cm) and I the applied current (A).

Figure 1.27 Surface profiler (Laboratoire de Physicochimie des Polymères et Interfaces, LPPI, Cergy-Pontoise University).

1.5. Fabrication procedure of perovskite solar cells (PSCs)

In this experiment, we incorporated our radio-synthesized conducting polymers in PSCs. Furthermore, according to their electronic properties as well as to their electrochemical characterizations, the radio-synthesized conducting polymers were used as hole transport materials (HTMs). Our devices were composed of a thin compact TiO_2 layer, a mesoporous TiO_2 layer filled and capped with the $CH_3NH_3PbI_3$ perovskite as the absorber material, a HTM layer and finally a thermally evaporated Au layer (**Scheme 1.1**).

For the devices elaboration, fluorine doped tin oxide coated glass slides (FTO) (TEC7, Pilkington) were used with an area of 12*12 mm. An area of 3*1 mm of the latter was cut for etching via powder of zinc and HCl (10%) (see scheme 1.1). It was then cleaned by using a concentrated 2.5 $mol \cdot L^{-1}$ NaOH ethanolic solution, rinsed with water, cleaned with a detergent, rinsed with Milli-Q water, dried with compressed air and placed under UV/O_3 for 15 min. The TiO_2 blocking layer was prepared by an aerosol spray pyrolysis technique as described in reference [53]. A precursor solution was prepared by mixing 0.6 mL of titanium isopropoxide (TTIP) and 0.4 mL of acetyl acetone in 7 mL of 2-propanol. Then 20 μL were spin coated at 2800 rpm then 1200 rpm for 25s. The layer was then dried on a hot plate at 125°C for 5 min. After the drying the thickness of the layer was measured with a Dektak profiler and it was found equal to 250 nm. Then, the mesoporous TiO_2 layer was spin coated by depositing 20 μL at 2000 rpm then 1200 rpm for 20s. The layer was then dried on a hot plate at 125°C for 5 min and subsequently annealed at 540 °C for 60 min (see scheme 1.1). The mesoporous TiO_2 layer was prepared by diluting the NR30-D paste from Dyesol with ethanol (1:8 mass ratio). The thickness of the layer was measured after drying procedure and found in our case equal to 200 nm.

For perovskite layer, The $CH_3NH_3PbI_3$ (MAPI) precursor solution was prepared by mixing 553 mg of PbI_2 and 190 mg of MAI (Dyesol) in 1 mL of DMSO solvent. The solution was heated at 70 °C until full dissolution. A 20 μL aliquot of this solution was deposited on the substrate and spun at 4000 rpm, then 1200 for 25 s. The perovskite layer was finally annealed at 100°C for 15 min on a hot plate. The thickness of this layer was found equal to 400 nm.

For Hole Transport layer (HTM), spiro-OMeTAD was used as standard to compare it with our radiosynthesized polymers: PEDOT, $PTAA_{H_2O}$, $PTAA_{CH_2Cl_2}$, $P3HT_{N_2}$, and $P3HT_{O_2}$. First, spiro-OMeTAD solution was prepared by dissolving 72 mg of Spiro-OMeTAD, in 1 mL chlorobenzene. While for other HTMs, solubility test was needed before solutions

preparation. **Table 1.5** summarizes the performed solubility tests. According to the solubility tests, 10 $mg.mL^{-1}$of HTMs were prepared in the appropriate following solvents: in THF containing PTAA, in chlorobenzene containing PEDOT and P3HT synthesized in DCM under N_2 or O_2. Subsequently, 10 µL of the HTM solution was spin-coated at 3000 rpm then 1200 rpm for 30 s. The thickness was then measured for each HTM: spiro-OMeTAD = 175 nm, PEDOT synthesized in DCM= 300 nm, P3HT synthesized in DCM under N_2 or O_2 =400 nm, PTAA synthesized in water =200 nm and PTAA synthesized in DCM= 250 nm.

Sample	Solvent				
	Chloroform	Chlorobenzene	DCM	THF	DMSO
PEDOT	Insoluble	Partially	Partially	Insoluble	Partially
P3HT 1	Soluble	Partially	Soluble	Soluble	No test
P3HT 2	Soluble	Partially	Soluble	Soluble	No test
PTAA 1	Insoluble	Insoluble	Partially	Partially	Soluble
PTAA 2	Insoluble	Insoluble	Partially	Soluble	Soluble

Table 1.5 Solubility of the prepared radio-synthesized conducting polymers in some common organic solvents

The final step was the deposition of the counter electrodes which are made of gold. The substrates were placed on a certain template (mask) obtained from LPPI laboratory before deposition of the electrodes onto the substrates by thermal evaporation of the golden metal. For this purpose, the apparatus PLASSYS ME 300 was used. The template was placed inside the apparatus and small pieces of gold were added in specific position within the apparatus. The apparatus was set at current of 200 A, corresponding to a temperature of about 600 °C. The thickness of the gold layer was set at 100 nm. The elaboration process can be summarized in the following **Scheme 1.1**.

As known, the aim of solar cells is to convert sunlight into electricity. Thus, the fabricated devices made of Spiro-MeOTAD as reference and made of our radio-synthesized CPs, were tested by measuring the current versus voltage under dark and under stimulated sunlight illumination by using Keithley 4200 semiconductor parameter analyzer (**Figure 1.28**).

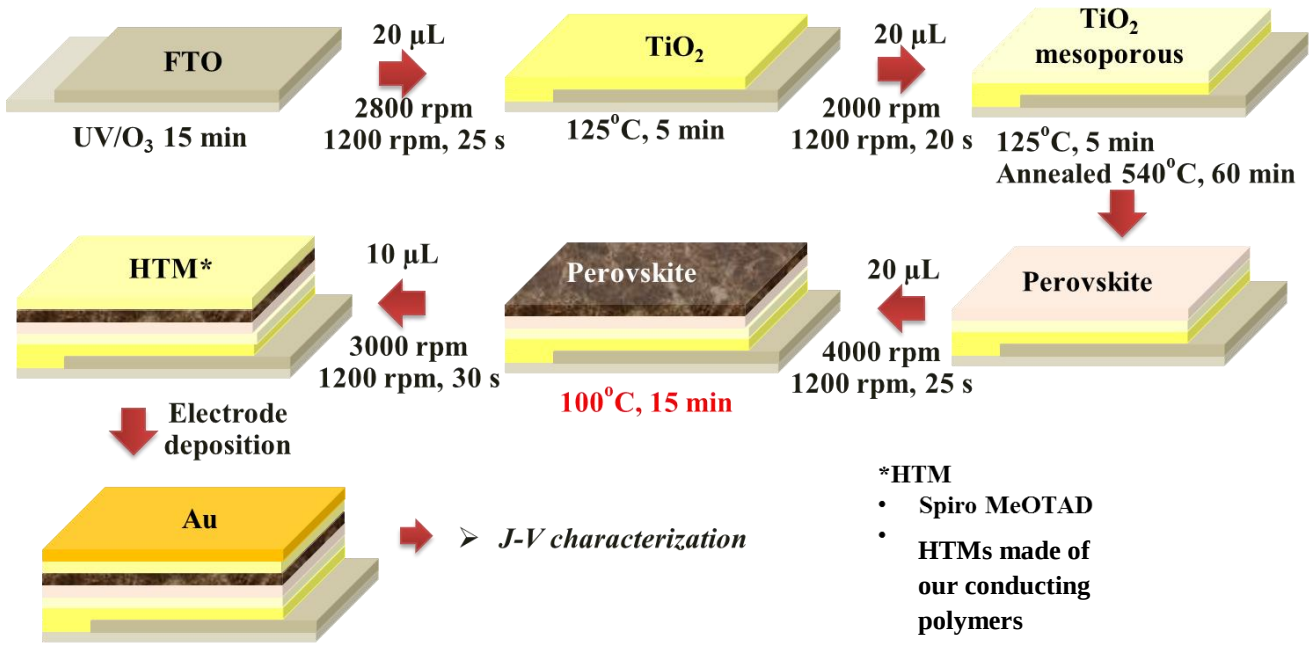

Scheme 1.1 Fabrication steps of solar cell devices

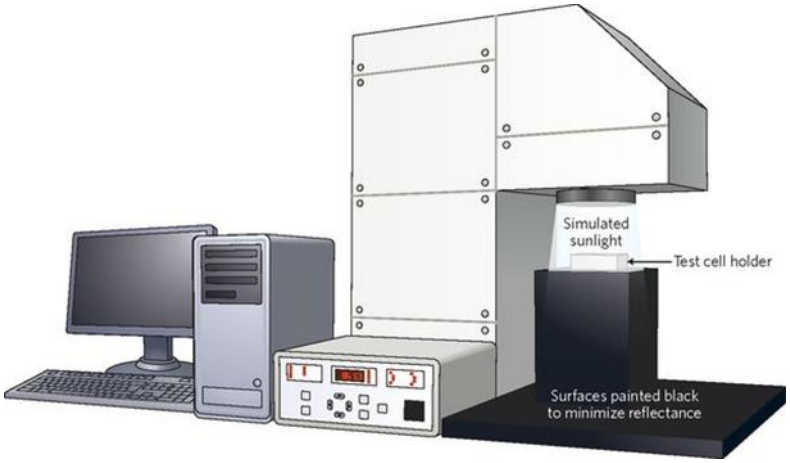

Figure 1.28 keithley 4200 semiconductor parameter analyzer(Laboratoire de Physicochimie des Polymères et Interfaces, LPPI, Cergy-Pontoise University).

The measurements were made at LPPI laboratory in University Cergy Pontoise. The obtained data were treated in order to calculate the fill factor (FF) and the efficiency (η) of the devices.

References

1. Roncali, J.; Blanchard, P.; Frere, P., 3,4 ethylenedioxythiophene(EDOT) as a versatile building block for advanced functional pi-conjugated systems. *Journal of Materials Chemistry* **2005,** *15*, 1589.

2. Sakmeche, N.; Aeiyach, S.; Aaron, J.-J.; Jouini, M.; Lacroix, J. C.; Lacaze, P.-C., Improvement of the Electrosynthesis and Physicochemical Properties of Poly(3,4-ethylenedioxythiophene) Using a Sodium Dodecyl Sulfate Micellar Aqueous Medium. *Langmuir* **1999,** *15* (7), 2566-2574.

3. Belaidi, F. S.; Civélas, A.; Castagnola, V.; Tsopela, A.; Mazenq, L.; Gros, P.; Launay, J.; Temple-Boyer, P., PEDOT-modified integrated microelectrodes for the detection of ascorbic acid, dopamine and uric acid. *Sensors and Actuators B: Chemical* **2015,** *214*, 1-9.

4. Lattach, Y.; Deniset-Besseau, A.; Guigner, J. M.; Remita, S., Radiation chemistry as an alternative way for the synthesis of PEDOT conducting Polymers under "soft" Conditions. *Radiat Phys Chem* **2013,** *82*, 44-53.

5. Bahry, T.; Cui, Z. P.; Deniset-Besseau, A.; Gervais, M.; Sollogoub, C.; Bui, T. T.; Remita, S., An alternative radiolytic route for synthesizing conducting polymers in an organic solvent. *New J Chem* **2018,** *42* (11), 8704-8716.

6. Wu, T.; Wang, L.; Zhang, Y.; Du, S.; Guo, W.; Pei, M., Electrochemical synthesis of poly(3-thiophene acetic acid) nanowires with water-soluble macromolecule templates. *RSC Advances* **2015,** *5* (22), 16684-16690.

7. Pam Cherry, A. D., Practical Radiotherapy: Physics and Equipment. *Oxford University Press* **1998,** *119*.

8. Grupen, C., Introduction to radiation protection: practical knowledge for handling radioactive source. *Springer* **2010,** *7*.

9. Jayson, G. G.; Parsons, B. J.; Swallow, A. J., The mechanism of the fricke dosimeter. *International Journal for Radiation Physics and Chemistry* **1975,** *7* (2), 363-370.

10. Karim, M. R.; Lee, C. J.; Lee, M. S., Synthesis of conducting polypyrrole by radiolysis polymerization method. *Polymers for Advanced Technologies* **2007,** *18* (11), 916-920.

11. Henglein, A., J. W. T. Spinks. R. J. Woods: An Introduction to Radiation Chemistry, Third Edition, John-Wiley and Sons, Inc., New York, Toronto 1990. ISBN 0-471-61403-3. 574 Seiten, Preis: DM 91, 45. *Berichte der Bunsengesellschaft für physikalische Chemie* **1991,** *95* (3), 451-451.

12. Ferradini, C.; Jay-Gerin, J. P., Radiolysis of water and aqueous solutions - History and present state of the science. *Can J Chem* **1999,** *77* (9), 1542-1575.

13. Ferradini, C.; Jay-Gerin, J. P., The effect of pH on water radiolysis: A still open question - A minireview. *Res Chem Intermediat* **2000,** *26* (6), 549-565.

14. Le Caër, S., Water Radiolysis: Influence of Oxide Surfaces on H2 Production under Ionizing Radiation. *Water* **2011,** *3* (1), 235-253.

15. Lousada, C. M.; Soroka, I. L.; Yagodzinskyy, Y.; Tarakina, N. V.; Todoshchenko, O.; Hänninen, H.; Korzhavyi, P. A.; Jonsson, M., Gamma radiation induces hydrogen absorption by copper in water. *Scientific Reports* **2016,** *6*, 24234.

16. Ma, J., Ultrafast electron transfer in solutions studied by picosecond pulse radiolysis. *Doctoral thesis* **2015**.

17. Spinks, J. W. T. W., R. J., An introduction to radiation chemistry. *John Wiley & Sons, Inc.* **1990,** *3*, 260.

18. Getoff, N., Radiation-induced degradation of water pollutants—state of the art. *Radiation Physics and Chemistry* **1996,** *47* (4), 581-593.

19. Schwarz, H. A.; Dodson, R. W., Equilibrium between hydroxyl radicals and thallium(II) and the oxidation potential of hydroxyl(aq). *The Journal of Physical Chemistry* **1984,** *88* (16), 3643-3647.

20. Elliot, A. J.; Geertsen, S.; Buxton, G. V., Oxidation of thiocyanate and iodide ions by hydrogen atoms in acid solutions. A pulse radiolysis study. *Journal of the Chemical Society, Faraday Transactions 1: Physical Chemistry in Condensed Phases* **1988,** *84* (4), 1101-1112.

21. Jayson, G. G.; Parsons, B. J.; Swallow, A. J., Some simple, highly reactive, inorganic chlorine derivatives in aqueous solution. Their formation using pulses of radiation and their role in the mechanism of the Fricke dosimeter. *Journal of the Chemical Society, Faraday Transactions 1: Physical Chemistry in Condensed Phases* **1973,** *69* (0), 1597-1607.

22. Buxton, G. V.; Greenstock, C. L.; Helman, W. P.; Ross, A. B., Critical Review of rate constants for reactions of hydrated electrons, hydrogen atoms and hydroxyl radicals (·OH/·O− in Aqueous Solution. *Journal of Physical and Chemical Reference Data* **1988,** *17* (2), 513-886.

23. Lattach, Y.; Deniset-Besseau, A.; Guigner, J.-M.; Remita, S., Radiation chemistry as an alternative way for the synthesis of PEDOT conducting Polymers under "soft" Conditions. *Radiation Physics and Chemistry* **2013,** *82*, 44-53.

24. Hart, E. J., Research potentials of the hydrated electron. *Accounts of Chemical Research* **1969,** *2* (6), 161-167.

25. Cui, Z.; Bahry, T.; Dazzi, A.; Bui, T.-T.; Goubard, F.; Remita, S., Conducting polymers synthesized by γ-radiolysis in very acidic aqueous medium. *Radiation Physics and Chemistry* **2019,** *159*, 47-56.

26. Jonsson, M.; Lind, J.; Eriksen, T. E.; Merenyi, G., Redox and Acidity Properties of 4-Substituted Aniline Radical Cations in Water. *Journal of the American Chemical Society* **1994,** *116* (4), 1423-1427.

27. Lind, J.; Shen, X.; Eriksen, T. E.; Merenyi, G., The one-electron reduction potential of 4-substituted phenoxyl radicals in water. *Journal of the American Chemical Society* **1990,** *112* (2), 479-482.

28. Alfassi, Z. B.; Harriman, A.; Huie, R. E.; Mosseri, S.; Neta, P., The redox potential of the azide/azidyl couple. *The Journal of Physical Chemistry* **1987,** *91* (8), 2120-2122.

29. Lattach, Y.; Coletta, C.; Ghosh, S.; Remita, S., Radiation-Induced Synthesis of Nanostructured Conjugated Polymers in Aqueous Solution: Fundamental Effect of Oxidizing Species. *ChemPhysChem* **2014,** *15* (1), 208-218.

30. Cui, Z., Radaition induced synthesis of conducting polymers and their metal nancomposites. *Doctoral thesis* **2017**.

31. Saunders, B. B., Reactions of thiophene with radiolytically produced radicals. 2. The solvated electron and the hydrogen atom. *The Journal of Physical Chemistry* **1978,** *82* (2), 151-154.

32. Belloni, J.; Mostafavi, M.; Remita, H.; Marignier, J.-L.; Marie-Odile Delcourt, a., Radiation-induced synthesis of mono- and multi-metallic clusters and nanocolloids. *New Journal of Chemistry* **1998,** *22* (11), 1239-1255.

33. Cui, Z.; Coletta, C.; Dazzi, A.; Lefrançois, P.; Gervais, M.; Néron, S.; Remita, S., Radiolytic Method as a Novel Approach for the Synthesis of Nanostructured Conducting Polypyrrole. *Langmuir* **2014,** *30* (46), 14086-14094.

34. Coletta, C.; Cui, Z.; Archirel, P.; Pernot, P.; Marignier, J.-L.; Remita, S., Electron-Induced Growth Mechanism of Conducting Polymers: A Coupled Experimental and Computational Investigation. *The Journal of Physical Chemistry B* **2015,** *119* (16), 5282-5298.

35. Coletta, C.; Cui, Z.; Dazzi, A.; Guigner, J.-M.; Néron, S.; Marignier, J.-L.; Remita, S., A pulsed electron beam synthesis of PEDOT conducting polymers by using sulfate radicals as oxidizing species. *Radiation Physics and Chemistry* **2016,** *126*, 21-31.

36. Deng, Y.; Ezyske, C. M., Sulfate radical-advanced oxidation process (SR-AOP) for simultaneous removal of refractory organic contaminants and ammonia in landfill leachate. *Water Research* **2011,** *45* (18), 6189-6194.

37. Jian, Z.; Zhiping, Z.; Shengkang, Y., Study of gamma-ray radiation-induced polymerization of butadiene in ethanol. *International Journal of Radiation Applications and Instrumentation. Part C. Radiation Physics and Chemistry* **1991,** *37* (2), 263-266.

38. Mengping, Q.; Ye, Y.; Baokang, C.; Zhili, X., Radiation-induced polymerization of acrylamide in ethanol and its application in medical x-ray film as a covering agent. *Radiation Physics and Chemistry* **1993,** *42* (1), 193-196.

39. Russell, J. C.; Freeman, G. R., Radiolysis of ethanol. V. Reactions of the primary reducing species in the liquid phase. *The Journal of Physical Chemistry* **1967,** *71* (3), 755-762.

40. Abadie, M. J. M., Radiolysis of liquid chloroform in an oxygen free atmosphere. *Radiation Physics and Chemistry (1977)* **1982,** *19* (1), 63-71.

41. Emmi, S. S.; Beggiato, G.; Casalbore-Miceli, G., Transient species in the pulse radiolysis of methylene chloride and the self-reaction of chloromethyl radicals. *International Journal of Radiation Applications and Instrumentation. Part C. Radiation Physics and Chemistry* **1989,** *33* (1), 29-37.

42. B. Alfassi, Z.; Mosseri, S.; Neta, P., Reactivities of chlorine atoms and peroxyl radicals formed in the radiolysis of dichloromethane. **1989,** *93*.

43. Emmi, S. S.; D'Angelantonio, M.; Beggiato, G.; Poggi, G.; Geri, A.; Pietropaolo, D.; Zotti, G., The generation and spectral characterization of oligothiophenes radical cations. A pulse radiolysis investigation11This paper was presented at the 10th International Meeting on Radiation Processing, 11–16 May 1997, Anaheim, California, U.S.A. *Radiation Physics and Chemistry* **1999,** *54* (3), 263-270.

44. Chen, T. H.; Wong, K. Y.; Johnston, F. J., RADIOLYSIS OF CHLOROFORM AND CARBON TETRACHLORIDE. *The Journal of Physical Chemistry* **1960,** *64* (8), 1023-1025.

45. Isse, A. A.; Lin, C. Y.; Coote, M. L.; Gennaro, A., Estimation of Standard Reduction Potentials of Halogen Atoms and Alkyl Halides. *The Journal of Physical Chemistry B* **2011,** *115* (4), 678-684.

46. Ushida, K.; Yoshida, Y.; Kozawa, T.; Tagawa, S.; Kira, A., Evidence of Oxidation of Aromatic Hydrocarbons by Chloromethyl Radicals: Reinvestigation of Intersolute Hole Transfer Using Pulse Radiolysis. *The Journal of Physical Chemistry A* **1999,** *103* (24), 4680-4689.

47. Emmi, S. S.; Poggi, G.; D'Angelantonio, M.; Russo, M.; Favaretto, L., The solvatochromic effect on some oligothiophene radical cations: a pulse radiolysis and semiempirical investigation. *Radiation Physics and Chemistry* **2003,** *67* (3), 251-256.

48. Li, W.; Chen, L.; Pan, Y.; Yan, S.; Dai, Y.; Liu, J.; Yu, Y.; Qu, X.; Song, Q.; Ouyang, M.; Zhang, C., Electrochromic Properties of Polymers/Copolymers via Electrochemical Polymerization Based on Star-Shaped Thiophene Derivatives with Different Central Cores. *Journal of The Electrochemical Society* **2017,** *164* (4), E84-E89.

49. Roncali, J.; Garreau, R.; Yassar, A.; Marque, P.; Garnier, F.; Lemaire, M., Effects of steric factors on the electrosynthesis and properties of conducting poly(3-alkylthiophenes). *The Journal of Physical Chemistry* **1987,** *91* (27), 6706-6714.

50. Connelly, N. G.; Geiger, W. E., Chemical Redox Agents for Organometallic Chemistry. *Chemical Reviews* **1996,** *96* (2), 877-910.

51. Smits, F. M., Measurement of Sheet Resistivities with the Four-Point Probe. *Bell System Technical Journal* **1958,** *37* (3), 711-718.

52. Ghosh, S.; Remita, H.; Ramos, L.; Dazzi, A.; Deniset-Besseau, A.; Beaunier, P.; Goubard, F.; Aubert, P.-H.; Brisset, F.; Remita, S., PEDOT nanostructures synthesized in hexagonal mesophases. *New Journal of Chemistry* **2014,** *38* (3), 1106-1115.

53. Wang, P.; Shao, Z.; Ulfa, M.; Pauporté, T., Insights into the Hole Blocking Layer Effect on the Perovskite Solar Cell Performance and Impedance Response. *The Journal of Physical Chemistry C* **2017,** *121* (17), 9131-9141.

Chapter 2 Radiation induced polymerization of conducting polymers: from water to dichloromethane radiolysis

2.1 Recent advancements towards facile preparation of processable CPs

Intrinsically conducting polymers CPs are extraordinary class of material that combines the electrical properties of metals and semiconductors with a polymer's ability to flex and/or stretch.[1] Generally, the synthesis of CPs is feasible and easy, however, CPs have some limitations which restrict their applications due to the poor processability which is attributed to the rigidity and interchain interactions of the polymer chains.[2] Moreover, these polymers are highly branched and crosslinked due to polaron/bipolaron charge interaction. CPs are therefore poorly soluble in common industrial solvents. Thus, the key hurdle to uptake these polymers in commercial products is lack of existing facile synthetic methods of producing useful quantities as well as simple approaches for processing bulk polymer into useful forms.[1]

Nowadays, the scientific community is tremendously endeavoring to develop and upgrade new synthesis methodologies of CPs.[3-4] The main methods to synthesize CPs are chemical oxidation or electrochemical polymerization.[5-7] Based on these conventional methods, numerous studies were carried out to optimize, to structuralize and to functionalize CPs.[8] Research reports showed that nanostructured conducting polymers in the form of nanofibers and nanosponges, showed significantly improved capacitance values as compared to their non-nanostructured counterparts.[9] For this purpose, reverse micro-emulsion polymerization[10-11] and CPs composite with carbon nanotubes (CNTs)[12-13] have been employed to fabricate polymers nanotubes[14], wires[15], nano-rods[16], fibers[17], etc. Furthermore, polymer-metal oxide nanocomposites were used to enhance their thermal, mechanical and chemical properties.[18] Even though these previously mentioned methods are well understood and controlled, still remain many obstacles to overcome such as chemical contamination, purification steps and processability. In literature, there are several approaches that have been adopted towards production of processable forms of CPs:[1, 19]

i. Removal of inter-chain charge interactions by reducing CPs to their non-conducting state making them soluble in some solvent such as DMF and DMSO.
ii. Resorting to use of substituted polymer by flexible and long alkyl chain rendering them soluble in common solvent (chloroform, toluene, etc).
iii. Preparation of water soluble CPs using a template-guided enzymatic approach.
iv. Preparation of aqueous colloidal dispersions of CPs in the presence of a water soluble polyelectrolyte such as polystyrene sulfonic acid.
v. Vapor phase polymerization method to produce thin films of both soluble and insoluble CPs, and nanocomposites thereof.

vi. Self-doping approach for increasing the solubility of CPs in aqueous solution by using ionizable functional groups.

For the sake of simplifying the preparation of nanostructured CPs with the view to obtain processable polymers, finding an alternative synthesis and processing approaches would be immensely helpful. In this respect, radiolysis synthesis is already known as an interesting method for the synthesis of non-conducting polymers.[20] However, radiation induced polymerization via the interaction of high energetic rays with the matter is narrowly used to prepare CPs.[21] The preparation of CPs using gamma irradiation was predominantly accompanied by the addition of chemical oxidants. As reported in the literature, ionizing radiation affects polymer morphology and leads to tailoring their nano-structure. Indeed, Karim *et al.* synthesized PPy using γ-radiation induced oxidative polymerization with ammonium peroxy-disulfate (APS) as chemical oxidant.[22] And besides, he prepared buckyball shaped conducting polythiophene by gamma induced polymerization method in presence of $FeCl_3$.[23] However, radiation induced polymerization in the absence of any external oxidizing species has never been used to produce CPs. Radiation method based on radiation chemistry with γ-irradiation or pulse radiolysis for the synthesis of CPs in aqueous solutions has recently been developed by Remita's team.[21] Hence, we concisely preview in this chapter all the potential approaches to proceed with CPs production by radiolysis methodology with all the tools and means that have been employed to ameliorate their preparation in the recent times. It is worth mentioning that, even if this preliminary work began before my joining Samy Remita's group and it was not exclusively carried out for my thesis, in fact, I took part in this research work and made some of the experiments related below which led to the publications of articles where I appear as co-author.

2.2 Preface to radiation induced oxidative polymerization of CPs in aqueous solutions

It is well known that γ-rays and X-rays radiolysis are very often used at ambient temperature and pressure in order to initiate, in the absence of external chemical initiators, oxidation or reduction reactions through the control of the initiator radicals which depend on the nature of the medium (atmosphere, solvent, potential solute).[24-27] The principle is that upon irradiation the deoxygenated aqueous solutions at neutral pH 7 generate the following various radiolytic species (chapter 1,equation 1.3)[28-30]

$$H_2O \rightsquigarrow e_{aq}^-, HO^\bullet, H^\bullet, H_3O^+, H_2O_2, H_2 \quad (1.3)$$

The radiolytic products of water radiolysis are varied between oxidizing species and reducing ones. In the presence of air, $H^{\bullet}$ atoms and solvated electrons e_{aq}^{-} are scavenged by molecular oxygen O_2 to produce respectively perhydroxyl radicals ($HO_2^{\bullet}$) and superoxyde radicals ($O_2^{\bullet-}$) which are the two acido-basic forms of the couple $HO_2^{\bullet}/O_2^{\bullet-}$ (pKa ($HO_2^{\bullet}/O_2^{\bullet-}$) = 4.8 at 298 K).[29, 31] As a consequence, when irradiating aerated aqueous solutions at neutral pH, only two short-lived transient species are formed: hydroxyl radicals ($HO^{\bullet}$) and $O_2^{\bullet-}$ with radiolytic yields of 2.8×10^{-7} mol J^{-1} and 3.4×10^{-7} mol J^{-1}, respectively. [32] The standard redox potential of $HO^{\bullet}$ at pH = 7 is quite high and amounts to $E°'(HO^{\bullet}/H_2O)$ = 2.2 V_{SHE}.[29] On the contrary, $O_2^{\bullet-}$ is almost a poor oxidizing species with relatively low redox potential that amounts to $E°'(HO_2^{\bullet}/H_2O_2)$ = 0.9 V_{NHE}.[29] With this in mind, one can say that $HO^{\bullet}$ radicals are strong oxidizing species and enables evidently oxidation induced polymerization of some interesting organic monomers, such as 3,4-ethylenedioxythiophene (EDOT) (chapter1, Figure 1.1) which has oxidation potential that amounts to 1.4 V versus Ag/AgCl.[33] EDOT molecules are soluble in water and present some specific chemical properties which make them interesting building blocks for the synthesis of functional π-conjugated systems such as PEDOT. In fact, due to their strong electron donor effect, the ether groups at the β and β' positions of thiophene rings, which confer a high reactivity to the free α and α' positions, prevent the formation of parasite α-β' linkages during polymerization. Thanks to these merits owns by EDOT, enabled Remita et al. to successfully synthesized PEDOT polymers by using γ-irradiation.[21] Starting from an aqueous solution of EDOT monomers, it was possible to synthesize polymers under soft conditions: at air and at room temperature without introduction of any external chemical initiators.[21] In addition, the synthesis was feasible under various conditions (O_2 and N_2O).[21, 34] In comparison with the usual electrochemical methods, this new γ-rays-based radiolytic way presented some advantages concerning the easy preparation of the samples, where no supporting electrolyte was needed, and the ability to work under atmospheric conditions without purging solutions with an inert gas. Besides, contrarily to the electrochemical way which leads to the direct deposition of CPs onto conducting substrates, the described radiolysis method leads to the formation of CPs dispersed in water enabling their further deposition over conducting or even non-conducting surfaces.

Radiation induced polymerization of CPs is promising method towards producing processable CPs and exhibits noticeably several advantages over other conventional methods. As it appears, radiation-based method does not require special equipments, can be performed

under various conditions, and it is free from the metal contaminations. Moreover, this method leads to formation of suspended nano-structured CPs in aqueous solutions as well as directly onto substrates. Using radiolysis should also lead to chemical processes which can be switched on and off upon exposure or removal of ionizing radiation instead of using initiator or stopper molecules.

2.2.1 Studying kinetic mechanism of HO•-induced PEDOT polymerization in aqueous solution :

Understanding the mechanism of oxidative polymerization of conducting polymers and studying the reaction mechanism between the generated radicals from radiolysis process and the studied monomers is a pivotal point to advance the development of this original synthetic method. For this purpose, time resolved absorption spectroscopy coupled with pulsed radiolysis was used in order, first, to study EDOT oxidation mechanism and, second, to definitely identify the nature of PEDOT growth process. In this context, the reaction between hydroxyl radical and EDOT monomer was mainly followed with the aim to identify the different transient species involved in the first steps of HO•-induced PEDOT polymerization. Spectrokinetic analysis of experimental data and molecular simulations of absorption spectra were used to confirm the rate constants values and to identify the transient and stable species involved in the mechanism. The experimental setup (University of Paris-Sud in Orsay) includes: a picosecond laser-triggered electron accelerator ELYSE[35-36] coupled with a time-

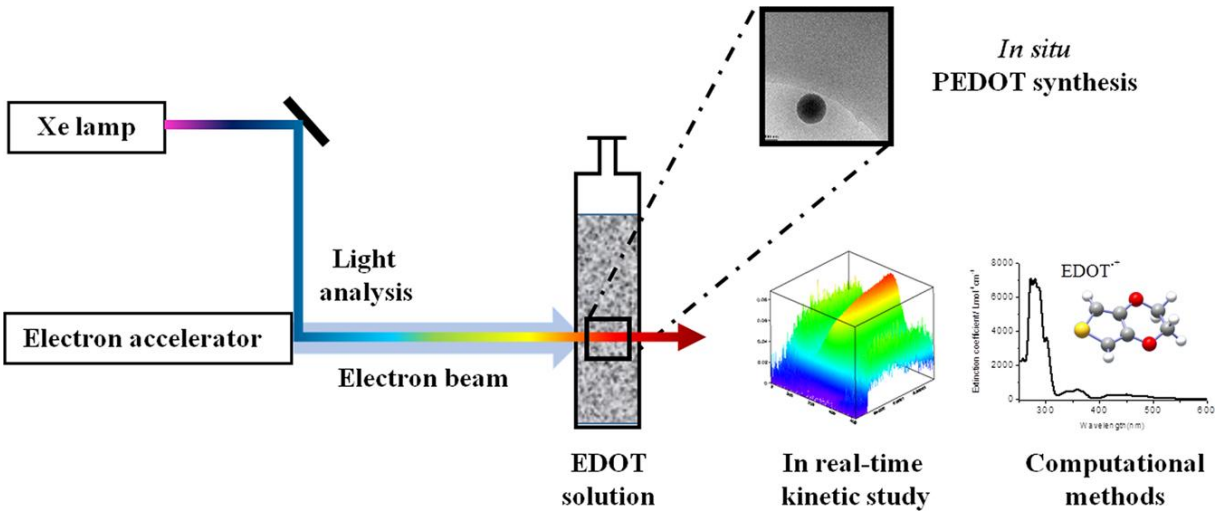

Figure 2.1 the picosecond laser-triggered electron accelerator ELYSE at University Paris-Sud (Orsay) coupled with a time-resolved absorption spectroscopic detection system. The figure shows the involvement in real-time kinetic study of molecular simulations of absorption spectra in the presented study as well as the Cryo-TEM image of PEDOT nanoparticles.[31]

resolved absorption spectroscopic detection system. A mixed simulation method was used, using the monte-carlo (MC) sampling of the molecular geometries, the density functional theory (DFT) calculation of the electron structures and the polarized continuum (PCM) modeling of the solvent (**Figure 2.1**). An N_2O-purged stock solution of 200 mL was used which circulated in the 10 x 10 mm fused silica irradiation cell at a flow rate of 100 mL/min by means of a peristaltic pump. Since the electron pulses were applied at a frequency of 5 Hz, the solution was renewed between each pulse and it was possible to apply up to 400 pulses for each kinetic measurement. All the experiments conditions and samples preparation can be found in details in the work of Cecilia Colletta.[31, 37]

In acidic and neutral aqueous solutions, $HO^{\bullet}$-induced oxidation of EDOT implies the oxidation of EDOT into a transient species, $EDOT^{\bullet+}$ radical cation (and possibly into $(EDOT\text{-}HO)^{\bullet}$ adduct, which dimerizes and deprotonates leading to a stable product, namely $EDOT_2$ dimer. In alkaline medium, this mechanism is mostly different since $HO^{\bullet}$ deprotonates into its alkaline form, $O_2^{\bullet-}$ oxide radical, which adds onto EDOT monomer. This addition leads to the formation of an open cycle which prevents any dimerization of EDOT and consequently any polymerization of PEDOT. Hence, in acidic and neutral aqueous solutions, after one pulse irradiation (40 Gy), no other products than $EDOT_2$ dimers were observed, demonstrating that no polymerization takes place. This proves that PEDOT polymerization is not a chain reaction. On the contrary, it has been demonstrated to proceed through a step-by-step mechanism made up of the following recurrent steps: (i) oxidation/activation, (ii) growth/chain length increase, (iii) deprotonation.[31] The amount of hydroxyl radicals generated by one pulse during the pulsed radiolysis study is then not enough to ensure polymerization. It only enables the incomplete transformation of EDOT monomers into dimers. The quantitative polymerization of EDOT into PEDOT requires a very much higher concentration in hydroxyl radicals which should reach at least twice that of EDOT. In pulse radiolysis experiment, the dose per pulse can‘t be significantly increased. Then, in order to check whether EDOT polymerization effectively proceeds through a step-by-step oxidation process and with the aim to synthesize conducting PEDOT polymers by using an electron beam, aqueous solutions containing 10 mM in EDOT in a closed cell under N_2O atmosphere were irradiated with a series of consecutive electron pulses of 40 Gy (delivered at a frequency of 10 Hz).

Taking into account the step by step polymerization process, 10 mM in hydroxyl radicals are needed for the quantitative dimerization of 10 mM in EDOT into 5 mM in $EDOT_2$, then an additional amount of 5 mM in $HO^{\bullet}$ is needed for the quantitative transformation of $EDOT_2$ into 2.5 mM in $EDOT_4$ and so on. This means that at least 20 mM in hydroxyl radicals are

necessary to ensure the quantitative polymerization of EDOT monomers into PEDOT polymers. The use of two $HO^{\bullet}$ radicals for one EDOT molecule is understandable since each EDOT monomer is bound to two EDOT neighbors inside the same polymer chain, which means that it must be twice oxidized. The theoretical irradiation dose (D_{max}) which should lead to the total oxidation of EDOT into PEDOT by $HO^{\bullet}$ radicals can be determined as follows:

$$D(Gy) = \frac{2[EDOT]_0 \ (mol\ L^{-1})}{G_{ox}\ (mol\ J^{-1})\ d\ (kg\ L^{-1})} \qquad (2.1)$$

Where D is the irradiation dose (in Grays, 1 Gy corresponding to 1 $J.kg^{-1}$or 1 $J.L^{-1}$ for diluted solution), where $[EDOT]_0$ is the initial concentration of EDOT monomers, where G_{ox} is the radiolytic yield of $HO^{\bullet}$ formation and where d is aqueous solution density ($d \sim 1\ kg.L^{-1}$).

According to equation 2.1, 37 kGy are necessary for the total polymerization of 10 mM in EDOT. Knowing that each pulse corresponds to a dose of 40 Gy, complete polymerization requires more than about 1000 successive pulses.

In order to quantitatively polymerize EDOT, the colorless and limpid aqueous solution of 10 mM in EDOT was irradiated at a dose of 180 kGy which corresponds to the accumulation of 4500 pulses of 40 Gy/pulse. After this irradiation, the solution became turbid. Its UV-Vis absorption spectrum is displayed (**Figure 2.2a**).[31] No noticeable absorption band is present in the spectrum. Nevertheless, a continuous scattering appears due to the presence of a brown-yellow suspension in the bulk of the irradiated solution (**inset of Figure 2.2a**). This spectrum and the turbidity of the solution are in good agreement with the results previously obtained by steady state γ radiolysis suggesting that polymerization effectively took place.[21]

The ATR-FTIR spectrum of the polymer powder is presented in the upper part of Figure 3.1b in the wave number region 1600-600 cm^{-1} together with the spectrum of pure non irradiated EDOT (**bottom of Figure 2.2b**).[31] The two spectra are in good agreement with those our group previously reported for PEDOT and EDOT when polymerization was induced by γ-rays. **Table 2.1** shows the absorption modes and the position of the observed peaks. The IR spectrum of the polymer powder displays vibrations at 1485, 1441 and 1365 cm^{-1} which are attributed to C=C and C-C stretching modes in the thiophene ring. The vibrations observed at 1288, 1240, 1171 and 1059 cm^{-1} are assigned to the bending vibration modes of the ethyledioxy groups (C-C and C-O-R-O-C). The vibration modes of C-S bond which are present in the thiophene ring can be observed at 941 and 901 cm^{-1}. Note that the intense =C-H vibration band at 754 cm^{-1}, observed in the spectrum of EDOT, is clearly absent in the ATR-

FTIR spectrum of polymers. This definitely demonstrates, without any ambiguity, that EDOT polymerization quantitatively took place thanks to α,α'-coupling reactions and that the resulting solid powder obtained after lyophilization is effectively composed of PEDOT polymers. This demonstrates that such as γ-irradiation, electron beam irradiation enables the radio-synthesis of PEDOT polymers.[33] It is worth to note that all of these bands presented in all of the recorded spectra for PEDOT polymers that have been synthesized in the present study, are signature of successful synthesis, even if they appear relatively slightly displaced. While one electron pulse leads to the formation of $EDOT_2$ dimers as stable products, the use of a series of successive pulses is necessary to generate enough hydroxyl radicals to form PEDOT polymers. It is evidenced that not only electron irradiation can be used as an alternative way for the synthesis of PEDOT polymers, but also that PEDOT growth effectively proceeds through a step by step oxidation process as expected.

Functional group	**Position (cm^{-1})**
C=C (symmetric stretching mode)	1485 and 1441
C-C (inter-ring stretching Mode)	1365
C-O-R-O-C (bending vibration in ethylenedioxy group)	1288, 1240, 1171 and 1059
C-S-C (stretching vibrations)	941 and 901
=C-H (in-plane and out-of-plane deformation vibrations)	754

Table 2.1 ATR-FTIR absorption peaks of EDOT and PEDOT polymers

Aqueous solutions containing 10 mM in EDOT and irradiated by the electron beam at 180 kGy were observed by Cryo-transmission electron microscopy just after irradiation in order to investigate the structure and morphology of PEDOT polymers in aqueous solution. Representative images show the presence of low density globular structures forming spherical nanoparticles with a diameter ranging between 200 and 250 nm (**Figure 2.2c**).[31] This result is in agreement with polymer size and shape found after γ-rays induced PEDOT synthesis. Since no other low density objects were observed during our Cryo-TEM experiments, these spherical nanoparticles are supposed to be made up of PEDOT polymers. Each observed nanoparticle should be composed of interdigitated polymer chains. Since no α-β' linkages could occur during polymerization, radiosynthesized PEDOT nanostructures should be composed of linear chain polymers which are no branched nor networked. Thus the globular structure observed on Figure 3.16 should correspond to a self-assembly of independent amorphous PEDOT chain polymers. The presence of ethylenedioxy groups (H-bond acceptors) should explain not only the hydrosolubility of PEDOT polymers but also the as-observed packing and nano-structuration of the spherical supramolecular PEDOT self-assemblies. In order to characterize the morphology of the polymer after a deposition

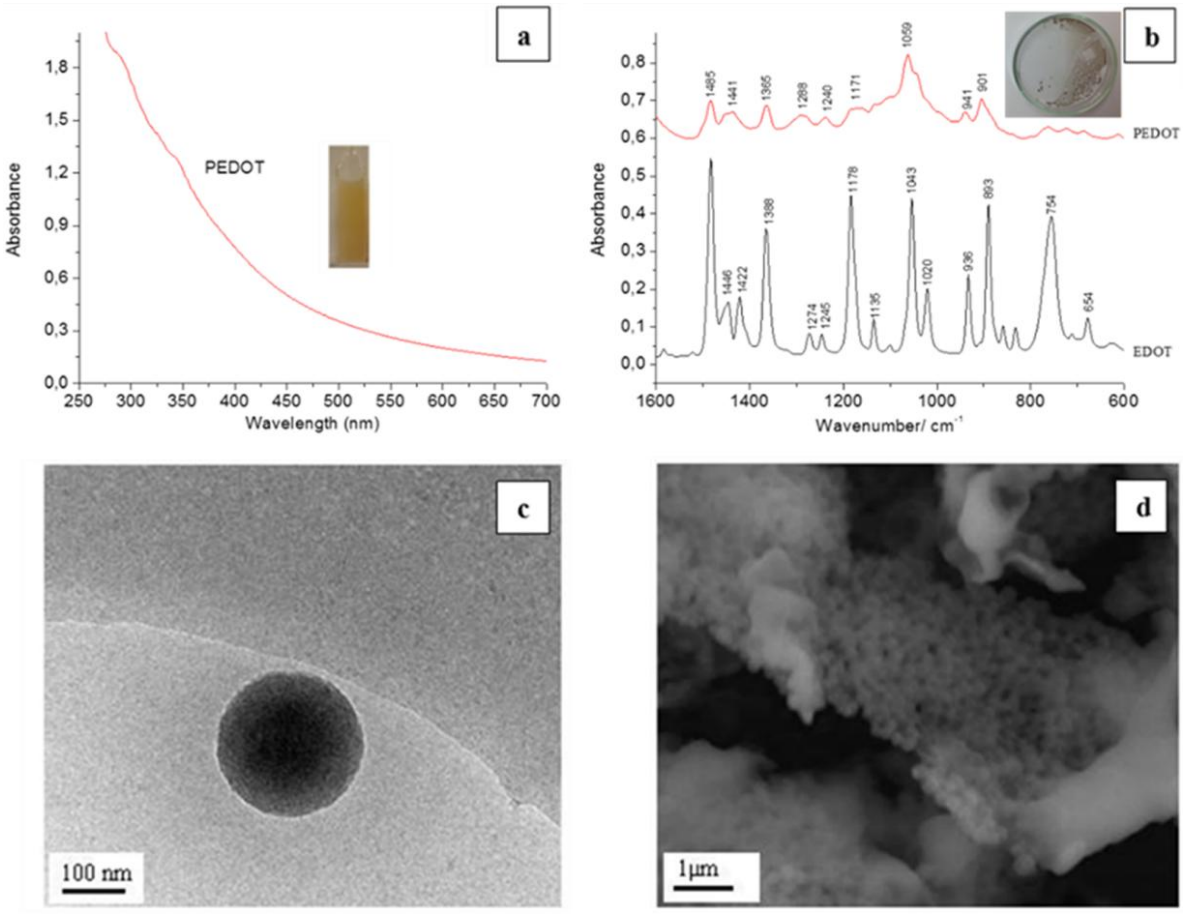

Figure 2.2 (a) Absorption spectrum of a N_2O-saturated aqueous solution of EDOT (10 mM) irradiated by an electron beam at a dose of 180 kGy (4500 pulses, 40 Gy/pulse). The reference was water, and path length was 1 mm; (inset) photograpgy of a cell containing PEDOT aqueous suspension radiosynthesized by an electron beam. (b) ATR-FTIR spectra of pure EDOT (bottom spectrum) and PEDOT polymers radiosynthesized at 180 kGy (top spectrum); (inset) photo of a cup containing the lyophilized radiosynthesized PEDOT powder. (c) Cryo-TEM image of radiosynthesized PEDOT in aqueous solution. A PEDOT nanoparticle of around 250 nm is observed. (d) SEM image of lyophilized radiosynthesized PEDOT powder. Aggregates of spherical PEDOT nanoparticles are observed.[31]

procedure, the 180 kGy-irradiated sample was lyophilized and the black powder obtained was deposited then characterized by SEM microscopy. The images indicate the presence of very close packed polymeric particles (**Figure 2.2d**).[31]

Once again PEDOT polymers appear as spherical nanoparticles. These structures should come from the globular nanostructures already observed in aqueous solution by Cryo-TEM. The particles observed by SEM are almost monodisperse in size with a mean diameter of 220 nm which is close to that observed by Cryo-TEM in aqueous solution. This proves that neither phase transition nor deposition procedure affect the size and shape of PEDOT nanoparticles. This would imply the existence of very strong hydrogen-bond interactions into each polymer nanoparticle. Therefore, the synthesis of PEDOT polymers is successful thanks to the

electrons beam irradiation of EDOT aqueous solution. The radiosynthesized PEDOT polymers form monodisperse nanoparticles the morphology of which is kept after deposition onto substrate.

Further investigation based on pulsed electron beam irradiation were proceeded to oxidize EDOT monomers and to induce polymers growth by using sulfate radicals, $SO_4^{\bullet-}$ instead of hydroxyl radicals, $HO^{\bullet}$.[38] The purpose of this study was to check the influence of the nature of the oxidizing species and of the presence of an inorganic compound (namely $K_2S_2O_8$) onto the morphology of radio-synthesized polymers. The results demonstrated the versatility of our methodology based on pulsed electron beam irradiation, and highlighted, without any ambiguity, the efficiency of alternative oxidizing radicals, such as sulfate radicals for the preparation of nanostructured conducting polymers. The success of PEDOT polymers synthesis by using accumulated electron pulses, definitely demonstrates that conducting polymers growth proceeds through a step-by-step oxidation mechanism and not according to a chain reaction.

2.2.2 Gamma-radiation induced oxidative polymerization of EDOT in aerated aqueous solutions at neutral pH :

The incipient form of this method was initially instituted by γ- radiolysis of aerated aqueous solutions of 3,4-ethylenedioxythiophene (EDOT).[21] The concept is that the radiolysis of aerated aqueous solutions provides the medium with several oxidizing species namely $HO^{\bullet}$ and $O_2^{\bullet-}$. These generated oxidizing species can insure the oxidation of EDOT monomers. Accordingly, the irradiation conditions were studied in details to get the product in optimal form. Within this framework, to approach the synthesis of PEDOT by γ-radiolysis, the yield of oxidation is needed to determine. As elucidated in our studies,[21, 31] by knowing the extinction coefficients of EDOT in aqueous solution that are calculated from UV-Vis absorption spectrum, one can deduce the initial radiolytic yield of EDOT consumption from the variation of EDOT concentration as a function of the irradiation dose. The extrapolated value of the radiolytic yield of EDOT consumption under air corresponds actually to the same radiolytic yield of $HO^{\bullet}$ that amounts to $G_{-EDOT\,0} = G_{HO^{\bullet}} = 2.8 \times 10^{-7} \mathrm{mol.J^{-1}}$.[21] Noting that this value is almost constant no matter what is the initial concentration of EDOT. That means EDOT is sufficient to scavenge all the hydroxyl radicals and also demonstrates that only hydroxyl radicals react with EDOT. As mentioned above, $HO^{\bullet}$ is a strong oxidizing species since its apparent standard redox potential at pH=7 amounts to $E^{\circ}{}_{SHE}(HO^{\bullet}/H_2O) = 2.2\ V_{SHE}$ [29] enabling oxidation of EDOT. Contrariwise, the formed $O_2^{\bullet-}$ radicals possess very low

redox potential [E°_{SHE} ($O_2^{\bullet-}/H_2O_2$) = 0.9 V_{SHE}][29], that making them being considered as poor oxidizing species. As a consequence, the relatively low apparent redox potential of $O_2^{\bullet-}$ does not allow the reaction with EDOT the oxidation potential of which amounts to 1.4 V $Ag/AgNO_3$ [33]. Whatever EDOT concentration ranging from 1 to 10 mM, the results show that EDOT disappearance parallels the formation of species which absorb at both 290 and 350 nm. These absorption maxima should be attributed to dimers and oligomers of EDOT which could be formed according to the step by step oxidation process highlighted by pulse radiolysis:

$$EDOT + HO^{\bullet} \rightarrow (EDOT - HO)^{\bullet} \text{ or } EDOT^{\bullet+} + HO^{-} \qquad (2.2)$$

$$2(EDOT - HO)^{\bullet} \text{ or } 2EDOT^{\bullet+} \rightarrow \text{ dimers then oligomers} \qquad (2.3)$$

These bands are in agreements with the absorption spectra of dimers found experimentally by our previous pulsed radiolysis studies.[31] Auxochromic substitution (by the ethylenedioxy group) in EDOT dimers can explain the shift in their absorption maxima as compared with those of bithiophene molecules which are known to absorb at 246 nm and 301 nm.[39] The yield of EDOT oxidation, $G_{-EDOT\,0}$ decreases with the dose and becomes much lower than $G_{HO^{\bullet}}$ at high doses. This is because of the competitive reactions of hydroxyl radicals with EDOT dimers and oligomers which take place in the medium and which become more and more preponderant as the amount of EDOT decreases. Indeed, the oxidation potential of the dimers and the oligomers is lower than that of the monomers enabling their oxidation by hydroxyl radicals. So the process of oxidative coupling of the units continues as the polymer grows.[40]

On the other hand, the yield of EDOT consumption does not depend on the initial EDOT concentration. This demonstrates that the process attributed to PEDOT radio-induced synthesis does not proceed through a chain reaction. In particular, $EDOT^{\bullet+}$ radical cation does not react with EDOT monomer. This is consistent with the pulsed radiolysis results obtained in literature in the case of thiophene monomers and with the results we obtained with our pulsed radiolysis study on EDOT: PEDOT radio-induced synthesis could only proceed through a recurrent $HO^{\bullet}$ oxidation process: $HO^{\bullet}$ reacts with EDOT monomers, then with dimers, then with oligomers. The quantitative synthesis of PEDOT polymers throughout such a step-by-step mechanism necessarily implies the use of two $HO^{\bullet}$ radicals for the oxidation of one EDOT molecule (in α and α' positions). Thus, the theoretical irradiation dose (D_{max}) which should lead to the total oxidation of EDOT into PEDOT can be calculated from

equation (3.1). For instance, 7.4 kGy and 74 kGy are necessary for the total oxidation of 1 and 10 mM in EDOT respectively.

In the respect of PEDOT characterizations, the ATR-FTIR observations evidenced their successful formation. [21] Moreover, the obtained spectra are in very good agreement with those previously reported for PEDOT in literature [41-43] and for PEDOT synthesized by accelerated electrons as highlighted before.[31] The PEDOT nature of the radiosynthesized polymers which compose the solid phase was also proved thanks to the determination of its melting point. Indeed, a temperature of 145°C was measured which is very close to the PEDOT melting point value (146°C) reported.[44] This result should also prove the absence of impurities in our product. The morphological features were also observed directly in the aqueous solution by Cryo-TEM and after deposition onto substrate by AFM.[21] The microscopic observations revealed formation of globular self-assembled structures made up of PEDOT polymeric chains. The mean diameter of the observed particles is 200 nm. The dimensions of the nano-objects observed by Cryo-TEM closely match those of AFM. As at will be demonstrated in the next paragraph, the presence of substituted hydroxyl groups along the polymer chains explains the packing and the nano-structuration of the observed spherical supramolecular PEDOT self-assemblies besides their hydrosolubility and the solvation of PEDOT polymers.

In order to enhance the yield of oxidation and in order to check whether other oxidizing species can enable the oxidative polymerization in aqueous solutions, the radiolysis methodology took further advances by varying the experimental conditions (atmosphere and additive). For this purpose, the radiolytic methodology was extended to the synthesis of PEDOT polymers in N_2O-saturated aqueous solutions in the presence and in the absence of sodium azide. The oxidative polymerization was induced through two different oxidizing species: $HO^{\bullet}$ (hydroxyl) and $N_3^{\bullet}$ (azide) radicals, as will be discussed below.

2.2.3 Effect of oxidizing species on radiation-induced synthesis of PEDOT:

The original radiolytic methodology was extended to the synthesis of PEDOT polymers in N_2O-saturated aqueous solutions of EDOT at neutral pH. In these conditions, and depending on the presence of sodium azide salt, two different oxidizing species are formed, namely hydroxyl radicals ($HO^{\bullet}$) and azide radicals ($N_3^{\bullet}$).[34] Since the redox potentials of these two oxidative radicals (which are higher than that of EDOT monomers) and since their well-known oxidation mechanisms are quite different, one can expect the formation of two kinds of PEDOT polymers with tuned characteristics. As already explained and justified, under N_2O in the absence of NaN_3, e_{aq}^- are quantitatively and immediately converted into $HO^{\bullet}$. As a

consequence, when irradiating N_2O-saturated aqueous solutions at neutral pH, only two short-lived transient species are formed: $HO^{\bullet}$ and $H^{\bullet}$ (hydrogen atoms). $HO^{\bullet}$ radicals can be considered as the only oxidizing species, and their radiolytic yield of formation [$G(HO^{\bullet}) = 5.6 \times 10^{-7} mol.J^{-1}$] is higher than that obtained under aerated conditions ($G_{HO^{\bullet}} = 2.8 \times 10^{-7} mol.J^{-1}$). On the other hand, in aqueous solutions containing sodium azide (NaN_3 at 10 mM for 1mM in EDOT or 100 mM for 10 mM in EDOT, dissociated into Na^+ and N_3^- ions) and saturated by nitrous oxide, $HO^{\bullet}$ radicals are very quickly scavenged by N_3^- ions leading to the quantitative formation of $N_3^{\bullet}$. In the presence of NaN_3, the concentration of EDOT monomers being always ten times lower than that of N_3^- ions, the direct oxidation of EDOT by $HO^{\bullet}$ can be neglected. Thus, when irradiating N_2O-saturated aqueous solutions at neutral pH in the presence of NaN_3, as in the case of EDOT solutions, the radiolytic yield of formation of $N_3^{\bullet}$ amounts to $5.6 \times 10^{-7} mol.J^{-1}$. Under these conditions $H^{\bullet}$ atoms are present in medium with radiolytic yield amounts to $G_{H^{\bullet}} = 0.6 \times 10^{-7} mol.J^{-1}$. Nevertheless, due to its relatively small amount and unknown reactivity, the presence of $H^{\bullet}$ atoms is often neglected.[51]

In the absence of NaN_3, the total irradiation dose (D_{max}) that should enable the quantitative synthesis of PEDOT in N_2O-saturated aqueous solutions is thus twice the dose necessary for the total oxidation of EDOT monomers and, as a consequence, can be calculated as previously explained, but by using $G(HO^{\bullet})$ instead of $G_{HO^{\bullet}}$. In a N_2O-saturated aqueous solution containing 1 and 10 mm EDOT, the dose that is necessary for the total oxidation of EDOT amounts to 1.8 and 18 kGy, respectively, and the dose D_{max} that is necessary for the complete synthesis of PEDOT amounts to 3.6 and 36 kGy, respectively.

In the absence of sodium azide salt, N_2O-saturated aqueous solutions containing 10 mm in EDOT were irradiated at increasing doses up to 70 kGy. This latter dose is high enough to ensure the total polymerization of EDOT (at 10 mm). **Figure 2.3a** displays the evolution of the UV/Vis absorption spectrum of this solution as a function of the dose. The spectra show at low irradiation doses, up to about 20 kGy (the dose that produces 10 mm hydroxyl radicals), two absorption bands which appear at 290 and 350 nm (**Figure 2.3a**), which demonstrates the formation of dimers as highlighted by pulsed radiolysis study.[31] Above 20 kGy, no absorption band is observed around 250 nm. This clearly indicates that EDOT has completely disappeared. If the dose is higher than the total irradiation dose, as observed in the case of the 70 kGy irradiation in **Figure 2.3a**, the absorption bands of the dimers disappear and an intense absorption band appears around 370 nm together with continuous scattering, the intensity of which increases with the irradiation dose. This should result from the lengthening

of the EDOT oligomers. In fact, at doses higher than 36 kGy, the appearance of a continuous scattering component, in the extinction spectrum of the irradiated solutions, is due to the formation of a brown-yellow suspension in the bulk solution. This suspension becomes denser and the solution appears more turbid as the irradiation dose increases. After the deposition of this suspension onto the ITO substrate, the resulting film displays an intense absorption band at 550 nm. According to the performed ATR-FTIR analysis, this indicates that the suspension is made up of polymers, denoted PEDOT-OH, formed at high doses thanks to the recurrent step-by-step $HO^{\bullet}$ oxidation process. After irradiation at high doses (from 36 to 70 kGy), very slow precipitation of the suspension was observed. This precipitation corresponds to a sedimentation process of the PEDOT-OH polymers of relatively high molecular weights. This precipitation cannot be assigned to the hydrophobia of the radiosynthesized polymers. Indeed, after adding either cyclohexane or dichloromethane to the aqueous suspensions (v/v) and after stirring and decantation, the polymer particles always remain in the aqueous phase, whereas the organic phase appears colorless, as illustrated in the case of dichloromethane (**Figure 2.3a, inset**). This result proves the hydrophilic properties of PEDOT-OH polymers.

The second condition is γ-radioysis under N_2O in the presence of NaN_3. In this case, $HO^{\bullet}$ radicals are scavenged by N_3^- leading to $N_3^{\bullet}$ radicals which can then be considered as the only oxidizing species able to react with EDOT. $N_3^{\bullet}$ radicals are known as an alternative oxidizing system more selective than $HO^{\bullet}$. It is a soft one-electron oxidant $E^{\circ}(N_3^{\bullet}/ N_3^-) = 1.33\ V_{SHE}$ at pH=7. By analogy with the case of hydroxyl radicals, in the presence of NaN_3, the total irradiation dose (D_{max}) which should enable the quantitative synthesis of PEDOT in N_2O-saturated aqueous solutions is twice the dose necessary for the total oxidation of EDOT monomers and can be calculated as previously explained, but by using $G(N_3^{\bullet})$ instead of $G(HO^{\bullet})$ or $G_{HO^{\bullet}}$. In a N_2O-saturated aqueous solution containing 10 mM in EDOT in the presence of azide salt, the dose which enables the total oxidation of EDOT amounts to 18 kGy and the dose D_{max} which is necessary for the complete production of PEDOT is then about 36 kGy. Accordingly, in the presence of sodium azide salt, N_2O-saturated aqueous solutions containing a higher concentration in EDOT (10 mM) were irradiated at increasing doses up to 70 kGy. The evolution of the UV-visible absorption spectrum of this solution as a function of the dose is displayed (**Figure 2.3b**). At low irradiation doses, up to about 20 kGy (the dose which produces 10 mM in azide radicals), two shoulders appear and grow up at 290 and 350 nm demonstrating once again the formation of dimers. When the dose becomes higher than the total irradiation dose, as observed in the case of the 70 kGy-irradiation on **Figure 2.3b**, the absorption bands of dimers disappear and a more intense absorption band grows up around

370 nm. Again, this should result from the lengthening of EDOT oligomers. Moreover, a brown-colored suspension is observable within the bulk which quickly deposits at the bottom of the solution. Note that the fast precipitation process, observed here, explains the absence of any scattering component in the extinction spectra of **Figure 2.3b**. After the deposition of this suspension onto ITO substrate, the resulting film displays a broad absorption between 500 and 600 nm. This indicates that the suspension is made of polymers, noted PEDOT-N_3, formed at high doses thanks to the $N_3^{\bullet}$-induced oxidation process. After irradiations at high doses (from 36 to 70 kGy), a precipitate is systematically observed. This precipitation is not only due to a sedimentation process of the PEDOT-N_3 polymers of relatively high molecular weight. It also results from the poor hydrophilic properties of these systems. Indeed, after adding either cyclohexane or dichloromethane solvents to the aqueous suspensions (v/v) and after stirring and decantation, the polymer particles always remain at the organic solvent-water interface as illustrated in the case of cyclohexane (Insert of **Figure 2.3b**). This result proves the amphiphilic properties of PEDOT-N_3 polymers. Note that at the interface, these polymers appear as clustered fibers. One can note that, for the same initial concentration in EDOT (10 mM), the spectral evolution in the presence of NaN_3 (**Figure 2.3b**) is similar to that observed in the absence of this salt (**Figure 2.3a**). However, when comparing both evolutions, one can note that for a given irradiation dose, the maximal absorption is always lower in the presence of NaN_3. Even if hydroxyl radicals and azide radicals oxidize EDOT and induce polymerization through the formation of EDOT dimers, it seems that the two implied mechanisms are somewhat different. Maybe the kinetic growth of dimers, oligomers and polymers is slower in the case of $N_3^{\bullet}$. This would induce a lower polymerization yield and lower values of the maximal absorbance. However, such an interpretation is not in agreement with the observed dose effect. On another hand, the products of EDOT oxidation could be chemically and structurally different depending on $N_3^{\bullet}$ or $HO^{\bullet}$ nature of the oxidizing radicals. This could explain the different spectral properties of the products obtained either in the presence or in the absence of azide salt. In addition, the poor hydrophilic properties of the products formed in the presence of NaN_3 lead to their deposition at the bottom of the solution and their adsorption onto the walls of the samples.

The assertion of the successful formation of PEDOT-OH and PEDOT-N_3 was realized by ATR-FTIR and melting point measurements. The obtained results are in good agreement with those previously reported about PEDOT in literature. The melting point both PEDOT-OH and PEDOT-N_3 was determined at a temperature of 145 $^{\circ}$C which is very close to the PEDOT melting point value (146 $^{\circ}$C) already reported. This result demonstrates the high purity of our

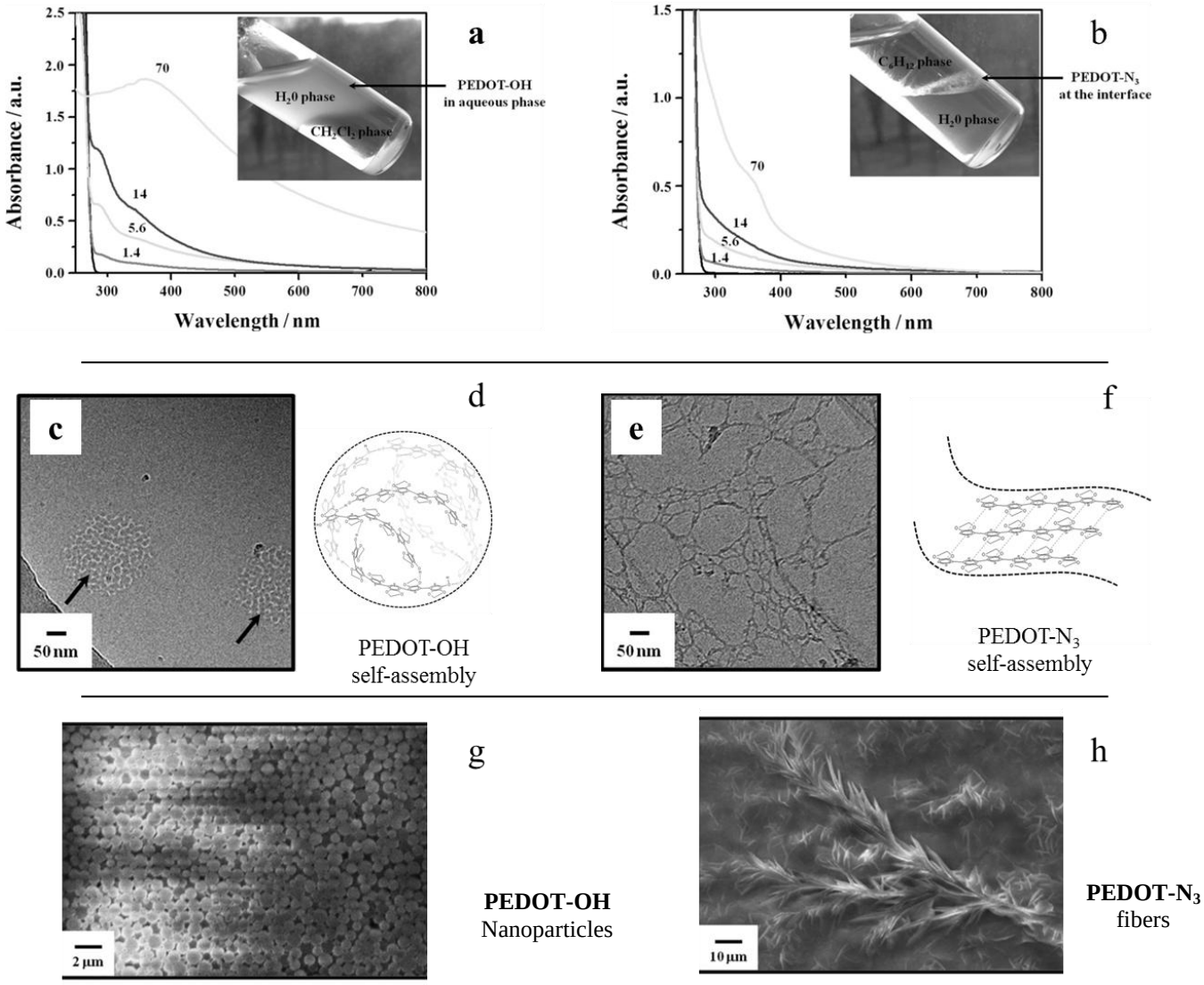

Figure 2.3 Absorption spectra of a N_2O-saturated aqueous solution containing 10 mm EDOT irradiated in the absence of NaN_3 (a) and in presence of NaN_3 (b) with increasing doses: 0, 1.4, 5.6, 14, and 70 kGy. The optical path length was 0.1 cm. The reference was water. Inset (a) Image of an aqueous solution irradiated at 70 kGy after the addition of dichloromethane as a denser organic phase (v/v): PEDOT-OH suspension remains in the upper aqueous phase. Inset (b) Image of an aqueous solution irradiated at 70 kGy after the addition of cyclohexane as a less dense organic phase (v/v): PEDOT-N_3 polymers remains at the interface between the two liquid phases. Cryo-TEM images of aqueous samples containing 10 mM in EDOT irradiated at 36 kGY under N_2O atmosphere: (c) in the absence of NaN_3 (PEDOT-OH) and (e) in the presence of NaN_3 (PEDOT-N_3). (d) A schematic representation of a single spherical polymer nanoparticle which highlights H-bond interactions between the chains. (f) A schematic representation of a single nanostructure highlights π-stacking interactions between the chains. SEM images of PEDOT polymers after deposition onto gold substrates. Polymers were obtained after irradiation at 70 kGy: (g) in the absence of NaN_3 (PEDOT-OH) and (h) in the presence of NaN_3 (PEDOT-N_3).[34]

products and thus the efficiency of our procedure. While, the recorded ATR-FTIR spectra demonstrate, without any ambiguity, that $N_3^{\bullet}$ and $HO^{\bullet}$-induced EDOT polymerizations have

both taken place thanks to α-α'coupling reactions and that the resulting solid powders obtained after centrifugation are effectively composed of PEDOT polymers. Interestingly though the wave number region 4000-700 cm^{-1} of the spectra of PEDOT-OH and PEDOT-N_3 are very much alike, significant differences can be observed above 2000 cm^{-1}.The spectrum of PEDOT-OH exhibits a very large band between 3200 cm^{-1} and 3600 cm^{-1} and is attributed to the presence of hydroxyl groups all along the polymers, while the spectrum of PEDOT-N_3 is characterized by an absorption in two different infrared regions: between 2110-2065 cm^{-1} and between 3565-3525 cm^{-1} and are attributable to the presence of azide anions. The explanation of the noticeable differences between these two kinds of polymers is explained by the difference that exists between the well-known oxidizing behaviors of $HO^{\bullet}$ and $N_3^{\bullet}$: whereas $HO^{\bullet}$ radical either adds onto aromatic molecules to afford radical adducts or abstract electrons leading to radical cations, $N_3^{\bullet}$ azide radicals form only radical cations through electron abstraction. The presence of hydroxyl groups in PEDOT-OH (coming from $HO^{\bullet}$-adducts) demonstrates the existence of strong intermolecular interactions between the functionalized polymers through hydrogen bonds. It also confers to PEDOT-OH polymers hydrophilic properties which explain their poor solubility into organic solvents as previously discussed. Contrarily to PEDOT-OH, PEDOT-N_3 polymers, which result from $N_3^{\bullet}$-induced EDOT oxidation, should not contain alcohol functionalities. This was proven by the absence of a large O-H band in the ATR-FTIR spectrum of PEDOT-N_3. The absence of such a polar group in the PEDOT-N_3 polymer impacts its solubility in water and explains its poor hydrophilic properties.

From what has been observed in the spectral findings (UV-Vis and ART-FTIR), no doubt that the difference between oxidizing behaviors of $HO^{\bullet}$ and $N_3^{\bullet}$ have influenced the nano-structure and have changed the configuration of polymer chains of PEDOT-OH and PEDOT-N_3. The captured Cryo-TEM images clearly showed these differences in nanostructures (**Figure 2.3c** and **Figure 2.3e**).[34] $HO^{\bullet}$ induces the polymerization of EDOT leading to spherical nanoparticles with a diameter comprised between 100 and 300 nm. These observations are consistent with our previous results which concerned hydroxyl-induced radiosynthesis of PEDOT under air atmosphere. Each observed nanoparticle has a complex structure and seems to be composed of interdigitated polymer chains. Since no parasite α–β' linkages could occur during polymerization, radiosynthesized PEDOT-OH nanostructures must be composed of linear chain polymers which are neither branched nor networked. Thus, each globular structure observed by Cryo-TEM should correspond to a self-assembly of independent amorphous PEDOT-OH chain polymers as schematically represented (**Figure**

2.3d). The presence of hydroxyl groups, which has previously been demonstrated, should explain not only the hydrosolubility of PEDOT-OH polymers but also the as-observed packing and nanostructuration of the spherical supramolecular PEDOT-OH self-assemblies. Note that ethylenedioxy groups (H-bond acceptors) present all along the polymer chains could also be involved in hydrogen-bonds with the hydroxyl groups.

$N_3^{\bullet}$ induces the polymerization of EDOT leading to different nanostructures quite different from these obtained in the case of PEDOT-OH. Instead of a compact spheroid surface morphology which was found in the case of PEDOT-OH (**Figure 2.3c)**, the obtained Cryo-TEM images clearly display nano-objects forming fibrillar or lamellar (plate-like) nanostructures, more or less folded, with a maximal fiber thickness of 10 nm and a length which can reach several microns **(Figure 2.3e)**.[34] Since no parasite α-β' linkages could occur during polymerization, the nanofibers are not branched nor bonded to each other. Then nodes observed by cryo-TEM correspond to the crossing between independent nanofibers. Due to the thickness of the fibers, each of them should correspond to a self-assembly of linear PEDOT-N_3 polymer chains as schematically represented in **Figure 2.3f**. Since hydroxyl groups are not present in PEDOT-N_3 polymers, the packing of these polymers can‘t result from H-bonds. This self-assembling should come from π-stacking interactions between conjugated polymers (and aromatic monomers) which maintain the polymer chains parallel to each other and which can maybe confer to the polymers a lamellar structure. On another hand, this self-assembling could explain the macroscopic observation of PEDOT-N_3 polymers as clustered fibers at the interface between water and organic solvent. Also, the fact that PEDOT-N_3 polymers can either interact by van der Waals interactions (π-stacking interactions) or by hydrogen bonds, thanks to the presence of ethylenedioxy groups, could explain the amphiphilic properties of these polymers.

The observed nanostructures of PEDOT-OH and PEDOT-N_3 by Scanning Electron Microscopy (SEM) after a deposition procedure, as might be expected, are consistent with what has been observed by cryo-TEM in aqueous solution. SEM image of PEDOT-OH indicates the presence of very close-packed spheroid polymeric particles (**Figure 2.2g**). The particles observed by SEM after deposition are polydisperse in size with a diameter comprised between 200 nm and 1 μm. The SEM image of PEDOT-N_3 demonstrates the presence of close-packed lamellar (plate-like) structures characterized by a maximal thickness of about 1 μm (**Figure 2.2h**).

As demonstrated above that changing oxidizing species ($HO^{\bullet}$ or $N_3^{\bullet}$) leads to different absorption properties, different hydrophilicities and different morphologies. This approach was extended to the use of another inorganic salt namely, potassium persulfate ($K_2S_2O_8$). Upon irradiation of aqueous solution containing $K_2S_2O_8$ by pulsed electron beam a very strong oxidizing species in aqueous solution, namely $SO4^{\bullet-}$ is sufficiently generated. These $SO4^{\bullet-}$ radicals enabled us to oxidize EDOT monomers and to induce polymers growth. [38] This study once again showed the versatility of our methodology based on pulsed electron beam irradiation, and highlight, without any ambiguity, the efficiency of alternative oxidizing radicals, such as sulfate radicals for the preparation of nanostructured conducting polymers.

2.2.4 Extension the radiolytic procedure to the synthesis of polypyrrole (PPy)

To demonstrate the versatility of the radiolytic method in water under N_2O, the radiolytic procedure that based on $HO^{\bullet}$-induced polymerization was extended to the successful synthesis of another representative CP, namely PPy starting from Py (**Scheme 2.1**).[45] Similar properties, in terms of nano-structuration and hydrophilicity, were obtained in case of PPy when comparing to PEDOT-OH. In solution and after deposition, PPy shows as highlighted by Cryo-TEM, SEM and AFM (**Figure 2.3**) chaplet like spherical nanoparticles with diameters comprised between 80 and 200 nm. The merit of the work is that radio-synthesized PPy nanostructures are characterized by a very good thermal stability and an electrical conductivity that is 5 times higher than that of chemically synthesized PPy.

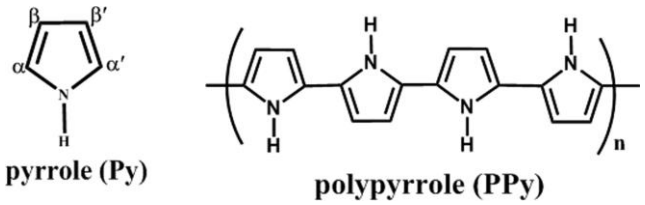

Scheme 2.1 Chemical structure of Pyrrole (Py) and Polypyrrole (PPy)[45]

As we demonstrated the versatility of our method in neutral media, we now want to study in acidic media. Knowing that in alkaline medium, the polymerization as demonstrated by pulsed radiolysis[31] is mostly different since $HO^{\bullet}$ deprotonates into its alkaline form, oxide radical, which adds onto EDOT monomer. This addition leads to an open cycle and prevents any dimerization of EDOT and consequently any polymerization of PEDOT.

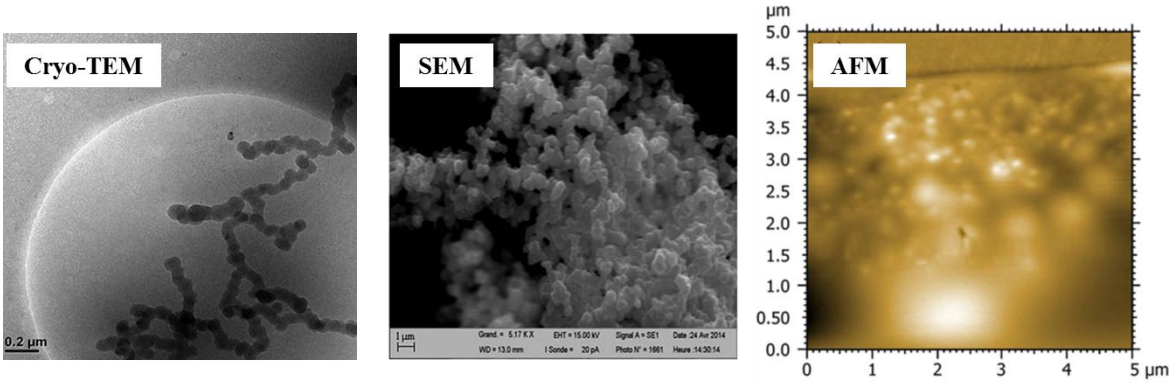

Figure 2.3 Cryo-TEM, SEM and AFM from left to right respectively of radio-synthesized PPy in aqueous solutions under N_2O at 72 kGy.[45]

2.2.5 Effect of pH on the polymerization of EDOT monomers

It has been shown in literature that low pHs prevent conducting polymers from overoxidation[46] and improve their electrical conductivity by doping effect[47] and structural optimization [48]. We therefore wanted to use γ-irradiation in order to radiolytically prepare for the first time conducting organic materials in acidic aqueous media and then to study their properties. In this framework, the endeavor was to polymerize EDOT in very acidic aqueous solutions under N_2O or N_2 (at pH 0 in presence of $HClO_4$ or HCl), by exploiting the oxidizing species produced by γ-radiolysis ($HO^\bullet$ or $Cl_2^{\bullet-}$) (see chapter 1, 1.2.2.1d).[49] In case of using $HClO_4$ to adjust the pH of the aqueous solution under N_2O, knowing that perchlorate ions (ClO_4^-) remain unreactive upon radiolysis, two reactive species should be considered: $HO^\bullet$ and $H^\bullet$ with radiolytic yield amounts to $G(HO^\bullet) = 2.8 \times 10^{-7} mol.J^{-1}$ and $G(H^\bullet) = 3.4 \times 10^{-7} mol.J^{-1}$. $HO^\bullet$ is known as a very oxidizing species which enables in particular oxidation-induced polymerization of EDOT monomers in neutral aqueous solutions. While $H^\bullet$ generally known as less reactive and its reactions are often neglected in neutral media due to its low G value at pH = 7.[31] Nevertheless, $H^\bullet$ becomes predominant at pH 0 and thus its reactivity onto EDOT monomers cannot be omitted as demonstrated in some cases in literature.[39] Interestingly, when hydrochloride acid (HCl) is used (instead of $HClO_4$) in order to adjust the pH, $HO^\bullet$ radicals are quantitatively transformed into dichloride radical anions, $Cl_2^{\bullet-}$.[50] Therefore, the main species produced by γ-radiolysis of very acidic aqueous solutions containing HCl under N_2O are $Cl_2^{\bullet-}$ (instead of $HO^\bullet$) and $H^\bullet$.[51] While the total radiolytic yield of production of $H^\bullet$ atoms remains the same as that found in the case of $HClO_4$, the radiolytic yield of $Cl_2^{\bullet-}$ amounts to $G(Cl_2^{\bullet-}) = 2.8 \times 10^{-7} mol.J^{-1}$. Such as $HO^\bullet$, $Cl_2^{\bullet-}$ is a strong oxidizing species with a very high standard redox potential: $E^\circ (Cl_2^{\bullet-}/Cl^-) = 2.1\ V_{SHE}$.[52] As in

the case of hydroxyl radicals, the oxidation of EDOT monomers and their polymerization into PEDOT should be possible thanks to $Cl_2^{\bullet-}$.[49]

Thus, under N_2O at pH 0, in presence of $HClO_4$ or with HCl, $HO^{\bullet}$ or $Cl_2^{\bullet-}$ should quantitatively oxidize EDOT. If we assume, in both cases, effective oxidation yields of $2.8 \times 10^{-7} mol.J^{-1}$, the dose needed for quantitative polymerization of 10 mM in EDOT amounts to 72 kGy at pH 0 according to equation (3.1). Acidic aqueous solution containing 10 mM in EDOT and 1 M in $HClO_4$ and acidic aqueous solution containing 10 mM in EDOT and 1 M in HCl were then both irradiated at 72 kGy under N_2O atmosphere. Also, for comparison purpose a neutral aqueous solution containing 10 mM in EDOT in the absence of acids was irradiated under N_2O at the same dose. The pictures of the three solutions after irradiation (**in insert Figure 2.4**) as well as their UV-Vis absorption spectra are displayed on **Figure 2.4**. After a 72 kGy-irradiation, the solution prepared in neutral medium appears yellow (photography c in insert of **Figure 2.4**) and its absorption spectrum (spectrum c of **Figure 2.4**) displays an intense absorption band at around 350 nm in total agreement with our previous works[21, 34, 53]. This band was shown to be characteristic of PEDOT oligomers produced in the neutral medium by water radiolysis. Differently, after irradiation at 72 kGy, the solutions prepared at pH 0 in the presence of HCl (photography a in insert of **Figure 2.4**) or in the presence of $HClO_4$ (photography b) both appear as dark blue suspensions, which is the typical color of PEDOT polymers when obtained in their oxidized state.[54-55] Remarkably, when considering the absorption spectra of the two acidic solutions irradiated at 72 kGy in presence of HCl (spectrum a of **Figure 2.4**) or $HClO_4$ (spectrum b), two shoulders are observed in both cases at 350 and 450 nm, which can be attributed to the presence, in very acidic medium, of PEDOT polymers prepared upon irradiation. As a matter of fact, PEDOT polymers are known to usually display, in solution, characteristic peaks in this wavelength region which are assigned to π-π^* transitions in the polymer backbones. In addition to these shoulders, a large absorption band was observed in both cases at around 700 nm in the case of HCl (spectrum a) and in the case of $HClO_4$ (spectrum b). This large band can be considered as polaron or bipolaron bands, which are both characteristic of PEDOT polymers when obtained in their oxidized state (p-type doping).[56]

The *in situ* doping process of PEDOT polymers radio-synthesized in very acidic aqueous solutions in presence of HCl was definitely confirmed by both ATR-FTIR spectroscopy and Energy-Dispersive X-ray (EDX) analysis: first EDX enabled the detection of an additional chemical element, namely chlorine atom, not present in the organic monomers but found homogeneously dispersed in the deposited solid sample; second, ATR-FTIR spectrum of

PEDOT polymers radio-synthesized in very acidic aqueous solutions highlighted the presence of a less common infrared band located at 1640 cm^{-1}.[12, 57] This band has already been observed in earlier works in the case of PEDOT polymers doped with chloride ions. The presence of this band together with the results obtained by EDX highlight the doping of PEDOT by Cl^- and is in full agreement with the results obtained by UV-vis absorption spectroscopy (absorption band at 700 nm). This peak originates from the quinoidal structure of thiophene ring. Further consideration, the infrared spectrum obtained after irradiation shows the absence of the strong band of C-Cl bond which should appear between 600 and 700 cm^{-1}.

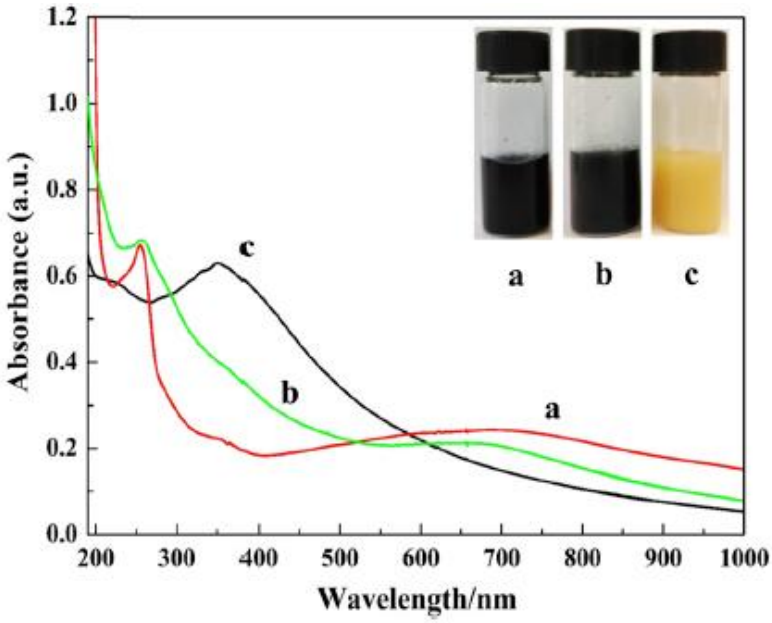

Figure 2.4 UV-Vis absorption spectra of PEDOT polymers synthesized after 72 kGy irradiation of aqueous solutions containing 10 mM in EDOT under N_2O atmosphere (a) in presence of HCl (1 M) at pH = 0, (b) in presence of $HClO_4$ (1 M) at pH = 0 and (c) in the absence of acids at neutral pH. All the spectra were recorded after 10 times dilution. The optical path length was 0.2 cm. The reference was water. Insert: photographies of the corresponding aqueous solutions.[49]

This means that no chlorine atom is covalently bonded to PEDOT polymers chains. It is worth noting that same results demonstrated the doping with ClO_4^- in case of PEDOT in presence of $HClO_4$. This interesting result, which is in total agreement with the colors of the irradiated solutions, demonstrates that contrarily to PEDOT oligomers produced in neutral medium, polymers synthesized under the same atmosphere (N_2O) at pH 0 are found doped. The doping of radiosynthesized PEDOT polymers should result from the presence in the medium of considerable amounts (1M) of hydrochloric acid or perchloric acid. PEDOT polymers produced in presence of either HCl or $HClO_4$ seem to be in the same oxidized state

since the doping bands are located at approximatively the same wavelength. In terms of morphology, the observations made by SEM and AFM microscopies, showed that PEDOT polymers self-assemble into polydisperse globular particles (size comprised between 200 and 500 nm).[49] Since PEDOT morphology in very acidic medium is comparable to that of PEDOT polymers obtained in neutral aqueous medium, one can conclude that neither the acidity of the medium (presence of HCl at 1 M) nor the reactivity of $Cl_2^{\bullet-}$ radicals affect the final morphology of PEDOT polymers.

2.3 Radiation-Induced synthesis of PEDOT by reduction-polymerization route

Usually CPs synthesized by oxidation of monomers as shown previously. Some work in literature concern the synthesis by reduction of monomers.[58] We wanted to check whether reducing radiolytic species produced by γ-radiolysis are able to lead to CPs. In particular we wanted to check if γ-rays-based reduction-polymerization route for synthesizing PEDOT polymers under N_2 atmosphere is feasible thanks to the produced reducing species from water radiolysis, namely hydrated electrons (e_{aq}^-). Contrarily to our common approach based on the use oxidizing radicals, such as hydroxyl radicals ($HO^\bullet$), azide radicals ($N_3^\bullet$) or sulfate radicals ($SO_4^{\bullet-}$), hydrated electrons produced by water radiolysis are used to reduce EDOT and then to initiate the reduction–polymerization of PEDOT polymers through coupling reactions. Evidently in order to reduce EDOT and then to synthesize PEDOT, hydroxyl radicals must be scavenged. This is possible, under N_2 atmosphere, in the presence of isopropanol, $(CH_3)_2CHOH$ (at a relatively high concentration, 0.2 mol.L^{-1} for instance). In these conditions $HO^\bullet$ are quantitatively converted into $(CH_3)_2C^\bullet OH$ isopropanol radicals [59-60] which not able to oxidize EDOT. In fact, they are almost reducing species, the redox potential of which amounts to -1.8 V_{SHE} at pH = 7. As a consequence, when irradiating N_2-saturated aqueous solutions in the presence of isopropanol, as in the case of our EDOT solutions, in addition to hydrated electrons ($G_{e_{aq}^-} = 2.8 \times 10^{-7} \mathrm{mol.J^{-1}}$), only an additional reducing short-lived transient species is quantitatively formed, namely isopropanol radicals, the radiolytic yield of which being: $G((CH_3)_2C^\bullet OH) = G_{HO^\bullet} = 2.8 \times 10^{-7} \mathrm{mol.J^{-1}}$.

We demonstrated that the yield of EDOT reduction is equal to $G_{e_{aq}^-}$.[61] This means that isopropanol radicals don't reduce EDOT and since only hydrated electrons react onto EDOT molecules. Consequently, the doses which are necessary for the total reduction of 1 mM and 10 mM in EDOT, amount to 3.6 and 36 kGy respectively, while the doses D_{max} which are necessary for the complete synthesis of PEDOT, according to equation (3.1) amount to 7.2

and 72 kGy, respectively. Indeed from kinetic point of view, the dose effect study showed that similarly to hydroxyl radicals, the process initiated by hydrated electrons and which lead to $PEDOT_{red}$ radio-induced synthesis does not proceed through a chain reaction. In fact, the quantitative synthesis of $PEDOT_{red}$ polymers throughout a reduction-polymerization process proceeds through a step-by-step mechanism and therefore the use of two hydrated electrons per EDOT molecule is needed. In terms of the optical properties, the recorded UV-visible absorption spectrum of the solution irradiated (at 72 kGy) under N_2 in the presence of isopropanol does not show any change or shift when comparing to the spectrum we previously obtained for $PEDOT_{ox}$ (PEDOT formed by oxidation at the same dose) under N_2O. When it comes to ATR-FTIR, the spectra appear relatively slightly displaced. Nevertheless, the findings prove, without any ambiguity, that PEDOT polymers are obtained by radiolysis either by reduction-polymerization or by oxidation polymerization.[61]

To discuss the resulted morphological structures of $PEDOT_{red}$ synthesized thanks to e_{aq}^-, we view in **Figure 2.5** the collected images from cryo-TEM, SEM and AFMIR. Representative cryo-TEM image showed the presence of low density globular structures forming polydisperse spherical nanoparticles with a diameter comprised between 100 and 500 nm as observed on **Figure 2.5 a**. The mean size, the shape and the polydispersity of $PEDOT_{red}$ polymer nanostructures obtained through reduction-polymerization, are the same as those of $PEDOT_{ox}$ polymers already synthesized through oxidation-polymerization routes induced either by γ-rays or by accelerated electrons. The displayed SEM image in **Figure 2.5 b** depicts very close-packed spheroidal polymeric particles. These structures should come from the globular nanostructures already observed in aqueous solution by cryo-TEM (**Figure 2.5 a**). All these observations are consistent with the reported characterizations of $PEDOT_{ox}$ polymers synthesized by oxidation polymerization. The particles observed by SEM after deposition are polydisperse in size with a diameter comprised between 100 and 500 nm. These SEM observations agree well with the morphology of $PEDOT_{red}$ particles previously observed in aqueous solution by cryo-TEM (**Figure 2.5 a**) without any significant change in the mean size and in the shape. Then, the packing of the particles and their flattening onto the substrate when deposited and dried do not seem to affect the nano-structuration of $PEDOT_{red}$ polymers.

In order to further prove that the spherical nanoparticles already observed by cryo-TEM and SEM are made up of PEDOT polymer chains, a drop of the yellow suspension was deposited on the upper surface of a ZnSe prism, dried naturally and finally imaged and characterized by AFM-IR (**Figure 2.5**). According to the AFM image of $PEDOT_{red}$ recorded

in contact mode (**Figure 2.5 c**), the bottom dark areas having no thickness correspond to the substrate. The topography of $PEDOT_{red}$ displayed as the bright areas correspond to the thicker regions made up of close-packed spherical nanoparticles (100 to 300 nm in diameter). This

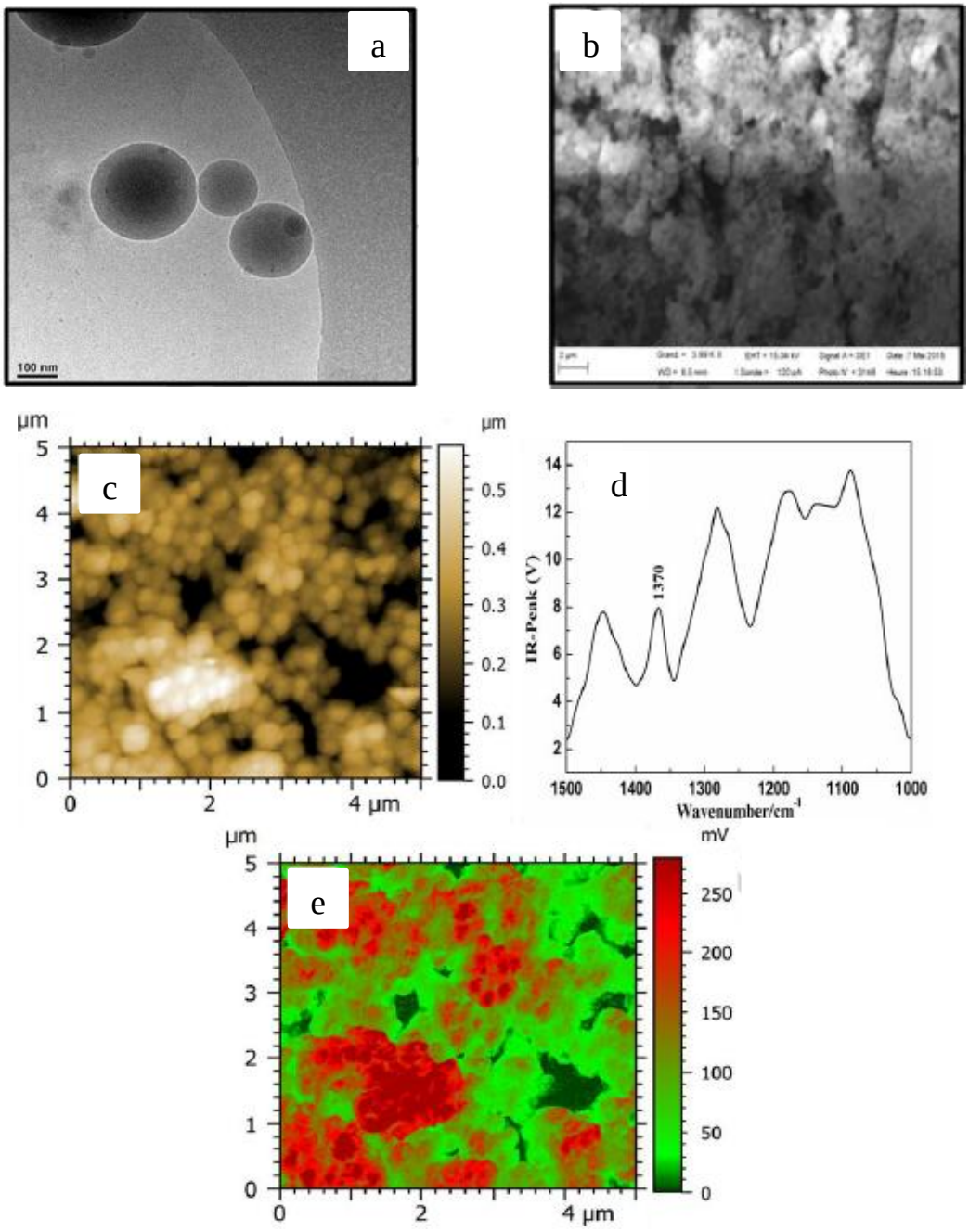

Figure 2.5 Microscopic and AFM-IR characterizations of of aqueous samples containing 10 mM in EDOT irradiated at 72 kGy under N_2 in the presence of isopropanol. a) Cryo-TEM image of $PEDOT_{red}$ polymers exhibiting spherical nano-objects with diameters comprised between 100 and 500 nm attributed to self-assembled b) SEM images of $PEDOT_{red}$ polymers after lyophilization and deposition onto carbon tape adhered to aluminum mounts c) AFM topographic image of $PEDOT_{red}$ polymers in contact mode after lyophilization and deposition onto ZnSe prism (d) AFM-IR spectrum of $PEDOT_{red}$ polymers and (e) AFM-IR chemical mapping of $PEDOT_{red}$ polymers with the IR source tuned to the C-C band at 1370 cm^{-1}.[61]

AFM observation agrees well with the morphology of $PEDOT_{red}$ globular particles previously observed in aqueous solution by Cryo-TEM (**Figure 2.5** a) without any significant change in the mean size and in the shape. Then, the packing of the particles and their flattening onto ZnSe substrate when deposited and dried do not seem to affect the nanostructuration of the polymers.

In order to confirm that these nanoparticles are made up of PEDOT polymers, the sample was observed by AFM-IR in the range of 1000~1500 cm^{-1} (**Figure 3.4** d). The spectrum of **Figure 2.5 d** displays a peak at 1370 cm^{-1} which corresponds to the C-C stretching band of PEDOT as observed in typical ATR-FTIR spectra. This definitely demonstrates that the nanoparticles observed in **Figure 2.5 a, b and c**, contain close-packed $PEDOT_{red}$ polymer chains. Since the AFM-IR technique also enables the chemical mapping of the sample, this wavenumber 1370 cm^{-1} was chosen for AFM-IR chemical mapping of our sample. The chemical map was scanned and the absorption strength was recorded (**Figure 2.5** e). In **Figure 2.5 e**, the red areas indicate a stronger absorption at the characteristic wavenumber which is caused by a thick layer of $PEDOT_{red}$ (~300 nm) linked onto the prism. When comparing the topography (**Figure 2.5 c**) and the chemical mapping (**Figure 2.5** e), one can observe that the stronger absorbing areas fit very well with the thicker regions, which implies that the spherical nanoparticles are mainly composed by PEDOT polymer chains. Therefore, we conclude, without any ambiguity that radiation chemistry in reducing conditions (in the presence of hydrated electrons) leads to the reduction of EDOT monomers and to the growth of PEDOT polymers which self-assemble into spherical nanoparticles (of few hundred nanometers in diameter), those we observed by cryo-TEM, SEM and AFM (**Figure 2.5)**.

2.4 Radiation-Induced synthesis of PEDOT/Ag nanocomposites

After synthesis of CPs by reduction we wanted to know if it was possible to synthesis nanocomposites and thus we tried PEDOT/Ag. In literature, PEDOT/Ag nanocomposites have already been successfully synthesized by the means of either chemical or electrochemical methods [62-64] and have also been shown to possess various potential applications.[65-67] According to the synthetic methodologies, two-step method or one-pot method are usually applied to synthesize CPs nanocomposites.[68-69] These latter usually show core shell structure, the composition of which fundamentally depends on the preparation procedure.[70-71]

In fact the use of radiation-induced synthesis of shape controlled silver nanoparticles in aqueous solution has been already conducted by Remita *et al.*[72-73] on one hand, and the radiolytic preparation of nanostructured conducting PEDOT polymers has been realized as

previously highlighted on the other hand.[21, 34] Thus, these two approaches represent good omens for the successful synthesis of PEDOT/Ag composites by radiolysis. Starting from an aqueous solution containing metal ions and EDOT monomers, the use of radiation chemistry for the *in situ* producing hydrated electrons as a reducing species or hydroxyl radicals as an oxidizing species in order to synthesize CPs/metal nanocomposites is certainly feasible.[53]

Based on γ-radiolysis, PEDOT/Ag nanocomposites can simply be prepared by both two-step and one pot method. According to the two-step method, PEDOT polymers are first synthesized by either oxidation ($PEDOT_{ox}$) or reduction ($PEDOT_{red}$) of EDOT monomers and then, PEDOT/Ag nanocomposites are prepared by the further reduction of silver ions into metal nanoparticles. Differently, according to the one pot method, polymerization and metal ions reduction are achieved in parallel, in one step. As lastly previewed in reduction-polymerization route, γ-induced synthesis of $PEDOT_{red}$ proceeds in N_2-saturated aqueous solutions and in the presence of isopropanol. Under these conditions, two short-lived reactive transient species are formed, namely e_{aq}^- and (CH3)2C$^{\bullet}$OH radicals, with corresponding radiolytic yields (G values) which amount to 2.8×10^{-7} mol.J^{-1} and 3.4×10^{-7} mol.J^{-1}.[74] Note that isopropanol radical is a reducing species with a redox potential of -1.8 V_{SHE} at pH = 7 which can quantitatively can act as reducing species towards Ag^+ but which cannot reduce EDOT monomers.[75] Consequently, EDOT is reduced with a radiolytic yield $G_{red}(EDOT) = 2.8 \times 10^{-7} mol.J^{-1}$, while silver ions Ag^+ are reduced by e_{aq}^- and $(CH_3)_2C^{\bullet}OH$, with radiolytic yield: $G((CH_3)_2C^{\bullet}OH) + G_{e_{aq}^-} = G_{red}(Ag^+) = 6.2 \times 10^{-7} mol.J^{-1}$.[76] The ratio between EDOT and Ag was changed in case of pot method, from 10:1 to 10:20, by varying the amount of AgClO4 (from 1 to 20 mM). Whatever the ratio of EDOT to Ag, the aqueous solutions were always added with isopropanol (0.2 M), degassed with N_2 and irradiated at 72 kGy, which enables in all cases the total reduction of both EDOT and Ag^+ and production of $(PEDOT/Ag)_{red}$. Regarding two steps method, PEDOT polymers were first synthesized either by reduction (10 mM in EDOT in N_2-saturated aqueous solutions and in the presence of isopropanol, 0.2 M) or by oxidation of EDOT molecules as demonstrated before (10 mM in EDOT in N_2O-saturated aqueous solutions)[34], and then silver nanoparticles are obtained by reduction of silver ions (10 mM in $AgClO_4$ in N_2-saturated aqueous solutions and in the presence of isopropanol, 0.2M). The formed CPs nanocomposites from these two step methods are so called "$PEDOT_{red}/Ag_{red}$" and "$PEDOT_{ox}/Ag_{red}$". At each step a dose of 36 kGy is delivered to enable the quantitative synthesis of PEDOT/Ag nanocomposites.[53]

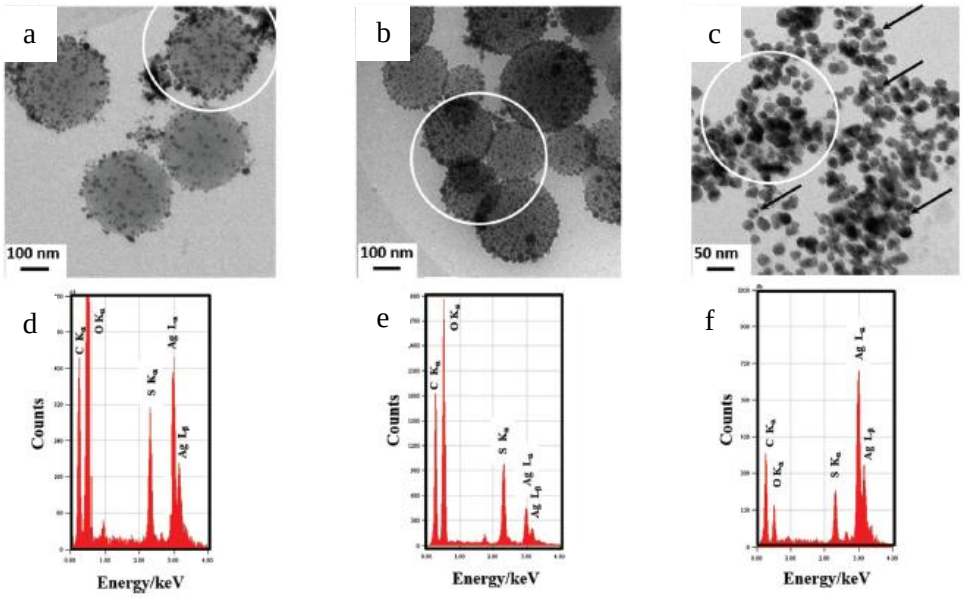

Figure 2.6 Cryo-TEM images of (a) sample containing ($PEDOT_{ox}/Ag_{red}$) synthesized according to two step method, (b) sample containing ($PEDOT_{red}/Ag_{red}$) synthesized according also to two step method and (c) sample containing $(PEDOT/Ag)_{red}$ prepared according to the one-pot. Energy-Dispersive X-ray (EDX) spectra (d), (e) and (f) corresponding to the elemental analysis of the circled areas of the cryo-TEM images.[53]

UV-Vis absorption spectrophotometry, ATR-FTIR spectroscopy (spectra not shown) and EDX spectroscopy (displayed in **Figure 2.6)** [53] have showed that no matter what is the opted procedure, all the prepared nanocomposites are made of PEDOT polymers and silver nanoparticles. More interestingly, they are found to be doped with perchlorate anions.[74] The morphologies of PEDOT/Ag nanocomposites are almost different and depend on the preparation procedure. As can be seen from the presented cryo-TEM images in **Figure 2.6 a** and **b**, the observations made on ($PEDOT_{ox}/Ag_{red}$) and ($PEDOT_{red}/Ag_{red}$) in aqueous solution appear similar. In both cases, representative images show the presence of low density globular structures forming polydisperse spherical nanoparticles with a diameter comprised between 100 and 500 nm. This result is in very good agreement with the observations already made in the case of PEDOT synthesized, alone (in the absence of silver) by radiolysis, either by EDOT oxidation or by EDOT reduction. Thus, these low density globular objects are made of PEDOT polymers. Each globular structure should correspond to the self-assembly of independent amorphous PEDOT chains. As can be seen in **Figure 2.6 a** and **b**, smaller nanoparticles (from few nm to 50 nm), which appear very more contrasted (darker), are systematically found adsorbed onto the bigger globular PEDOT nanoparticles. The relatively high contrast of these small particles suggests their metal nature. Since no other objects are

observed during our Cryo-TEM experiments, we suppose that these small spherical nanoparticles are made up of silver.

When it comes to $(PEDOT/Ag)_{red}$ formed by one pot method, the structure and morphology shown in **Figure 2.6 c**, appear as granular mixtures. This observation is totally different from those obtained in case of ($PEDOT_{ox}/Ag_{red}$) and ($PEDOT_{red}/Ag_{red}$). Indeed, **Figure 2.6 c** shows the presence of low density globular structures forming polydisperse spheroidal nanoparticles with a diameter between 10 and 50 nm. These organic particles, made of PEDOT polymers and obtained via the one-pot method, are ten times smaller than the PEDOT nanoparticles obtained via the two-step method. On the other hand, as can also be observed of in **Figure 2.6 c** smaller nanoparticles, which appear much more contrasted (darker), are found to be embedded into the core of the bigger globular PEDOT nanoparticles. Some of these dark nanoparticles are indicated in the figure by arrows. The relatively high contrast of these smaller particles suggests once again that they are made of silver

During Cryo-TEM observations, *in situ* Energy-Dispersive X-ray (EDX) spectroscopy was used to check the chemical composition of radiosynthesized materials in order to prove the presence of sulfur atoms (which are only present in PEDOT polymers, one sulfur atom per EDOT molecule) and of silver atoms (which would be the signature of silver nanoparticles). The aim was also to check the molar ratio between both atoms in radiosynthesized PEDOT/Ag composites. EDX spectra (**Figure 2.6**, spectra **a**, **b** and **c**) which correspond respectively to the elemental analysis of the surrounded areas of cryo-TEM images of **Figure 2.6 a**, **b** and **c**, highlight the presence, in all samples, of the following chemical elements: O (Kα 0.525 keV), C (Kα 0.277 keV), S (Kα 2.31 keV) and Ag (Lα 2.98 keV and Lβ 3.15 keV). The presence of oxygen and carbon atoms is related to the presence of PEDOT polymers. Nevertheless, their preponderance in EDX spectra is certainly due to the ice which surrounds all the observed nanomaterials and to the carbon-coated grid itself (which is used for Cryo-TEM observations). Contrarily to oxygen and carbon atoms, the detection of sulfur and silver elements definitely demonstrates, as expected, the concomitant presence, in the analyzed areas of images a, b and c of **Figure 2.6**, of both PEDOT polymers and silver nanoparticles.

To estimate S and Ag atomic percentages in the surrounded areas of **Figure 2.6**, a quantitative analysis was performed. It was found 39 % S and 61 % Ag in spectrum a, 67 % S and 33 % Ag in spectrum b and 21 % S and 79 % Ag in spectrum c. Even if these percentages are not far from those expected (50 % S and 50 % Ag) starting from 10 mM in EDOT and 10 mM in $AgClO_4$, they were found to be dependent on the analyzed area. In fact, sulfur and silver were systematically detected in all the nanoparticles observed by cryo-TEM.

But their atomic percentage was found to vary from 20 % to 80 %. Note that sulfur and silver atoms were only observed into the nanomaterials and were never found in the surrounding aqueous medium. As demonstrated by cryo-TEM microscopy and EDX spectroscopy, composites prepared by two-step method are made of large spherical PEDOT nanoparticles at the surface of which smaller silver nanoparticles adsorb.

Due to the two-step method used to produce ($PEDOT_{ox}/Ag_{red}$) and ($PEDOT_{red}/Ag_{red}$), PEDOT polymers are first synthesized, in the absence of inorganic ions, and self-assemble thanks to Van der Waals interactions into globular organic nanoparticles. Silver nanoparticles are formed only during the second step. This explains their presence outside PEDOT nanoparticles. Nevertheless, in spite of all our cryo-TEM investigations, metal nanoparticles are never found isolated in the aqueous phase. They are always found adsorbed onto PEDOT spherical nanostructures. Maybe, during the second step, silver nanoparticles are radiolytically synthesized in the bulk of the aqueous solution and then diffuse and adsorb at the surface of PEDOT thanks to weak Van der Waals interactions. But, more probably, prior to irradiation, silver ions first strongly interact with PEDOT particles and bind, as soft Lewis acids, with the sulfur atoms (soft Lewis bases) present all along the polymer chains. These coordinated silver ions are further reduced in the vicinity of PEDOT nanoparticles.

By contrast, in the one-pot method, silver ion reduction takes place in parallel with EDOT reduction. Then, since silver reduction is faster than that of EDOT as demonstrated in our work[53], metal nanoparticles can form prior to the existence of the PEDOT nanoparticles. As shown in **Figure 2.6**, image c, all silver nanoparticles are found surrounded by an organic shell. This could mean that EDOT reduction and polymerization occur in the vicinity of silver nanoparticles. Such a growth mechanism could be explained by the strong interaction which exists between silver ions (or even atoms) and the sulfur atoms of the EDOT monomers. Or maybe, PEDOT polymers are formed far from the silver nanoparticles, in the bulk of the aqueous solution, and then diffuse and adsorb at their surface, due to weak van der Waals interactions, enabling the thermodynamic stabilization of silver particles and avoiding their aggregation and sedimentation. This effect of polymers on silver nanoparticles has already been reported in the literature.[77]

SEM was also used as another corroboratory tool to verify the nanostructure of PEDOT/Ag nanocomposites.[53] In case of ($PEDOT_{ox}/Ag_{red}$) and ($PEDOT_{red}/Ag_{red}$), the composite nanoparticles observed using SEM after deposition are polydisperse in size with a diameter comprised between 100 and 500 nm. These SEM observations agree well with the size and the shape of the ($PEDOT_{ox}/Ag_{red}$) and ($PEDOT_{red}/Ag_{red}$) particles previously

observed in aqueous solution using cryo-TEM (**Figure 2.6,** images **a** and **b**). In contrast to these observations made on ($PEDOT_{ox}/Ag_{red}$) and ($PEDOT_{red}/Ag_{red}$), respectively, no spherical nanoparticles were observed in case of $(PEDOT/Ag)_{red}$, which may be due to the fact that their relatively small size avoids their observation during SEM microscopy. In fact, SEM characterization shows that the $(PEDOT/Ag)_{red}$ composites become a compact hybrid after deposition. Also, when varying the EDOT/Ag ratio, from 10:5 to 10: 20, as the proportion of silver increases, the $(PEDOT/Ag)_{red}$ composites become denser and form more compact blocks.

2.5 The electrical and physical properties of radio-synthesized CPs in aqueous solution

The importance of radiation induced polymerization is to achieve effective and simple synthesis of processable and usable forms of conducting polymer. The radiation based methodology that is evolved by *Remita's et al*, is certainly the appropriate technique for promising production of CPs. As previewed, the methodology is versatile and reliable. Interestingly though the radiation induced synthesis methodology necessitates more researches to parallel the current requirements, the radio-synthesized material are comparable to materials that were obtained by commonly used methods, in terms of physical and electrical properties.

One of the most important properties that recognize the polymers is generally their molecular weight. Indeed, the presence of long polymer chains, or more precisely having high $\pi-\pi^*$ conjugation gives CPs their remarkable electrical properties. Thus, I chose to use size exclusion chromatography analysis (SEC) in order to characterize the molecular weight and the chain length for the radio-synthesized conducting polymers. Another important property of CPs is their electrochemical characterization. Thus, I highlighted the electrochemical behaviors of some polymers synthesized by radiation based method in aqueous solutions by using cyclic voltammetry analysis and optical band gap E_g (optical) calculations. The CV analysis enabled the determination of oxidation and reduction potentials of radio-synthesized polymers and thus the estimation of the energy level of the highest occupied molecular orbital (HOMO) from the ionization potential, the energy level of the lowest unoccupied molecular orbital (LUMO) from the electronic affinity, as well as the electronic band gap E_{gap}. In addition, the electrical conductivity of the radio-synthesized CPs and CPs nanocomposites measured by using the four-point probe technique was also checked and compared with the electrical conductivities reported in literature of CPs synthesized by conventional methods.

Lastly, I highlighted the physical properties of the radio-synthesized CPs and CPs nanocomposites in aqueous by using thermogravimetric analysis (TGA).

2.5.1 SEC analysis

The weight average molecular weight (Mw) and the molar mass at the maximum peak (Mp) of some processable CPs obtained with a polystyrene calibration and were estimated from Size exclsion chromatography (SEC). The SEC data of 3 $mg.mL^{-1}$ in THF of these radiosynthesized conducting polymers in aqueous solutions are displayed in **table 2.1**. Mw and Mp were found to be 2630 (~18 units) and 1297 (~9 units) $g.mol^{-1}$for the PEDOT-OH, 4145 (~29 units) and 2484 $g.mol^{-1}$ (~17 units) for $PEDOT_{red}$ and 1423 (~10 units) and 1128 (~8 units) $g.mol^{-1}$ for PEDOT (at pH 0).

SEC data shows that all the radio-synthesized polymers have reasonable molecular weight. However, the obtained molecular weights are not approximate. If we look at the molecular weight at Mp, $PEDOT_{red}$ radiosynthesized polymers have clearly the highest value among the other. Nevertheless, the solubility of these radiosynthesized PEDOT (PEDOT-OH, $PEDOT_{red}$ and PEDOT at pH 0) are not the same in THF solvent. As a consequence, a more likely reason of SEC findings is the poor solubility of the prepared polymers in THF which prevents complete solubilization of the polymers with higher molecular weight.

2.5.2 Optical and electronic band gaps

The electronic and optical band gap E_{gap} of radiosynthesized PEDOT polymers (PPy, PEDOT-OH, PEDOT-N_3, $PEDOT_{red}$ and PEDOT at pH 0) are shown in **table 2.2**. Note that the cyclic voltammetry measurements were carried out only on PEDOT at pH 0. As a consequence, the cyclic voltammetry measurements enabled us to calculate the electronic energy band gap (E_{gap}) of PEDOT at pH 0 that amounts to 1.04 eV, while the UV-Vis absorption spectrum (see Figure 2.4 spectrum a) enable us to calculate the optical energy band gap that amounts 1.14 eV. In case of the other radiosynthesized CPs, the optical energy band gaps were calculated from the UV-Vis absorption spectra obtained in previous work[34, 45, 61] and amount to 1.90 eV for PPy, 2.00 eV for PEDOT-OH, 2.30 eV for PEDOT-N_3 and 1.90 eV for $PEDOT_{red}$. As seen from table 1.2, the radio-synthesized PEDOT polymers that obtained by reduction-polymerization route ($PEDOT_{red}$) present lower optical band gap in comparison to radio-synthesized PEDOT polymers obtained by oxidation polymerization route (PPy, PEDOT-OH and PEDOT-N_3). This difference is evidently originated from the fact the $PEDOT_{red}$ are characterized by higher molecular weight (see table 3.1) than PEDOT-OH and PEDOT-N_3 polmyers. Interestingly, the radiosynthesized polymers in very acidic medium

(PEDOT at pH 0) represent the lowest optical and electrical band gaps in comparison to the other radiosynthesized CPs despite its low molecular weight. Moreover, these E_{gap} (electronic and optical) values are attributed to the *in situ* doping by Cl^- ions.[49] However, these results are incompatible with SEC data. A more likely reason of these findings is that because of poor solubility of the prepared polymers prevents the detection by SEC of polymers with higher molecular weight.

Polymer	**Optical band gap E_g(optical) (ev)**	**Electronic band gap E_g(electronic) (ev)**	**SEC data**	
			Molar mass Mp ($g.mol^{-1}$)	**Weight average molecular weight (Mw) ($g.mol^{-1}$)**
PEDOT-OH	2.00	-	1297 (~9 units)	2630 (~18 units)
PEDOT-N_3	2.30	-	-	-
$PEDOT_{red}$	1.90	-	2484 (~17 units)	4145 (~29 units)
PEDOT (at pH 0)	1.14	1.04	1128 (~8 units)	1423 (~10 units)
PPy	1.90	-	-	-

Table 2.2 Summary of some calculated optical and electronic band gaps for some conducting polymers radio synthesized in aqueous solutions as well as to their analyzed molecular weight by SEC

2.5.3 Electrical conductivities measurements

The electrical conductivities of some radio-synthesized conducting polymers measured using the four-point probe technique are all reported in **Table 2.3**. The electrical conductivities of the radio-synthesized polymers obtained by the all possible radiolytic routes in aqueous solutions were found interestingly remarkable. For instance, the radiosynthesized PPy in N_2O-saturated aqueous solutions has electrical conductivity after doping process equal to 57×10^{-3} S. cm^{-1}.[45] This value was found nearly five times higher than that of chemically synthesized PPy ($\approx 12 \times 10^{-3}$ S. cm^{-1}). The measured electrical conductivities of the radiosynthesized PEDOT in N_2O-saturated aqueous solution ($PEDOT_{ox}$) and radiosynthesized PEDOT in N_2 saturated aqueous solution and in presence of isoprobanol ($PEDOT_{red}$) are 9.8×10^{-3} S.cm^{-1} and 3.4×10^{-3} S.cm^{-1}, respectively.[61] The value found in the case of

$PEDOT_{red}$ is somewhat lower than that of $PEDOT_{ox}$. Note that PEDOT polymers synthesized through accelerated electron also possess remarkable electrical conductivity ($\approx 9 \times 10^{-4}$ S. cm^{-1}). Furthermore, the electrical conductivity of PEDOT/Ag nanocomposites which were prepared according to two-step method or one-pot method, are all in the same order of magnitude (10^{-3} $S.cm^{-1}$) and not far from those values that have been found for $PEDOT_{ox}$ and $PEDOT_{red}$.[53]

Polymer	**Electrical conductivity/S.cm^{-1}**
Radio-synthesized PPy	57×10^{-3}
Chemically synthesized PPy	12×10^{-3}
PEDOT-OH	9.8×10^{-3}
$PEDOT_{red}$	3.4×10^{-3}
PEDOT by accelerated electron	0.9×10^{-3}
$PEDOT_{ox}/Ag_{red}$	3.2×10^{-3}
$(PEDOT/Ag)_{red}$	3.6×10^{-3}
$PEDOT_{red}/Ag_{red}$	5.6×10^{-3}
PEDOT at pH 0	3.3×10^{-3}

Table 2.3 List of electrical conductivities measured by using the four-point probe technique for some CPs nanocomposites and CPs radio synthesized in aqueous solutions.

The conductivity of PEDOT polymers synthesized in very acidic aqueous medium was found to be 3.3×10^{-3} $S.cm^{-1}$, which is of the same order of magnitude as the conductivities of PEDOT we already synthesized by radiolysis in neutral aqueous solutions and remains close to the conductivities reported in literature for PEDOT polymers produced by conventional methods.[56, 78-79] The obtained electrical conductivity findings prove that the radio-synthesized materials are certainly semiconductors and no doubt about their implementation in practical applications.

2.5.4 Physico-chemical properties

In this paragraph I summarized the physico-chemical properties of radiosynthesized CPs and CPs nanocomposites in aqueous solutions analyzed by TGA. The TGA analysis of $PEDOT_{red}$ polymers and their degradation processes were found quite similar for PEDOT polymers synthesized by oxidation-polymerization. In case of PEDOT/Ag composites, TGA

revealed that all are characterized by the same thermal stability, which remains higher, over a wide range of temperatures, than that of pure PEDOT polymers synthesized in aqueous solutions by both radiolytic routes (oxidation and reduction). Also, the TGA analysis showed that the thermal stability can be enhanced by increasing the amount of silver into the composites. In case of PPy, a comparative study has been carried out between chemical synthesized PPy by using $K_2S_2O_8$ as oxidant and radiosynthesized conducting PPy in aqueous solutions under N_2O. TGA analysis showed that both PPy polymers possess comparable and good thermal stability.[45] Moreover, the TGA analysis was found in very good agreement with TGA data already reported in the literature concerning PPy polymers.[80]

2.6 Comparative studies between radiolytic methodology in aqueous solutions and conventional methodologies

In these studies that have been performed on PEDOT and PPy polymers, we were able to prove their very good properties, in comparison with the ones that obtained by chemical and electrochemical methods. According to the comparative study between radio-synthesized conducting PEDOT in aerated aqueous solutions and electro-synthesized one (100 mM $LiClO_4$)[21], both polymers showed comparable UV-visible spectral features and capacitive current behavior in the cyclic voltammetry analysis.[21] In case of UV-visible absorption spectroscopy, the electrosynthesized and radiosynthesized PEDOT films were characterized onto ITO substrate. The recorded absorption spectrum of radiosynthesized PEDOT looks like that of electrochemically synthesized PEDOT polymers. Both spectra display an intense absorption band at 550 nm in addition to a shoulder around 750 nm. This result is in agreement with the fact that polymer films which are characterized by longer conjugation lengths in the solid state absorb at higher wavelengths than oligomers in solution.[81] This result is also in agreement with absorption spectra of solid films of doped polythiophenes which are characterized by absorption maxima in the region 480–520 nm.[81] Thus, the similarity in the spectra of both radiosynthesized and electrosynthesized PEDOT polymers definitely demonstrates that we succeeded in the radiation induced synthesis of PEDOT polymers which are doped.[21] Another study has been performed between chemically synthesized PPy by using $K_2S_2O_8$ as oxidant and radiosynthesized conducting PPy in aqueous solutions under N_2O. In this study, the observed optical properties by UV-Vis absorption spectroscopy for both PPy polmyers were more or less share the same spectral features.[45] As mentioned earlier in this chapter, these radiosynthesized PPy polymers were characterized by a very good thermal

stability and an electrical conductivity that is 5 times higher than that of chemically synthesized PPy.[45]

2.7 Towards radiation-Induced synthesis of conducting polymers in organic solvents

All what previously has been done was in water (oxidation, reduction, changing atmosphere, and changing oxidizing species), so what about changing the solvent. This is important for instance in order to synthesize CPs starting from hydrophobic monomers such as 3-hexylthiphene (3HT). The extension of original radiolytic methodology to the use of organic solvents is a need since radiation-induced polymerization in aqueous solution cannot always be used. In fact, there are several obstructions that have been faced with γ-radiolysis of aqueous solutions, such as the poor processability, low solubility and even sometimes the insolubility of some of concerned monomers, namely 3, alkylthiophenes. In this part, we wanted to check in which organic solvent would be easier to work. To check the solvents, we decided to use 3HT monomers which are insoluble in water but soluble in many organic solvents (see chapter 1, figure 1.5)

Initially, the polymerization of P3HT was studied in aqueous solution starting from 3HT (20 mM) in the presence of surfactants (200 mM SDS) under N_2O. The UV-Vis absorption spectrum of the irradiated aqueous solution is quite different from the spectrum before irradiation (**Figure 2.7 A**). After irradiation, a shoulder clearly appears around 300 nm and, furthermore, the resulted solution was almost pale yellow (Insert of **Figure 2.7 A**). This shoulder was also observed when using different concentrations in 3HT in the same solvent. It is ascribed to the formation of oligomers of P3HT. Nevertheless, P3HT polymers with long chains and high molecular weight, which are characterized by absorption at higher wavelength, were never observed. This is not due to their insolublitiy in water since no deposition nor suspension were observed. In order to check whether chemical method leads to the synthesis of P3HT in aqueous solution in the presence of SDS and in order to compare the obtained results with those obtained by radiolysis, we tried to polymerize 3HT (20 mM) chemically by using iron chloride (60 mM) as oxidant in the presence of SDS surfactants. As in the case of radiolytic method, the obtained solution and the recorded UV-Vis absorption spectra as well did not show any formation of P3HT polymers. This result could be explained as follows: 3HT monomers are hydrophobic and remain encapsulated into SDS micelles. Since iron ions (in case of chemical method) are hydrophilic and since $HO^{\bullet}$ radicals (in case of radiolytic method) are formed from water molecules, outside the micelles, one can suppose that the oxidation of 3HT is not efficient. On the other hand, due to the relatively high

concentration of SDS, in comparison with that of 3HT, the probability of the oxidation of SDS by $HO^{\bullet}$ radicals under N_2O is certainly higher than that of organic monomers.

Since, no way to synthesize P3HT in water even in presence of surfactant, γ-radiolysis of many organic solvents was investigated in presence of 3-hexylthiophene (3HT). Furthermore, changing the solvent should presumably enable to tune the morphology through polymer functionalization, and subsequently to adjust polymers physio-chemical properties. At the outset of this study, a solubility test was checked for 3HT in many solvents. In ethanol, 3HT showed quite good solubility in ethanol solvent (higher than 50 mM) with high molar extinction coefficient (ε_{238}= 3460 $cm^{-1}.mol^{-1}$). We first tried in ethanol since many organic polymers have already been synthesized by ethanol radiolysis in literature.[82-83] In order to induce P3HT polymerization in ethanol under N_2O, and since the exact radiolytic yields of the primary radicals are not well known in these conditions, we chose to use the same conditions, which were used in aqueous systems. Thus, we irradiated ethanol solutions containing 20 mM in 3HT at 72 kGy. The recorded UV-Vis absorption spectrum did not indicate any formation of P3HT after irradiation (**Figure 2.7 B**). Only a slight increase of the absorbance was observed at 238 nm. We then concluded that the radicals formed by ethanol radiolysis, such as $O_2^{\bullet -}$ do not allow 3HT oxidation. Maybe their redox potentials are too low. Therefore, the polymerization of P3HT under these conditions seems inappropriate.

To proceed further with our endeavors to gamma-induced polymerization in an organic solvent, halo-methanes have been taken into account. Indeed, halo-methanes are very good solvents for many organic compounds and their gamma radiolysis have been widely studied under different conditions. Moreover, γ-irradiation of halo-methane solvents yields several oxidizing species which could enable first the oxidation of dissolved organic monomers and then their polymerization into CPs.

In fact, the use of organic solvent to chemically synthesize CPs was investigated by Koizumi *et al*. who studied the mechanism of oxidative polymerization of conducting polymers in several organic solvents by γ-irradiation.[84] The study was performed on 3-octylthiophene, 3OT, and the oxidative polymerization initiated by γ-radiolysis of chloroform, hexane and neat monomer solution. The polymerization was successfully induced in chloroform. The study showed that, the products contain large amount of small oligomers, and the yield of polymers with high molecular weight was found low. Furthermore, high irradiation dose and removal of the oligomers was shown to be necessary to obtain usable polymers for any potential applications.

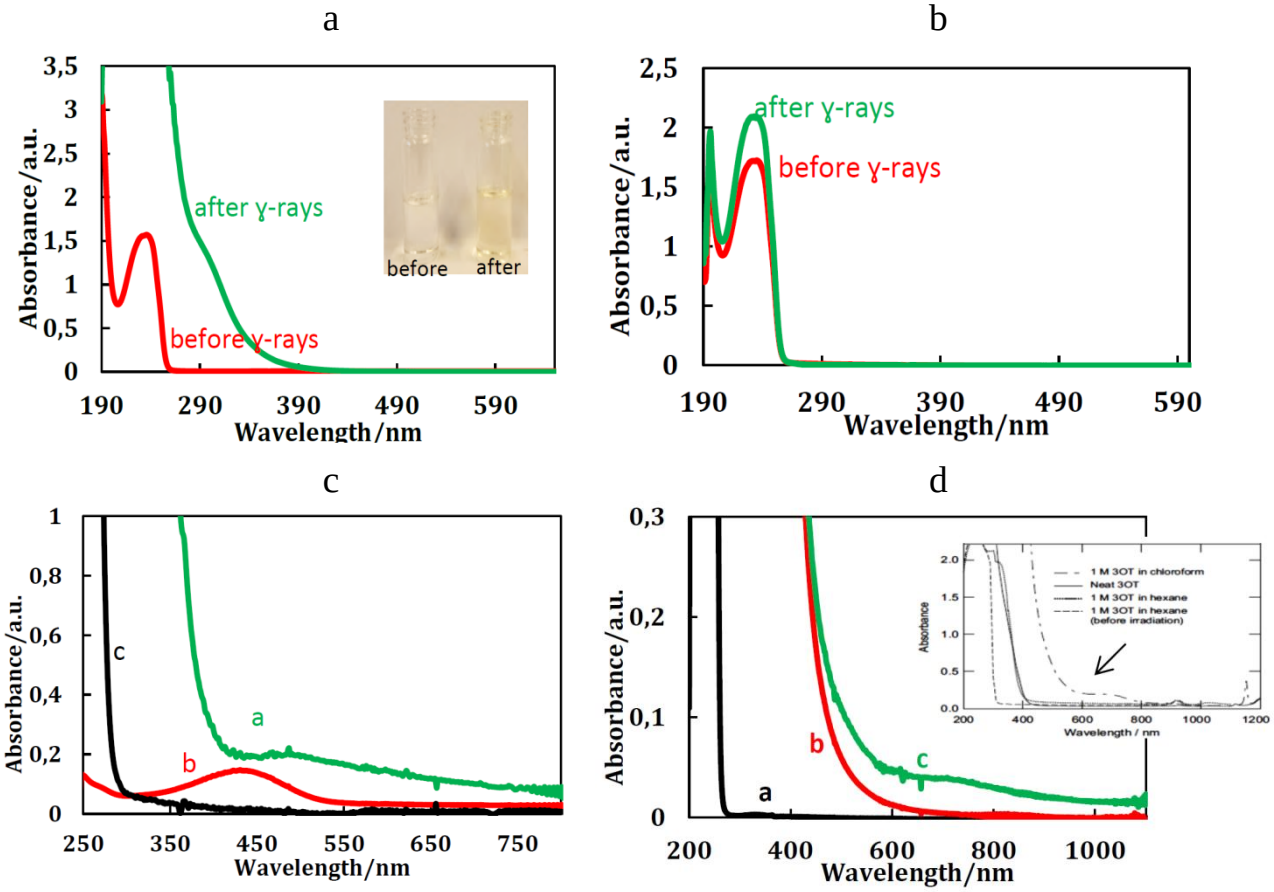

Figure 2.7 UV-Vis absorption spectra of **(A)** 20 mM in 3HT in water in presence of a surfactant (200 mM SDS) under N_2O before and after ɣ-irradiation at 72 kGy, dilution: 4 times. The reference: was water+SDS. In insert, photo of the solutions before and after irradiation **(B)** 20 mM in 3HT in ethanol before and after γ-irradiation at 72 kGy under N_2O, dilution: 5 times. The reference: was ethanol **(C)** 50 mM in 3HT in CCl_4 solvent: (a) by radiolysis under N_2 at 106 kGy (b) by chemical method with $FeCl_3$ (c) before irradiation. The reference: was CCl_4. **(D)** 50 mM in 3HT in $CHCl_3$ and CH_2Cl_2 solvents under N_2: (a) before irradiation (b) radiosynthisized P3HT in $CHCl_3$ (c) radiosynthisized P3HT in CH_2Cl_2. The reference: pure solvent. Insert D: absorption spectra of radiosynthesized 3OT in several organic solvents. Path length: 2 mm.

The solubility tests showed that 3HT has quite good solubility in halo-methane solvents (more than 50 mM in CCl_4, $CHCl_3$ and CH_2Cl_2) and high molar extinction coefficient (ε_{238} (CH_2Cl_2) = 5570 $cm^{-1}.mol^{-1}$, $\varepsilon_{251}(CCl_4)$= 4338 $cm^{-1}.mol^{-1}$ and $\varepsilon_{238}(CHCl_3)$= 4506 $cm^{-1}.mol^{-1}$). As a consequence, we decided to use halo-methane solvents (CCl_4, $CHCl_3$ and CH_2Cl_2) to induce P3HT polymerization. Evidently, we varied the atmosphere (presence of N_2O, O_2, N_2 or Ar), the concentration in 3HT, the dose rate, as well as the irradiation dose (From 36 kGy to 106 kGy). After irradiation and whatever the solvent used, the obtained solutions became yellow. Nevertheless, at higher dose and higher 3HT concentration, the solutions were always darker, certainly due to the presence of high number of P3HT polymers with increased

molecular weight. For instance we irradiated a CCl_4 solution containing 50 mM in 3HT under N_2 at a dose of 106 kGy. The UV-Vis absorption spectrum obtained after irradiation which is different from that of 3HT monomers (spectrum a **Figure 2.7 C**) exhibits a weak absorption band between 450 and 600 nm (Spectrum b, **Figure 2.7 C**). In order to chemically identify the species which absorb in this wavelengths region, we evaporated the solvent and characterized the obtained glutinous material by ATR-FTIR spectroscopy (Results not shown). The IR spectrum was found consistent with that of P3HT given in literature.[85] We then concluded that γ-radiolysis of CCl_4 solution led to the formation of P3HT polymers.

For comparison, we also synthesized P3HT in CCl_4 by chemical method thanks to the use of iron chloride (3.5 mM in $FeCl_3$). The absorption spectrum obtained in this case (Spectrum c, **Figure 2.7 C**) is also different. The difference in the absorption spectra of the differently synthesized P3HT polymers could be also due to their different chain length or to their doping level. According to the obtained spectra and, in comparison with the reported results in literature [84], we can deduce that 3HT was polymerized by radiolysis under the studied conditions. Indeed, $Cl^{\bullet}$ and $CCl_3^{\bullet}$ radicals (see chapter 1, table 1.3) are known as strong oxidizing species, where the redox potential of $Cl^{\bullet}$ is estimated to be about 2.59 V_{SHE}.[86] However, studying the polymerization of P3HT in CCl_4 did not proceed for further investigation due to the toxicity of this solvent.

In parallel, we performed the same experiments in $CHCl_3$ and CH_2Cl_2 solvents. Solutions of 50 mM in 3HT were once again prepared under N_2 and irradiated at 106 kGy. In both solvents, the obtained solutions obtained after irradiation have the same color as that of the commercial P3HT solution. The UV-Vis absorption spectra of P3HT polymers synthesized in $CHCl_3$ and CH_2Cl_2 solvents are displayed in **Figure 2.7 D** (spectra b and c respectively). The two spectra exhibit an absorption band (more pronounced in case of CH_2Cl_2), which is red-shifted in comparison with that of P3HT in CCl_4. Interestingly, the irradiated sample in CH_2Cl_2 exhibits a shoulder with an absorbance maximum around 750 nm. These results are in good agreement with a recent study on radiation induced polymerization of 3OT [84] (Insert of **Figure 2.7 D**), where P3OT polymers were found to absorb at the same wavelength. The absorption spectra obtained in our case are then attributed to the formation of P3HT polymers.

In order to confirm the polymerization of 3HT and to characterize the obtained polymers, infrared spectra were recorded for monomers of 3HT, commercial P3HT and radiosynthesized P3HT in all the previously described conditions but we chose to present only some of the more representative data. The IR spectra obtained in the case of radiosynthesized P3HT in CH_2Cl_2, commercial P3HT and 3HT monomers are displayed in **Figure 2.8**.

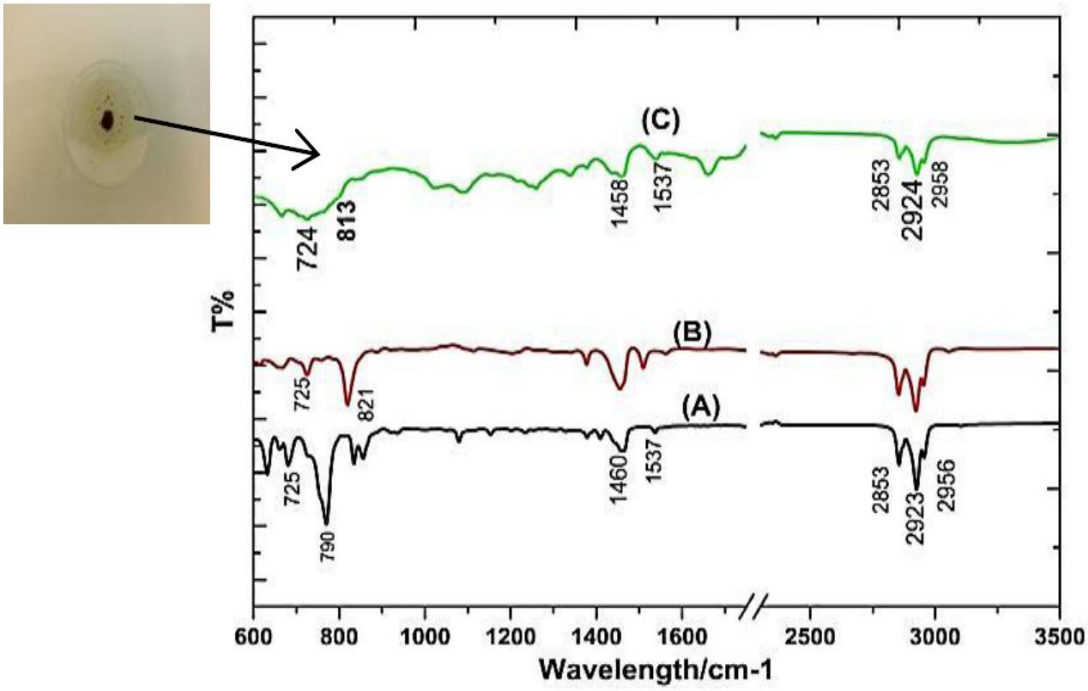

Figure 2.8 ATR-FTIR spectra of: a) pure 3HT- b) commercial P3HT- c) P3HT synthesized in CH_2Cl_2 solvent in presence of 50 mM in 3HT by γ-radiolysis after irradiation at 106 kGy under N_2. Insert, photo of radiosynthesized P3HT polymers after solvent evaporation.

Table 2.4 displays the absorption modes and the positions of the representative peaks of 3HT monomers and P3HT polymers. The IR spectrum of 3HT monomers (**Figure 2.8,** spectrum A) shows several distinguishable absorption peaks which are represented by: the stretching vibration of C=C bond between 1450-1460 cm^{-1}; the aliphatic C–H stretches at 2956, 2923 and 2853 cm^{-1}; The bands at 790 and 833 cm^{-1} are attributed to the =C-H in-plane and out-of-plane deformation vibration modes of 3HT; The peak at 723 cm^{-1} is the characteristic absorption on the in-planeand out-of-plane rocking vibration of $-(CH2)_n-$. The IR spectrum obtained in the case of commercial P3HT is shown in **Figure 2.8,** spectrum B. In comparison with the IR spectrum of 3HT monomers, P3HT polymers have the same main characteristic bands in its spectrum. The band around 1664 cm^{-1} is attributed to carbonyl groups that formed due to the overoxidation of P3HT polymers. However, the out-of-plane aromatic -C-H absorption peaks are weaker and less intense in case of P3HT polymers, which is ascribed to the fact that 3HT monomers have more aromatic C-H bonds than that ones in P3HT polymers. It is worth mentioning that, these spectra will be once again described in details chapter 5. All in all, the IR spectrum obtained in case of radiosynthesized P3HT in

CH_2Cl_2 (**Figure 2.8,** spectrum C) was found in agreement with IR spectrum of commercial P3HT polymers and with the reported ones in literature [85].

According to the obtained data from UV-Vis absorption spectra and IR spectra, we vouched the formation of P3HT polymers thanks to CCl_4, $CHCl_3$ and CH_2Cl_2 solvents radiolysis.

Functional group	Position (cm^{-1})
C=C (symmetric stretching mode)	1450 and 1460
-C-H (symmetric and asymmetric Stretching vibration)	2956, 2923 and 2853
$-(CH_2)_n-$ (in-planeand and out-of-plane rocking vibration)	724 and 725
C-S-C (stretching vibrations)	678
=C-H (in-plane and out-of-plane deformation vibrations)	790 and 833

Table 2.4 ATR-FTIR absorption peaks of 3HT and P3HT polymers

Earlier, we described the gamma radiolysis of CCl_4, $CHCl_3$ and CH_2Cl_2 under N_2 (Table 1.3). The interaction of γ-rays with these solvents leads to the formation of many strong oxidizing species, in particular solvent radical cations, chlorine radicals and halide alkyl radicals. It was reported in literature that hydrocarbons can be oxidized by chloromethyl radicals [87], which are produced by the radiolysis of $CHCl_3$ and CH_2Cl_2. These radicals are known to react onto hydrocarbon molecules yielding to the formation of radical cations. On the base of what we know concerning the reactivity of $HO^{\bullet}$ radicals onto EDOT molecules, we can propose that cations of 3HT are first produced by the interaction of chlorine radicals and halide alkyl radicals with 3HT then these produced radical cations react with each other according to a step by step reaction leading to polymers of P3HT. Thus, the UV-vis absorption spectra as well as ATR-FTIR characterizations enabled us to claim that we succeeded in the synthesis of P3HT thanks to ɣ-radiolysis, starting from organic solutions of CCl_4, $CHCl_3$ and CH_2Cl_2 containing 50 mM in 3HT. the results and data that came out from CH_2Cl_2 were more encouraging and promising than those obtained with $CHCl_3$. Thus, the study of P3HT synthesis in CH_2Cl_2 will be continued in more details in chapter 5.

Cyro-TEM technique was used for further characterization in solutions of the radiosynthesized polymers of P3HT in CH_2Cl_2 containing 50 mM in 3HT irradiated at 106 kGy. Representative images are shown in **Figure 2.9 A**. In cryo-TEM image, well dispersed nanostructures can be observed. The contrasted objects correspond to nanofibers of P3HT polymers, which is the common structure found in case of regioregular P3HT [88]. After irradiation, CH_2Cl_2 solvent was evaporated and the obtained P3HT was observed by SEM microscopy (**Figure 2.9 B**). **Figure 2.9 B** exhibits SEM image of polymers of P3HT obtained

by γ-radiolysis in CH_2Cl_2 under N_2 after irradiation of 50 mM in 3HT at 106 kGy. The image shows the morphology of curly and well dispersed particles of P3HT. The observed image is in good agreement with SEM images of commercial polymers of P3HT and P3OT polymers described in literature [89]. In order to check whether the morphology of P3HT polymers depends on the solvent used during irradiation, we irradiated at 106 kGy $CHCl_3$ solution containing 50 mM in 3HT under N_2. After irradiation, chloroform was removed and the obtained polymers were observed by SEM (**Figure 2.9 C**). SEM image exhibits soft and flat surface of well dispersed particles of P3HT (**Figure 2.9 C**). These obtained images definitely prove the success of our methodology in polymerization of 3HT.

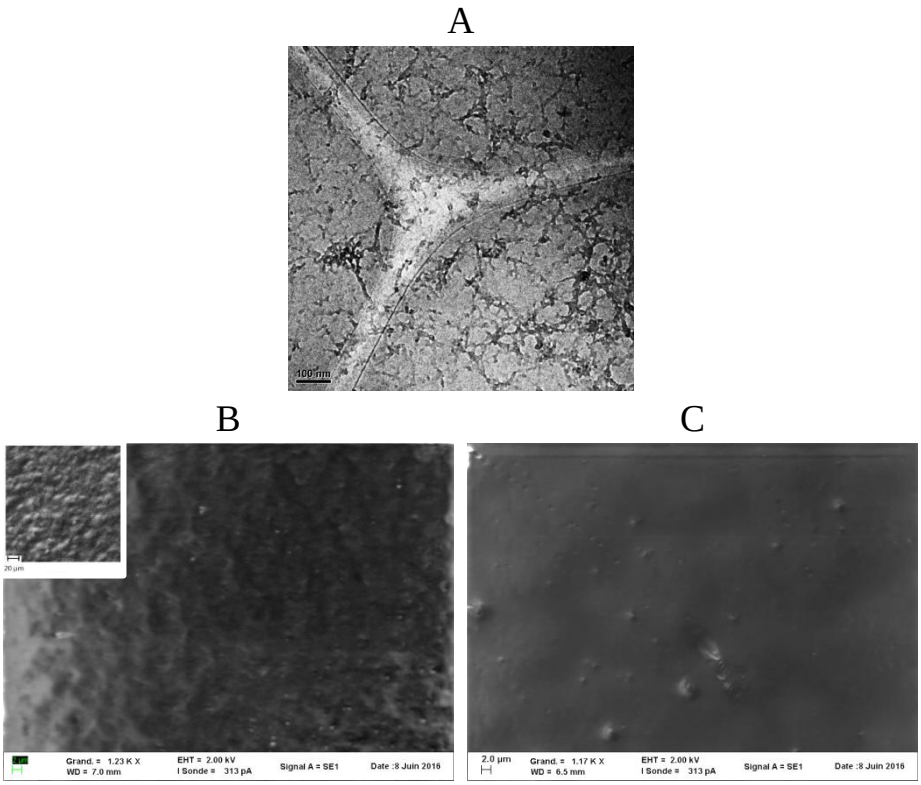

Figure 2.9 Microscopic characterizations by Cryo-TEM and SEM of radiosynthesized P3HT: **(A)** cyro-TEM images of solutions of dichloromethane containing P3HT obtained by CH_2Cl_2 radiolysis under N_2 after irradiation of 50 mM of 3HT at 106 kG **(B)** and **(C)** SEM images of the nanostructures of the radiosynthesized P3HT obtained by (B) γ-radiolysis of CH_2Cl_2 under N_2 after irradiation of 50 mM of 3HT at 106 KGy (C) γ-radiolysis of $CHCl_3$ under N_2 after irradiation of 50 mM 3HT at 106 kGy.

Based on all obtained results concerning P3HT, one can say that radiolysis of water (with SDS) and ethanol do not lead to CPs polymers. However, the findings suggest that irradiation of CCl_4, $CHCl_3$ and CH_2Cl_2 solutions should enable the preparation of CPs. The success in the synthesis of P3HT was demonstrated by spectroscopic analysis represented by UV-Vis

absorption spectroscopy and ATR-FTIR spectroscopy. In addition, the morphology of the polymers was characterized in solution by cyro-TEM microscopy and after deposition by SEM microscopy.

As said before, the findings that obtained from CH_2Cl_2 were more encouraging and promising than those obtained with $CHCl_3$. Thus, in the next chapters I will investigate the synthesis of other conducting polymer in CH_2Cl_2 under different experimental conditions (different atmospheres, different irradiation doses, different dose rates, etc.)

2.8 Summary

According to the work presented in this chapter of Samy Remita's team in which I participated in some parts, synthesis of conducting polymers (CPs) with radiation method (e-beam irradiation and γ-rays irradiation) has been developed by the synthesis of conducting poly (3,4- ethylenedioxythiophene) (PEDOT) in aqueous solutions. Using γ-radiolysis of aerated aqueous solutions of 3,4- ethylenedioxythiophene (EDOT) in the absence of any external chemical initiators, PEDOT polymers were successfully synthesized with spherical appearance. By use of pulse radiolysis, the polymerization mechanism was shown to be a step-by-step oxidation process. By changing the oxidizing species (from $HO^{\bullet}$ and $SO_4^{\bullet -}$ to $N_3^{\bullet}$), PEDOT nanoparticles and nanofibers were prepared using γ-irradiation of aqueous solutions of EDOT degased with N_2O. It is proved that PEDOT-OH polymers self-assemble in aqueous solutions into globular nanostructures thanks to hydrogen-bond interactions. While, PEDOT-N_3 polymers self-assembly should come from π-stacking interactions between conjugated polymers forming fibrillar nanostructures. The versatility of radiolytic method in water has been proved by the successful synthesis of polypyrrole (PPy). The effect of synthetic conditions (pH and soft template) on the polymerization of EDOT has also been reported. The morphology and properties of conducting polymers (CPs) can be affected and adjusted by the synthetic conditions (soft template and pH). Nevertheless, In alkaline medium irradiated EDOT monomers undergo degradation. Spectroscopic studies proved that poly (3,4-ethylenedioxythiophene) (PEDOT) polymers are obtained in reduced state in very acidic medium at pH =0. Furthermore, the radiolytic procedure was extended to the synthesis of CPs by the way of a reduction route instead of an oxidation procedure. In these conditions, the polymerization of EDOT is initiated by hydrated electrons (e_{aq}^-) produced from γ-radiolysis of water. In aqueous solution, the preparation of PEDOT/Ag composites, made of PEDOT

conducting polymers and silver nanoparticles, was achieved by using different radiolytical procedures.

All the radio-synthesized polymers are characterized by remarkable optical and electrical conductivity and additionally their performance is comparable to other conducting polymers synthesized by chemical or electrochemical methods.

Just lately, our strategy based on radiation chemistry was opened up to the preparation of conducting polymers in organic solvents. A seemingly self-doping process is associated with γ-radiolysis of halo-methanes. However, the improvement of synthetic conditions needs further research.

In order to develop a new radiation-based synthetic method and to study mechanism of oxidative polymerization of CPs in organic solvents, particularly dichloromethane, we need to proceed with further investigations. In particular, controlling the morphology and increasing the molecular weight of the radiosynthesized polymers could enhance their optical and electrical properties of the radiosyntheiszed polymers. In the next chapter, we studied in details all the possible radiolytic routes to synthesize conducting polymers of PEDOT in dichlormethane considering different atmospheres, absorbed dose and dose rates.

References

1. Michael S. Freund BS; Bhavana A. Deore, *Self-Doped Conducting Polymers*. John Wiley & Sons, Ltd 2007; p 1-74.

2. Ruiz, J.; Gonzalo, B.; Dios, J. R.; Laza, J. M.; Vilas, J. L.; León, L. M., Improving the Processability of Conductive Polymers: The Case of Polyaniline. *Advances in Polymer Technology* **2013,** *32* (S1), E180-E188.

3. Heeger, A. J., Semiconducting and Metallic Polymers: The Fourth Generation of Polymeric Materials. *The Journal of Physical Chemistry B* **2001,** *105* (36), 8475-8491.

4. MacDiarmid, A. G., "Synthetic Metals": A Novel Role for Organic Polymers (Nobel Lecture). *Angewandte Chemie International Edition* **2001,** *40* (14), 2581-2590.

5. Gospodinova, N.; Terlemezyan, L., Conducting polymers prepared by oxidative polymerization: polyaniline. *Progress in Polymer Science* **1998,** *23* (8), 1443-1484.

6. Paradee, N.; Sirivat, A., Synthesis of poly(3,4-ethylenedioxythiophene) nanoparticles via chemical oxidation polymerization. *Polymer International* **2014,** *63* (1), 106-113.

7. Zhang, X.; Manohar, S. K., Bulk Synthesis of Polypyrrole Nanofibers by a Seeding Approach. *Journal of the American Chemical Society* **2004,** *126* (40), 12714-12715.

8. Roncali, J., Conjugated Poly(Thiophenes) - Synthesis, Functionalization, and Applications. *Chem Rev* **1992,** *92* (4), 711-738.

9. Tebyetekerwa, M.; Yang, S.; Peng, S.; Xu, Z.; Shao, W.; Pan, D.; Ramakrishna, S.; Zhu, M., Unveiling Polyindole: Freestanding As-electrospun Polyindole Nanofibers and Polyindole/Carbon Nanotubes Composites as Enhanced Electrodes for Flexible All-solid-state Supercapacitors. *Electrochimica Acta* **2017,** *247*, 400-409.

10. Zhang, X. T. Z., J.; Song, W. H.; Liu, Z. F., Controllable Synthesis of Conducting Polypyrrole Nanostructures. *J. Phys. Chem. B* **2006,** *110* (3), 1158–1165.

11. Siju, C. R.; Narasimha Rao, K.; Ganesan, R.; Gopal, E. S. R.; Sindhu, S., Synthesis of poly(3, 4 ethylenedioxythiophene) nano structure using reverse microemulsion polymerization. *physica status solidi c* **2011,** *8* (9), 2739-2741.

12. Zhou, H.; Han, G.; Chang, Y.; Fu, D.; Xiao, Y., Highly stable multi-wall carbon nanotubes@poly(3,4-ethylenedioxythiophene)/poly(styrene sulfonate) core–shell composites with three-dimensional porous nano-network for electrochemical capacitors. *Journal of Power Sources* **2015,** *274*, 229-236.

13. Gupta, B.; Mehta, M.; Melvin, A.; Kamalakannan, R.; Dash, S.; Kamruddin, M.; Tyagi, A. K., Poly (3,4-ethylenedioxythiophene) (PEDOT) and poly (3,4-ethylenedioxythiophene)-few walled carbon nanotube (PEDOT-FWCNT) nanocomposite

based thin films for Schottky diode application. *Materials Chemistry and Physics* **2014,** *147* (3), 867-877.

14. Zhang, X.; Lee, J.-S.; Lee, G. S.; Cha, D.-K.; Kim, M. J.; Yang, D. J.; Manohar, S. K., Chemical Synthesis of PEDOT Nanotubes. *Macromolecules* **2006,** *39* (2), 470-472.

15. Choi, W.; An, T.; Lim, G., Fabrication of conducting polymer nanowire sensor array. *SENSORS, 2009 IEEE* **2009**, 1151-1153.

16. Jang, J.; Yoon, H., Formation Mechanism of Conducting Polypyrrole Nanotubes in Reverse Micelle Systems. *Langmuir* **2005,** *21* (24), 11484-11489.

17. Huang, J., Syntheses and applications of conducting polymer polyaniline nanofibers. *pac* **2006,** *78* (1), 15.

18. Aydın, M.; Durmus, Z.; Kavas, H.; Esat, B.; Sözeri, H.; Baykal, A.; Yılmaz, F.; Toprak, M. S., Synthesis and characterization of poly(3-thiophene acetic acid)/Fe3O4 nanocomposite. *Polyhedron* **2011,** *30* (6), 1120-1126.

19. Brooke, R.; Cottis, P.; Talemi, P.; Fabretto, M.; Murphy, P.; Evans, D., Recent advances in the synthesis of conducting polymers from the vapour phase. *Progress in Materials Science* **2017,** *86*, 127-146.

20. Chapiro, A., Radiation induced polymerization. *Radiation Physics and Chemistry (1977)* **1979,** *14* (1), 101-116.

21. Lattach, Y.; Deniset-Besseau, A.; Guigner, J.-M.; Remita, S., Radiation chemistry as an alternative way for the synthesis of PEDOT conducting Polymers under "soft" Conditions. *Radiation Physics and Chemistry* **2013,** *82*, 44-53.

22. Karim, M. R.; Lee, C. J.; Lee, M. S., Synthesis of conducting polypyrrole by radiolysis polymerization method. *Polymers for Advanced Technologies* **2007,** *18* (11), 916-920.

23. Karim, M.; Jae Lee, C.; Jin Kim, H.; Tauhidul Islam Bhuiyan, M.; Sang Lee, M., Preparation of Buckyball-Shaped Conducting Polythiophene by the Gamma Radiation-Induced Polymerization Method. *Macromolecular Symposia* **2007,** *249-250*, 234-240.

24. Remita, S., [Radiation induced lipid peroxidation: factors which determine the oxidizability of lipids]. *Canadian journal of physiology and pharmacology* **2001,** *79*, 144-53.

25. Remita, S.; Fontaine, P.; Lacaze, E.; Borensztein, Y.; Sellame, H.; Farha, R.; Rochas, C.; Goldmann, M., X-ray radiolysis induced formation of silver nano-particles: A SAXS and UV–visible absorption spectroscopy study. *Nuclear Instruments and Methods in Physics Research Section B: Beam Interactions with Materials and Atoms* **2007,** *263* (2), 436-440.

26. Varmenot, N.; Remita, S.; Abedinzadeh, Z.; Wisniowski, P.; Strzelczak, G.; Bobrowski, K., Oxidation Processes of N,S-Diacetyl-l-cysteine Ethyl Ester: Influence of S-Acetylation. *The Journal of Physical Chemistry A* **2001,** *105* (28), 6867-6875.

27. Attia, J.; Rémita, S.; Jonic, S.; Lacaze, E.; Fauré, M. C.; Larquet, E.; Goldmann, M., Radiation-Induced Synthesis and Cryo-TEM Characterization of Silver Nanoshells on Linoleate Spherical Micelles. *Langmuir* **2007,** *23* (19), 9523-9526.

28. Spinks, J. W. T. W., R. J., An Introduction to Radiation Chemistry. *John Wiley & Sons, Inc.: New York* **1990,** *3*, 251-256.

29. Ferradini, C.; Jay-Gerin, J.-P., La radiolyse de l'eau et des solutions aqueuses : historique et actualité. *Canadian Journal of Chemistry* **1999,** *77* (9), 1542-1575.

30. Ferradini, C.; Jay-Gerin, J.-P., The effect of pH on water radiolysis: A still open question — A minireview. *Research on Chemical Intermediates* **2000,** *26* (6), 549-565.

31. Coletta, C.; Cui, Z.; Archirel, P.; Pernot, P.; Marignier, J.-L.; Remita, S., Electron-Induced Growth Mechanism of Conducting Polymers: A Coupled Experimental and Computational Investigation. *The Journal of Physical Chemistry B* **2015,** *119* (16), 5282-5298.

32. Buxton, G. V.; Greenstock, C. L.; Helman, W. P.; Ross, A. B., Critical Review of rate constants for reactions of hydrated electrons, hydrogen atoms and hydroxyl radicals (·OH/·O− in Aqueous Solution. *Journal of Physical and Chemical Reference Data* **1988,** *17* (2), 513-886.

33. Lattach, Y.; Garnier, F.; Remita , S., Influence of Chemical and Structural Properties of Functionalized Polythiophene-Based Layers on Electrochemical Sensing of Atrazine. *ChemPhysChem* **2012,** *13* (1), 281-290.

34. Lattach, Y.; Coletta, C.; Ghosh, S.; Remita, S., Radiation-Induced Synthesis of Nanostructured Conjugated Polymers in Aqueous Solution: Fundamental Effect of Oxidizing Species. *ChemPhysChem* **2014,** *15* (1), 208-218.

35. Belloni, J.; Monard, H.; Gobert, F.; Larbre, J. P.; Demarque, A.; De Waele, V.; Lampre, I.; Marignier, J. L.; Mostafavi, M.; Bourdon, J. C.; Bernard, M.; Borie, H.; Garvey, T.; Jacquemard, B.; Leblond, B.; Lepercq, P.; Omeich, M.; Roch, M.; Rodier, J.; Roux, R., ELYSE—A picosecond electron accelerator for pulse radiolysis research. *Nuclear Instruments and Methods in Physics Research Section A: Accelerators, Spectrometers, Detectors and Associated Equipment* **2005,** *539* (3), 527-539.

36. Marignier, J. L.; de Waele, V.; Monard, H.; Gobert, F.; Larbre, J. P.; Demarque, A.; Mostafavi, M.; Belloni, J., Time-resolved spectroscopy at the picosecond laser-triggered electron accelerator ELYSE. *Radiation Physics and Chemistry* **2006,** *75* (9), 1024-1033.

37. Coletta, C., Study of growth mechanism of conducting polymers by pulse radiolysis. *PhD thesis* **2016,** *1* (37).

38. Coletta, C.; Cui, Z.; Dazzi, A.; Guigner, J.-M.; Néron, S.; Marignier, J.-L.; Remita, S., A pulsed electron beam synthesis of PEDOT conducting polymers by using sulfate radicals as oxidizing species. *Radiation Physics and Chemistry* **2016,** *126*, 21-31.

39. Saunders, B. B.; Kaufman, P. C.; Matheson, M. S., Reactions of thiophene with radiolytically produced radicals. 1. The hydroxyl radical. *The Journal of Physical Chemistry* **1978,** *82* (2), 142-150.

40. Bhattacharya, A.; Amitabha, D.; Mandal, P. C., Carbonate radical induced polymerisation of pyrrole: A steady state and flash photolysis study. *Journal of Radioanalytical and Nuclear Chemistry* **1998,** *230* (1), 91-95.

41. Randriamahazaka, H.; Noël, V.; Chevrot, C., Nucleation and growth of poly(3,4-ethylenedioxythiophene) in acetonitrile on platinum under potentiostatic conditions. *Journal of Electroanalytical Chemistry* **1999,** *472* (2), 103-111.

42. Kvarnström, C.; Neugebauer, H.; Blomquist, S.; Ahonen, H. J.; Kankare, J.; Ivaska, A., In situ spectroelectrochemical characterization of poly(3,4-ethylenedioxythiophene). *Electrochimica Acta* **1999,** *44* (16), 2739-2750.

43. Bazzaoui, E. A.; Aeiyach, S.; Lacaze, P. C., Electropolymerization of bithiophene on Pt and Fe electrodes in an aqueous sodium dodecylsulfate (SDS) micellar medium. *Synthetic Metals* **1996,** *83* (2), 159-165.

44. Irwin, M. D.; Roberson, D. A.; Olivas, R. I.; Wicker, R. B.; MacDonald, E., Conductive polymer-coated threads as electrical interconnects in e-textiles. *Fibers and Polymers* **2011,** *12* (7), 904.

45. Cui, Z.; Coletta, C.; Dazzi, A.; Lefrançois, P.; Gervais, M.; Néron, S.; Remita, S., Radiolytic Method as a Novel Approach for the Synthesis of Nanostructured Conducting Polypyrrole. *Langmuir* **2014,** *30* (46), 14086-14094.

46. Tehrani, P.; Kanciurzewska, A.; Crispin, X.; Robinson, N. D.; Fahlman, M.; Berggren, M., The effect of pH on the electrochemical over-oxidation in PEDOT:PSS films. *Solid State Ionics* **2007,** *177* (39), 3521-3527.

47. Ouyang, J., Solution-processed PEDOT:PSS films with conductivities as indium tin oxide through a treatment with mild and weak organic acids. *ACS applied materials & interfaces* **2013,** *5* (24), 13082-13088.

48. Yun, D. J.; Jeong, Y. J.; Ra, H.; Kim, J. M.; Park, J. H.; Park, S.; An, T. K.; Seol, M.; Park, C. E.; Jang, J.; Chung, D. S., Effective Way To Enhance the Electrode Performance of Multiwall Carbon Nanotube and Poly(3,4-ethylenedioxythiophene): Poly(styrene sulfonate) Composite Using HCl–Methanol Treatment. *J. Phys. Chem. C* **2016,** *120* (20), 10919-10926.

49. Cui, Z.; Bahry, T.; Dazzi, A.; Bui, T.-T.; Goubard, F.; Remita, S., Conducting polymers synthesized by γ-radiolysis in very acidic aqueous medium. *Radiation Physics and Chemistry* **2019,** *159*, 47-56.

50. Jayson, G. G.; Parsons, B. J.; Swallow, A. J., Some simple, highly reactive, inorganic chlorine derivatives in aqueous solution. Their formation using pulses of radiation and their role in the mechanism of the Fricke dosimeter. *Journal of the Chemical Society, Faraday Transactions 1: Physical Chemistry in Condensed Phases* **1973,** *69* (0), 1597-1607.

51. Elliot, A. J.; Geertsen, S.; Buxton, G. V., Oxidation of Thiocyanate and Iodide Ions by Hydrogen Atoms in Acid Solutions. *J. Chern. Soc., Faraday Trans. I* **1988,** *84* (4), 1101-1112.

52. Schwarz, H. A.; Dodson, R. W., Equilibrium between Hydroxyl Radicals and Thallium(I I) and the Oxidation Potential of OH (aq). *The Journal of Physical Chemistry* **1984,** *88* (16), 3643-3647.

53. Cui, Z.; Coletta, C.; Bahry, T.; Marignier, J.-L.; Guigner, J.-M.; Gervais, M.; Baiz, S.; Goubard, F.; Remita, S., A novel radiation chemistry-based methodology for the synthesis of PEDOT/Ag nanocomposites. *Materials Chemistry Frontiers* **2017,** *1* (5), 879-892.

54. Heuer, H. W.; Wehrmann, R.; Kirchmeyer, S., Electrochromic window based on conducting poly(3,4-ethylenedioxythiophene)-poly(styrene sulfonate). *Adv. Funct. Mater.* **2002,** *12* (2), 89-94.

55. Pei, Q. B.; Zuccarello, G.; Ahlskogt, M.; Ingan, O., Electrochromic and highly stable poly(3,4-ethylenedioxythiophene) switches between opaque blue-black and transparent sky blue. *POLYMER* **1994,** *35* (7), 1347-1351.

56. Rumbau, V.; Pomposo, J. A.; Eleta, A.; Rodriguez, J.; Grande, H.; Mecerreyes, D.; Ochoteco, E., First enzymatic synthesis of water-soluble conducting poly(3,4-ethylenedioxythiophene). *Biomacromolecules* **2007,** *8* (2), 315-317.

57. Jang, J.; Chang, M.; Yoon, H., Chemical Sensors Based on Highly Conductive Poly(3,4-ethylenedioxythiophene) Nanorods. *Advanced Materials* **2005,** *17* (13), 1616-1620.

58. Kitada, K.; Ozaki, S., Reductive Polymerization of Halothiophene. *Polymer Journal* **1995,** *27* (12), 1161-1166.

59. Song, L.; Wang, M.; Cong, Y.; Liu, W.; Ge, X.; Zhang, Z., The mechanism of 60Co γ-ray radiation induced interfacial redox reaction in inverse emulsion and its application in the synthesis of polymer microcapsules. *POLYMER* **2007,** *48* (1), 150-157.

60. Belloni, J.; Mostafavi, M.; Remita, H.; Marignier, J.-L.; Marie-Odile Delcourt, a., Radiation-induced synthesis of mono- and multi-metallic clusters and nanocolloids. *New Journal of Chemistry* **1998,** *22* (11), 1239-1255.

61. Cui, Z.; Coletta, C.; Rebois, R.; Baiz, S.; Gervais, M.; Goubard, F.; Aubert, P.-H.; Dazzi, A.; Remita, S., Radiation-induced reduction–polymerization route for the synthesis of PEDOT conducting polymers. *Radiation Physics and Chemistry* **2016,** *119*, 157-166.

62. Gangopadhyay, R.; De, A., Conducting Polymer Nanocomposites: A Brief Overview. *Chemistry of Materials* **2000,** *12* (3), 608-622.

63. Xu, P.; Han, X.; Zhang, B.; Du, Y.; Wang, H.-L., Multifunctional polymer–metal nanocomposites via direct chemical reduction by conjugated polymers. *Chemical Society Reviews* **2014,** *43* (5), 1349-1360.

64. Armel, V.; Winther-Jensen, O.; Kerr, R.; MacFarlane, D. R.; Winther-Jensen, B., Designed electrodeposition of nanoparticles inside conducting polymers. *Journal of Materials Chemistry* **2012,** *22* (37), 19767-19773.

65. Roncali, J.; Blanchard, P.; Frère, P., 3,4-Ethylenedioxythiophene (EDOT) as a versatile building block for advanced functional π-conjugated systems. *Journal of Materials Chemistry* **2005,** *15* (16), 1589-1610.

66. Groenendaal, L.; Jonas, F.; Freitag, D.; Pielartzik, H.; Reynolds, J. R., Poly(3,4-ethylenedioxythiophene) and Its Derivatives: Past, Present, and Future. *Advanced Materials* **2000,** *12* (7), 481-494.

67. Jung, H.-R.; Lee, W.-J., Ag/poly(3,4-ethylenedioxythiophene) nanocomposites as anode materials for lithium ion battery. *Solid State Ionics* **2011,** *187* (1), 50-57.

68. Mo, Z.; Zuo, D.; Chen, H.; Sun, Y.; Zhang, P., Synthesis of graphite nanosheets/AgCl/polypyrrole composites via two-step inverse microemulsion method. *European Polymer Journal* **2007,** *43* (2), 300-306.

69. Pillalamarri, S. K.; Blum, F. D.; Tokuhiro, A. T.; Bertino, M. F., One-Pot Synthesis of Polyaniline−Metal Nanocomposites. *Chemistry of Materials* **2005,** *17* (24), 5941-5944.

70. Fujii, S.; Aichi, A.; Akamatsu, K.; Nawafune, H.; Nakamura, Y., One-step synthesis of polypyrrole-coated silver nanocomposite particles and their application as a coloured particulate emulsifier. *Journal of Materials Chemistry* **2007,** *17* (36), 3777-3779.

71. Feng, X.; Huang, H.; Ye, Q.; Zhu, J.-J.; Hou, W., Ag/Polypyrrole Core−Shell Nanostructures: Interface Polymerization, Characterization, and Modification by Gold Nanoparticles. *The Journal of Physical Chemistry C* **2007,** *111* (24), 8463-8468.

72. Remita, S.; Mostafavi, M.; Delcourt, M. O., *Stabilization, growth and reactivity of silver aggregates produced by radiolysis in the presence of edta*. 1994; Vol. 18, p 581-588.

73. Mostafavi, M.; Remita, S.; Delcourt, M.; Belloni, J., Ligand effects on solvated metal cluster properties. *J. Chim. Phys.* **1996,** *93*, 1828-1842.

74. Remita, S., Effect of ligands on thermadynamics, kinetics and spectral properties of metalic aggregates synthesized by radiloysis. *Doctoral thesis* **1995**.

75. Mostafavi, M.; Dey, G. R.; François, L.; Belloni, J., Transient and Stable Silver Clusters Induced by Radiolysis in Methanol. *The Journal of Physical Chemistry A* **2002,** *106* (43), 10184-10194.

76. Remita, S.; Fontaine, P.; Rochas, C.; Muller, F.; Goldmann, M., Radiation induced synthesis of silver nanoshells formed onto organic micelles. *Eur. Phys. J. D* **2005,** *34* (1-3), 231-233.

77. Remita, S.; Orts, J. M.; Feliu, J. M.; Mostafavi, M.; Delcourt, M. O., Stm Identification of Silver Oligomer Clusters Prepared by Radiolysis in Aqueous-Solution. *Chem Phys Lett* **1994,** *218* (1-2), 115-121.

78. Van de Ruit, K.; Cohen, R. I.; Bollen, D.; Van Mol, T.; Yerushalmi-Rozen, R.; Janssen, R. A. J.; Kemerink, M., Quasi-One Dimensional in-Plane Conductivity in Filamentary Films of PEDOT:PSS. *Adv. Funct. Mater.* **2013,** *23* (46), 5778-5786.

79. Jones, B. H.; Cheng, K.-Y.; Holmes, R. J.; Lodge, T. P., Nanoporous Poly(3,4-ethylenedioxythiophene) Derived from Polymeric Bicontinuous Microemulsion Templates. *Macromolecules* **2012,** *45* (1), 599-601.

80. Hazarika, J.; Kumar, A., Controllable synthesis and characterization of polypyrrole nanoparticles in sodium dodecylsulphate (SDS) micellar solutions. *Synthetic Metals* **2013,** *175*, 155-162.

81. Tour, J. M.; Wu, R., Synthesis and UV-visible properties of soluble α-thiophene oligomers. Monomer to octamer. *Macromolecules* **1992,** *25* (7), 1901-1907.

82. Jian, Z.; Zhi-Ping, Z.; Shang-Kang, Y., Study of gamma-ray radiation induced polymerization of butadiene in ethanol. *International Journal of Radiation Applications and Instrumentation. Part C. Radiation Physics and Chemistry* **1990,** *36* (3), 393-397.

83. Mengping, Q.; Ye, Y.; Baokang, C.; Zhili, X., Radiation-induced polymerization of acrylamide in ethanol and its application in medical x-ray film as a covering agent. *Radiation Physics and Chemistry* **1993,** *42* (1), 193-196.

84. Ishigaki, A.; Koizumi, H., Radiation-induced polymerization of 3-octylthiophene. *Radiation Physics and Chemistry* **2012,** *81* (7), 803-806.

85. Yue, G.; Wu, J.; Xiao, Y.; Lin, J.; Huang, M., Flexible solar cells based on PCBM/P3HT heterojunction. *Frontiers of Optoelectronics in China* **2011,** *4* (1), 108-113.

86. Isse, A. A.; Lin, C. Y.; Coote, M. L.; Gennaro, A., Estimation of Standard Reduction Potentials of Halogen Atoms and Alkyl Halides. *The Journal of Physical Chemistry B* **2011,** *115* (4), 678-684.

87. Ushida, K.; Yoshida, Y.; Kozawa, T.; Tagawa, S.; Kira, A., Evidence of Oxidation of Aromatic Hydrocarbons by Chloromethyl Radicals: Reinvestigation of Intersolute Hole Transfer Using Pulse Radiolysis. *The Journal of Physical Chemistry A* **1999,** *103* (24), 4680-4689.

88. Tremel, K.; Ludwigs, S., Morphology of P3HT in Thin Films in Relation to Optical and Electrical Properties. In *P3HT Revisited – From Molecular Scale to Solar Cell Devices*, Ludwigs, S., Ed. Springer Berlin Heidelberg: Berlin, Heidelberg, 2014; pp 39-82.

89. Ramani, R.; Alam, S., A comparative study on the influence of alkyl thiols on the structural transformations in P3HT/PCBM and P3OT/PCBM blends. *POLYMER* **2013,** *54* (25), 6785-6792.

Chapter 3 An alternative radiolytic route for synthesizing PEDOT conducting polymers in an organic solvent

Monomers oxidation induced polymerization, by using oxidizing species, is the way to obtain conducting polymers [1, 2]. The most common approaches which are used to synthesize CPs are either chemical polymerization through adding oxidizing reagents [2, 3] or electro-polymerization by applying a potential across a solution containing the monomers [4]. In literature, PEDOT is usually synthesized by oxidation-polymerization routes thanks to the initial oxidation of 3,4-ethylenedioxythiophene monomers (EDOT) (**Figure 3.1**) and to the further coupling reactions in α, α' positions. Even though these two methods are well understood and their mechanism is relatively well known, still remain some problems such as chemical contamination, purification steps and sometimes need to use a catalyst. On the other hand, conducting polymers have some limitations which restrict their applications due to difficult processability, low solubility in common solvents and poor thermal stability [5].

Apart from traditional methods of polymers synthesis, ionizing radiation induced polymerization by γ-rays or accelerated electrons is not commonly used in the field of CPs synthesis [6]. In previous studies, our group has developed a new methodology based on radiation chemistry to polymerize some of those conducting polymers in aqueous solutions [7, 8, 9, 10, 11] thanks to the oxidation of dissolved organic monomers by oxidizing radicals *in situ* produced in the medium during water radiolysis. Additionally, pulse radiolysis was used to study and to understand the growth mechanism of PEDOT polymers initiated by these radicals in aqueous solution [12]. In this way, we demonstrated that the growth of conducting polymers is not a chain reaction. In fact, it proceeds through a step-by-step recurrent oxidation process where monomers, then dimers, then oligomers are successively oxidized.

Unfortunately, radiation-induced polymerization in aqueous solution cannot always be used due to poor processability, low solubility and even sometimes insolubility of some of concerned monomers. Contrarily to water, halo-methanes are very good solvents for many organic compounds [13] and their gamma radiolysis has been widely studied under different conditions [14, 15]. Moreover, γ-irradiation of halo-methane solvents yields to several oxidizing species [13] which could enable first the oxidation of dissolved organic monomers and then their polymerization into CPs.

Among halo-methane solvents, dichloromethane (DCM), CH_2Cl_2, has been used to carry out electrochemical or radiolytical one-electron oxidation of solutes [13, 16], and it has been proved that irradiated DCM is a good oxidizing system [15]. Yet, to the best of our knowledge, oxidative polymerization of conducting polymers induced by gamma-irradiation of

dichloromethane solutions has never been studied in literature. In order to develop a new synthetic and processable method for conducting polymers production, to control the optical properties of radiosynthesized materials, to tune polymers morphology and to overcome the low solubility issue, we extend our methodology based on radiation chemistry through a new synthetic approach in order to polymerize EDOT in an organic solvent by exploiting the oxidizing species produced from γ-irradiation of CH_2Cl_2 (DCM).

In this study here presented, firstly, the oxidative polymerization of EDOT was investigated in dichloromethane under different atmospheres: N_2, air and O_2. Dose effect studies were used to get approximate estimation of the radiolytic yield under the corresponding environmental conditions. Based on the performed studies, the oxidative polymerization of EDOT under N_2 was found the most appropriate radiolysis routes to synthesis PEDOT. The chapter then reviewed few possibilities to enhance the molecular weight of produced PEDOT polymers under the optimized conditions. The radio-synthesized polymers were characterized by many microscopic techniques after checking their chemical and physical properties. The last part was dedicated to investigate the electrical features and to probe the electronic performance for any application opportunities.

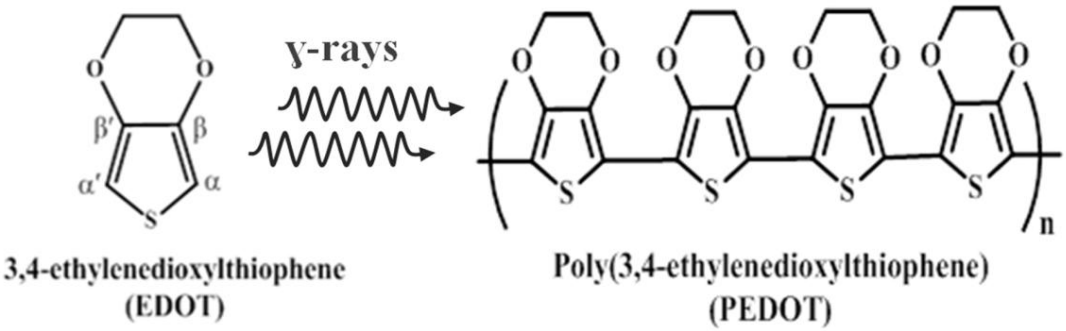

Figure 3.1 Radiation-induced polymerization of 3,4-ethylenedioxythiophene

3.1 Radiolysis methodology

3.1.1 Solutions preparation and irradiation:

Dichloromethane solutions containing 10 mM in EDOT monomers were prepared at ambient temperature. Note that the used concentration is lower than EDOT solubility in dichloromethane at 25°C (which is over than 20 mM as found by a UV-Vis absorption spectroscopy study (results not shown). This concentration remains also much lower than dichloromethane molecules concentration (15.6 M). This enables one to neglect the direct effect of ionizing radiation on EDOT monomers. Dichloromethane solutions were kept under air or degassed with N_2 and O_2, respectively, for 20 min, sealed in glass ampoules. The solution were then irradiated with a ^{60}Co γ-source with increasing doses at a dose rate 4.2 $kGy.h^{-1}$. In the dose rate effect study the following dose rates were considered: 3.4 $kGy.h^{-1}$, 2 $kGy.h^{-1}$, 1.8 $kGy.h^{-1}$and 1.3 $kGy.h^{-1}$.

3.1.2 Radiolysis of dichloromethane solutions and radio-synthesis of PEDOT under N_2 or under air:

It is known that the oxidative polymerizations are induced by formation of cations of the monomers [17]. This could be possible by ionizing radiation of aerated and/or deaerated solutions of DCM. Indeed, it is well established that γ-irradiation of deoxygenated solutions of dichloromethane (under N_2 for instance) leads, within short nanosecond time scale, to the formation of solvated electrons in addition to neutral radicals and solvent radical cations which quickly lead to dichloromethyl ($^{\bullet}CHCl_2$) and chloromethyl ($^{\bullet}CH_2Cl$) radicals [16, 18] (see chapter 1, equation 1.30)

All the generated radicals are well known as strong oxidizing agents towards organic materials. For instance, chlorine radicals [$Cl^{\cdot}/Cl^{-}$] have an ionization potential of 11.48 eV [19], while the dichloromethane radical cations [$CH_2Cl_2^{\cdot+}/CH_2Cl_2$] have an ionization potential of 11.35 eV [15]. In addition, it has been proved the possibility of oxidation of aromatic hydrocarbons by neutral dichloromethyl and chloromethyl ($^{\bullet}CH_2Cl$ and $^{\bullet}CHCl_2$) radicals in spite of their relatively lower redox potentials [15, 20]. As a consequence, due to the low redox potential of EDOT [21], one can expect its effective radiation-induced oxidation by $^{\bullet}CH_2Cl$ and $^{\bullet}CHCl_2$ radicals when dissolved in dichloromethane under N_2 atmosphere.

Note that, in aerated dichloromethane solutions, the produced dichloromethyl and chloromethyl radicals are rapidly scavenged by molecular oxygen (O_2) producing the

corresponding peroxyl radicals: $CH_2ClO_2^{\bullet}$ and $CHCl_2O_2^{\bullet}$ [14, 16]. Nevertheless, even if the oxidizing power of peroxyl radicals is higher than that of neutral chloromethyl and dichloromethyl carbon centred radicals [16], the work under nitrogen atmosphere enable us to avoid any overoxidation of our materials in DCM.

Emmi et al. elucidated the oxidation of thiophene and oligothiophenes by means of pulse radiolysis in aerated and deaerated solutions of dichloromethane[18]. On the other hand, Alfassi et al. calculated the total yield of oxidation of various solutes by pulse radiolysis of aerated DCM solutions [16]. It has been shown in these latter conditions that the total yield of solutes oxidation by peroxyl radicals, G_{max}, amounts to 7.77×10^{-7}mol.J^{-1} for solute concentrations higher than 3.3 mM [16]. Since oxidizing power of peroxyl radicals generated in aerated solutions is higher than that of chloromethyl and dichloromethyl radicals formed in deaerated DCM solutions, one can deduce that the yield, G_{ox}, of solutes oxidation under N_2 atmosphere is necessarily lower than G_{max}. This should be the case for our deaerated dichloromethane solutions under N_2 containing 10 mM in EDOT monomers.

The concentration of EDOT oxidized through dichloromethane radiolysis can be expressed as a function of the irradiation dose, D, expressed in Gray (Gy, 1 Gy corresponds to 1 J.kg^{-1}) according to:

$$[\text{Oxidized EDOT}]\ (\text{mol.L}^{-1}) = \text{D(Gy)} \times G_{ox}\ (\text{mol.J}^{-1}) \times \text{d}\ (\text{kg.L}^{-1}) \qquad (3.1)$$

where G_{ox} is the effective yield of EDOT oxidation and where d is dichloromethane density (d = 1.35 kg.L^{-1}).

In aerated dichloromethane solutions, the yield of oxidation of EDOT monomers, G_{max}, by the generated oxidizing radicals is 7.77×10^{-7}mol.J^{-1}. Subsequently, the dose for oxidation of 10 mM in EDOT is 10 kGy. Then, starting from equation (2) and knowing that under N_2 atmosphere, the yield of EDOT oxidation, G_{ox}, is lower than G_{max}, one can deduce that a dose higher than 10 kGy is needed for the quantitative oxidation of 10 mM in EDOT monomers dissolved in deaerated dichloromethane solutions (under N_2).

As demonstrated in our previous studies [10, 12], PEDOT growth is not a chain reaction but proceeds through a step-by-step oxidation mechanism made up of recurrent oxidation reactions: oxidizing radicals oxidize monomers, then dimers, then oligomers, and so on. According to this growth mechanism, the quantitative formation of PEDOT polymers requires the radiolytic production of a high concentration in oxidative species which should reach at least twice that of EDOT monomers [12]. This is consistent with the fact that, in a PEDOT

polymer, all the monomers apart from the terminal ones, are bound to two neighbors in α and α' positions. Thus, the theoretical irradiation dose which should lead to the quantitative formation of PEDOT is twice the dose necessary for the total oxidation of EDOT monomers. As a consequence, in aerated DCM solutions containing 10 mM in EDOT, the required dose for complete EDOT polymerization reaches 20 kGy. In a N_2-saturated dichloromethane solution containing 10 mM in EDOT, while the dose needed for the total oxidation of EDOT by $CHCl_2^{\cdot}$ and $CH_2Cl^{\cdot}$ radicals should be higher than 10 kGy, the dose which is necessary for the complete synthesis of PEDOT should be higher than 20 kGy, dependently on the effective yield, G_{ox}, of EDOT oxidation, according to:

$$\mathrm{D(Gy)} = \frac{2[\mathrm{EDOT}]_0(\mathrm{mol.L^{-1}})}{G_{ox}\ (\mathrm{mol.J^{-1}}) \times \mathrm{d\ (kg.L^{-1})}} \qquad (3.2)$$

where $[EDOT]_0$ is the initial concentration of EDOT.

Conversely, the determination of the dose, D, necessary for the quantitative polymerization of PEDOT should enable the estimation of the value of the yield of EDOT oxidation under nitrogen, G_{ox}, thanks to equation (3).

In this context, in order to check the dose effect and to evaluate the required irradiation dose for quantitative PEDOT preparation and then to determine the effective yield of EDOT oxidation, solutions of dichloromethane containing 10 mM in EDOT under N_2 atmosphere were irradiated at increasing doses up to 70 kGy. After irradiation, in order to extract PEDOT polymers and to evaporate the organic solvent, irradiated solutions were dried under reduced pressure. The obtained PEDOT powders were then used for further characterizations and spectral analysis.

3.1.3 Radiolysis of dichloromethane solutions and radio-synthesis of PEDOT under O_2

As mentioned above, in aerated solution of dichloromethane, the produced dichloromethyl and chloromethyl radicals are rapidly scavenged by the molecular oxygen (O_2) to produce the corresponding peroxyl radicals: $CH_2ClO_2^{\bullet}$ and $CHCl_2O_2^{\bullet}$[16, 18]:

$$^{\bullet}\mathrm{RCl} + \mathrm{O_2} \rightarrow \mathrm{RClOO^{\bullet}} \qquad (4)$$

According to radiolysis studies carried out on dichloromethane [16, 18, 20], introducing oxygen in dichloromethane solution containing oligothiophenes ($n \geq 3$) is facilitating their

oxidation due to the fact that the peroxyl radicals possess higher oxidizing power with the respect to original carbon centered radicals [18]. (See reaction 3.3)

$$RClOO^{\bullet} + 3(4,5,6)T \rightarrow nT^{+\bullet} + RClOO^{-} \quad (3.3)$$

Emmi et al.[18], investigated the oxidation of thiophene and oligothiophene by means of pulse radiolysis in aerated and deaerated solutions of dichloromethane. Within this context, Alfassi et al. calculated the total yield of oxidation by pulse radiolysis of aerated dichloromethane solutions containing various solutes. It has been shown, dependently on the solute concentration, that total yield of oxidation by the primary radicals and the peroxyl radicals amounts to 7.77×10^{-7} mol.J^{-1}.

However, despite the fact that peroxyl radicals will lead to overoxidation and deterioration of PEDOT polymers, a lower dose would presumably be enough for the quantitative polymerization. To verify the calculated radiolytic yield that was calculated by Alfassi et al. and in addition to determine the effective yield of EDOT oxidation in oxygen saturated solutions, 10 mM in EDOT was prepared in dichloromethane under air and O_2 atmosphere. Afterward, the solutions were irradiated at increasing doses up to 54 kGy.

3.2 Results and discussion

3.2.1 Radiation induced synthesis of PEDOT and dose effect study under N_2:

A dichloromethane solution containing 10 mM in EDOT was prepared under N_2 and its UV-vis absorption spectrum was recorded before irradiation (insert of **Figure 3.2a**). As observed, the prepared EDOT solution exhibits two absorption maxima at 242 and 259 nm which are features of π-π* electronic transitions in the thiophene rings within dichloromethane solvent [7]. This is consistent with the fact that pure thiophene molecules absorb light in the UV region between 225 and 245 nm, this absorption being ascribed to π-π* transition [22]. Within this context, EDOT showed good solubility in dichloromethane which is higher than 20 mM (results not shown). Also, at the two absorption maxima, the extinction coefficients of EDOT were found to be $\varepsilon_{242} = 4747$ and $\varepsilon_{259} = 6020$ L.mol^{-1}.cm^{-1}.

As elucidated in our previous work [6], knowing the extinction coefficients of EDOT, one can deduce the initial radiolytic yield of EDOT consumption from the variation of EDOT concentration as a function of the irradiation dose. Nevertheless, in the present work, it was impossible to follow up the decrease in EDOT absorption since from the beginning of the

irradiation, even at lower doses, radiolytic products appeared to also absorb in the UV region of the spectrum (results not shown). These products could come either from EDOT oxidation or from the radiolysis of dichloromethane solvent. Indeed, it has been demonstrated in literature that the products of dichloromethane radiolysis in an oxygen-free atmosphere, namely (1,1-dichloroethane, 1,2-dichloroethane, 1,1,2-trichloroethane and 1,1,2,2-tetrachloroethane), absorb light between 230 and 400 nm [23]. This evidently prevents the direct study of EDOT decay. Nevertheless, detecting the formation of PEDOT polymers by following their UV-Vis absorption spectra as a function of the dose should allow us to estimate the approximate irradiation dose needed to achieve the complete oxidative polymerization of EDOT monomers into PEDOT polymers in dichloromethane solution.

In order to follow the progressive formation of PEDOT polymers, dichloromethane solution containing 10 mM in EDOT was irradiated under N_2 at increasing doses up to 70 kGy with fixed dose rate 4.2 kGy.h^{-1} (**Figure 3.2c**) and its absorption spectrum was recorded as a function of the irradiation dose (**Figure 3.2a** and **3.2b**). Up to an irradiation dose of 36 kGy, progressively and remarkably, two peaks were being protruded at 490 and 650 nm (**Figure 3.2a**). These peaks can be attributed to the radiation induced formation of PEDOT polymers. Indeed, it's worth noting that PEDOT polymers usually display, in solution, characteristic peaks at approximately 400 to 700 nm which are ascribed to the π-π* transitions along the polymer chains [24, 25]. Differently, the observed large absorption band which progressively grows up between 800 and 1000 nm can be attributed to polaron and/or bipolaron bands, which are characteristic of oxidized state of PEDOT [26 27]. This will be proved later in this chapter, moreover. As far as we can say that the considerable amount of hydrochloride acid produced from γ-irradiation of dichloromethane, yields to different doping states of PEDOT. As a consequence, the doped PEDOT polymers with chloride ions show an absorption maximum at approximately 900 nm corresponding to the charge carrier band of the charged polymers [27]. Note that proceeding the solutions with irradiation doses higher than 36 kGy leads to gradual decrease in the absorption of PEDOT polymers at 490 and 650 nm (**Figure 3.2b**).

Dichloromethane solution containing 10 mM in EDOT appears colorless before irradiation (**Figure 3.2c**). Nevertheless, γ-radiolysis induces a progressive change in the color of the solution. After 6 kGy-irradiation, the solution got a sky-blue color. This color darkened with proceeding the irradiation with higher doses up to 36 kGy. Dark blue and black precipitants were systematically observed in solutions irradiated at doses comprised between

28 and 36 kGy. However, when exceeding the dose of 36 kGy and continuing the irradiation up to70 kGy, the solution gradated toward brown, then yellow and finally orange, while the black precipitant appeared to be glue. These color fluctuations above 36 kGy and the spectral variations upon using overdose, are ascribed to the overoxidation of PEDOT polymers (as it will be demonstrated by ATR-FTIR spectroscopy and SEC chromatography), which evidently leads to degradation and breaking down of the polymer chains.

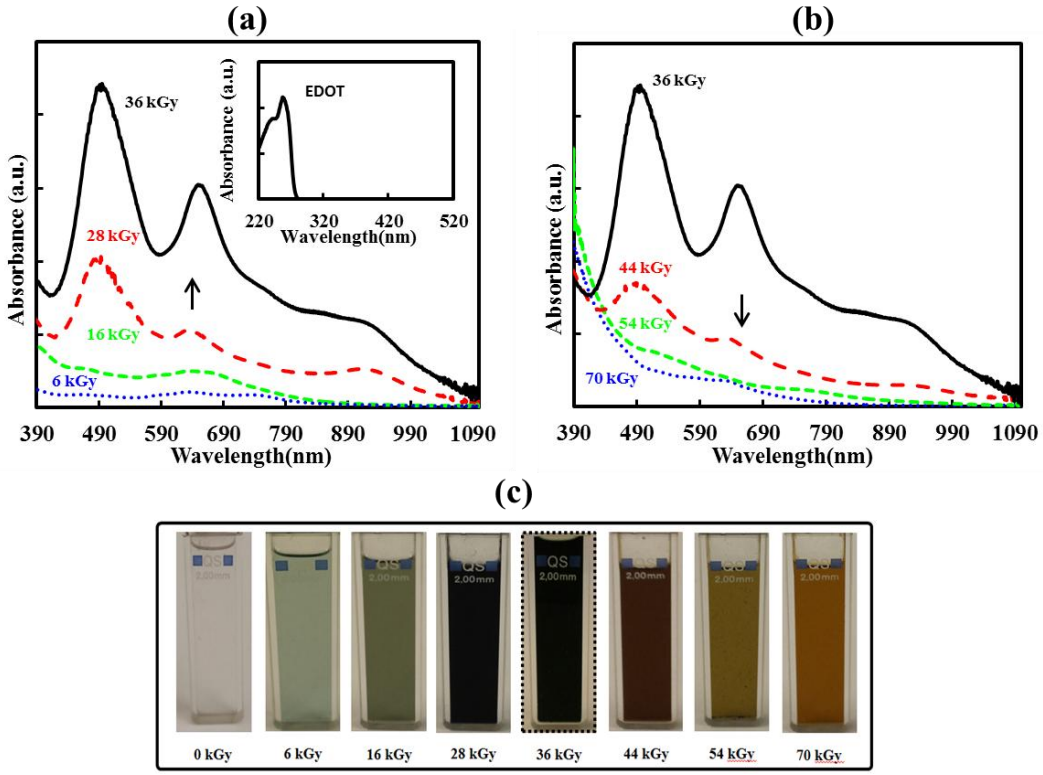

Figure 3.2 UV-Vis absorption spectra of DCM solutions containing 10 mM in EDOT and irradiated under N_2 atmosphere at constant dose rate of 4.2 kGy.h^{-1} and at increasing doses from: (a) 0 to 36 kGy and (b) from 36 to 70 kGy. The solutions were diluted 5 times. The reference was DCM. Path length = 0.2 cm (c) Photographs of DCM solutions before and after irradiation at increasing doses.

Size exclusion chromatography (SEC) was used to check the appearance of oligomeric structures synthesized in DCM solutions at increasing irradiation doses (**Figure 3.3**). The molar masses, M_p, at the maxima of the peaks were measured as the calculation of the average molecular weights, M_n, may be influenced by the overlapping of the different peaks. The more intense peak, peak (a), around the molar mass of 1100 g.mol^{-1} (obtained with a polystyrene calibration), which corresponds to 8 EDOT units, was observed as soon as the irradiation dose is equal or above 16 kGy (elution times between 19.5 and 21 min.). The molar masses, M_p, at this peak are reported in insert of **Figure 3.3** When increasing the dose,

one can observe an enlargement and a slight shift of peak (a) to shorter elution times, meaning that the molecular weight slightly increases with the dose. Polymers with higher molecular weight (up to 20 EDOT units were also detected from 36 kGy). Nevertheless, even if longer polymers are obtained at higher irradiation doses, more and more oligomers of lower molecular weight (elution times between 21 and 21.5, peak (b)) are formed at doses above 36 kGy, indicating the occurrence of damages and breaking down of the polymer chains. As it will be later demonstrated thanks to ATR-FTIR spectroscopy, these polymers which were exposed to overdoses exhibit absorption peaks corresponding to overoxidized state.

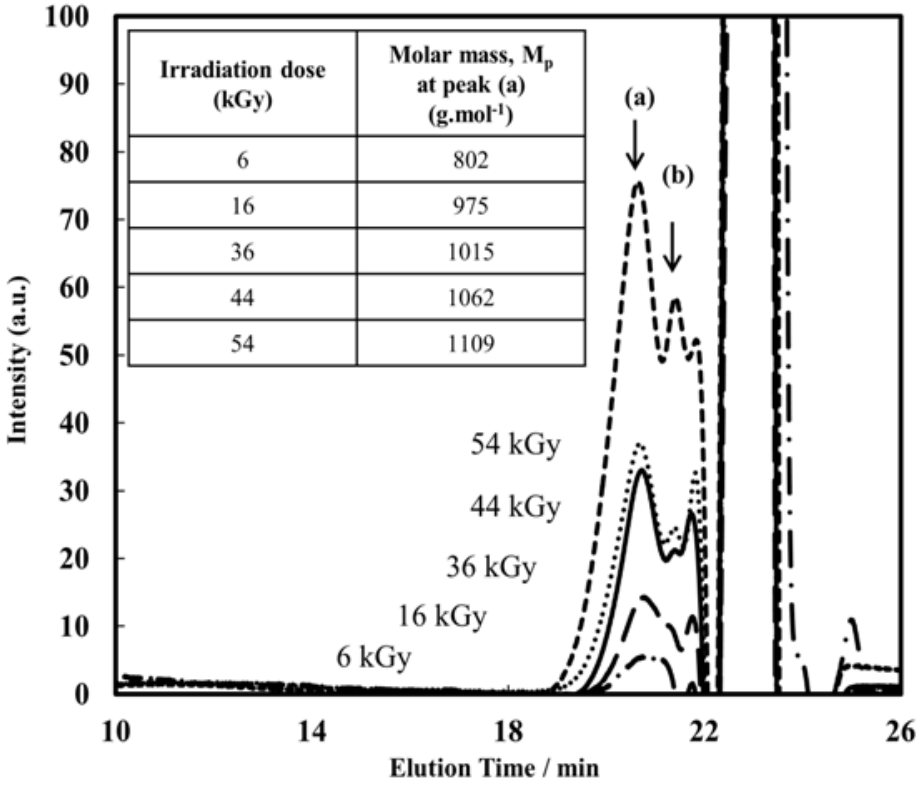

Figure 3.3 SEC chromatograms of PEDOT polymers synthesized in DCM under N_2 by γ-radiolysis at constant dose rate 4.2 kGy.h^{-1} and at increasing doses. The initial concentration of EDOT was 10 mM.

The low molecular weight obtained can be originated from poor solubility of PEDOT polymers in the solutions used in SEC analysis and thus, the longer PEDOT polymers have not been detected and analyzed by SEC.

Subsequently, these findings suggest that the oxidative polymerization of EDOT (10 mM) in dichloromethane can be proceeded with an irradiation dose of 36 kGy. This dose can be considered as the dose, D, necessary for the quantitative production of PEDOT starting from 10 mM in EDOT. From equation (3), one can then estimate the value of the effective

yield of EDOT oxidation under nitrogen: $G_{ox} = 4.12 \times 10^{-7}$ mol.J^{-1}. It is clear that, under our experimental conditions under N_2, the radiation induced oxidative polymerization of EDOT can be initiated by the generated oxidizing species in dichloromethane. As expected, the yield of oxidation, G_{ox}, is lower than G_{max} (7.77×10^{-7} mol.J^{-1}) since chloromethyl and dichloromethyl radicals are less oxidant than peroxyl radicals.

Attenuated total reflectance Fourier transform infrared spectroscopy (ATR-FTIR) was used to assert the successful formation of PEDOT polymers and also to verify the oxidative polymerization in dichloromethane solutions at different doses. After irradiation, in order to get pure PEDOT polymers, samples were dried under reduced pressure enabling DCM evaporation and EDOT monomer residues elimination. In case of solutions irradiated at 16 and 36 kGy, solvent removal led to dark solid powders while in case of sample irradiated at 54 kGy, drying process led to a glutinous product. The dried compounds were then characterized by ATR-FTIR spectroscopy and their spectra were compared with that of pure non-irradiated EDOT within wavenumber region from 3600 to 600 cm^{-1} (**Figure 3.4**).

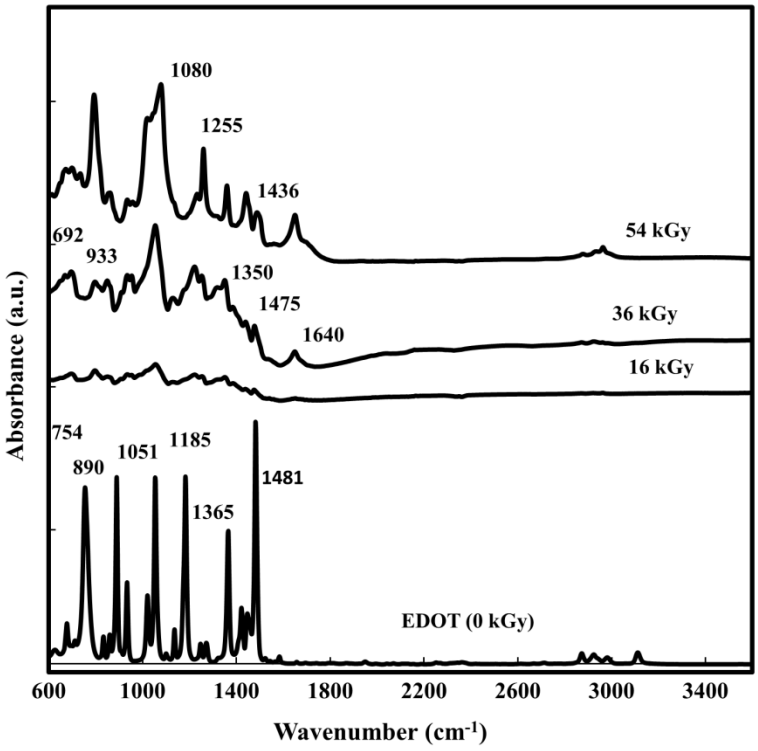

Figure 3.4 ATR-FTIR spectra of pure EDOT monomers and of PEDOT polymers radiosynthesized in DCM solvent in presence of 10 mM in EDOT at constant dose rate of 4.2 kGy.h^{-1} and at irradiation doses of 16, 36 and 54 kGy under N_2 atmosphere.

Table 3.1 displays the absorption modes and the positions of the representative peaks of EDOT monomers and PEDOT polymers As observed on **Figure 3.4**, infrared spectra of

EDOT and PEDOT (whatever the irradiation dose) are in good agreement with earlier reports. The vibration bands at 1051, 1128 and 1249 cm^{-1} are attributed to bending vibration mode of the C-O-C bond in the ethylenedioxy group. Also, the stretching vibration modes of the C–S bond which is present in the thiophene ring can be observed at 684, 790, 840 902 and 935. [25, 28 R] One can note also, as highlighted in EDOT spectrum, absorption bands located at 1475 and 1436 cm^{-1} which can be assigned to symmetric stretching mode. The absorption peaks at 1313, 1349 and 1384 cm^{-1} can be assigned to C-C inter-ring stretching mode. More interestingly, the infrared spectrum of pure EDOT displays typical band at 754, attributed to the =C-H in-plane and out-of-plane deformation vibrations of pure EDOT [6, 28, 29], which is not observed in the spectra of PEDOT. The absence of this band after irradiation implies the formation of PEDOT polymers thanks to α,α'-coupling reactions (**Figure 3.1**).[7]

Functional group	**Position (cm^{-1})**
C=C (Symmetric stretching mode)	1436 and 1475
C=C (asymmetrical stretching vibrations mode of quinoid configuration in thiophene ring)	1640
C-C (Inter-ring stretching mode)	1313, 1349 and 1384
C-O-R-O-C (Bending vibration in ethylenedioxy group)	890, 1050, 1128, 1185 and 1255
C-S-C (Stretching vibrations)	684, 790, 840 902 and 935
=C-H (In-plane and out-of-plane deformation vibrations)	754
C=O (Stretching vibrations)	1730
S=O (symmetric and antisymmetric vibrations from the sulfone groups in the thiophene units)	1080 and 1228

Table 3.1 ATR-FTIR absorption peaks of EDOT and PEDOT polymers

The infrared spectra obtained after irradiation reveal the typical bands of PEDOT polymers. Nevertheless, one can note the presence, whatever the irradiation dose, of a less common infrared band located at 1640 cm^{-1}. This band has already been observed in earlier works in the case of PEDOT polymers doped with chloride ions [30, 27]. The presence of this band highlights the doping state of PEDOT for all irradiation doses [27] and is in full agreement with the results obtained by UV-vis absorption spectroscopy (absorption band at 900 nm).

This peak originates from the quinoidal structure of doped PEDOT polymers. [25], [31] **Figure 3.5** illustrates the electronic arrangement in quinoidal structure of doped PEDOT polymers with bromines.[32] As depicted in **Figure 3.5**, the quinoid structure of PEDOT is different from that of benzoid structure (see **Figure 3.1**) and therefore the the position of absorption peak of C=C stretching vibration mode can be shifted depending on PEDOT conformation and its doping degree.[33] Remarkably, this peak resulting from polymers doping has never been observed in our previous works about radiation induced synthesis of PEDOT in aqueous media [6]. Note the absence in the infrared spectra obtained after irradiation of the strong band of C-Cl bond which should appear between 600 and 700 cm^{-1}. This means that no chlorine atom is covalently bonded to PEDOT polymers chains. When comparing the absorption spectra of PEDOT on **Figure 3.4**, one can observe the specific presence, in case of an irradiation dose of 54 kGy, of a broad band from 1650 to 1730 cm^{-1} which is the sign of an overoxidation state [34]. That band could be attributed to the formation of carbonyl group (C=O). At 54 kGy, one can also observe two bands at 1080 and 1228 cm^{-1} the might be ascribed to the symmetric and antisymmetric vibrations from the sulfone groups in the thiophene units as reported in literature concerning PEDOT overoxidation.[34]

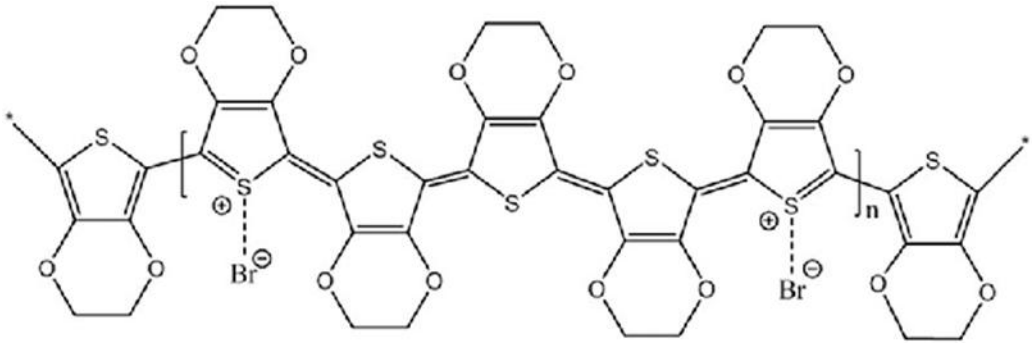

Figure 3.5 Electronic arrangement of the quinoidal structure of PEDOT polymers doped with bromine[33]

The referred peaks in **table 3.1** are slightly shifted in comparison to the assigned peaks for PEDOT polymer in aqueous media that were mentioned in **table 2.1**. This definitely is due to the pre-doping process with chloride ions and formation of different PEDOT conformations.

The study by UV-vis absorption spectrophotometry and by ATR-FTIR spectroscopy of the dose effect enables us to claim that we succeeded in the radiation induced synthesis of PEDOT polymers in DCM under N_2 atmosphere. Whatever the irradiation dose, the polymers are found doped with chloride anions generated in the medium through dichloromethane radiolysis. As demonstrated by UV-vis absorption spectrophotometry, ATR-FTIR

spectroscopy and SEC chromatography, 36 kGy is the optimal irradiation dose which enables quantitative polymerization of EDOT. Above this irradiation dose, an overoxidation is systematically observed, which leads to degradation and breaking down of PEDOT polymer chains.

3.2.2 Dose effect study under different atmospheres (air and O_2)

In the same manner as done before, the progressive formation of PEDOT polymers were followed by the evolution of the UV-visible absorption spectra of aerated solutions and oxygen saturated solution of dichloromethane in presence of 10 mM in EDOT. The solutions were then irradiated at doses ranging between of 6 and 54 kGy. **Figure 3.6a** and **Figure 3.6b** exhibit the UV-visible absorption spectra of irradiated dichloromethane solutions at increasing doses. The recorded absorption spectra maintain the same characteristic peaks. In both atmospheres, remarkably, two peaks were being protruded at 490 and 650 nm and ascribed to the π-π* transitions along the polymer chains. The doping bands were also monitored approximately around 800 to 1000 nm.

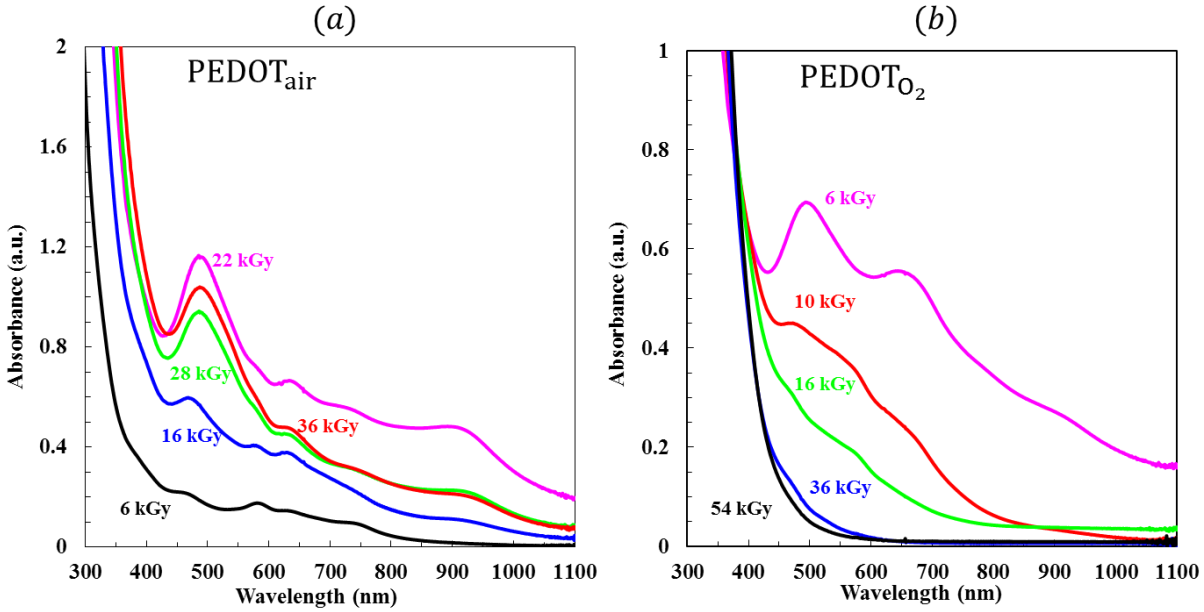

Figure 3.6 UV-Vis absorption spectra of DCM solutions containing 10 mM in EDOT and irradiated under air (a) and O_2 (b) atmospheres at constant dose rate of 4.2 kGy.h^{-1} and at increasing doses from: (a) 0 to 36 kGy and (b) from 6 to 54 kGy. The reference was DCM. Path length = 0.2 cm.

In another vein, the spectral behavior is completely different between the studied atmospheres. In case of air, the progressive formation of PEDOT polymers is clearly evolving up to 22 kGy. This is totally consistent with the yield of oxidation $G_{max} = 7.77 \times 10^{-7}$mol.J^{-1} as proposed in literature in case of DCM solutions under air. After this dose, degradation of

PEDOT polymers occurs. By contrast, proceeding the irradiation of oxygen saturated solution with dose higher than 6 kGy leads to continuous decrease in the absorption of PEDOT polymers at 490 nm and 650 nm. Indeed, as previously mentioned, the presumed initial radiolytic yield of EDOT oxidation into PEDOT polymers in aerated dichloromethane amounts to 7.77 $\times 10^{-7}$ mol.J^{-1} and therefore 20 kGy of irradiation dose are foreseeable to proceed with polymerization of 10 mM in EDOT. This is definitely consistent with our experimental results. Introducing oxygen to dichloromethane solutions boosts up the oxidative polymerization and leads to drastic decrease in irradiation dose which is needed to proceed with the oxidative polymerization.

3.2.3 Attempts to increase the molecular weight of PEDOT polymers in DCM under N_2

Synthesis conducting polymers having relatively high molecular weight is foreseeable to get better polymeric properties. In Particular, increasing the molecular weight is a key factor for fine-tuning the distribution of electron-poor and electron-rich units along the polymer backbone. Therefore, it is important to enhance the practical performance for any application opportunity. For that purpose we carried out few experiments by adjusting some parameters with the view of obtaining higher molecular weight.

3.2.3.1 *By varying the dose rate:*

As the dose rate increases the concentration of free radicals per unit of time becomes greater. This leads to a higher number of oxidations per second and then finally to more polymers with shorter chain length[35]. The use of lower dose rate by turn will reduce the number of generated dimers and trimers per unit of time and subsequently would give sufficient time for EDOT monomers to propagate and produce longer chains. In these experiments, dichloromethane solutions containing 10 mM in EDOT under N_2 atmosphere were irradiated at different dose rates: 4.2 kGy.h^{-1}, 3.4 kGy.h^{-1}, 2 kGy.h^{-1}, 1.8 kGy.h^{-1}and 1.3 kGy.h^{-1} at the optimal absorbed dose 36 kGy.

In this context, the formation of PEDOT polymers were followed by UV-Vis absorption spectra and their molar masses were measured by SEC chromatography. The obtained UV-Vis absorption spectra are shown in **Figure 3.7** and the molar masses (obtained with a polystyrene calibration), at M_p, are reported in the insert of **Figure 3.7**. The recorded UV-Vis absorption spectra share the typical absorption peaks of PEDOT obtained that were earlier synthesized 36 kGy at highest dose rate (4.2 kGy.h^{-1}). The spectra exhibit the characteristic peaks of π-π^* transitions at approximately 650 nm and a broad absorption of polaron and

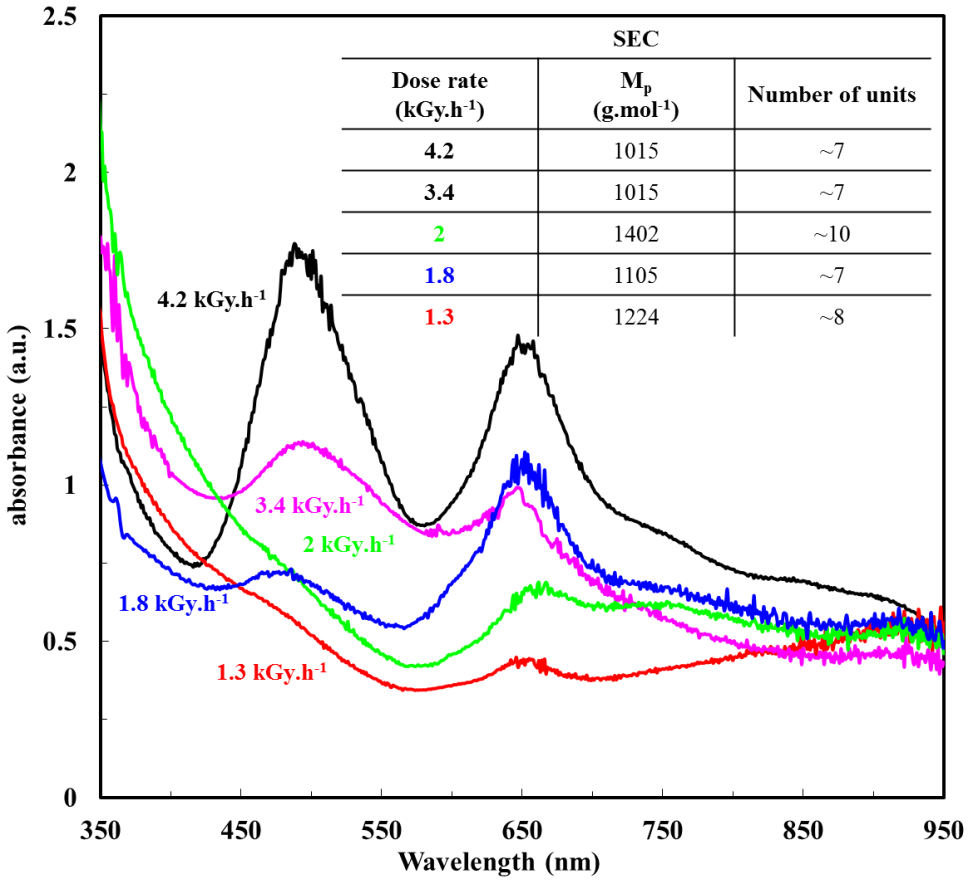

Figure 3.7 UV-Vis absorption spectra of DCM solutions containing 10 mM in EDOT and irradiated under N_2 atmosphere at dose 36 kGy at different dose rates: 1.3 kGy.h^{-1}, 1.8 kGy.h^{-1}, 2 kGy.h^{-1} , 3.4 kGy.h^{-1} and 4.2 kGy.h^{-1}. The solutions were diluted 3 times. Insert is SEC data of the irradiated solutions. The reference was DCM. Path length = 0.2 cm.

bipolaron at approximately 800 to 1000 nm which is characteristic of oxidized PEDOT with high conjugation length [36]When comparing the results obtained at the different dose rates, there is no concrete change in the main features of the obtained UV-Vis absorption spectra. However, a slight increase in the intensity of the broad band at 900 nm is perceptible upon decreasing the dose rate. The intensity of the polaron and/or bipolaron band at dose rate equals to 1.3 kGy.h^{-1} is higher than that of others, suggesting that the highest doping level occurs in the case of the lower dose rate[36]. The absorption peak at 490 nm is distinctly decreasing when dose rate decreases. This is associated with increase in the absorption peak at 650 nm that becomes more prominent than the absorption peak at 490 nm with lower dose rate. Those spectra findings could be explained by the formation of PEDOT polymers with higher molecular weight upon using lower dose rate. However, SEC data are not in accordance with our spectral observations. Indeed, the measured molar mass of PEDOT polymers, M_p, is in average equal to 9 units independently of the applied dose rate.

This is contradictory with UV-Vis observations which expect to lead to higher molecular weight. The most probable reason of these results is the poor solubility of PEDOT polymers in dichloromethane. This solubility decreases with increasing the chain length. The major part of the produced polymers is indeed precipitate or suspended in the solution. This fact makes the detection of polymers of high molecular barely infeasible. Based on these findings, we decided to keep using the highest dose rate (4.2 kGy.h^{-1}) for all performed irradiations.

3.2.3.2 *Irradiation by consecutively accumulation of EDOT concentration:*

The purpose of this experiment is to stimulate the elongation of preexisted and short polymers. Such a procedure should enable the production of PEDOT polymers at high degree of polymerization.

To do so, a solution containing 10 mM in EDOT was prepared in 50 ml of dichloromethane and then irradiated under N_2 at dose of 36 kGy with dose rate 4.2 kGy.h^{-1}. Right after γ-irradiation, 5 mL were taken from the irradiated solution to record UV-Vis absorption and to carry out afterward SEC analysis. Later, 10 mM in EDOT was prepared in the pre-irradiated solution containing already PEDOT polymers and again the solution was

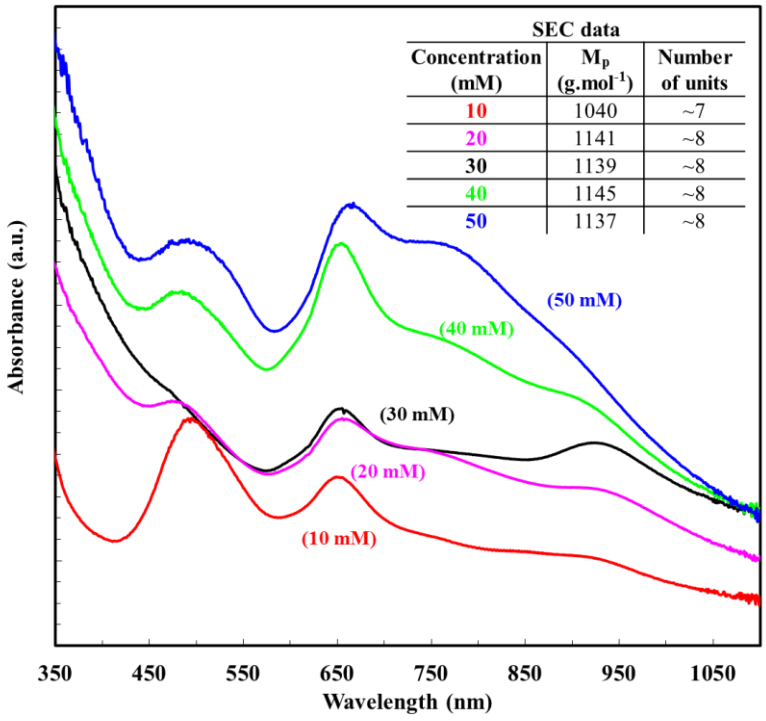

Figure 3.8 UV-Vis absorption spectra of DCM solutions containing PEDOT polymers prepared by γ-irradiation under N_2 atmosphere at dose 36 kGy and dose rates 4.2 kGy.h^{-1}. The γ-irradiation was done in five steps by consecutive and cumulative additives of 10 mM in EDOT for five times. The solutions were diluted 5 times. The reference was DCM. Path length = 0.2 cm. Insert is SEC data of the irradiated solutions.

irradiated under N_2 at dose of 36 kGy with dose rate 4.2 kGy.h^{-1}. This procedure was repeated until we reached out to five consecutive and cumulative additives of 10 mM in EDOT.

For SEC analysis, the 5 mL of each irradiated solution was placed under the hood for evaporating the solvent. After solvent evaporation, 5 ml of THF were added to the samples and then vortexed for 5 mins, THF solutions were filtrated using filter papers (55 µm), and then the resulted solutions were used for SEC analysis.

The obtained UV-Vis absorption spectra are shown in **Figure 3.8** and the molar masses (obtained with a polystyrene calibration), at M_p, are reported in the insert of **Figure 3.8**. There is no observable change in the molecular weight at M_p. As shown in table, one monomer accretion is obtained for the first additive concentration and then the M_p become static for higher concentrations. From UV-Vis absorption spectra we can see the same main spectral features that were observed earlier for dose rate effect. It is possible to recognize that the peak at 490 nm decreases while the absorption peak at 650 nm increases at each step. Interestingly, one additional peak at 770 nm protrudes gradually and becomes discernible at the fifth additive concentration. These spectral behaviors are characteristic features of oxidized PEDOT with high conjugation length. However, these results are incompatible with SEC data. A more likely reason of these findings is the poor solubility of the prepared polymers in THF which prevents the solubilization of the polymers with higher molecular weight and which should explain the inconsistencies between UV-Vis and SEC observations. Hence, one can say that the recorded SEC chromatograms are only originated from solubilized PEDOT. oligomers in THF solvent.

3.2.4 Doping and dedoping of radio-synthesized PEDOT:

The synthesis of PEDOT polymers induced by γ-radiation of dichloromethane in presence of 10 mM in EDOT was optimized at irradiation doses up to 36 kGy under N_2 and ambient temperature at dose rate 4.2 kGy.h^{-1} (see section 3.2.1). Under these conditions, PEDOT polymers were synthesized and then dried under reduced pressure in order to evaporate the solvent and eliminate the eventual monomer residues. Later, to check their absorption spectra after this post treatment procedure, 10 mg of the dark solid powder was solubilized in 1 mL of the following solvents: chloroform ($CHCl_3$), dimethylsolphoxide (DMSO). **Figure 3.9a** shows the UV-Vis absorption spectra of PEDOTs in different solvents with 4 times dilution. PEDOT polymers exhibit different solubilities with similar spectral behavior. As seen in the figure, all UV-Vis absorption spectra share the typical absorption peaks of the neutral form of PEDOT with the oxidized PEDOT chains in polaron and/or

bipolaron state. The spectra exhibit the characteristic peaks of π-π* transitions at approximately 650 nm and a broad absorption of polaron at approximately 800 to 1000 nm [36]. This spectral behavior is in good agreement with early reports about doped PEDOTs with HCl [30]. It is worth noting that, such spectra with broad absorption bands near infrared region have not been observed in our previous work in the case of γ-induced oxidation-polymerization of PEDOT in aqueous solution[6, 9]. To verify the fact that the produced PEDOTs from ɣ-radiation of dichloromethane are pre-doped with HCl and to check their different doping states, the pre-doped radiosynthesized PEDOTs were first dedoped through washing by mixed solvent system of (1:1; v/v) of ethanol and ammonium hydroxide (NH_4OH; 5M), in order to remove the yielded chloride ions. Later, part of dedoped PEDOTs were then solubilized in chloroform at concentration of 10 mg. mL^{-1} (**Figure 3.9b**, spectrum A). The other part of dedoped PEDOTs were washed again with hydrochloride acid (HCl; 5M) and solubilized in chloroform at concentration of 10 mg. ml^{-1}, resulting in re-doping of PEDOTs. **Figure 3.9b** exhibits UV-Vis absorption spectra of PEDOTs at different doping levels. Where, spectrum A represents depoded PEDOTs and spectrum B represents re-doped PEDOTs. After dedoping, PEDOT spectrum does not show the absorption peak at 900 nm corresponding to charge carrier band. On the other hand, when the dedoped PEDOT were re-doped with HCl (5M), the spectrum exhibits absorption at approximately 900 nm with a free tail extending into the near-

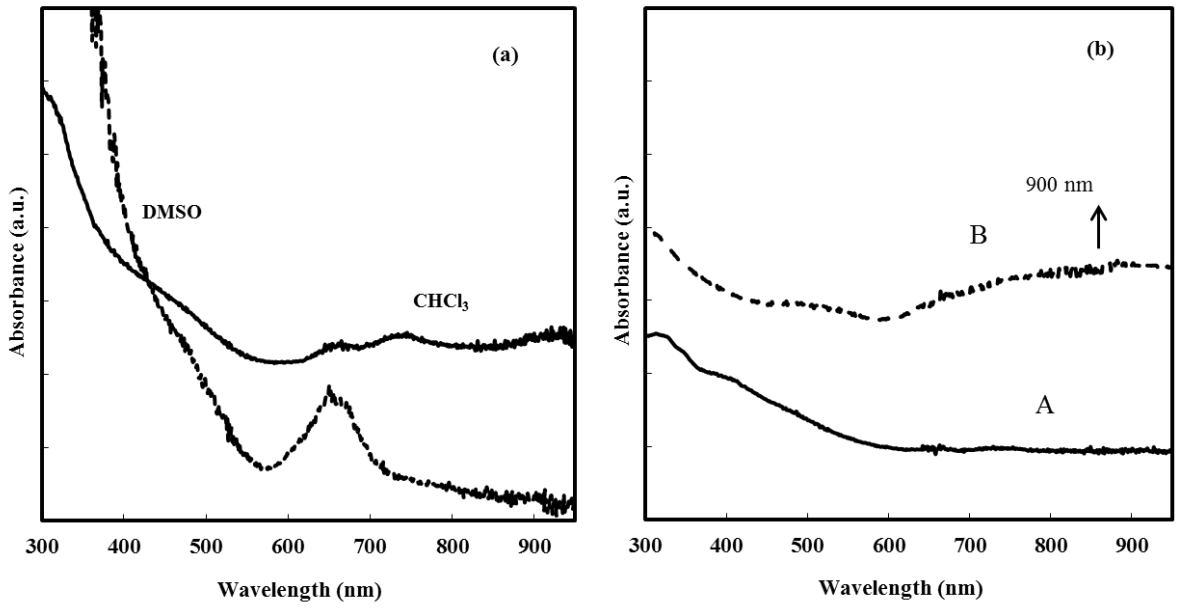

Figure 3.9 UV-Vis absorption spectra of 10 mg of PEDOT in 1 mL solvent (diluted 4 times). (a) pre-doped PEDOT in different solvents and (b) PEDOT in Chloroform: A) dedoped PEDOT with 5M NH_4OH:EtOH and B) redoped PEDOT with 5M HCl:EtOH. PEDOTs were synthesized in DCM solvent under N_2 in presence of 10 mM in EDOT by γ-radiolysis after irradiation at dose of 36 kGy; ; dose rate 4.2 $kGy.h^{-1}$; path length= 2 mm; reference: pure solvent.

infrared region, indicating the formation of charged PEDOTs.

3.2.5 Structural and morphological characterizations of radio-synthesized PEDOTunder N_2

From now, we will focus on the characterization of PEDOT polymers produced under N_2 from DCM radiolysis at the optimal irradiation dose of 36 kGy and dose rate 4.2 kGy.h^{-1}.

In order to check the morphology of PEDOT polymers synthesized under N_2 atmosphere in a dichloromethane solution containing 10 mM in EDOT, cryo-TEM microscopy was used just after a 36 kGy-irradiation and before any sedimentation (**Figure 3.10**). Thanks to sample freezing, this technique enables *in situ* observation, into dichloromethane solvent, of radiosynthesized polymers, avoiding any phase transition and any PEDOT aggregation which could result from drying procedures.

Figure 3.10a displays a zoom of one of the circular holes of the holey-carbon grid coated with PEDOT polymers in DCM solvent. As depicted in the figure, this hole is fully coated with more or less spherical contrasted objects. As explained and demonstrated in our previous works, these globular structures correspond to self-assemblies of independent amorphous PEDOT chain polymers. The full coverage of the hole and the packing of the spheroidal PEDOT particles indicate the high local concentration of these PEDOT self-assemblies into the holes of the carbon grid. In the vicinity of the holes (**Figure 3.10b**), concentration of PEDOT particles clearly appears lower due to the smaller thickness of the frozen sample outside the holes, enabling the clear observation of individual spheroidal PEDOT particles

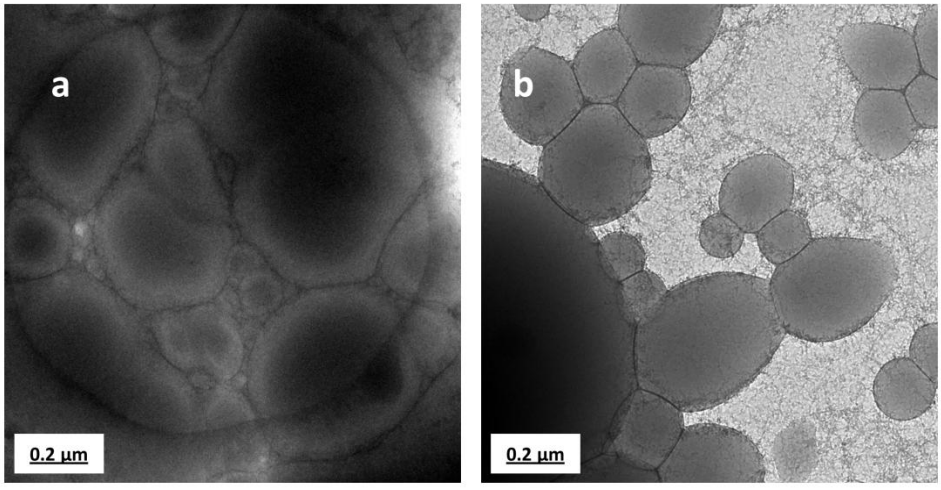

Figure 3.10 Cryo-TEM images of PEDOT polymers self-assembled in DCM solvent right after a 36 kGy-irradiation. The polymers were synthesized under N_2 atmosphere in DCM solvent in presence of 10 mM in EDOT at dose rate 4.2 kGy.h^{-1}.

which nevertheless remain packed. PEDOT particles are heterogeneous in size with diameters comprised between 100 nm and 1 µm. Each observed particle should be composed of interdigitated polymer chains. Since no α−β′ linkages could occur during polymerization, radio-synthesized PEDOT should be composed of linear chain polymers which are neither branched nor networked but in weak interactions.

After irradiation, samples were dried under reduced pressure, DCM solvent was evaporated and black PEDOT powder was extracted and collected for further characterizations. XRD analysis was then used to check the crystallinity of PEDOT polymers synthesized by gamma-radiolysis of DCM solutions. In particular, powder X-ray diffraction pattern was studied in order to analyze the structure of PEDOT polymers synthesized at 36 kGy (**Figure 3.11**).

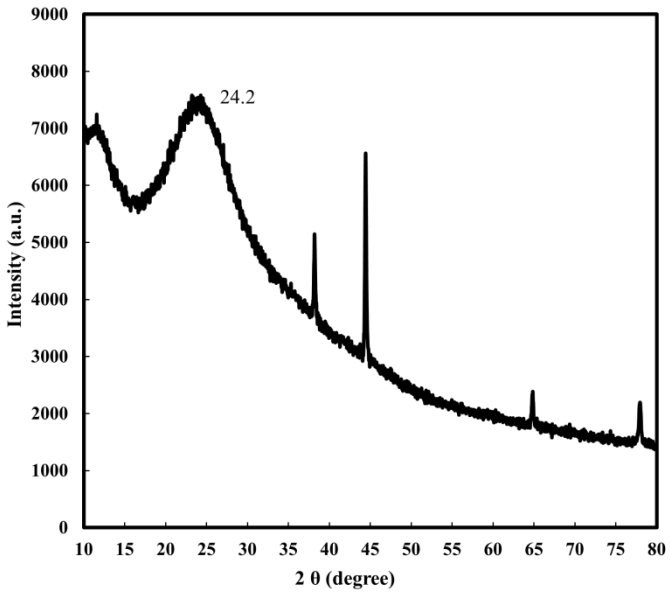

Figure 3.11 XRD pattern of dried PEDOT polymers powder obtained after DCM evaporation. The polymers were synthesized by gamma-radiolysis at 36 kGy of a DCM solution containing 10 mM in EDOT under N_2 atmosphere at dose rate 4.2 kGy.h^{-1}. The substrate used for XRD analysis was aluminum**.**

The typical XRD pattern, exhibited in Figure 3.9 in the case of radio-synthesized PEDOT closely matches those earlier reported in literature in the case of chemically synthesized PEDOT polymers [37, 38]. The diffraction peaks at about 38°, 44°, 64° and 78° are originated from the aluminum support used in this work. More interestingly, the amorphous nature of PEDOT is highlighted and confirmed from the diffraction peak at 2θ ~ 24° which is a feature of interchain planar ring stacking [38,36].

In order to investigate the morphology of PEDOT polymers powders obtained after a 36 kGy irradiation of an EDOT-containing DCM solution and after solvent evaporation, SEM microscopy was used. SEM images recorded after deposition of dried PEDOT polymers powder onto carbon tape adhered to aluminum mounts and gold coating are displayed on **Figure 3.12.** Note that without gold coating, similar images were obtained but with lower resolution. SEM image of **Figure 3.12a** displays a comprehensive view of creased film of PEDOT. Without gold coating, *in situ* Energy-Dispersive X-ray spectroscopy (EDX) was carried out in order to identify the chemical composition of the materials and to perform the elemental analysis in different areas of the film. EDX highlighted the presence of sulfur (in addition to carbon and oxygen) in the whole sample demonstrating that the film is effectively made of PEDOT. Moreover, EDX enabled the detection of chlorine atoms homogeneously dispersed in the film. This observation definitely demonstrates that radiosynthesized PEDOT are doped with chloride ions, in total agreement with our results obtained by UV-vis absorption spectrophotometry and by ATR-FTIR spectroscopy.

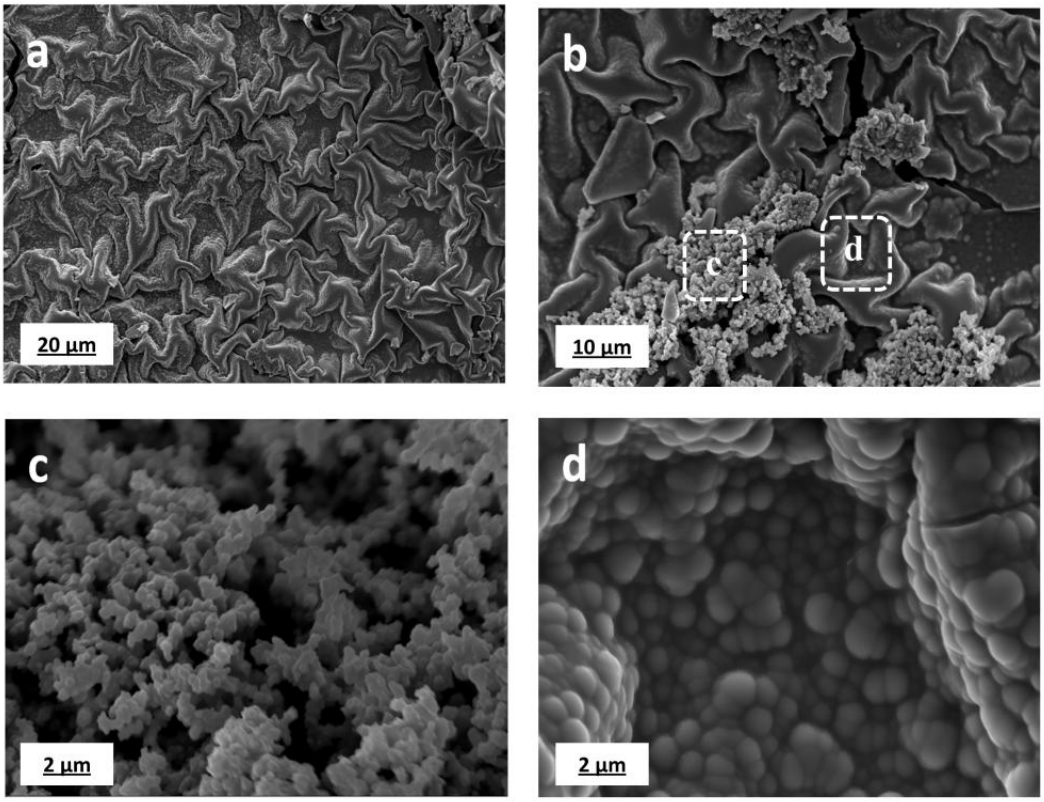

Figure 3.12 SEM images of dried PEDOT polymers powder after deposition onto carbon tape adhered to aluminummounts and gold coating. The powder was obtained after solvent evaporation. PEDOT polymers were synthesized by gamma-radiolysis at 36 kGy of a DCM solution containing 10 mM in EDOT under N_2 atmosphere at dose rate 4.2 kGy.h^{-1}.

Figure 3.12b which shows a closer view of PEDOT film, highlights the presence of aggregated spheroidal particles at its surface. These packed globular particles can be clearly seen in **Figure 3.12c** (first zoom of **Figure 3.12b**). These PEDOT particles have a mean diameter of few hundreds nm. Another zoom of the film (**Figure 3.12d**, second zoom of **Figure 3.12b**, which was realized in a region of **Figure 3.12b** where no apparent particles were observable) depicts the presence of bigger spheroidal PEDOT particles with a mean diameter between 1 and 1.5 µm. This means that the whole film is made of very close-packed PEDOT particles. These results are in good agreement with previous observations reported in literature concerning PEDOT films prepared by electrochemical method and doped with Cl [30].

Interestingly, as observed by SEM microscopy, PEDOT particles are heterogeneous in size with diameters comprised between 100 nm and 1.5 µm. This is in agreement with cryo-TEM observations. Then the particles observed by SEM after deposition should come from the globular structures initially dispersed in DCM solvent and already observed by cryo-TEM (Figure 3.8). The drying process as well as the deposition procedure have clearly no effect on the size of the particles nor on their shape. This would imply the existence of relatively strong interactions (π-stacking and/or hydrogen-bonds interaction) into each polymers particle.

For further characterization and to definitely prove that the spheroidal particles observed by cryo-TEM and SEM are made of PEDOT polymers, Atomic Force Microscopy coupled with infrared nanospectroscopy (AFM-IR) was used. PEDOT polymers powder obtained after irradiation at 36 kGy and after DCM evaporation was solubilized in ethanol and then a small drop of the ethanolic solution was deposited onto the upper surface of ZnSe prism and dried naturally at air. The obtained film was then scanned and imaged by AFM-IR as shown in **Figure 3.13**.

In **Figure 3.13a** and **Figure 3.13b**, the bottom dark areas having no thickness correspond to the prism. Distinctly, the topography of the deposited materials displayed as the bright areas corresponds to the thicker regions made up of more or less aggregated spheroidal particles. The AFM topography image in **Figure 3.13a** recorded in contact mode reveals the presence of big particles with diameters comprised between 0,5 and 3,5 µm. Nevertheless, if we spot on one of these big particles as shown in **Figure 3.13b**, it is possible to observe that the apparently big spheroidal particle is constructed by smaller aggregated particles. By scanning the whole substrate, we found that the smallest identifiable particles are heterogeneous in size with diameters comprised between 100 nm and 1.5 µm. The particles observed by AFM have then the same size as the particles we already observed by cryo-TEM and SEM, those we previously considered as radiosynthesized PEDOT particles.

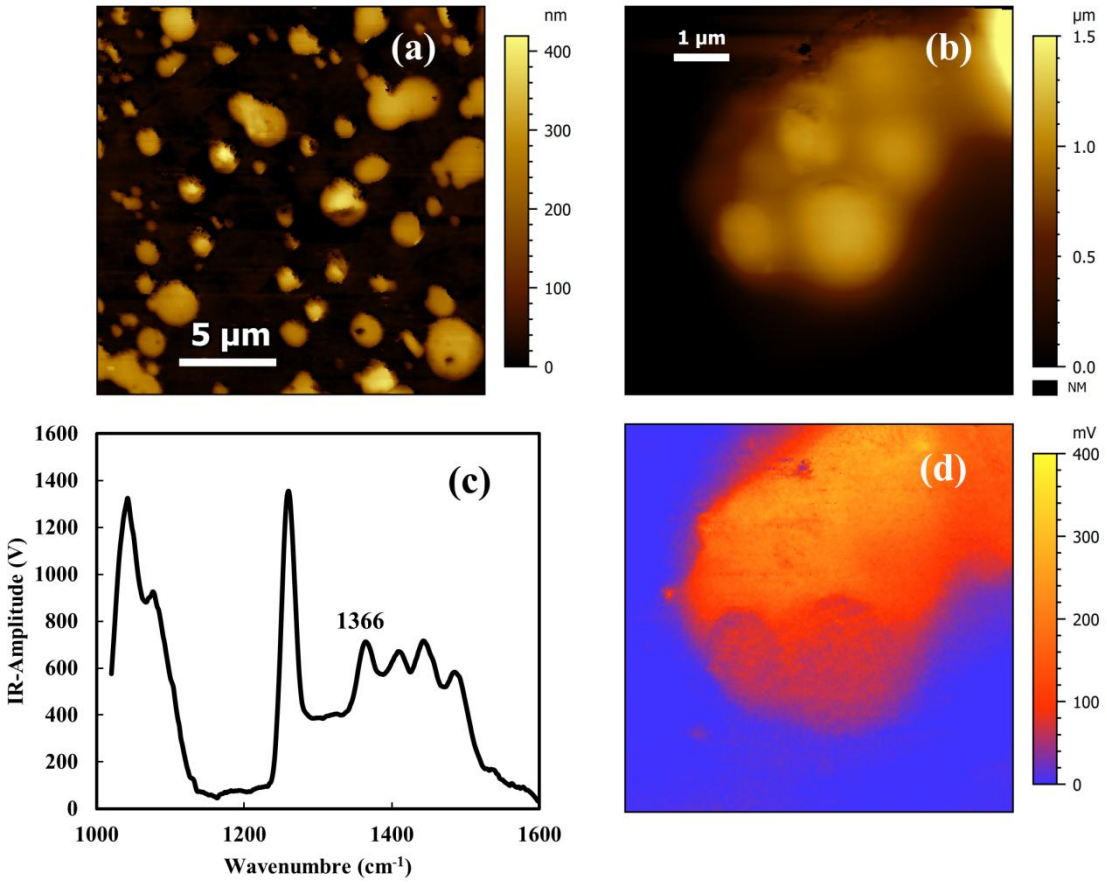

Figure 3.13 AFM-IR images of PEDOT polymers after deposition onto the upper surface of ZnSe prism. PEDOT polymers were synthesized by gammaradiolysis at 36 kGy of a DCM solution containing 10 mM in EDOT under N_2 atmosphere at dose rate 4.2 kGy.h^{-1}. (a) and (b) AFM topographic images of PEDOT polymers in contact mode. (c) AFM-IR spectrum of PEDOT. (d) AFM-IR chemical mapping of PEDOT with the IR source tuned to the C–C band at 1366 cm^{-1}.

In order to definitely demonstrate that these particles and then those previously observed by SEM and cryo-TEM are made of PEDOT, we performed AFM-IR experiments. Indeed, changing by AFM-IR the wavenumber on a fixed position of the tip gives a local infrared spectrum. Thanks to AFM-IR, we recorded the local infrared absorption spectrum of the particles observed in **Figure 3.13b** in the range of 1020-1600 cm^{-1} (**Figure 3.13c**). Note that all the particles observed by AFM onto the prism display the same infrared spectrum, which means that they all have the same chemical structure. The infrared spectrum of **Figure 3.13c** matches with the ATR-FTIR spectra recorded in the case of PEDOT radiosynthesized at different irradiation doses (16, 36 and 54 kGy, **Figure 3.4**). This proves that the spheroidal particles observed by AFM (and thus by SEM and cryo-TEM) contain close-packed PEDOT polymer chains.

Now, scanning the surface by AFM-IR at a given wavenumber enables to reveal the chemical map of the sample. We considered in particular, in the spectrum of **Figure 3.13c**, the

peak at 1366 cm^{-1} which is a feature of C-C stretching band in PEDOT, we selected the corresponding wavenumber to carry out the chemical mapping of the sample and we recorded the absorption strength (**Figure 3.13d**). In this figure, the orange-red areas indicate a stronger absorption at the characteristic wavenumber which is caused by a thick layer of PEDOT linked onto the ZnSe prism. When comparing the topography (**Figure 3.13b**) and the chemical mapping (**Figure 3.13d**), one can observe that the stronger absorbing areas fit well with the thicker regions. This implies that the observed particles are mainly composed by PEDOT polymer chains.

The observations made by cryo-TEM, SEM and AFM microscopies as well as the characterizations conducted by XRD analysis, EDX spectroscopy and AFM-IR nanospectroscopy enable us to conclude without any ambiguity that radiolysis of DCM leads to the oxidation of EDOT monomers and to the production of amorphous PEDOT polymers doped with chloride ions. As observed in the case of a 36 kGy-irradiation, radiosynthesized PEDOT polymers self-assemble into polydisperse globular particles (diameters comprised between 100 nm and 1.5 µm), those we observed in this work by cryo-TEM, SEM and AFM-IR.

3.2.6 Physicochemical and Electrochemical performances of radiosynthesized PEDOT

Thermogravimetric analysis (TGA) was used in order to check the thermal stability of PEDOT polymers synthesized by radiolysis under N_2 atmosphere in a dichloromethane solution containing 10 mM in EDOT. The TGA profile obtained in the case of PEDOT polymers radiosynthesized at an irradiation dose of 36 kGy and at dose rate 4.2 $kGy.h^{-1}$ is displayed in **Figure 3.14**.

As observed in **Figure 3.14**, TGA curve exhibits the typical decomposition behavior of PEDOT polymers synthesized by traditional methods [29, 38]. Before 100°C, no weight loss is observed. However, above 150°C, a more or less progressive weight loss happens resulting from PEDOT fragmentation and carbon oxidation. It can be clearly observed two pronounced falls which occur between 150°C and 450°C. The first weight loss observed between 150°C and 300°C should correspond to the degradation of the shortest PEDOT oligomers with relatively low molecular weight, while the second weight loss observed above 300°C should correspond to the decomposition of longer polymers. This TGA analysis of radiosynthesized PEDOT is in very good agreement with TGA data already reported in the literature concerning PEDOT polymers produced by conventional methodologies [29, 38]. This result

evidently highlights the good thermal stability of PEDOT polymers synthesized by gamma-radiolysis in DCM solvent.

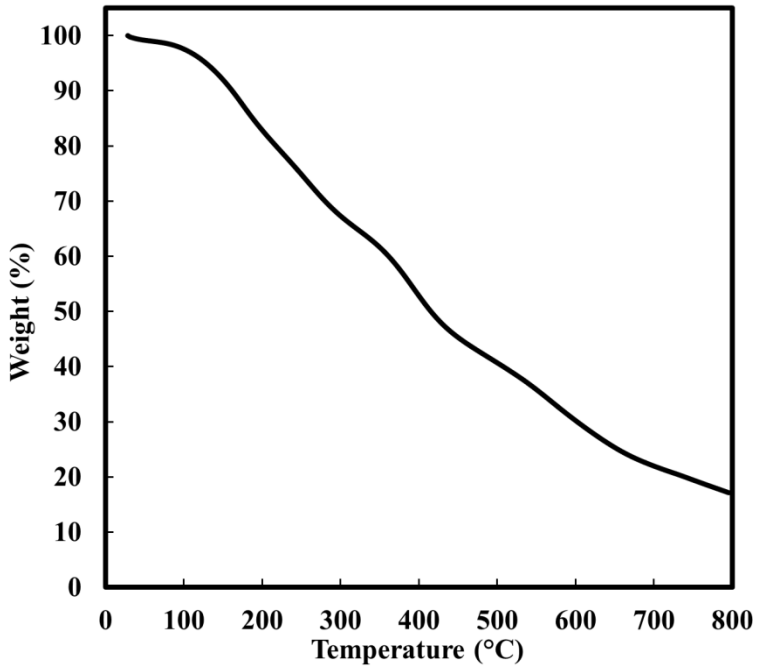

Figure 3.14 Thermogravimetric analysis (TGA) graph of dried PEDOT polymers powder. The polymers were synthesized by gamma-radiolysis at 36 kGy of a DCM solution containing 10 mM in EDOT under N_2 atmosphere at dose rate 4.2 $kGy.h^{-1}$.

In order to investigate the electronic properties of PEDOT polymers radiosynthesized in DCM for future applications in optoelectronics and electrocatalysis, it is evidently necessary to determine by using cyclic voltammetry (CV) measurements their oxidation and reduction potentials and then to estimate the energy level of the highest occupied molecular orbital (HOMO) from the ionization potential, the energy level of the lowest unoccupied molecular orbital (LUMO) from the electronic affinity, as well as the band gap.

Cyclic voltammetry (CV) was then used to study the electrochemical behavior of PEDOT polymers synthesized by radiolysis at 36 kGy in a dichloromethane solution containing 10 mM in EDOT under N_2 atmosphere. PEDOT powder obtained after solvent evaporation was dissolved in DCM at a concentration of 1 $mg.mL^{-1}$. Then, 1 mL of this solution was mixed with 5 mL of acetonitrile solution containing tetrabutylammonium hexafluorophosphate ($TBAPF_6$) used as electrolyte at a concentration of 0.1 M. The electrochemical behavior of PEDOT polymers and their characteristic oxidation and reduction peaks are presented in **Figure 3.15**. The several peaks which are clearly observed from the sinuous cyclic voltammogram of **Figure 3.15** could be assigned to the polydispersity in size of the PEDOT oligomers and polymers which are present in the electrochemical cell. According to CV

profile displayed in **Figure 3.15**, main PEDOT p-doping (oxidation) process occurs at onset potential, Eox, of + 0.85 V while n-doping starts at onset potential, E_{red}, of -0.61 V. Knowing these two potential values, one can calculate, from the equations given in legend of **Figure 3.15**, the HOMO/LUMO energy levels of radiosynthesized PEDOT: EHOMO and ELUMO amount respectively to -5.45 eV and -3.84 eV [39]. As a consequence, the corresponding electrochemical band gap is -1.61 eV. Note that the optical band gap deduced from the UV-Vis absorption spectrum of PEDOT irradiated at 36 kGy (Figure 3.2a, at λ = 750 nm) amounts to -1.65 eV. We can notice the similarity between the two estimated values of the band gap and also the good agreement with results earlier reported in literature for PEDOT polymers synthesized by conventional methods. [38, 40]

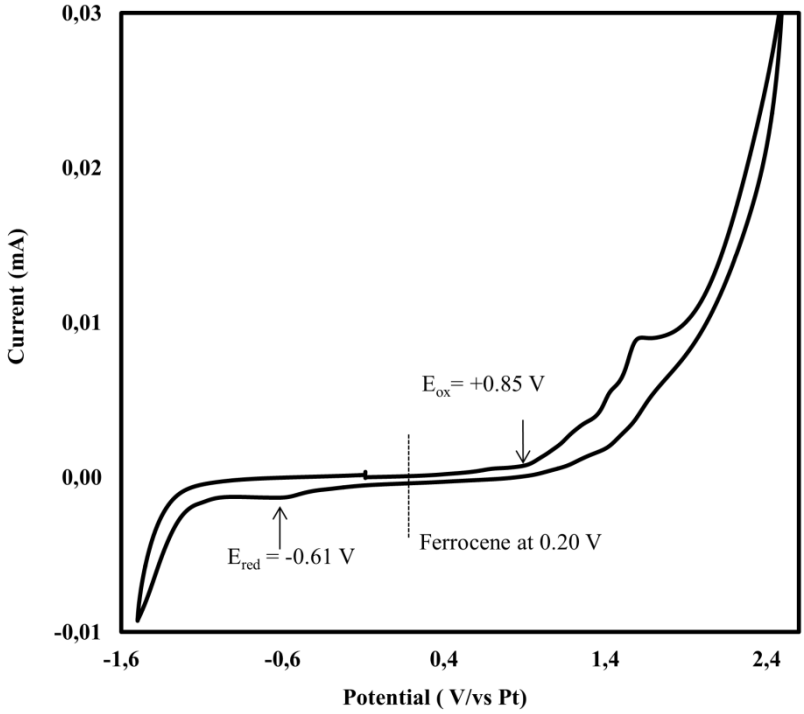

Figure 3.15 Cyclic voltammogram of PEDOT polymers recorded in acetonitrile containing 0.1 M of $TBAPF_6$ at a scan rate of 20 mV s^{-1}. PEDOT polymers were radiosynthesized at 36 kGy in a DCM solution containing 10 mM in EDOT under N_2 atmosphere at dose rate 4.2 $kGy.h^{-1}$. Ferrocenium/ferrocene (Fc^+/Fc) redox potential was measured in order to calibrate the pseudo reference electrode (0.2 V vs. Pt in the present study). The HOMO/LUMO energetic levels of PEDOT are determined as follows: E_{HOMO} (eV) from ionization potential = -4.8 - e(E_{ox} - 0.2) and E_{LUMO} (eV) from electronic affinity =-4.8 - e(E_{red} _ 0.2) where e is the elementary charge.

Eventually, four-point probe technique was used to measure the electrical conductivity of PEDOT polymers synthesized by radiolysis at 36 kGy in a dichloromethane solution containing 10 mM in EDOT under N_2 atmosphere at dose rate 4.2 $kGy.h^{-1}$. PEDOT powder

obtained after irradiation and solvent evaporation was dissolved in DCM at a concentration of 10 $mg.mL^{-1}$. Then, 100 µL of the solution were spin-coated on a clean glass substrate and the obtained PEDOT film was doped with $NOBF_4$ (10 mM) in acetonitrile. After measuring the thickness of the film by a surface profiler, its conductivity was determined by four-point probe technique and found to be 2.6 x 10^{-3} $S.cm^{-1}$. The conductivity of PEDOT polymers synthesized by radiolysis in DCM is then close to the conductivities of PEDOT polymers we earlier synthesized by high energy radiation (gamma-rays or accelerated electrons) in aqueous solution [9, 12]and remains close to those already reported in literature for PEDOT polymers produced by conventional synthetic methods. [28, 41]

The measurements and characterizations made by thermogravimetric analysis, cyclic voltammetry and four-point probe technique enable us to conclude that PEDOT polymers synthesized in dichloromethane by our alternative radiolytic method have not only a good thermal stability but also present interesting electronic properties (band gap and conductivity), which are comparable to those reported in literature for PEDOT polymers synthesized by chemical or electrochemical methodologies. Thus, the obtained material are really promising and surely usable for practical applications.

3.3 Conclusion

In the previous works and for the first time in literature, radiolysis (by γ-rays or accelerated electrons) was used in the host laboratory as a new methodology for the synthesis of conducting polymers in aqueous solution in the absence of any external chemical initiators. Oxidation of monomers was shown to result from the action of oxidizing radicals *in situ* produced by water radiolysis while growth of polymers was shown to proceed through a recurrent step-by-step oxidation process. Starting from Py and EDOT monomers, nanostructured conducting PPy and PEDOT polymers were then successfully prepared. Nevertheless, high energy radiation induced polymerization cannot systematically be used in aqueous solution due to poor solubility into water and even sometimes insolubility of monomers.

Herein, our strategy based on radiation chemistry was extended to the preparation of conducting polymers into organic solvents. In particular, starting from EDOT monomers dissolved in dichloromethane (DCM) solvent, we elaborated and optimized the synthesis by gamma-rays of PEDOT polymers. The choice of DCM was justified by the fact that it is a good solvent for many organic compounds. Moreover, its radiolysis is relatively well-known

and leads to *in situ* production of oxidizing radicals which should enable first the oxidation of dissolved organic monomers and second their polymerization into conjugated polymers.

In this work, we succeeded in the simple radiation induced oxidative polymerization of EDOT and in the synthesis of PEDOT polymers in DCM under N_2 atmosphere. For all irradiation doses, oligomers with several EDOT units were observed. Some polymers with higher molecular weight up to 20 EDOT units were also detected from 36 kGy. Also, whatever the irradiation dose, the polymers were found naturally doped with chloride anions generated in the medium through dichloromethane radiolysis. As demonstrated by UV-vis absorption spectrophotometry, ATR-FTIR spectroscopy and SEC chromatography, the dose of 36 kGy is the optimal irradiation dose which enables quantitative polymerization of 10 mM in EDOT and as a consequence, the yield of EDOT oxidation in DCM, under N_2 atmosphere, amounts to 4.12×10^{-7} mol.J^{-1}. Above this irradiation dose, an overoxidation is systematically observed, which leads to degradation of PEDOT polymer chains.

Within the context, other environmental conditions were considered: EDOT oxidation in DCM, under O_2 atmosphere and EDOT oxidation in DCM, under air atmosphere. It was evident that the oxidative polymerization in aerated solutions of dichloromethane proceeds favourably with the generated primary radicals and the two chloromethyl and dichloromethyl peroxyl radical. Thanks to their high oxidizing power, the yield of EDOT oxidation was increased. In aerated DCM solution, the yield of EDOT oxidation amounts to 7.7×10^{-7} mol.J^{-1}. Several attempts were tried out to increase the molecular weight of produced PEDOT polymers in DCM, under N_2 atmosphere at 36 kGy. For this purpose, two approaches were followed: study the effect of irradiation at different dose rates and irradiation by consecutively accumulation of EDOT concentration.

The morphology of PEDOT polymers radiosynthesized at an irradiation dose of 36 kGy was checked in DCM solution and after deposition. The observations and characterizations made by cryo-TEM, SEM and AFM microscopies, by XRD analysis, EDX spectroscopy and AFM-IR nanospectroscopy demonstrated that radiolysis of DCM leads to the production of amorphous PEDOT polymers doped with chloride ions and highlighted the self-assembly of these polymers into polydisperse globular particles (size comprised between 100 nm and 1.5 µm). Besides, physico-chemical and electrochemical performances of PEDOT polymers radiosynthesized at an irradiation dose of 36 kGy were evaluated by thermogravimetric analysis, cyclic voltammetry and four-point probe technique. PEDOT polymers synthesized by the original radiolytic method were found to be characterized by good thermal stability and by interesting electronic properties (band gap and conductivity), which are comparable to

those reported in literature for PEDOT polymers synthesized by chemical or electrochemical methodologies. Our radiation chemistry-based methodology definitely appears as a promising method for the production, not only in water but also in organic solvents, of usable conducting polymers for practical applications.

Current research aims to develop new synthesis strategies and new conducting polymers with tuned morphologies and optimized properties. The present results encourage us to investigate the radiation induced polymerization of other conducting polymers, such as poly(3- hexylthiophene) (P3HT, the monomers of which are insoluble in water) or some other polythiophene derivatives such as poly (3-Thiophene acetic acid) (PTAA, the monomers of which are soluble in water and in DCM solvent) in DCM solvent as well as in other alternative organic solvents (chloroform, cyclohexane…).

Due to the fact that, the synthesis of PTAA polymers is not easy to be done by conventional polymerization methods. Thus in the next chapter, we would like to use our original radiolytic methodologies (radiation induced polymerization in water and DCM) to polymerize 3-Thiophene acetic acid (TAA) without using oxidizing agents or any prior esterification.

References

1. Jiang, C. Q.; Chen, G. M.; Wang, X., High-conversion synthesis of poly(3,4-ethylenedioxythiophene) by chemical oxidative polymerization. *Synth. Met.* **2012,** *162* (21-22), 1968-1971.

2. Sugimoto, R.; Takeda, S.; Gu, H. B.; Yoshino, K., Preparation of soluble polythiophene derivatives utilizing transition metal halides as catalysts and their property. *Chem. Express* **1986,** *1* (11), 635-638.

3. Roncali, J., Conjugated Poly(Thiophenes) - Synthesis, Functionalization, and Applications. *Chem. Rev.* **1992,** *92* (4), 711-738.

4. Lattach, Y.; Fourati, N.; Zerrouki, C.; Fougnion, J. M.; Garnier, F.; Pernelle, C.; Remita, S., Molecularly imprinted surface acoustic wave sensors: The synergy of electrochemical and gravimetric transductions in chemical recognition processes. *Electrochim. Acta* **2012,** *73*, 36-44.

5. Ruiz, J.; Gonzalo, B.; Dios, J. R.; Laza, J. M.; Vilas, J. L.; León, L. M., Improving the Processability of Conductive Polymers: The Case of Polyaniline. *Adv. Polym. Tech.* **2013,** *32*, E180-E188.

6. Lattach, Y.; Deniset-Besseau, A.; Guigner, J. M.; Remita, S., Radiation chemistry as an alternative way for the synthesis of PEDOT conducting Polymers under "soft" Conditions. *Radiat. Phys. Chem* **2013,** *82*, 44-53.

7. Lattach, Y.; Coletta, C.; Ghosh, S.; Remita, S., Radiation-Induced Synthesis of Nanostructured Conjugated Polymers in Aqueous Solution: Fundamental Effect of Oxidizing Species. *Chemphyschem* **2014,** *15* (1), 208-218.

8. Cui, Z. P.; Coletta, C.; Dazzi, A.; Lefrancois, P.; Gervais, M.; Neron, S.; Remita, S., Radiolytic Method as a Novel Approach for the Synthesis of Nanostructured Conducting Polypyrrole. *Langmuir* **2014,** *30* (46), 14086-14094.

9. Cui, Z. P.; Coletta, C.; Rebois, R.; Baiz, S.; Gervais, M.; Goubard, F.; Aubert, P. H.; Dazzi, A.; Remita, S., Radiation-induced reduction-polymerization route for the synthesis of PEDOT conducting polymers. *Radiat. Phys. Chem* **2016,** *119*, 157-166.

10. Coletta, C.; Cui, Z. P.; Dazzi, A.; Guigner, J. M.; Neron, S.; Marignier, J. L.; Remita, S., A pulsed electron beam synthesis of PEDOT conducting polymers by using sulfate radicals as oxidizing species. *Radiat. Phys. Chem* **2016,** *126*, 21-31.

11. Cui, Z.; Bahry, T.; Dazzi, A.; Bui, T.-T.; Goubard, F.; Remita, S., Conducting polymers synthesized by γ-radiolysis in very acidic aqueous medium. *Radiation Physics and Chemistry* **2019,** *159*, 47-56.

12. Coletta, C.; Cui, Z. P.; Archirel, P.; Pernot, P.; Marignier, J. L.; Remita, S., Electron-Induced Growth Mechanism of Conducting Polymers: A Coupled Experimental and Computational Investigation. *J. Phys. Chem. B* **2015,** *119* (16), 5282-5298.

13. Emmi, S. S.; Poggi, G.; D'Angelantonio, M.; Russo, M.; Favaretto, L., The solvatochromic effect on some oligothiophene radical cations: a pulse radiolysis and semiempirical investigation. *Radiat. Phys. Chem* **2003,** *67* (3-4), 251-256.

14. Chen, T. H.; Wong, K. Y.; Johnston, F. J., Radiolysis of Chloroform and Carbon Tetrachloride. *J. Phys. Chem.* **1960,** *64* (8), 1023-1025.

15. Emmi, S. S.; Beggiato, G.; Casalboremiceli, G., Transient Species in the Pulse-Radiolysis of Methylene-Chloride and the Self-Reaction of Chloromethyl Radicals. *Radiat. Phys. Chem* **1989,** *33* (1), 29-37.

16. Alfassi, Z. B.; Mosseri, S.; Neta, P., Reactivities of Chlorine Atoms and Peroxyl Radicals Formed in the Radiolysis of Dichloromethane. *J. Phys. Chem.* **1989,** *93* (4), 1380-1385.

17. Ishigaki, A.; Koizumi, H., Radiation-induced polymerization of 3-octylthiophene. *Radiat. Phys. Chem* **2012,** *81* (7), 803-806.

18. Emmi, S. S.; D'Angelantonio, M.; Beggiato, G.; Poggi, G.; Geri, A.; Pietropaolo, D.; Zotti, G., The generation and spectral characterization of oligothiophenes radical cations. A pulse radiolysis investigation. *Radiat. Phys. Chem* **1999,** *54* (3), 263-270.

19. Isse, A. A.; Lin, C. Y.; Coote, M. L.; Gennaro, A., Estimation of Standard Reduction Potentials of Halogen Atoms and Alkyl Halides. *J. Phys. Chem. B* **2011,** *115* (4), 678-684.

20. Ushida, K.; Yoshida, Y.; Kozawa, T.; Tagawa, S.; Kira, A., Evidence of oxidation of aromatic hydrocarbons by chloromethyl radicals: Reinvestigation of intersolute hole transfer using pulse radiolysis. *J. Phys. Chem. A* **1999,** *103* (24), 4680-4689.

21. Lattach, Y.; Archirel, P.; Remita, S., Influence of the Chemical Functionalities of a Molecularly Imprinted Conducting Polymer on Its Sensing Properties: Electrochemical Measurements and Semiempirical DFT Calculations. *J. Phys. Chem. B* **2012,** *116* (5), 1467-1481.

22. Beiting, E. J.; Zeringue, K. J.; Stickel, R. E., Absorption-Spectra of Thiophene between 225-Nm and 246-Nm at Elevated-Temperatures. *Spectrochim. Acta A* **1985,** *41* (12), 1413-1418.

23. Truszkowski, S.; Szymański, W., Stable products and radicals in the radiolysis of dichloromethane and 1,1,-dichloroethane gamma-irradiated in an oxygen-free atmosphere. *J. Radioanal. Nucl. Chem* **1994,** *177* (2), 415-423.

24. Nie, T.; Zhang, K. X.; Xu, J. K.; Lu, L. M.; Bai, L., A facile one-pot strategy for the electrochemical synthesis of poly(3,4-ethylenedioxythiophene)/Zirconia nanocomposite as an effective sensing platform for vitamins B-2, B-6 and C. *J. Electroanal. Chem* **2014,** *717*, 1-9.

25. Hohnholz, D.; MacDiarmid, A. G.; Sarno, D. M.; Jones, W. E., Uniform thin films of poly-3,4-ethylenedioxythiophene (PEDOT) prepared by in-situ deposition. *ChemComm* **2001,** (23), 2444-2445.

26. Kim, T.; Kim, J.; Kim, Y.; Lee, T.; Kim, W.; Suh, K. S., Preparation and characterization of poly(3,4-ethylenedioxythiophene) (PEDOT) using partially sulfonated poly(styrene-butadiene-styrene) triblock copolymer as a polyelectrolyte. *Curr. Appl. Phys.* **2009,** *9* (1), 120-125.

27. Jang, J.; Chang, M.; Yoon, H., Chemical sensors based on highly conductive poly(3,4-ethylenedioxythiophene) nanorods. *Adv. Mater.* **2005,** *17* (13), 1616-1620.

28. Ghosh, S.; Remita, H.; Ramos, L.; Dazzi, A.; Deniset-Besseau, A.; Beaunier, P.; Goubard, F.; Aubert, P. H.; Brisset, F.; Remita, S., PEDOT nanostructures synthesized in hexagonal mesophases. *New J. Chem* **2014,** *38* (3), 1106-1115.

29. Behniafar, H.; Yousefzadeh, D., Chemical synthesis of PEDOT/Ag nanocomposites via emulsion technique in silver colloid. *Designed Monomers and Polymers* **2015,** *18* (1), 6-11.

30. Zhou, H. B.; Han, G. Y.; Chang, Y. Z.; Fu, D. Y.; Xiao, Y. M., Highly stable multi-wall carbon nanotubes@poly(3,4-ethylenedioxythiophene)/poly(styrene sulfonate) core-shell composites with three-dimensional porous nano-network for electrochemical capacitors. *J. Power Sources* **2015,** *274*, 229-236.

31. Choi, J. W.; Han, M. G.; Kim, S. Y.; Oh, S. G.; Im, S. S., Poly(3,4-ethylenedioxythiophene) nanoparticles prepared in aqueous DBSA solutions. *Synth. Met.* **2004,** *141* (3), 293-299.

32. Pistillo, B. R.; Menguelti, K.; Arl, D.; Addiego, F.; Lenoble, D., PRAP-CVD: how to design high conformal PEDOT surfaces. *RSC Advances* **2017,** *7* (31), 19117-19123.

33. Olivares, A. J.; Cosme, I.; Sanchez-Vergara, M. E.; Mansurova, S.; Carrillo, J. C.; Martinez, H. E.; Itzmoyotl, A., Nanostructural Modification of PEDOT:PSS for High Charge Carrier Collection in Hybrid Frontal Interface of Solar Cells. *Polymers (Basel)* **2019,** *11* (6), 1034.

34. Hui, Y.; Bian, C.; Wang, J. F.; Tong, J. H.; Xia, S. H., Comparison of Two Types of Overoxidized PEDOT Films and Their Application in Sensor Fabrication. *Sensors* **2017,** *17* (3).

35. Woods, R. J.; Spinks, J. W. T., THE RADIOLYSIS OF SOME ORGANIC HALOGEN COMPOUNDS IN AQUEOUS SOLUTION. *Canadian Journal of Chemistry* **1960,** *38* (1), 77-93.

36. Zhao, Q.; Jamal, R.; Zhang, L.; Wang, M. C.; Abdiryim, T., The structure and properties of PEDOT synthesized by template-free solution method. *Nanoscale Res. Lett.* **2014,** *9*.

37. Feng, W.; Li, Y.; Wu, J.; Noda, H.; Fujii, A.; Ozaki, M.; Yoshino, K., Improved electrical and optical properties of Poly(3,4-ethylenedioxythiophene) via ordered microstructure. *J. Phys. Condens. Matter* **2007,** *19* (18).

38. Gupta, B.; Mehta, M.; Melvin, A.; Kamalakannan, R.; Dash, S.; Kamruddin, M.; Tyagi, A. K., Poly (3,4-ethylenedioxythiophene) (PEDOT) and poly (3,4-ethylenedioxythiophene)-few walled carbon nanotube (PEDOT-FWCNT) nanocomposite based thin films for Schottky diode application. *Mater. Chem. Phys.* **2014,** *147* (3), 867-877.

39. Pommerehne, J.; Vestweber, H.; Guss, W.; Mahrt, R. F.; Bassler, H.; Porsch, M.; Daub, J., Efficient 2-Layer Leds on a Polymer Blend Basis. *Advanced Materials* **1995,** *7* (6), 551-554.

40. Farah, A. A.; Rutledge, S. A.; Schaarschmidt, A.; Lai, R.; Freedman, J. P.; Helmy, A. S., Conductivity enhancement of poly(3,4-ethylenedioxythiophene)-poly(styrenesulfonate) films post-spincasting. *J. Appl. Phys.* **2012,** *112* (11).

41. Jones, B. H.; Cheng, K. Y.; Holmes, R. J.; Lodge, T. P., Nanoporous Poly(3,4-ethylenedioxythiophene) Derived from Polymeric Bicontinuous Microemulsion Templates. *Macromolecules* **2012,** *45* (1), 599-601.

Chapter 4 Radiation induced synthesis of poly (3-thiophene acetic acid), PTAA, in water and dichloromethane

In chapter 2, we described our methodology based on radiation chemistry to polymerize some of conducting polymers (CPs) in aqueous solutions (PEDOT and PPy) thanks to the oxidation of dissolved organic monomers by solvent radicals *in situ* produced in the medium during water radiolysis [1-4]. As mentioned in previous chapters 2 and 3, our strategy based on radiation chemistry was opened up to the preparation of conducting polymers into organic solvents (CCl_4, $CHCl_3$ and CH_2Cl_2) [5]. By taking the advantage of dichloromethane which is able to dissolve a wide range of organic compounds and which is a good oxidizing system upon irradiation [6], gamma induced oxidative polymerization in dichloromethane was successfully employed to polymerize 3,4-ethylenedioxythiophene into poly(3,4-ethylenedioxythiophene), PEDOT polymers [5] as described in chapter 4. PEDOT polymers produced in DCM were found not similar from those obtained in water (i.e. optical properties, chemical properties, electrical properties, etc.).

In this context, poly (3-thiophene acetic acid), PTAA as one of the most important polythiophenes derivatives members, is an excellent and practical conducting polymer due to its various interesting properties such as high conductivity, good thermal and environmental stability in addiation to important biocompatibility [7]. However, additionally to what is mentioned above concerning the common synthesis methods problems there are some issues towards the synthesis of this polymer, in particular. Namely, when using chemical induced polymerization an esterification reaction is essential to protect the carboxylic acid moiety of the monomer from an oxidative decomposition [8-9]. In another meaning, several steps are required to accomplish the synthesis. Moreover, TAA is characterized by a limited solubility in aqueous media and by an oxidation potential which is higher than that of water decomposition. As a consequence, when using an electrochemically induced polymerization PTAA cannot be produced in aqueous media. PTAA is then mainly electro-polymerized in organic media such as boron triflouride diethyletherate (BFEE) and trifluoroacetic (TFA)[7, 10-12].Therefore, with these in mind, we discuss in the current chapter the use of two different radiolysis routes to induce the oxidative polymerization of 3-thiophene acetic acid (TAA) in one step synthesis, starting from monomers dissolved either in water or in dichloromethane (without using oxidizing agents or any prior esterification) (**Scheme 4.1**).

We show here a simple example to synthesize and then to modulate the morphological nanostructure of PTAA ($PTAA_{H_2O}$ and $PTAA_{CH_2Cl_2}$) conducting polymers thanks to oxidizing species generated from γ-irradiation of both solvents.

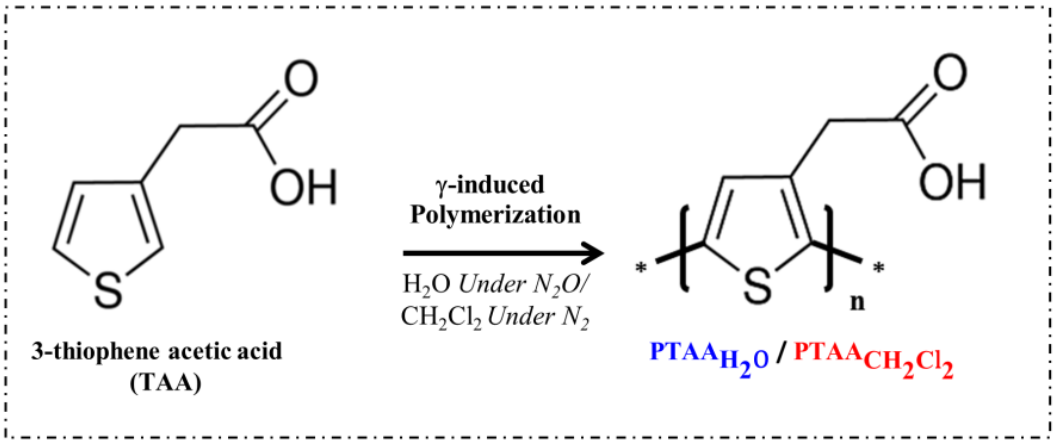

Scheme 4.1 One step synthesis of poly (3-thiophene acetic acid) (PTAA) via γ-radiolysis of dichloromethane and water

4.1. Experimental

4.1.1. Solutions Preparation

Dichloromethane solutions containing 10 mM in TAA monomers were prepared at ambient temperature. Note that the used concentration is lower than TAA solubility in dichloromethane at 25°C (which is over than 50 mM as found by UV-Vis absorption spectroscopy study (see chapter 1)). This concentration remains also much lower than dichloromethane molecules concentration (15.6 M). This enables one to neglect the direct effect of ionizing radiation on TAA monomers. In the same manner, aqueous solutions containing 10 mM in TAA were prepared at room temperature. The chosen TAA concentration, which is lower than TAA solubility in water, was always checked by UV-vis absorption spectroscopy.

The pH of the solutions was measured before and after irradiation. Dichloromethane and aqueous solutions were degassed with N_2 and N_2O, respectively, for 20 min, sealed in glass ampoules and then irradiated with a ^{60}Co ɣ-source with increasing doses up to 72 kGy at a dose rate of 3.65 kGy.h^{-1}.

4.1.2. Radiolytic methods

In water. As already explained and justified in chapter 2, under N_2O $HO^{\bullet}$ radicals can be considered as the only oxidizing species and their radiolytic yield of formation is $G_{HO^{\bullet}} = 5.6 \times 10^{-7}$ mol·J^{-1}. This radiolytic yield is equivalent to the yield of oxidation of organic monomers.

$$G_{HO^{\bullet}} = G_{ox} = 5.6 \times 10^{-7}\, mol.J^{-1} \quad (4.1)$$

Thus, for quantitative polymerization of CP, the concentration of oxidative species ($HO^{\bullet}$) should be twice that of TAA monomers ($[TAA]_0$. As a consequence, the dose D_{max} needed for a quantitative polymerization of TAA can be calculated as follows:

$$D\ (Gy) = \frac{2[TAA]_0\ (mol\ L^{-1})}{G_{ox}\ (mol\ J^{-1})\ d\ (kg\ L^{-1})} \qquad (4.2)$$

Where d=1 in these conditions

It thus amounts to 36 kGy for 10 mM in TAA. TAA aqueous solutions were then irradiated up to this dose.

In dichloromethane. When irradiation proceeds under N_2-saturated dichloromethane solutions, the radiolytic yield of the generated oxidizing species and these of oxidation has been shown in chapter 3 to be G_{ox} is 4.1×10^{-7} $mol \cdot J^{-1}$ (see also chapter 1). The concentration of TAA oxidized through dichloromethane radiolysis can be expressed as a function of the irradiation dose, D, according to equation (4.2).

The dose D_{max} needed for a quantitative polymerization of TAA can be expressed according to equation 4.2 but with d=1,35 $kg.L^{-1}$. The dose D_{max} needed for a quantitative polymerization of 10 mM in TAA in dichloromethane solutions amounts to 36 kGy as can be calculated from equation **4.2**.

Both TAA aqueous solution and TAA dichloromethane solutions were then irradiated up to 36 kGy

4.2. Results and Discussion

4.2.1. Radiation induced formation of PTAA and dose effect study:

Aqueous and dichloromethane solutions containing 10 mM in TAA were prepared under N_2O and N_2 respectively for the corresponding solvent, and their representative UV-Vis absorption spectra which are displayed in insert of **Figure 4.1a and Figure 4.1b**. The UV-Vis absorption spectra of TAA molecules in water and dichloromethane, show maximum absorption at 235 nm with molar extinction coefficients as found by our study: ε_{235} (H_2O) = 7304 and ε_{235} (CH_2Cl_2) = 6896 $L.mol^{-1}.cm^{-1}$. This consistent with thiophene molecules absorb light in the UV region between 225 and 245 nm, and this absorption is ascribed to a π-π* transition [13].

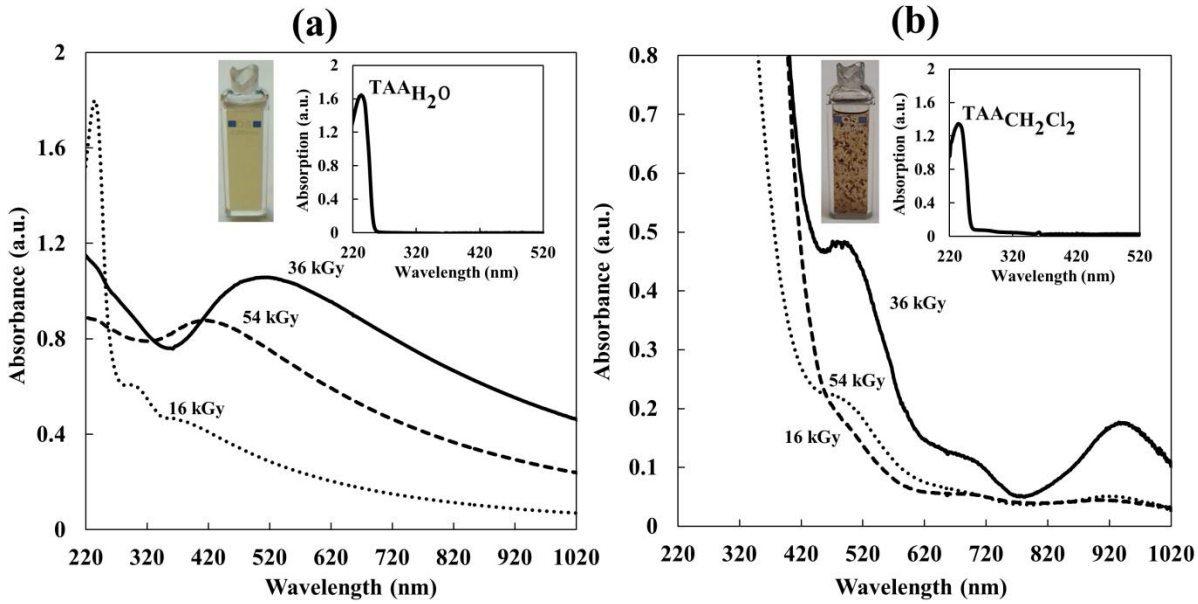

Figure 4.1 UV-Vis absorption spectra of (a) aqueous solutions containing 10 mM in TAA irradiated with increasing doses: 0, 16 kGy, 36 kGy and 54 kGy under N_2O (b) DCM solutions containing 10 mM in TAA and irradiated under N_2 atmosphere at increasing doses 0, 16, 36 and 54 kGy. The reference was the pure solvents. Inserts: photographs of PTAA solutions in water and DCM after γ-irradiation at 36 kGy and UV-Vis absorption spectra of 10 mM in TAA in water and 10 mM in TAA in DCM diluted 10 times; Reference is pure solvents; l = 0.2 cm.

In the previous works concerning gamma induced polymerization of conducting polymers in aqueous solutions, it has been demonstrated that EDOT or pyrrole molecules dissolved in water were oxidized, under N_2O, by $HO^{\bullet}$ radicals, into PEDOT and Ppy conducting polymers (CPs) [3-4]. This was possible thanks to the relatively high redox potential of $HO^{\bullet}$ which amounts to $E^{0'}(HO^{\bullet}/H_2O_2)$ = 2.2 V_{SHE} [14] and which is higher than that of EDOT/ Py monomers. Under N_2O, the yield of EDOT/Py oxidation was found equal to the radiolytic yield of $HO^{\bullet}$ formation ($G_{HO^{\bullet}}$ =5.6×10^{-7} mol.J^{-1}) which means that PEDOT/Ppy polymerization is a step by step oxidation process. Therefore, polymerization of PTAA was studied in the samy way in aqueous solution at increasing doses, in order to follow the progressive formation of PTAA. Aqueous solutions containing 10 mM in TAA were irradiated under N_2O at increasing doses up to 54 kGy and their absorption spectra were recorded as a function of the irradiation dose (**Figure 4.1a**). Gradually and up to 36 kGy, TAA disappearance represented by the absorption at 235 nm parallels the formation of species which absorb at 500 nm as illustrated on **Figure 4.1a**. According to literature, this absorption can be attributed to the radiation induced formation of PTAA oligomers and polymers and come from the π-π* transitions along the polymer chains [9, 15]. These polymers formed by water radiolysis are called $PTAA_{H_2O}$. In regards to the continuous scattering whose intensity

increases with irradiation dose (All the spectra are not represented in Figure 4.1a for clarity), this scattering should result from the presence of a dark yellow suspension in the medium as observed in **Figure 4.1a**. This suspension becomes denser and the solution appears more turbid as the irradiation dose increases. As it will be demonstrated later, this suspension corresponds to $PTAA_{H_2O}$ polymers formed at high doses thanks to the $HO^{\bullet}$-induced oxidation process.

In the same manner, we reported in **Figure 4.1b**, the UV-Vis absorption spectra of dichloromethane solution containing 10 mM in TAA irradiated under N_2 at increasing doses up to 54 kGy. Contrary to TAA in water, it is infeasible to conceive of TAA consumption and formation of TAA oligomers due to the presence of stable products of the γ-radiolysis of dichloromethane which perturb TAA absorption between 230 and 400 nm [16]. However, up to an irradiation dose of 36 kGy, remarkably, broad peak is being protruded between 490 and 720 nm (**Figure 4.1b**) and that is concurrent with formation of suspended brownish clumps of PTAA in dichloromethane solution. These polymers formed by dichloromethane radiolysis are called $PTAA_{CH_2Cl_2}$. As it will be demonstrated later, these absorption peaks and suspension correspond to $PTAA_{CH_2Cl_2}$ polymers formed thanks the oxidizing species produced from γ-irradiation of dichloromethane. Indeed, PTAA polymers usually display, in solution, characteristic peaks at approximately 400 to 500 nm which are ascribed to π-π* transitions along the polymer chains [9, 15], while the red-shift absorption band between 550 and 750 nm can be ascribed to different elongation of the PTAA's delocalized π-electron chain sequence. The observed absorption band which progressively grows up at 940 nm can be attributed to polaron and/or bipolaron bands, which are characteristic of oxidized state of pre-doped PTAA with chloride ions (The same result was obtained for PEDOT in DCM) [17]. Likewise our study concerning PEDOT polymers in dichloromethane [5], the oxidative polymerization of TAA (10 mM) in dichloromethane can be proceeded with an irradiation dose of 36 kGy.

This dose can be considered as the dose D_{max}, which enabled quantitative polymerization of PTAA, as discussed previously. Furthermore, as stated at EDOT γ-induced polymerization in dichloromethane, exceeding the dose of 36 kGy and continuing the irradiation up to 54 kGy, leads up to the degradation and the breaking down of the polymer chains. This can be seen on Figure 4.1a and 4.1b where the absorption spectra appears less intensive as irradiation dose increased above 36 kGy. Distinctly, the dose about 36 kGy seems the optimal irradiation

dose which enables quantitative polymerization of 10 mM in TAA in both corresponding solvents.

By looking at the recorded UV-Vis absotption spectra in both solvents, in particular, those recorded for irradiation doses of 36 kGy, clearly seen, PTAA polymers in dichloromethane absorb at higher wavelengths and are featured with formation of polaron and/or bipolaron bands which are characteristic of oxidized state of PTAA. This is due to the considerable amount of hydrochloride acid produced from γ-irradiation of dichloromethane, yielding to different doping states of PTAA. As a consequence, the doped PTAA polymers with chloride ions show an absorption maximum at approximately 900 nm corresponding to the charge carrier band of the charged polymers [18]. In principle, one can say that PTAA polymers induced by γ-irradiation of dichloromethane and by water are optimally produced at 36 kGy. Furthermore, PTAA induced by dichloromethane radiolysis is optically more ascendant than PTAA induced by water radiolysis under our experimental conditions.

4.2.2. Chemical characterization and chain length determination of PTAAs

The turbid solutions obtained after irradiation of 36 kGy were centrifuged at 13k rpm for 15 min to recuperate a solid phase. The obtained solid powders were dried by laboratory oven at temperature 50 °C for 24 h (**Scheme 4.2**).

Size exclusion chromatography (SEC) was used to check the molecular weight of PTAAs oligomeric/polymeric structures. For this purpose, solutions of 3 $mg.L^{-1}$ of PTAAs were prepared in THF (Scheme 4.2). The molecular weights obtained with a polystyrene calibration and calculated from the SEC chromatograms are shown in **Figure 4.2**.

The obtained data from SEC analysis is displayed in the inserted table of **Figure 4.2**. $PTAA_{H_2O}$ has number average molecular weights (M_n) of 1350 $g.mol^{-1}$ and has weight average molecular weight (M_w) of 1712 $g.mol^{-1}$. $PTAA_{CH_2Cl_2}$ has number average molecular weights (M_n) of 1320 $g.mol^{-1}$ and has weight average molecular weight (M_w) of 1860 $g.mol^{-1}$. Maldi-TOF mass spectrometry was used to measure the degree of polymerization of $PTAA_{CH_2Cl_2}$ (thanks to its better solubility and prosscability in the matrix solution THF-trans-2-[3-(4-t-butyl-phenyl)-2-methyl-2-propenylidene] malononitrile (DCTB)). The maximum molecular weight of $PTAA_{CH_2Cl_2}$, as determined by Maldi-TOF mass spectroscopy, is found to be 2840 $g.mol^{-1}$ which corresponds to about 20 repeated units of 3HT monomers **(Figure 4.3)**. Although it is possible to detect relatively high molecular weights, MALDI-TOF spectrum shows also presence of oligomers of 11 units of TAA monomers (molar mass

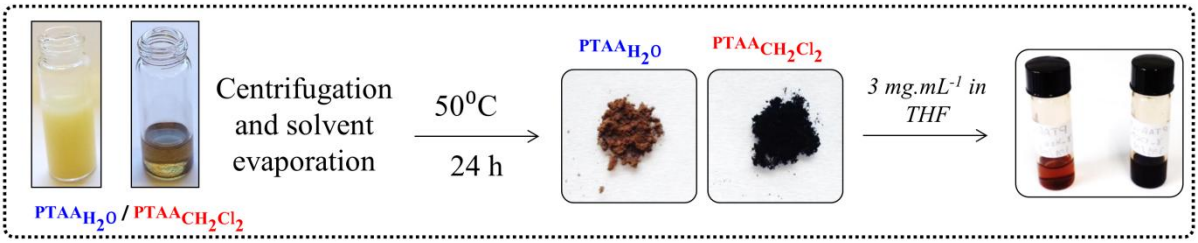

Scheme 4.2 The post processing of PTAAs polymers after gamma-irradiation

Polymer	Number Average Molecular Weight, M_n (g.mol^{-1})	Weight-Average molecular weight, M_w (g.mol^{-1})
$PTAA_{H_2O}$	1350 ≈ 9 units	1710 ≈12 units
$PTAA_{CH_2Cl_2}$	1320 ≈ 9 units	1860 ≈13 units

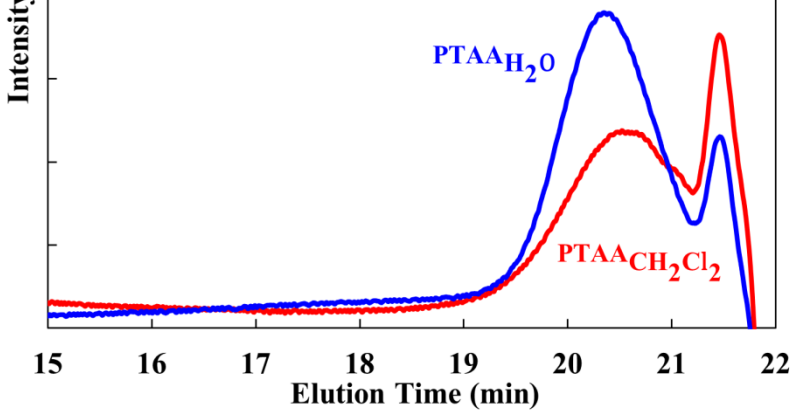

Figure 4.2 SEC chromatograms of 3 mg.mL^{1}of PTAAs polymers synthesized by γ-induced polymerization in water or DCM under N_2O or N_2 at irradiation dose of 36 kGy. The polymers powders were dissolved in THF for SEC experiments. The initial concentration of TAA was 10 mM.

of 1600 g.mol^{-1}) in abundance. The results obtained with MALDI-TOF are in good agreement with the results that were obtained with SEC analysis. Indeed, for both $PTAA_{H_2O}$ and $PTAA_{CH_2Cl_2}$, the measured mean size was found corresponding to oligomers with several TAA units around the molar mass of 1800 g.mol^{-1}, these values show that on the average there are about 13 monomer units in each polymer chain. In this regards, SEC's findings manifest no concrete influence on the molecular weight neither by the generated oxidizing radicals nor by solvents themselves.

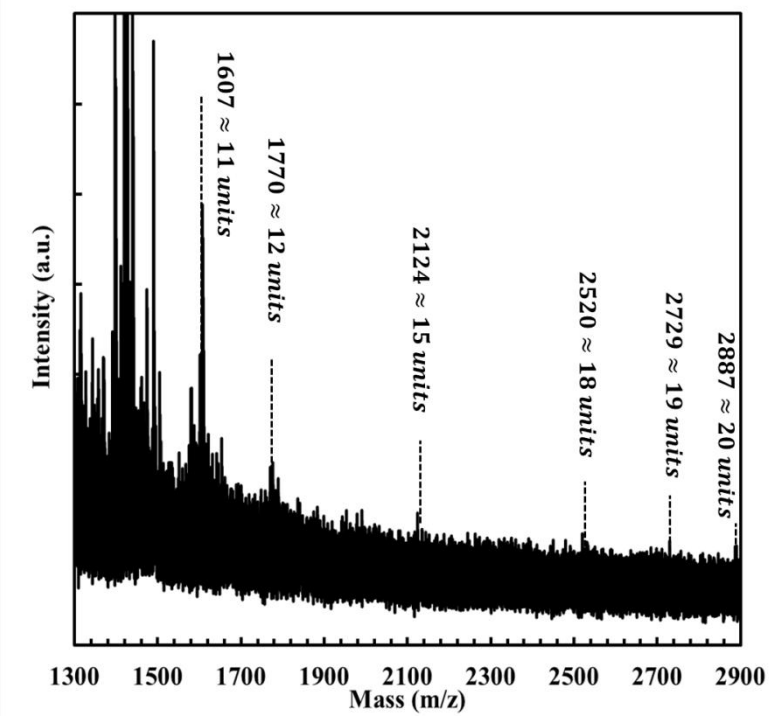

Figure 4.3 Maldi-TOF mass spectrum of $PTAA_{CH_2Cl_2}$prepared in THF-DCTB matrix solution. $PTAA_{CH_2Cl_2}$ polymers synthesized by γ-induced polymerization in DCM under N_2 at irradiation dose of 36 kGy.

Attenuated total reflectance Fourier transform infrared (ATR-FTIR) spectroscopy was used to investigate the chemical nature of the obtained PTAAs. For this purpose, the turbid solutions obtained after irradiation of 36 kGy were centrifuged at 13k rpm for 15 min to recuperate a solid phase. The obtained solid powders were dried by laboratory oven at temperature 50 °C for 24 h. ATR-FTIR spectra of both powders, radiosynthesized at 36 kGy by water radiolysis (spectrum b) and by dichloromethane radiolysis (spectrum c), are presented in **Figure 4.4** in the wave number region 4000-600 cm^{-1} together with the spectrum of pure non irradiated TAA powder (spectrum a). **Table 4.1** shows the absorption modes and the positions of the representative peaks of TAA monomers and PEDOT $PTAA_{H_2O}$ and $PTAA_{CH_2Cl_2}$ polymers

Quantitative polymerization was confirmed by the decrease of the 734 cm^{-1} absorption band which is attributed to the =Cα-H out-of-plane deformation vibration of thiophene ring in TAA monomers [19]. This peak is remarkable in the monomer spectrum and almost imperceptible in the polymers spectrum. Narrow peaks of low intensity are observed between 3000 and 2550 cm^{-1} for both the monomer and the polymers, and are attributed to the aliphatic (C-H) stretching vibration mode of aliphatic C-H bonds [19]. The absorption bands between 3200-3000 cm^{-1} attributed to the stretching vibration of the (C-H) bond on the thiophene ring.

The broad band between 3650 and 3100 cm^{-1} can be assigned to the (O-H) stretching vibration mode. [7] The (C=O) stretching vibration at 1690 cm^{-1} is related to the carboxylic group of the TAA monomer [19]. This vibration is shifted to 1706 cm^{-1} for $PTAA_{H_2O}$ polymers and to 1702 cm^{-1} for $PTAA_{CH_2Cl_2}$ (spectrum b and c). The presence of small shoulder at 1750 cm^{-1} in case of $PTAA_{H_2O}$ indicates that the carbonyl group is in a less associated state [20]. Noteworthy, C=O stretching vibration of $PTAA_{CH_2Cl_2}$ exhibits a sharper peak, indicating that the polymer is fully protonated [21]. This is ascribed to the presence of HCl which is generated by radiolysis of dichloromethane as stable product. Further consideration is the absence in the infrared spectra obtained after irradiation of the strong band of C-Cl bond between 600 and 700 cm^{-1}. This means that no chlorine atom is covalently bonded into the $PTAA_{CH_2Cl_2}$ polymers.

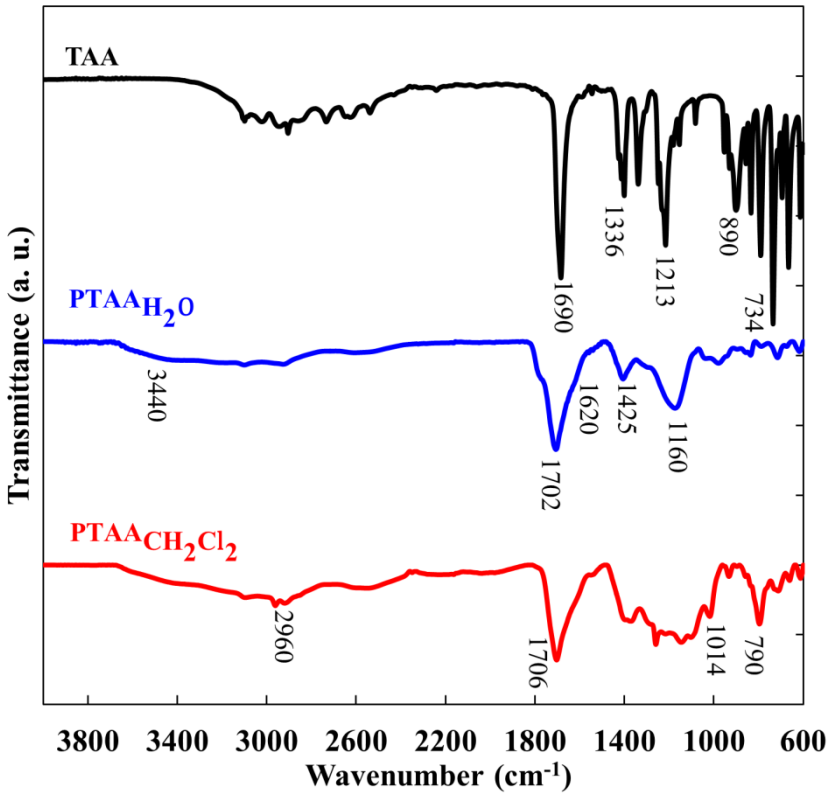

Figure 4.4 ATR-FTIR spectra of a) pure TAA monomers, b) **$PTAA_{H_2O}$** and c) **$PTAA_{CH_2Cl_2}$**. The polymers were synthesized by γ-induced polymerization in water or DCM under N_2O or N_2 atmosphere at an irradiation dose of 36 kGy. The initial concentration was 10 mM in TAA.

In turn, a shoulder around 1620 cm^{-1} is observed in the IR spectrum of $PTAA_{H_2O}$ which is related to the carboxylate anion saying that the carboxylic groups present in the partially. [21] The shoulder around 1612 cm^{-1} and the small peak at 1546 are observed in the IR spectrum of

$PTAA_{CH_2Cl_2}$ can be ascribed to asymmetrical stretching vibrations mode of quinoid configuration. The absorption at 1336 and 1365 cm^{-1} are assigned to the (C–C) stretching vibration of the thiophene ring. The bands around 1213, 1160 and 1014 cm^{-1} are attributed to the C–O bending vibrations belonging to the side chain of the thiophene. The bands at 933, 790 and 665 cm^{-1} are attributed to the C–S stretching vibration of the ring.[22] The band at 835 cm^{-1} is attributed to Cβ-H out-of-plane deformation vibration of thiophene ring.[15] As highlighted in IR spectra, absorption bands located between 1336 and 1425 cm^{-1} can be assigned to inter-ring stretching mode and symmetric stretching vibrations mode of C-C and C=C bonds, respectively. [8, 19, 23]

Functional group	Position (cm^{-1})
C=C (symmetric stretching mode)	≈1407 and 1427
C=C (asymmetrical stretching vibrations mode of quinoid configuration in thiophene ring)	≈1614 and 1546
C-C (inter-ring stretching mode)	≈1336 and 1365
C-O (bending vibration)	≈ 890, 1014, 1160 and 1214
C-S-C (stretching vibrations)	665, 790, and 933
=Cα-H (in-plane and out-of-plane deformation vibrations)	734
C=O (stretching vibrations)	≈1627 and 1705
O-H stretching vibration mode	≈ 3100 to 3600
=Cβ-H (out-of-plane deformation vibration)	≈835

Table 4.1 ATR-FTIR absorption peaks of TAA, $PTAA_{H_2O}$ and $PTAA_{CH_2Cl_2}$ polymers

As far as one can tell, the slight shifts in the recorded IR spectra of PTAAs descended evidently from the two distinct: hydrophilic aqueous medium and hydrophobic dichloromethane medium. Nevertheless, the infrared spectra obtained after irradiation reveal the typical bands of PTAA polymers and the careful interpretation of the data asserted the formation of PTAA polymers in both corresponding media.

Contrarily to chemical method, radiation induced polymerization in water and DCM successfully leads to formation of PTAA polymers in one step. Furthermore, γ-radiolysis of aqueous solutions enabled us to polymerize TAA, contrarily to electrochemical method. Thus, these findings proved the simplicity and reliability of radiation induced methodology in both solvent when comparing to conventional methods.

4.2.3. Evaluation of thermal stability of PTAAs

Thermogravimetric analysis (TGA) was used in order to detect and compare the thermo-degradability of the two different radio-synthesized PTAAs. The TGA data for $PTAA_{H_2O}$and

$PTAA_{CH_2Cl_2}$ are displayed in **Figure 4.5**. TGA curve exhibits about 8% initial weight loss observed up to 100 °C in the $PTAA_{H_2O}$ which is possibly due to the evaporation of the absorbed water on the hygroscopic polymer. On the contrary $PTAA_{CH_2Cl_2}$ is quite stable up to that temperature. From the $PTAA_{CH_2Cl_2}$ thermogram, it can be clearly observed two pronounced falls occurring at 130°C and then at 250°C. First process between 130°C and 250°C corresponds to the degradation of some $PTAA_{CH_2Cl_2}$ oligomers with relatively low molecular weight and second one corresponds to the decomposition of longer PTAAs. In regard to $PTAA_{H_2O,}$ the thermogram curve exhibits, above 130 °C, a continuous weight loss. This latter was observed until 20% of the initial weight of the polymer was lost at 700 °C.

The TGA findings suggest that $PTAA_{CH_2Cl_2}$ has better thermal stability at the initial stage of weight loss when comparing to $PTAA_{H_2O}$. This may be due to presence of longer $PTAA_{CH_2Cl_2}$polymers chains.

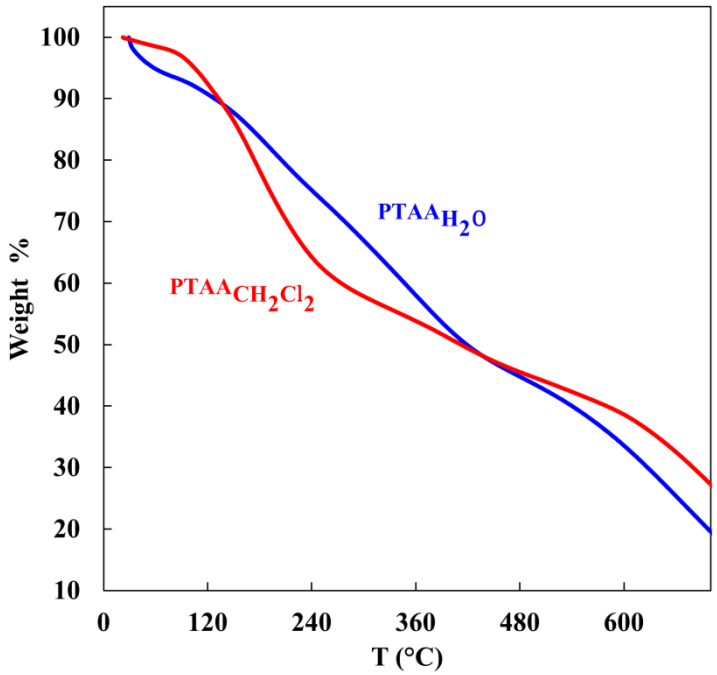

Figure 4.5 Thermogravimetric analysis (TGA) graph of dried **$PTAA_{H_2O}$** and **$PTAA_{CH_2Cl_2}$** polymers powder. The polymers were synthesized by γ-induced polymerization in water or DCM under N_2O orN_2 atmosphere at irradiation doses of 36 kGy. The initial concentration was 10 mM in TAA.

This TGA analysis of radiosynthesized PTAAs somehow matches TGA data already reported in the literature concerning PTAAs produced by conventional methodologies [24]. This

substandard behavior in comparison with PTAA polymers produced by conventional methodologies is due to relatively low molecular weight.

4.2.4. Structural and morphological characterizations of radio-synthesized PTAAs

In order to compare and to check morphologies of PTAAs which were produced by the two different radiolysis routes (water and dichloromethane radiolysis). The morphological features of radio-synthesized PTAAs were scrutinized thanks to several microscopic techniques.

4.2.4.1.Cryo-TEM observations

First and foremost, $PTAA_{H_2O}$ and $PTAA_{CH_2Cl_2}$ were characterized and investigated in solution by cryogenic-transmission electron micrograph (Cryo-TEM). For proper comparison, two solutions at concentration 3 $mg.mL^{-1}$ were prepared in water and dichloromethane for the corresponding polymers $PTAA_{H_2O}$ and $PTAA_{CH_2Cl_2}$, respectively. The recorded cryo-TEM images of $PTAA_{CH_2Cl_2}$ and $PTAA_{H_2O}$ are represented in **Figure 4.6a** and **Figure 4.6b**, respectively. Thanks to sample freezing, this technique enables *in situ* observation, into dichloromethane and aqueous solution, of radiosynthesized polymers, avoiding any phase transition and any aggregation which could result from drying procedures.

The representative cryo-TEM image of $PTAA_{H_2O}$ show the presence of low density globular structures forming polydisperse spherical nanoparticles with a diameter comprised between 300 and 800 nm as observed on **Figure 4.6a**. Given that no other low-density objects were observed during our cryo-TEM experiments, we deduce that these spherical nanoparticles are made up of PTAA polymers interacting by H-bonding into each spherical nano-particle. These observations are consistent with our previous results concerning the hydroxyl-induced radio-synthesis of PEDOT polymers in aqueous solutions.[1]

On the other hand, **Figure 4.6b** displays a zoom of one of the circular holes of the holey-carbon grid loaded with a granular cluster corresponds to 1.2 μm and comprises of granular nanoparticles with nanometric size between 50 and 80 nm. These were observed in the whole sample indicating that PTAA nanoparticles are aggregated in DCM and not isolated as in the case of water. This would imply the existence of new interparticles interaction in addition to the intraparticular ones. These interactions should come from the H-bond between the -COOH groups of the polymers located in the nanoparticles. Such as interaction is possible in

dichloromethane while it is not foreseeable in water. These aggregates observed here correspond to self-assemblies of independent PTAAs nanoparticles.

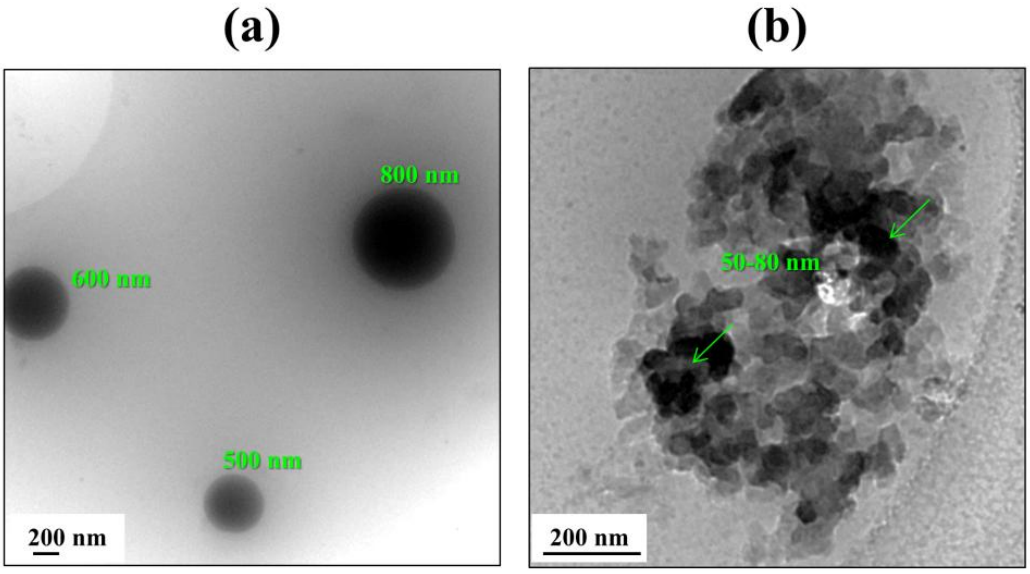

Figure 4.6 Cryo-TEM images of : (a) $\mathbf{PTAA_{H_2O}}$ polymers self-assembled into spherical nanoparticles in water under N_2O atmosphere after γ-irradiation at 36 kGy (b) $PTAA_{CH_2Cl_2}$ polymers self-assembled in clustered nanoparticles in DCM solvent under N_2 atmosphere after γ-irradiation at 36 kGy . The initial concentration in TAA was 10 mM.

4.2.4.2.XRD analysis

The samples were then dried in a laboratory oven at 50 °C for 24h after centrifugation procedure for further characterization by using X-ray diffraction. This aim was to analyze the structure and to check the crystallinity of PTAAs polymers synthesized by gamma-radiolysis of DCM and aqueous solutions. The typical XRD patterns are exhibited in **Figure 4.7**.

The diffraction peaks at about 38°, 44°, 64° and 78° are originated from the aluminum support used in this work. As can be seen in the XRD diffractograms, both XRD patterns are closely identical and no particular feature form of both PTAAs polymers is detected, as they are probably being amorphous polymers. The amorphous nature of PTAAs is highlighted and confirmed from the broad diffraction peak at 2θ ~ 21,5° which corresponds to interlayer stacked chain-to-chain distance [5]. All in all, both PTAAs diffracograms closely match those earlier reported in literature in the case of chemically synthesized PTAA polymers[25-26].

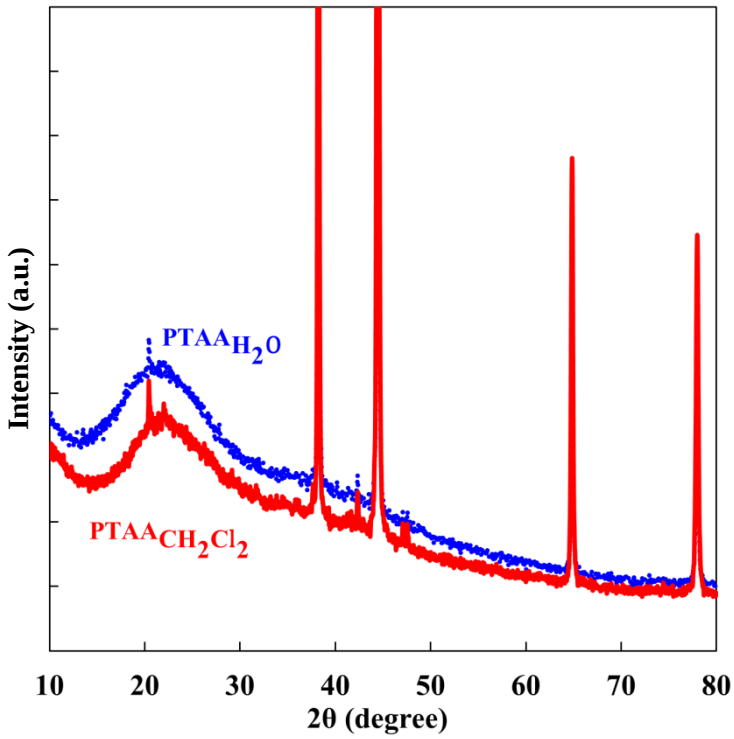

Figure 4.7 XRD diffractograms of dried **PTAA$_{H_2O}$** and **PTAA$_{CH_2Cl_2}$** polymers powders. The polymers were synthesized by γ-induced polymerization in water or DCM under N_2O or N_2 atmosphere at an irradiation dose of 36 kGy. The initial concentration was 10 mM in TAA. The substrate used for XRD analysis was aluminium.

4.2.4.3.SEM obeservations

In solid state after the deposition procedure and the drying steps, SEM microscopy was used. SEM images were recorded after deposition of the dried $PTAA_{H_2O}$ and $PTAA_{CH_2Cl_2}$ polymers powders onto carbon tape adhered to aluminum mounts and gold coating are displayed on **Figure 4.8**. Note that without gold coating. Some of these images similar images were obtained but with lower resolution. In **Figure 4.8a** SEM image of $PTAA_{H_2O}$ is presented. The image shows close-packed spherule beads with size range between 200 and 700 nm. These SEM observations agree well with the morphology of PTAAs previously observed in aqueous solution by Cryo-TEM (**Figure 4.6a**) without any significant change in the mean size and in the shape. Then, the packing of the particles and their flattening onto the substrate when deposited and dried do not seem to affect the nanostructuration of $PTAA_{H_2O}$ polymers.

SEM image of $PTAA_{CH_2Cl_2}$ is represented in **Figure 4.8b**. $PTAA_{CH_2Cl_2}$ appears outwardly as large aggregates of several micrometers. However, by looking very closely, it is possible to

recognize tightly packed granular nanoparticles of several hundreds of nanometers. The particles observed by SEM after deposition, are slightly bigger than the globular nanostructures observed by cryo-TEM in solution. The flattening of the particles upon deposition onto the substrate and their aggregation upon drying due to phase transition should explain the increase and the polydispersity in size observed in **Figure 4.8b**.

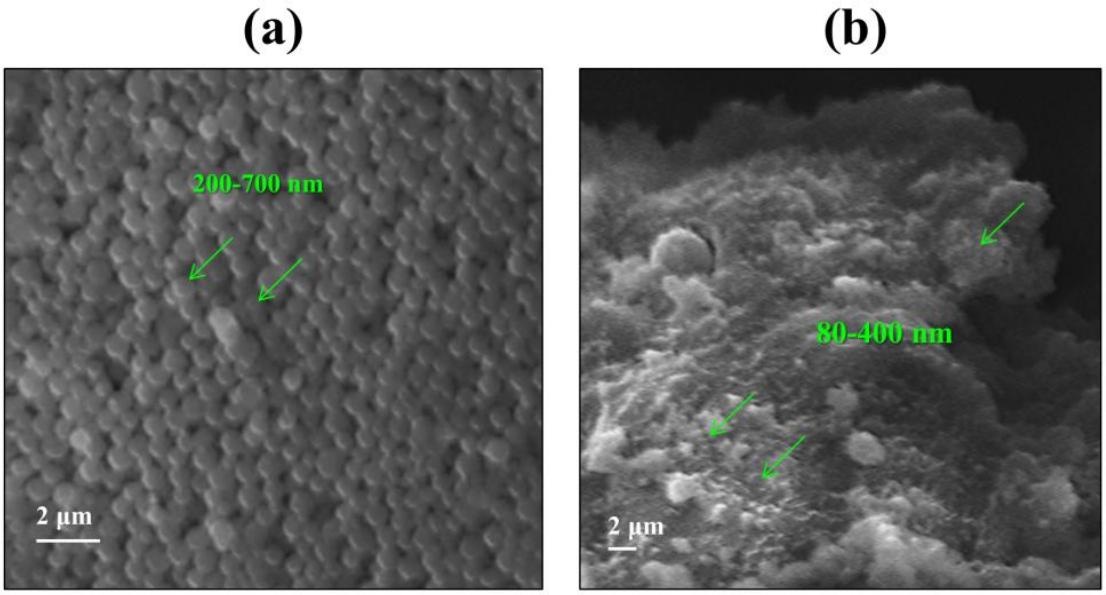

Figure 4.8 SEM images of dried $\mathbf{PTAA_{H_2O}}$ and $\mathbf{PTAA_{CH_2Cl_2}}$ polymers powders after deposition onto carbon tape adhered to aluminum mounts and gold coating. The powders were obtained after solvent evaporation. The polymers were synthesized by γ-induced polymerization in water or DCM under N_2O or N_2 atmosphere at irradiation dose of 36 kGy. The initial concentration was 10 mM in TAA.

4.2.4.4.EDX spectroscopy

During SEM obsevations and without gold coating, *in situ* Energy-Dispersive X-ray spectroscopy (EDX) was carried out in order to identify the chemical composition of the materials and to perform the elemental analysis in different areas of the deposited nanoparticles. EDX highlighted the presence of sulfur (in addition to carbon and oxygen) in the whole $PTAA_{CH_2Cl_2}$ and $PTAA_{H_2O}$ samples demonstrating that our materials are effectively made of PTAAs polymers. Particularly, EDX enabled the detection of chlorine atoms dispersed in $PTAA_{CH_2Cl_2}$ granular nanoparticles. This observation definitely demonstrates that differently to $PTAA_{H_2O}$ synthesized by water radiolysis, radiosynthesized $PTAA_{CH_2Cl_2}$ are doped with chloride ions, in total agreement with our results obtained by UV-Vis absorption spectrophotometry and by ATR-FTIR spectroscopy.

4.2.4.5.AFM observations

AFM microscopy was used to get better morphological analysis and characterization for the two PTAAs powders obtained after γ-irradiation at the optimal dose. First, $PTAA_{CH_2Cl_2}$and $PTAA_{H_2O}$ powders were solubilized in ethanol (3 $mg.mL^{-1}$) and then a small drop of each ethanolic solution was deposited onto the upper surface of ZnSe prism and dried naturally at air. Each of the obtained films was then scanned by AFM (**Figure 4.9**). According to the AFM images of the samples recorded in tapping mode (**Figure 4.9 a** and **b**), the bottom dark areas having no thickness correspond to the substrate, while, the bright areas correspond to the topography of the samples. In **Figure 4.9a** the AFM topography of $PTAA_{H_2O}$ is presented. Distinctly, the topography of $PTAA_{H_2O}$ displayed as the bright areas correspond to the thicker regions made up of nano-spherules with equivalent size in the range 300-700 nm.

The AFM topography of $PTAA_{CH_2Cl_2}$ presented in **Figure 4.9b**, shows markedly small granular nanoparticles of several tens of nanometers as well as aggregated granular clusters of 800 to 1200 nm. The observed aggregated clusters are ascribed to the fact that dichloromethane not a good solvent of $PTAA_{CH_2Cl_2}$nanoparticles. It cannot stabilize them and cannot screen the interparticular H-bond interactions. Subsequently $PTAA_{CH_2Cl_2}$ nano-granules get together to form large aggregations.

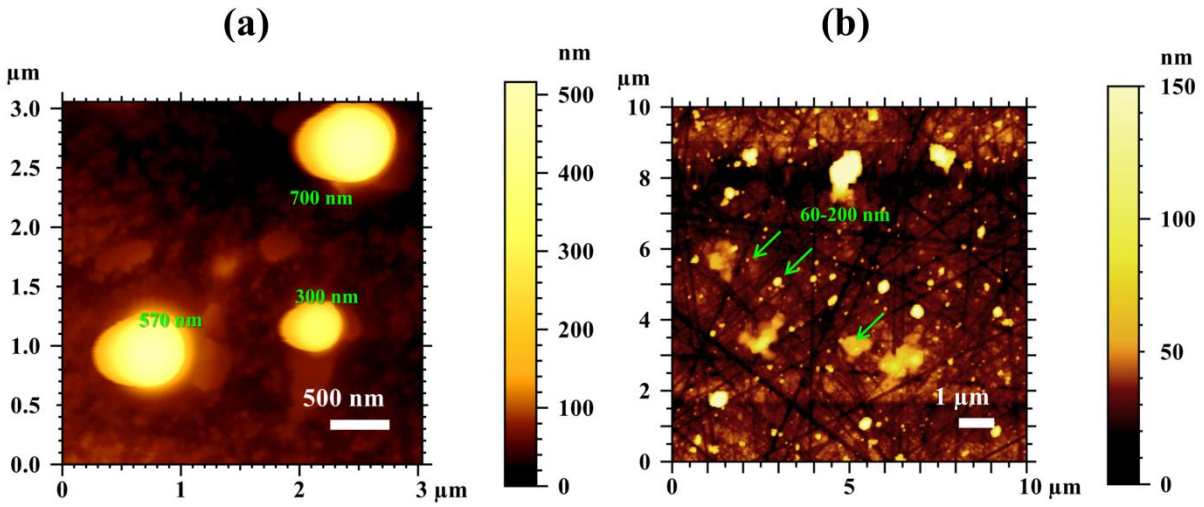

Figure 4.9 AFM topographic images of (a $\mathbf{PTAA_{H_2O}}$ and (b $PTAA_{CH_2Cl_2}$ polymers after deposition onto the CaF_2 disk. The polymers were synthesized by γ-induced polymerization in water or DCM under N_2O or N_2 atmosphere at irradiation dose of 36 kGy. The initial concentration was 10 mM in TAA.The AFM is used in tapping mode.

The small $PTAA_{CH_2Cl_2}$ nano-granules and $PTAA_{H_2O}$ nano-spherules which have been observed by AFM microscopy, are undoubtedly one and the same of those have been spotted by cryo-TEM.

We can conclude, on the whole, that the microscopic findings are all in good agreement. According to the microscopic observations (cryo-TEM, SEM and AFM), γ-radiation induced polymerization of TAA either in dichloromethane or in aqueous solution lead successfully up to two different nanostructures. These dissimilarities are indeed raised from the influence of polarity and the dissociating power of the two solvents. In addition as highlighted by EDX $PTAA_{CH_2Cl_2}$ is found doped. In consequence of different polymeric morphologies and nanostructures as well as different doping states, the radio-synthesized $PTAA_{CH_2Cl_2}$ and $PTAA_{H_2O}$ effectively possess distinct optical properties as already found (see **Figure 4.1**).

Let's now check the electrical properties and see if $PTAA_{H_2O}$ and $PTAA_{CH_2Cl_2}$ polymers also possess different electrical properties.

4.2.5. PTAAs Electrochemical performances of radio-synthesized PTAAs

$PTAA_{CH_2Cl_2}$ and $PTAA_{H_2O}$ powders obtained after γ-irradiation and solvent evaporation were dissolved in DCM at a concentration of 10 $mg.mL^{-1}$. Then, 100 µL of each solution were spin-coated on a clean glass substrate and the obtained films were doped with $NOBF_4$ (20 mM) in acetonitrile. After measuring the thickness of the films by a surface profiler, their conductivity was determined by four-point probe technique. The average electrical conductivities of $PTAA_{CH_2Cl_2}$ and $PTAA_{H_2O}$ were found to be 1.6×10^{-3} $S\cdot cm^{-1}$ and 0.6×10^{-3} $S\cdot cm^{-1}$, respectively. Remarkably, $PTAA_{CH_2Cl_2}$ has higher electrical conductivity, roughly 3 times higher than $PTAA_{H_2O}$. This should result from the difference in the morphology and the doping state of PTAAs. It is worth noting that, the amount of hydrochloride acid produced from γ-irradiation of dichloromethane, yields to doping of $PTAA_{CH_2Cl_2}$ while $PTAA_{H_2O}$ remains undoped. Now, the electrical conductivities measured for $PTAA_{H_2O}$ and $PTAA_{CH_2Cl_2}$ synthesized by γ-radiolysis show relatively higher conductivity in comparison with those already reported in literature for PTAA polymers produced by conventional synthetic methods [27].

The electronic properties of $PTAA_{H_2O}$ and $PTAA_{CH_2Cl_2}$ were investigated to inspect their potential applications. The oxidation and reduction potentials of $PTAA_{H_2O}$ and $PTAA_{CH_2Cl_2}$ were monitored under similar experimental conditions by using cyclic

voltammetry (CV) analysis (**Figure 4.10**). For this purpose, solutions of 3 mg.mL^{-1} of $PTAA_{H_2O}$ and $PTAA_{CH_2Cl_2}$ previously synthesized by radiolysis were dissolved in THF. Then, about 1 mL of each solution was mixed with 5 mL of acetonitrile solution containing tetrabutylammonium hexafluorophosphate ($TBAPF_6$) used as electrolyte at a concentration of 0.1 M.

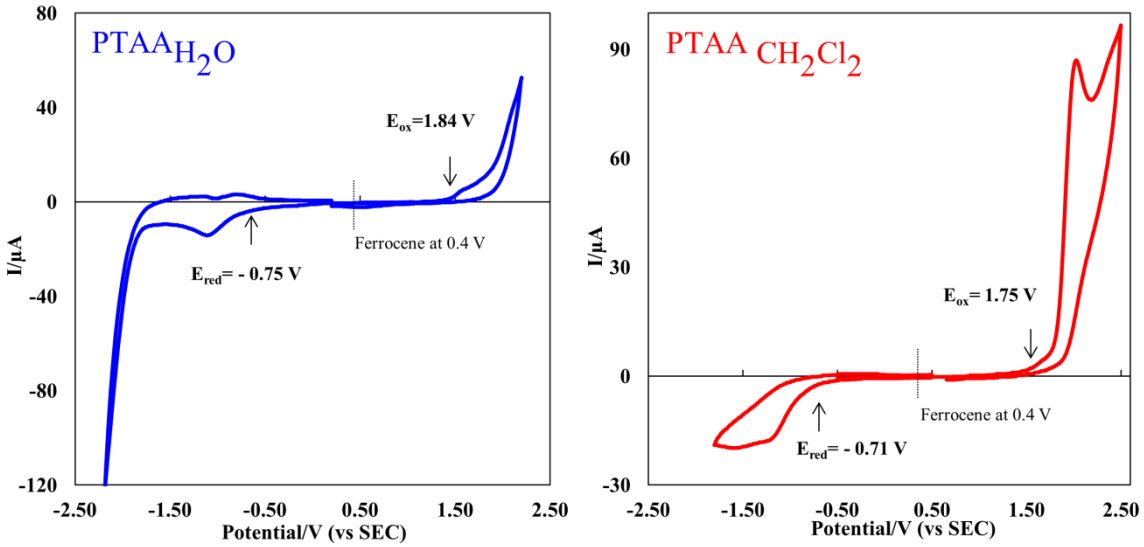

Figure 4.10 Cyclic voltammetry of 3 mg.L^{-1} of **$PTAA_{H_2O}$** and **$PTAA_{CH_2Cl_2}$** dissolved in THF recorded in acetonitrile containing 0.1 M of $TBAPF_6$ at a scan rate of 100 mV.S^{-1}. The polymers were synthesized at a dose of 36 kGy in corresponding solvent containing 10 mM in TAA. Ferrocenium/ferrocene (Fc^+/Fc) redox potential was measured in order to calibrate the pseud reference electrode (0.4 V vs SEC in the present study). The HOMO/LUMO energetic levels of PTAA are calculated as follows: E_{HOMO} (eV) from ionization potential = -4.8 – e(E_{ox}-0.4) and E_{LUMO} (eV) from electronic affinity = -4.8 – e(E_{red}-0.4) where e is the elementary charge.

The CV profiles show the main p-doping (oxidation) process occurs at onset potentials of +1.84 V ($PTAA_{H_2O}$) and +1.75 V ($PTAA_{CH_2Cl_2}$) while n-doping starts at -0.75 V ($PTAA_{H_2O}$) and -0.71 V ($PTAA_{CH_2Cl_2}$). Knowing these potential values, one can calculate, from the equations given in legend of **Figure 4.10**, the HOMO/LUMO energy levels of radiosynthesized $PTAA_{H_2O}$ and $PTAA_{CH_2Cl_2}$. Both the energy level of the highest occupied molecular orbital (HOMO) and the energy of the lowest unoccupied molecular orbital (LUMO) were calculated, from the ionization potential and the electronic affinity, respectively. E_{HOMO} and E_{LUMO} amount respectively to -6.24 eV and -3.65 eV ($PTAA_{H_2O}$) and -6.15 eV and -3.67 eV ($PTAA_{CH_2Cl_2}$), leading to an electrochemical band gap E_{gap} of 2.59 eV ($PTAA_{H_2O}$) and 2.48 eV ($PTAA_{CH_2Cl_2}$) as shown in **Figure 4.10 (a and b)**. The HOMO/LUMO energy levels of the material were calculated by using the ferrocene

ionization potential value as the standard. The corrected value of 4.8 eV vs vacuum of ferrocene is widely adopted. This value is based on the calculation obtained by Pommerehne *et al.*[28] It is fairly obvious that the oxidation and reduction onsets of $PTAA_{H_2O}$ and $PTAA_{CH_2Cl_2}$ provide matching values. The cyclic voltammetry findings suggest that both two polymers have the same electronic behavior and indeed, the results are consistent with SEC data since the two polymers roughly possess the same molecular weight and thus comparable electronic band gaps. Anyhow, the calculated electronics band gaps are closely matching results earlier reported in the literature for PTAA polymers which were synthesized by conventional chemical method by using $FeCl_3$.[23, 29]

On another hand, the optical band gaps measurement is important for applications such as solar cells and therefore, the cyclic voltammetry results were upheld by drawing on Tauc's plot, which was read it out from the recorded absorption spectra of $PTAA_{H_2O}$ and $PTAA_{CH_2Cl_2}$dissolved in THF, as depicted in **insert of Figure 4.10 (a** and **b).** The UV-Vis absorption spectrum of $PTAA_{H_2O}$in THF does not retain the same spectral features as observed in absorption spectrum **Figure 4.1a**. From the spectrum of $PTAA_{CH_2Cl_2}$, it is possible to discern that $PTAA_{CH_2Cl_2}$in THF retains the same absorption peaks as those observed in insert of **Figure 4.1b**, especially, the one attributed to doping effect. In the context of Tauc's plot, based on Tauc equation represented below, $(\alpha h\upsilon)^{1/n}$ is principally plotted as a function of photon energy ($h\upsilon$):

$$(\alpha h\upsilon)^{1/n} = A(h\upsilon - E_{gap}) \qquad (4.3)$$

Where α, h, υ and E_{gap} are respectively the absorption coefficient, Planck constant, light frequency, oprical band gap energy and A is a constant. The exponent n is 0.5 for direct allowed transitions, 1.5 for direct forbidden transitions, 2 for indirect allowed transitions, and 3 for indirect forbidden transitions. Here, n=2 corresponding to the amorphous nature of the two polymers, which indicates an allowed indirect transitions.

As a consequence, in our case if n=2

$$(\alpha h\upsilon)^{1/2} = A(h\upsilon - E_{gap}) \qquad (4.4)$$

$$(\alpha h\upsilon)^{1/2} = Ah\upsilon - AE_{gap} \qquad (4.5)$$

Thus, optical band gaps E_{gap} can be calculated from the linear relation of $(\alpha h\upsilon)^{1/2}$ as a function of $h\upsilon$ and are determined by linear fit extrapolations onto the x-axis. A plot of $(\alpha h\upsilon)^{1/2}$ versus photon energy ($h\upsilon$) gives the band gap energies of the $PTAA_{CH_2Cl_2}$ and $PTAA_{H_2O}$ by the intercept of the tangent to the x-axis, as shown in **Figure 4.11 (a** and **b)**. The optical band gap energies of the ($PTAA_{H_2O}$) and ($PTAA_{CH_2Cl_2}$) were estimated to be 2.37 eV and 2.00 eV, respectively. We can observe that the optical band gap values are smaller than the electrochemical band gaps (2.59 and 2.48 eV respectively). Indeed, usually, the electronic band gaps are larger than the optical band gaps since the measurements by electrochemistry require additional energy because of Coulomb interactions.

The calculated E_{gap} of optical band gap $PTAA_{CH_2Cl_2}$ exhibits considerable difference in comparison with E_{gap} of $PTAA_{H_2O}$. Here again, the pre-doping of $PTAA_{CH_2Cl_2}$ with chloride ions coming from dichloromethane radiolysis affords, as expected, lower E_{gap} on $PTAA_{H_2O}$ account. As a consequence, these materials can presumably be used in solar cells due to their appropriate and pertinent E_{gap} values in the field.

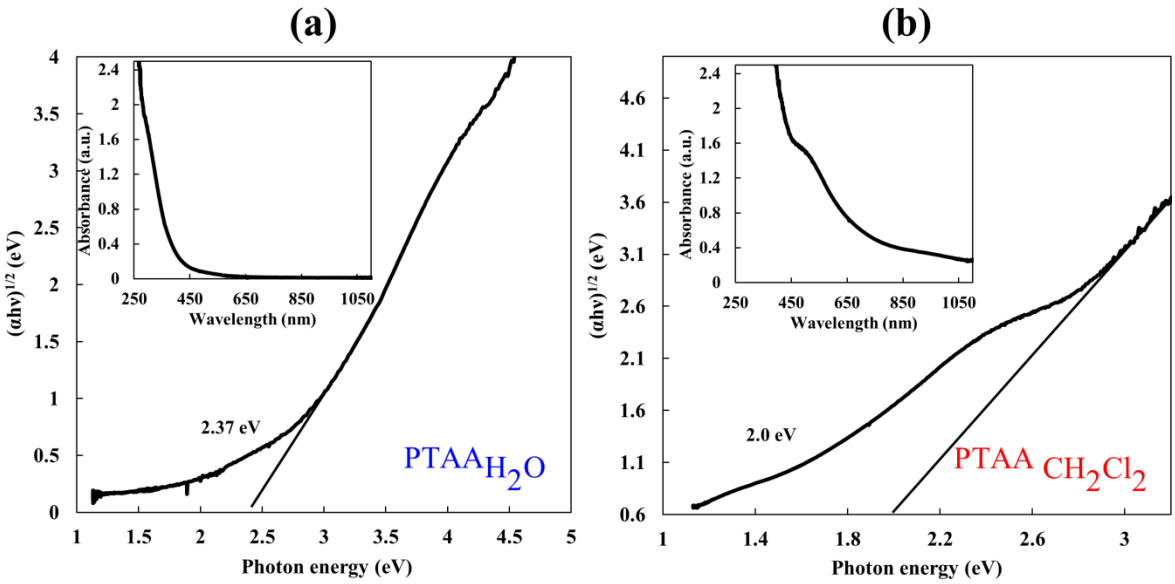

Figure 4.11 Tauc-plot analysis of UV-Vis absorption spectra $\mathbf{PTAA_{H_2O}}$ and $\mathbf{PTAA_{CH_2Cl_2}}$ in THF solvent for optical band gap assessment indicating the indirect transition for (a) $\mathbf{PTAA_{H_2O}}$ and (b) $\mathbf{PTAA_{CH_2Cl_2}}$. The UV-Vis absorption spectra of PTAAs dissolved in THF are given in insert. Reference is THF. L= 0.2 cm

4.2.6. Scrutinizing the electrochromic applicability of $PTAA_{CH_2Cl_2}$ and $PTAA_{H_2O}$

Thanks to the interesting optical and electrical properties of PTAAs polymers we wanted to check their electrochromic properties. To probe these electrochromic properties, we first dissolved $PTAA_{CH_2Cl_2}$ and $PTAA_{H_2O}$ polymers powder in DMSO solvent at approximate concentration of 5 mg.L^{-1} (Figure 4.11, before doping). Later on, few mg of pure $NOBF_4$ were (used as oxidant) added directly to DMSO solutions to chemically dope PTAA polymers. Thereafter, the solutions were vortexed, roughly for 2 min, before recording thier absorption spectra. The photographs of undoped and doped PTAA polymers are shown in **Figure 4.12**.

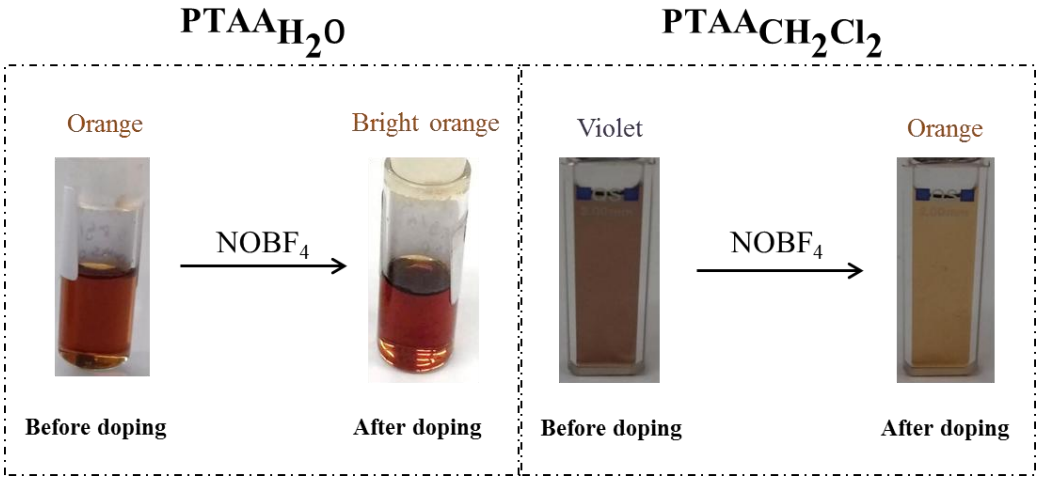

Figure 4.12 photographs of $PTAA_{H_2O}$ and $PTAA_{CH_2Cl_2}$ dissolved in dimethysulphoxide (DMSO) at a concentration of 5 mg.mL^{-1} before and after doping

In case of $PTAA_{H_2O}$, the initial colour of its solution in DMSO before doping with $NOBF_4$ is orange. This colour is getting slightly brighter after adding the dopant. In the latter case, $PTAA_{CH_2Cl_2}$ solution in DMSO has violet colour and upon the addition of $NOBF_4$ it becomes orange. The spectra of the corresponding solutions before and after doping are depicted in **Figure 4.13**.The UV-Vis spectrum of $PTAA_{H_2O}$ in DMSO before doping exhibits a shoulder around 300 nm. Worthy of note, this recorded absorption spectrum in DMSO looks like the absorption spectrum recorded in THF (Figure 4.11a, insert). Nothing noteworthy, after doping $PTAA_{H_2O}$, a modest change is observed in absorption spectrum where the shoulder is discernible around 360 nm. Then, only a slight shift in the spectra is noted which is in agreement with the slight change in the color of the solution upon doping. By looking at UV-Vis spectrum of $PTAA_{CH_2Cl_2}$ before the doping test, it is possible to observe a conspicuous absorption peak at 464 nm. The spectrum after $NOBF_4$ addition shows a red-shift of the

maximal absorption to 480 nm in addition to the appearance of broad absorption in the near infrared region. The change in the absorption spectrum is in this case more pronounced which is in agreement with the change in the color of the solution from violet to orange.

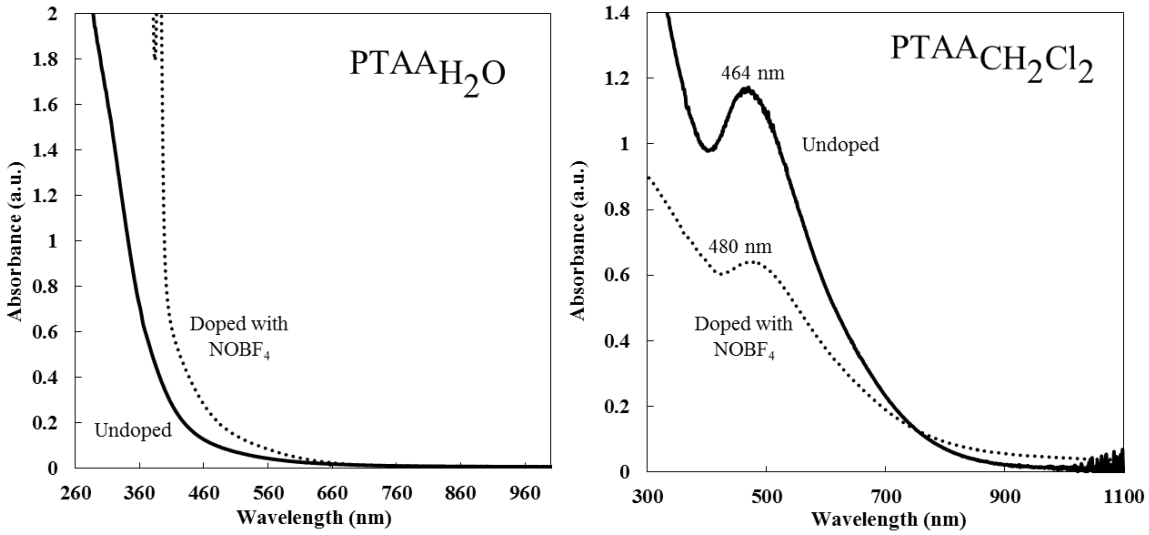

Figure 4.13 UV-Vis absorption spectra of 3 mg.mL^{-1}of PTAAs polymers dissolved in DMSO before and after doping with $NOBF_4$. The polymers were synthesized by γ-induced polymerization in water or in DCM under N_2O or N_2 at irradiation dose of 36 kGy. The initial concentration of TAA was 10 mM.

Although the spectral and optical changes are perceptible, the responses upon chemical doping are still insignificant and ordinary for electrochromism. These outcomes can be ascribed to relatively low molecular weight and to mal-distribution of electron-poor and electron-rich units along the polymer backbone. However, the electrochomic characteristics can be ameliorated by trying to synthesize polymers with higher molecular weight. Additionally, using a small subset of building blocks and resort to copolymerization will be immensely helpful to enhance the electrochromic properties.

4.3. Conclusion

Current research aims to develop new synthesis strategies and new conducting polymers with tuned morphologies and properties. We recently, and for the first time in the literature, used γ-radiolysis as an original simple alternative way for synthesizing nanostructured conducting PPy and PEDOT polymers in aqueous solution at ambient temperature and in the absence of any external oxidizing species. In order to develop a new processable method to

synthesize conducting polymers and also to overcome the low solubility issue, recently, our strategy based on radiation chemistry was extended to the preparation of conducting polymers into organic solvents.

In order to carry forward the development of our methodology based on radiation induced polymerization, to control the optical properties of radio-synthesized materials and to tune polymers morphology, in the present chapter, we exhibited two original and simple synthesis routes based on gamma radiation induced polymerization of PTAA in aqueous solutions and in dichloromethane without using oxidizing agents or any prior esterification. Starting from TAA monomers dissolved in aqueous solution or in dichloromethane, the oxidative polymerization of PTAA was successfully induced by gamma irradiation at a dose of 36 kGy. Depending on the solvent, two different PTAA polymers were formed (namely $PTAA_{H_20}$ and $PTAA_{CH_2Cl_2}$).

Whereas, the spectroscopic analysis represented by UV-Vis and ART-FTIR spectroscopy manifested distinct chemical and optical properties for both polymers SEC analysis showed that solvent has no influence on the molecular weight of the radio-synthesized. Both polymers are found amorphous as highlighted by XRD. TGA analysis demonstrated good and convergent thermal stabilities. The morphological analysis of $PTAA_{H_20}$ and $PTAA_{CH_2Cl_2}$was carried out in solution by cryo-TEM and after deposition onto substrate by XRD, SEM and AFM. The microscopic observations revealed that γ-synthesized PTAAs have two different nano-structures. In dichloromethane, $PTAA_{CH_2Cl_2}$was characterized by polymeric granular nano-structures of several tens of nanometer, whereas nano-spherules of few hundred nanometers size are the characteristic structures of $PTAA_{H_20}$ in aqueous solutions.

Cyclic voltammetry analysis and optical band gap calculations are favorable for any practical use. The electrical conductivity records are quite remarkable and even better than the electrical properties that have already been reported in literature highlighted the success of our radiation based synthesis leading to promising and usable polymers for practical applications. Ultimately, the optical and electrical features of $PTAA_{CH_2Cl_2}$outperform those of $PTAA_{H_20}$.

Nevertheless, the electrochromic test was not totally satisfactory and the electrochromic response has to be improved and therefore the synthesis of polymers having neat nanostructure with longer polymer chains is foreseeable to get better electrical and electrochromic properties. Let's take into account the fact that dichloromethane and water are immiscible solvents. This study on PTAA polymers posits the use of CH_2Cl_2/H_2O or

H_2O/CH_2Cl_2 microemulsions polymerization through gamma radiolysis with the view to having controlled morphology.

In another regard, this comparative study showed besides the influence of employed solvent and the versatility of both developed methodologies (in water and in organic solvent). In the next chapter we will introduce the synthesis of new conducting polymer, namely P3HT. Thus, the main objective of the next chapter is to synthesize P3HT polymer starting from 3HT monomers. Knowing that 3HT is insoluble in water, we will study only the polymerization in DCM solvent. Moreover, we will study the polymerization in DCM under different atmospheres in order to vary the oxidizing species and the yield of polymerization. We will also check the influence of the generated radicals on the morphology, the stability and on the optical and electrical properties.

References

1. Lattach, Y.; Coletta, C.; Ghosh, S.; Remita, S., Radiation-Induced Synthesis of Nanostructured Conjugated Polymers in Aqueous Solution: Fundamental Effect of Oxidizing Species. *ChemPhysChem* **2014,** *15* (1), 208-218.

2. Cui, Z.; Coletta, C.; Rebois, R.; Baiz, S.; Gervais, M.; Goubard, F.; Aubert, P.-H.; Dazzi, A.; Remita, S., Radiation-induced reduction–polymerization route for the synthesis of PEDOT conducting polymers. *Radiation Physics and Chemistry* **2016,** *119*, 157-166.

3. Cui, Z.; Coletta, C.; Dazzi, A.; Lefrançois, P.; Gervais, M.; Néron, S.; Remita, S., Radiolytic Method as a Novel Approach for the Synthesis of Nanostructured Conducting Polypyrrole. *Langmuir* **2014,** *30* (46), 14086-14094.

4. Coletta, C.; Cui, Z.; Archirel, P.; Pernot, P.; Marignier, J.-L.; Remita, S., Electron-Induced Growth Mechanism of Conducting Polymers: A Coupled Experimental and Computational Investigation. *The Journal of Physical Chemistry B* **2015,** *119* (16), 5282-5298.

5. Bahry, T.; Cui, Z.; Deniset-Besseau, A.; Gervais, M.; Sollogoub, C.; Bui, T.-T.; Remita, S., An alternative radiolytic route for synthesizing conducting polymers in an organic solvent. *New Journal of Chemistry* **2018,** *42* (11), 8704-8716.

6. Emmi, S. S.; Beggiato, G.; Casalbore-Miceli, G., Transient species in the pulse radiolysis of methylene chloride and the self-reaction of chloromethyl radicals. *International Journal of Radiation Applications and Instrumentation. Part C. Radiation Physics and Chemistry* **1989,** *33* (1), 29-37.

7. Wu, T.; Wang, L.; Zhang, Y.; Du, S.; Guo, W.; Pei, M., Electrochemical synthesis of poly(3-thiophene acetic acid) nanowires with water-soluble macromolecule templates. *RSC Advances* **2015,** *5* (22), 16684-16690.

8. Kim; Chen, L.; Gong; Osada, Y., Titration Behavior and Spectral Transitions of Water-Soluble Polythiophene Carboxylic Acids. *Macromolecules* **1999,** *32* (12), 3964-3969.

9. Yanagida, S.; Senadeera, G. K. R.; Nakamura, K.; Kitamura, T.; Wada, Y., Polythiophene-sensitized TiO2 solar cells. *Journal of Photochemistry and Photobiology A: Chemistry* **2004,** *166* (1), 75-80.

10. Najafisayar, P.; Bahrololoom, M. E., The effect of pulse electropolymerization on the electrochemical properties of polythiophene films. *Electrochim Acta* **2013,** *114*, 462-473.

11. Sato, M.-a.; Tanaka, S.; Kaeriyama, K., Electrochemical preparation of highly conducting polythiophene films. *Journal of the Chemical Society, Chemical Communications* **1985,** (11), 713-714.

12. Downard, A. J.; Pletcher, D., The influence of water on the electrodeposition of polypyrrole in acetonitrile. *Journal of Electroanalytical Chemistry and Interfacial Electrochemistry* **1986,** *206* (1), 139-145.

13. Beiting, E. J.; Zeringue, K. J.; Stickel, R. E., Absorption spectra of thiophene between 225 and 246 nm at elevated temperatures. *Spectrochimica Acta Part A: Molecular Spectroscopy* **1985,** *41* (12), 1413-1418.

14. Ferradini, C.; Jay-Gerin, J.-P., La radiolyse de l'eau et des solutions aqueuses : historique et actualité. *Canadian Journal of Chemistry* **1999,** *77* (9), 1542-1575.

15. Gomes, A. L.; Pinto Zakia, M. B.; Filho, J. G.; Armelin, E.; Alemán, C.; Sinezio de Carvalho Campos, J., Preparation and characterization of semiconducting polymeric blends. Photochemical synthesis of poly(3-alkylthiophenes) using host microporous matrices of poly(vinylidene fluoride). *Polymer Chemistry* **2012,** *3* (5), 1334-1343.

16. Truszkowski, S.; Szymański, W., Stable products and radicals in the radiolysis of dichloromethane and 1,1,-dichloroethane gamma-irradiated in an oxygen-free atmosphere. *Journal of Radioanalytical and Nuclear Chemistry* **1994,** *177*, 415-423.

17. Kim, T.; Kim, J.; Kim, Y.; Lee, T.; Kim, W.; Suh, K. S., Preparation and characterization of poly(3,4-ethylenedioxythiophene) (PEDOT) using partially sulfonated poly(styrene-butadiene-styrene) triblock copolymer as a polyelectrolyte. *Current Applied Physics* **2009,** *9* (1), 120-125.

18. Jang, J.; Chang, M.; Yoon, H., Chemical Sensors Based on Highly Conductive Poly(3,4-ethylenedioxythiophene) Nanorods. *Advanced Materials* **2005,** *17* (13), 1616-1620.

19. Yuan, X.; Floresyona, D.; Aubert, P.-H.; Bui, T.-T.; Remita, S.; Ghosh, S.; Brisset, F.; Goubard, F.; Remita, H., Photocatalytic degradation of organic pollutant with polypyrrole nanostructures under UV and visible light. *Applied Catalysis B: Environmental* **2019,** *242*, 284-292.

20. de França Mescoloto, A.; Pulcinelli, S. H.; Santilli, C.; Cristina Gonçalves, V., Structural and Thermal Properties of Carboxylic Acid Functionalized Polythiophenes. *Polimeros* **2014,** *24*, 31-35.

21. Giglioti, M.; Strixino, F.; Matsushima, J. T.; Bulhoes, L.; Pereira, E., Electrochemical and electrochromic response of poly(thiophene-3-acetic acid) films. *SOL ENERG MAT SOL C* **2004,** *82*, 413-420.

22. Mescoloto, A. d. F.; Pulcinelli, S. H.; Santilli, C. V.; Gonçalves, V. C., Structural and thermal properties of carboxylic acid functionalized polythiophenes. *Polímeros* **2014,** *24*, 25-30.

23. Shit, A.; Nandi, A. K., Interface engineering of hybrid perovskite solar cells with poly(3-thiophene acetic acid) under ambient conditions. *Physical Chemistry Chemical Physics* **2016,** *18* (15), 10182-10190.

24. Aydın, M.; Durmus, Z.; Kavas, H.; Esat, B.; Sözeri, H.; Baykal, A.; Yılmaz, F.; Toprak, M. S., Synthesis and characterization of poly(3-thiophene acetic acid)/Fe3O4 nanocomposite. *Polyhedron* **2011,** *30* (6), 1120-1126.

25. Ben Ishay, R.; Harel, Y.; Lavi, R.; Lellouche, J.-P., Multiple functionalization of tungsten disulfide inorganic nanotubes by covalently grafted conductive polythiophenes. *RSC Advances* **2016,** *6* (92), 89585-89598.

26. Floresyona, D.; Goubard, F.; Aubert, P.-H.; Lampre, I.; Mathurin, J.; Dazzi, A.; Ghosh, S.; Beaunier, P.; Brisset, F.; Remita, S.; Ramos, L.; Remita, H., Highly active poly(3-hexylthiophene) nanostructures for photocatalysis under solar light. *Applied Catalysis B: Environmental* **2017,** *209*, 23-32.

27. Ghosh, S.; Remita, H.; Ramos, L.; Dazzi, A.; Deniset-Besseau, A.; Beaunier, P.; Goubard, F.; Aubert, P.-H.; Brisset, F.; Remita, S., PEDOT nanostructures synthesized in hexagonal mesophases. *New Journal of Chemistry* **2014,** *38* (3), 1106-1115.

28. Pommerehne, J.; Vestweber, H.; Guss, W.; Mahrt, R. F.; Bässler, H.; Porsch, M.; Daub, J., Efficient two layer leds on a polymer blend basis. *Adv Mater* **1995,** *7* (6), 551-554.

29. Fernando, R.; Senadeera, G. K. R., Synthesis and characterization of carboxylated thiophene co-polymers and their use in photovoltaic cells. *Current Science* **2008,** *95* (6), 743-750.

Chapter 5 Radiation induced synthesis of poly (3-hexylthiophene), P3HT, in dichloromethane under N_2 and O_2 atmospheres

In general, thiophene monomers themselves have high oxidation potential (2 V_{SCE}).[1-3] However, introducing an alkyl group substituent at 3-β position in the thiophene ring decreases its oxidation potential (i.e. the oxidation potential of 3-methylthiophene, PC1T, is 1.8 V_{SCE}).[2, 4] Note that, the oxidation potential is almost constant when the length of the alky side chain increases (between 1.82 V_{SCE} to 1.85 V_{SCE} for alky side chain contains 1 to 18 carbon atoms).[4] In comparison with PEDOT that has relatively low oxidation potential (1.4 V_{SCE})[5], to polymerize 3-hexylthiophene (3HT) that has oxidation potential ~ 1.84 V_{SCE} (**Figure 5.1a**), for instance, we need to generate oxidizing species which possess higher oxidation potential than those needed for EDOT oxidation. Thus, in this chapter I will investigate the generation of different oxidizing species produced from dichloromethane radiolysis under different atmosphere to induce the oxidative polymerization of 3HT.

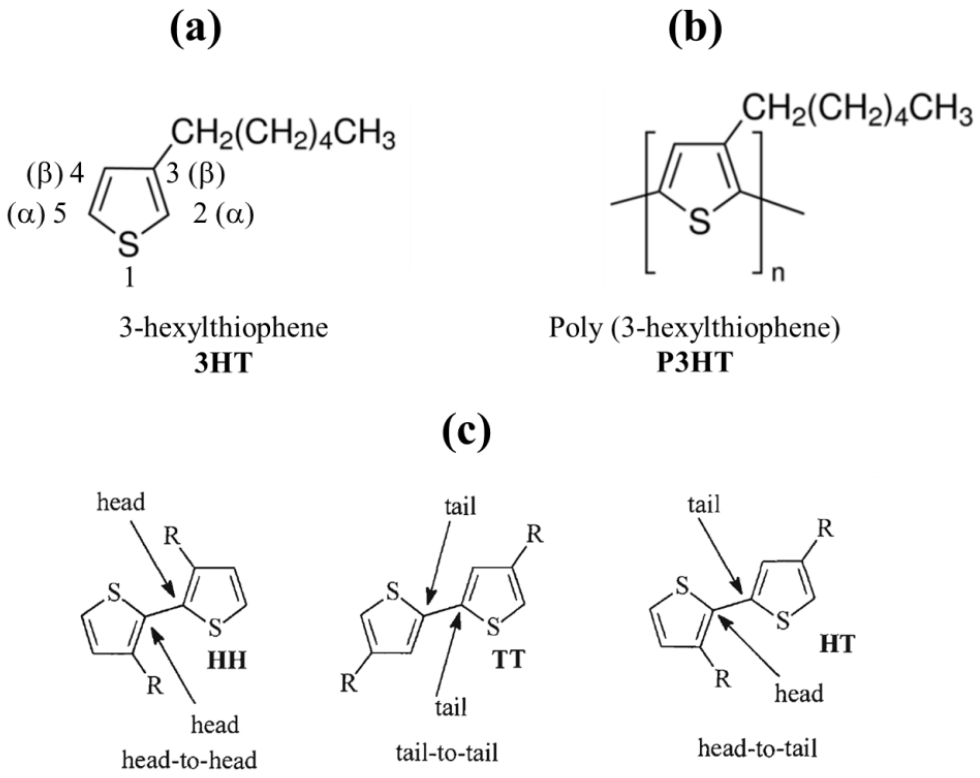

Figure 5.1 Chemical structures of: a) 3-hexylthiophene (3HT), b) poly (3-hexylthiophene) (P3HT) and c) the regiochemistry patterns of P3HT

The interest in Poly 3-hexylthiophene (P3HT) (**Figure 5.1b**) is originated from the fact that P3HT is considered as the best candidate for organic photovoltaic devices, due to its remarkable optical and conductive properties.[6-7] P3HT exhibits also good thermal stability, high processability, synthetic versatility and the susceptibility to tune and change its properties and morphology through simple ring modifications.[8] The spectroscopic and physical properties of poly (alkythiophenes) are sensitive to solvent, environmental changes and molecular weight. In fact the substitution at β position allows the polymerization to occur at the C-2 and C-5 positions of the ring (see **Figure 5.1a**), which is crucial for the extension of conjugation and hence conduction.[2] Moreover, presenting substituent at this position reduces mislinking that can occur via coupling reactions at the β position, which also inhibits conduction. The conductivity is effectively affected by two factors, namely stereoregularity (i.e. the degree of α-α' links in the polymer) and the planarity of the system.[9] Hence, the incorporation of alkyl substituents results in asymmetric thiophene monomers. Random polymerization methods can produce up to 4 different bonding arrangements, namely head-to-head (HH), head-to-tail (HT), tail-to-tail (TT) and the mixture of all three (**Figure 5.1c**).[2, 10] The polymers which have mixed pattern are called regiorandom while the polymers with coupling HT are referred as to regioregular. In fact, decreasing the torsional strain between thiophene rings by eliminating the unfavorable regiorandom polymers (HH and TT isomers) allows the chain to adopt low energy, planar configuration. As a consequence, red shift is observed in case of regioregular configuration due to increase of the conjugation along the polymer while blue shift is obtained in case of regiorandom pattern, which causes decreasing in the conjugation.[9] It is worth to note that, P3HT polymers with regioregular pattern can be consisted of 40 units and more, whereas the conjugation length for regiorandom P3HT polymers is short (i.e. the conjugation length for irregular poly(dodecylthiophene) was only 7 thiophenes in length).[2] Furthermore, the conductivity of random poly (alkythiophenes) decreases with increasing the chain length. By contrary, the conductivity of regioregular HT-poly (alkythiophenes) increases with increasing the chain length, which were found to undergo supermolecular ordering. The supermolecular ordering was not found to occur in irregular poly (alkythiophenes).[11] The conductivity of highly ordered of thin film of regioregular poly (3-methylthiophene) was found about 2000 $S.cm^{-1}$, regiorandom pattern has conductivity about 10^{-4} $S.cm^{-1}$ order of magnitude.[2]

P3HT is basically synthesized through oxidation reaction induced polymerization and thus the oxidative polymerization can be induced by formation of cations of the monomers.[12] In this context, ionizing radiation induced polymerization by γ-rays or X-rays without using oxidizing agents appears to be alternative and easy way to produce conducting polymers.[5] The cations can be generated by ionizing radiation under various conditions.[13] This could be possible by the ionizing radiation of aerated and/or deaerated solutions of dichloromethane; since all the generated radicals are well known as strong oxidizing agents towards organic materials.[14] In this regard, numerous studies were reported in the use of irradiated dichloromethane solutions for one electron oxidation.[15-16] Indeed, in the previous chapters, the oxidative polymerization of 3,4-ethylenedioxythiophene, EDOT and 3-thiophene acetic acid, 3TAA, were successfully induced by the ionizing radiation of deaerated solutions of dichloromethane. And besides, it is worthy to note that, attempts have been previously performed, by taking the same approach, to initiate the oxidative polymerization of 3-octylthiophene (3OT) in other organic solvents such as chloroform, hexane and neat monomer solution.[13]

In another regard, radiolytic method was well exploited the LCP's my group to synthesized nanostructured conducting polymers in aqueous solutions.[5] Effectively, nanostructured PEDOT materials were obtained by EDOT oxidation using either hydroxyl radical ($HO^{\bullet}$) [5, 17], azide radical ($N_3^{\bullet}$)[17] or sulfate radicals ($SO4^{\bullet-}$)[18] and even by EDOT reduction thanks to the use of hydrated electron (e_{aq}^-) generated by water radiolysis.[19] Interestingly, morphology of PEDOT polymers was found dependent on the nature of the initiating radiolytic species: while $HO^{\bullet}$ and e_{aq}^- lead to spherical nanoparticles, $N_3^{\bullet}$ leads to fibrillar structures.[17] However, the use of those radicals is no longer achievable due to the fact that 3HT monomers are completely insoluble in the aqueous solutions. As an alternative approach, the synthesis of P3HT has been made possible through dichloromethane radiolysis by means of dichlorometheyl, chloromethyl and their corresponding peroxyl radicals.

In this chapter, we endeavor to present an easy and original method to polymerize 3HT into P3HT in dichloromethane solvent without using oxidizing agents under different conditions: oxygen free solution, air saturated solution and oxygen saturated solution (**Scheme 5.1**). Under these atmospheres, three different polymers have been synthesized so-called "$P3HT_{N_2}$", "$P3HT_{air}$" and "$P3HT_{O_2}$". The produced materials were examined by several analytical techniques. The synthesis conditions by γ-radiolysis of dichloromethane

under different atmosphere were discussed. Later, based on the findings, detailed study was carried out on P3HT polymers which were polymerized by dichloromethyl, chloromethyl ($P3HT_{N_2}$) and their corresponding peroxyl radicals ($P3HT_{air}$ and $P3HT_{O_2}$). In addition, the morphological structure and the electrical properties of $P3HT_{N_2}$ and $P3HT_{O_2}$ were checked by several techniques.

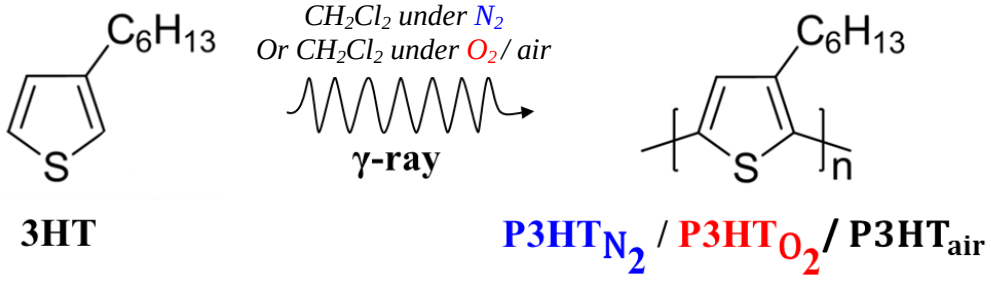

Scheme 5.1 Radiation-induced polymerization of poly(3-hexylthiophene) under different atmospheres

5.1. Experimental:

5.1.1. Solution preparation:

Dichloromethane solutions containing 10 mM in 3HT monomers were prepared at ambient temperature. Note that the used concentration is lower than 3HT solubility in dichloromethane at 25°C (which is over than 50 mM as found by UV-Vis absorption spectroscopy study (results are not shown)). This concentration remains also much lower than dichloromethane molecules concentration (15.6 M). This enables one to neglect the direct effect of ionizing radiation on 3HT monomers. Dichloromethane solutions were kept under air or degassed with N_2 and O_2, respectively, for 20 min, sealed in glass ampoules. The solutions were then irradiated with a ^{60}Co γ-source with increasing doses up to 140 kGy at a dose rate of 3.65 $kGy.h^{-1}$.

5.1.2. Radiolysis method:

Radiolysis under N_2. Under these experimental conditions, the possible oxidizing species that are generated can be solvated electrons in addition to $Cl^{\bullet}$ and solvent radical cations which quickly lead to dichloromethyl ($^{\bullet}CHCl_2$) and chloromethyl ($^{\bullet}CH_2Cl$) radicals.[14-15, 20] Those oxidizing species are known to generate radical cations of many organic compounds[15, 21] and even thiophenes and oligothiophenes ($Th^{\bullet+}$).[20] Thus, thanks to these species it will be

possible to initiate the oxidative polymerization of 3HT. However, the oxidation potential of 3HT is higher than that of EDOT and TAA (see chapter 4 and 5) and therefore it is predictable that the irradiation dose needed for quantitative polymerization of 10 mM in 3HT is higher than 36 kGy. In this context, to verify this dose, dose effect study was carried out to evaluate the required irradiation dose for quantitative preparation. In this context, solutions of dichloromethane containing 10 mM in 3HT were prepared under N_2 by degassing the samples for 20 min in sealed glass ampoules at ambient temperature. The solutions were then irradiated at doses ranging from 15 to 140 kGy, with γ-rays.

Radiolysis under air and O_2. In aerated and O_2 saturated solutions of dichloromethane, the produced dichloromethyl and chloromethyl radicals are rapidly scavenged by the molecular oxygen (O_2) to produce the corresponding peroxyl radicals: $CH_2ClO_2^{\bullet}$ and $CHCl_2O_2^{\bullet}$.[20] As shown in several studies in literature, peroxyl radicals possess higher oxidizing power with the respect to original carbon centered radicals and are effectively capable to oxidize the organic compounds.[15, 20] As said in chapter 4, the radiolytic yield of EDOT oxidation by dichloromethyl and chloromethyl peroxyl radicals under air and O_2 is much higher than $G_{ox} = 4.1\times10^{-7}$ mol·J^{-1}. Indeed the radiolytic yield of oxidation (G_{ox}) under air was calculated by Alfassi *et al*. and found to be $G_{ox} = 7.7\times10^{-7}$ mol·J^{-1} for several organic compounds [15]. This yield was also obtained in case of EDOT during our dose effect study in chapter 4. Therefore, to verify and to determine the radiolytic yield of 3HT oxidation by dichloromethyl and chloromethyl peroxyl radicals that are produced by dichloromethane under air and O_2, dose effect study was carried out. To do so, solutions of dichloromethane containing 10 mM in 3HT were prepared under air or saturated with O_2. The samples prepared under O_2 were degassed for 20 min in sealed glass ampoules at ambient temperature. The solutions were then irradiated up to doses between 15 and 65 kGy, with γ-rays.

5.2. Results and discussion:

5.2.1. Dose effect study and spectral analysis of irradiated solutions:

Normally, thiophene molecules absorb light in the UV region between 225 nm and 245 nm, and this absorption is ascribed to π-π* transition.[22] The absorption spectrum of 10 mM in 3HT is displayed in insert of **Figure 5.2**. The study of the variation of 3HT absorption as a function of its concentration in dichloromethane enabled us to find that 3HT is soluble up to 50 mM. Also thanks to Beer-Lambert law (results are not shown) the extinction coefficients were found to be ε_{238}= 5570 L.mol^{-1}.cm^{-1}. As stated in our previous study[5], thanks to the

calculated extinction coefficients, one can consider that the variation in EDOT concentration with the irradiation dose enables us to deduce the initial radiolytic yield of EDOT consumption. This approach is at variance with dichloromethane radiolysis. This is due to the fact that there are stable and transient products which are generated during gamma radiation of Dichloromethane. These products are dimers of (1,1-dichloroethane, 1,2-dichloroethane, 1,1,2-trichloroethane and 1,1,2,2-tetrachloroethane) which come from DCM radiolysis and which absorb light in the wavelength range 230-400 nm [23], at which, an overlap with the absorption of 3HT occurs.

Nevertheless, we successfully were able to calculate the approximate irradiation dose needed to achieve the complete oxidative polymerization of TAA and EDOT monomers into PTAA and PEDOT polymers in dichloromethane solution.[24] That was possible by detecting the formation of PTAA and PEDOT polymers by following their UV-Vis absorption as a function of the absorbed dose. Hence, with this aim the progressive formation of P3HT polymers were followed by the evolution of the UV-visible absorption spectra of the prepared solutions of dichloromethane under N_2, air and O_2 in presence of 10 mM in 3HT and irradiated to dose range of 15 to 140 kGy.

5.2.1.1. $P3HT_{N_2}$:

In order to follow the progressive formation of $P3HT_{N_2}$ polymers, dichloromethane solution containing 10 mM in 3HT was irradiated under N_2 at increasing doses up to 140 kGy and its absorption spectrum was recorded as a function of the absorbed dose and after concentrating the irradiated solution 10 times (**Figure 5.2a** and **Figure 5.2b**). From Figure 5.1a, it is possible to see that the irradiated solutions got colored with pale yellow right after gamma irradiation. This color parallelly darkens with proceeding the irradiation with doses up to 75 kGy. However, when resuming the irradiation and exceeding the absorbed dose up to 140 kGy, the yellow solutions turn pale again.

In return for this, the recorded UV-vis absorption spectra is showing red-shifted compared to the non-irradiated solution. The red shift is progressively increasing up to 75 kGy with the concomitant appearance of a peak around 750 nm. The observed red shift is attributed to the formation of $P3HT_{N_2}$ polymers. This red-shift is ascribed to the π-π* transition along the polymer chains.[13] Whereas the observed peak at approximately 750 nm is ascribed to polaron and/or bipolaron bands, originating from the oxidized state of doped P3HT polymers with chloride ions (which are produced by DCM radiolysis). [24-25] However, delivering overdose to the samples up to 140 kGy leads up to degradation and breaking down of the polymer chains.

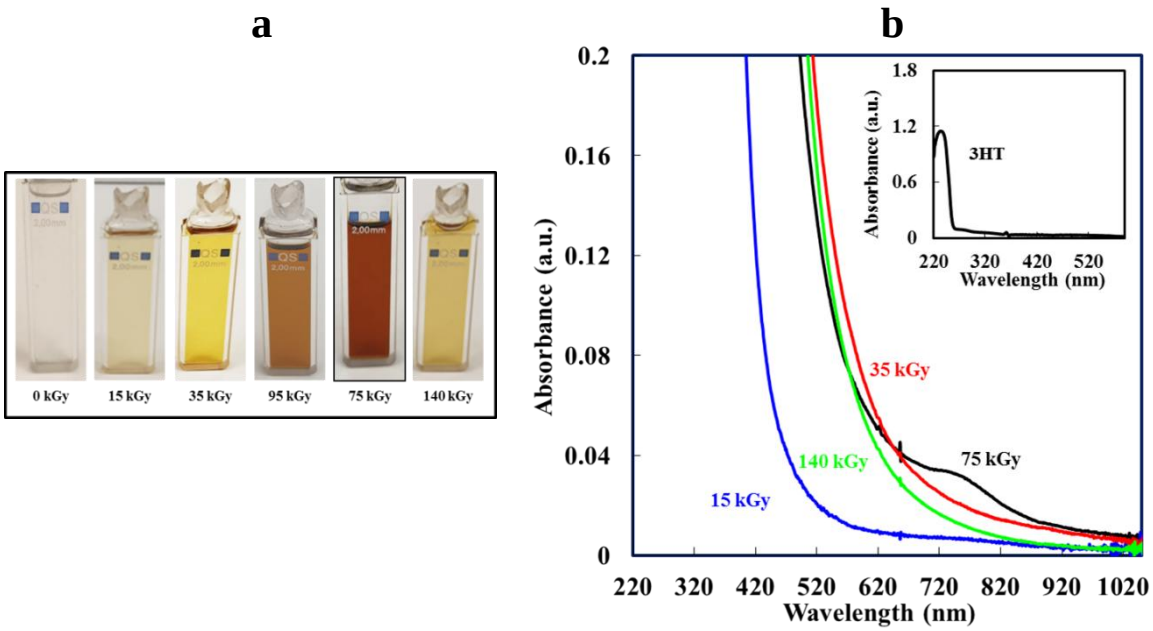

Figure 5.2 Dose effect study of 3HT in DCM under N_2 atmosphere: a) UV-Vis absorption spectra of DCM solutions containing 10 mM in 3HT and irradiated under N_2 atmosphere at increasing doses from 0 to 140 kGy. The reference was DCM. l = 0.2 cm. Insert UV-Vis absorption spectra of DCM solutions containing 10 mM in 3HT after 10 times dilution b) Photographs of DCM solutions before and after irradiation at increasing doses. The solutions were concentrated 10 times after irradiation.

The state of over oxidation and polymer degradation are already monitored in our previous chapters which is evidently due to deliver high dose to the irradiated solutions.

The dose effect study on the synthesis of P3HT polymers in dichloromethane under N_2 is at variance with those which were performed earlier on PEDOT and PTAA polymers. The findings suggest that the oxidative polymerization of 3HT in dichloromethane under N_2 can be proceeded with high irradiation dose which amounts roughly to 75 kGy. In other words, the oxidizing potential of the corresponding chloromethyl radicals are not sufficient to proceed with 3HT polymerization at 36 kGy. As previously mentioned, the presumed initial radiolytic yield of 3HT oxidation into P3HT polymers in deareated dichloromethane is much lower than 4.2×10^{-7} mol.J^{-1} and therefore 36 kGy of irradiation doses are not fairly enough to proceed with complete polymerization of 10 mM in 3HT under these conditions. This is consonant with the fact that 3HT monomers have relatively higher oxidation potential than some of the generated oxidizing species in dichloromethane and thus makes their oxidation harder.[4, 26] As a consequence to this issue, using air or oxygen saturated solutions of dichloromethane could immensely facilitate the oxidation of 3HT.

5.2.1.2. $P3HT_{air}$ and *$P3HT_{O_2}$*:

In the same manner, the dose effect study was performed on $P3HT_{air}$ and $P3HT_{O_2}$. In both cases, 10 mM in 3HT were prepared in dichloromethane under air or saturated with O_2. The solutions were then irradiated at increasing doses up to 65 kGy (**Figure 5.3a and Figure 5.3b**). The progressive formation of $P3HT_{air}$ and $P3HT_{O_2}$ polymers were followed by the evolution of the UV-visible absorption spectra of dichloromethane solutions under air or under O_2 containing 10 mM in 3HT irradiated to dose range of 15 to 55 kGy, as shown in **Figure 5.3c** and **Figure 5.3d**. As what has been observed in $P3HT_{N_2}$, it is remarkably possible to see that a shoulder and a peak are being protruded at 460 and 920 nm. The shoulder at 460 nm is evidently attributed to formation of $P3HT_{air}$ and $P3HT_{O_2}$ polymers originating from the π-π* transitions along the polymer chains.[13] Whereas the observed peaks at approximately 920 nm is attributed to polaron and/or bipolaron bands, which are characteristic of formation of doped polymers with chloride ions (generated by DCM radiolysis).[24-25]

From the recorded spectra, one can note that delivering irradiation doses between 15 and 35 kGy leads to the gradual appearance of a shoulder at 475 nm and of a peak at 920 nm in the absorption spectra of $P3HT_{O_2}$. This gradual increase in the absorption spectra remains in case of $P3HT_{air}$ up to 55kGy. The observed spectral features are clearly more prominent than those observed in case of $P3HT_{N_2}$. The doping band which corresponds to the formation of P3HT polymers in oxidized state are shifted to 920 nm. As it will be demonstrated later by SEC analysis, this red-shift is attributed to formation of P3HT polymers possessing higher molecular weight. In addition, the red shift also might be originated from formation of P3HT with (HT) pattern. This red shift is commonly observed in case of regioregular configuration due to the increase of the conjugation along the polymer, while blue shift is obtained in case of regiorandom pattern, which causes decreasing in the conjugation. The resulted decreasing comes from the twisting of the thiophene ring and from the lower number of π-π* interactions along the polymers.[2, 27] On the other hand, those spectral features are fading away by exceeding the irradiation dose of 35 kGy in case of $P3HT_{O_2}$ and of 55 kGy in case of $P3HT_{air}$. This is indubitably the indication of detrimental effect of delivering overdose to P3HT polymers.

The dose effect study on 3HT polymerization under the corresponding atmospheres is highlighting the influence of presence of oxygen in irradiated dichloromethane solutions. It is known that the chlorosubstituted methyl radicals react with O_2 to produce the corresponding

peroxyl radicals.[15, 20] Indeed, the formation of peroxyl radicals: $CH_2ClO_2^{\bullet}$ and $CHCl_2O_2^{\bullet}$ is the reason behind the decreasing of the irradiation doses that are needed to initiate and complete the polymerization of 3HT. Certainly, the use of oxygen saturated solution of dichloromethane during radiolysis leads to the total conversion of chloromethyl radicals to the corresponding peroxyl radicals.[20] However, the concentration of the oxygen in air saturated solution is less than of the solution saturated with O_2. As a consequence, the radiolytic yield of peroxyl radicals formation in dichloromethane oxygen saturated solutions is absolutely higher than those of aerated ones. These explain the fluctuation of spectral findings with the respect to irradiation dose which is needed to proceed with the oxidative polymerization in dichloromethane under different atmospheres.

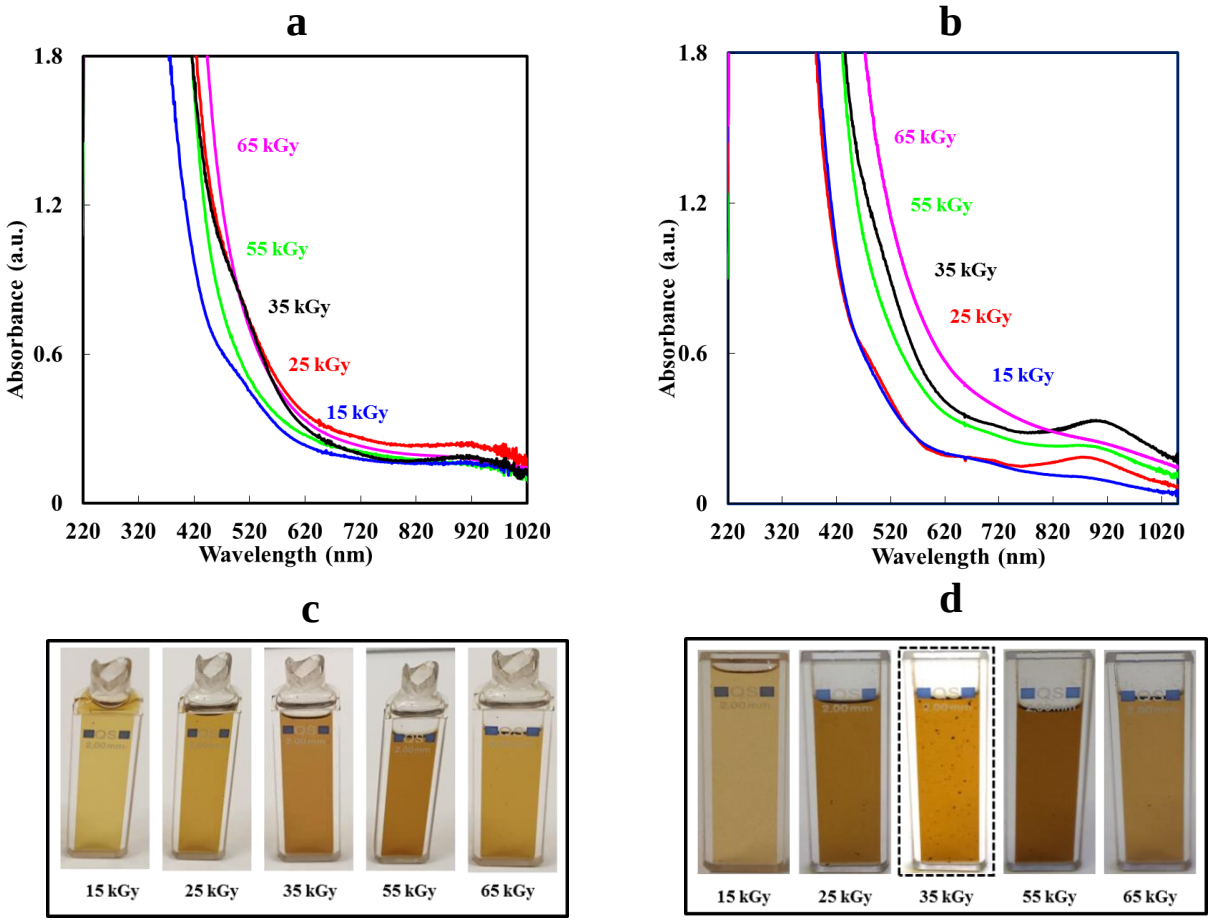

Figure 5.3 Dose effect study of 3HT in DCM under air and O_2 atmospheres: a) UV-Vis absorption spectra of aerated DCM solutions containing 10 mM in 3HT and irradiated directly at increasing doses from 0 to 65 kGy b) UV-Vis absorption spectra of DCM solutions containing 10 mM in 3HT and irradiated under O_2 atmosphere at increasing doses from 0 to 65 kGy. The reference was DCM. In both cases l=0.2 cm. c and d) Photographs of DCM solutions before and after irradiation at increasing doses under air (c) and under O_2 (d).

As far as, we can discern that halogenated alkyl peroxyl radicals boost up the oxidative polymerization and therefore facilitate the formation of P3HT polymers. The oxidation by the original carbon centered radicals is difficult to achieve unless we deliver high irradiation dose. The irradiation of dichloromethane under air is intermediate between the two extreme conditions: O_2-saturation and deareated solutions. Nevertheless, the spectral features seem to be similar in all cases (under N_2, air and O_2). In principle, one can say that $P3HT_{N_2}$, $P3HT_{air}$ and $P3HT_{O_2}$ polymers induced by γ-irradiation of dichloromethane are produced at irradiation doses which amounts to $75, 55$ and 35 kGy, respectively. Introducing oxygen to dichloromethane solution reduces the irradiation dose needed for quantitative polymerization. In the following characterizations, we will only consider the following two conditions: γ-induced synthesis of $P3HT_{N_2}$via chloromethyl radicals at 75 kGy and γ-induced synthesis of $P3HT_{O_2}$via chloromethyl peroxyl radicals at 35 kGy. The aerated conditions will not be considered in the next characterizations

5.2.2. Molecular weight analysis of polymers from irradiated solutions:

As we could see from the spectral analysis of the irradiated solutions, the notable shoulders and redshifts are ascribed to formation of $P3HT_{N_2}$and $P3HT_{O_2}$ polymers. To estimate the molecular weights and to check whether the halogenated alkyl peroxy radicals have any influence on the elongation of the polymer chain lengths, SEC analysis was used. For the comparison, SEC was performed on the polymers which were produced at the irradiation dose enabling quantitative polymerization (75 kGy for $P3HT_{N_2}$ and 35 kGy for $P3HT_{O_2}$). In order to do so, the glutinous solid parts (≈ 10 mg) that were obtained after solvent evaporation from $P3HT_{N_2}$ and $P3HT_{O_2}$ were dissolved in 1mL THF (**scheme 5.2**).

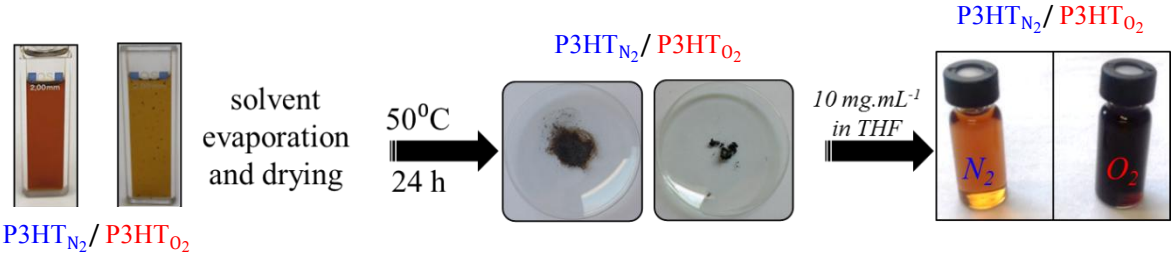

Scheme 5.2 The post processing of P3HT polymers after gamma irradiation

The obtained SEC chromatograms are shown in **Figure 5.4** and the molar masses of P3HT polymers (obtained with a polystyrene calibration), at M_p, are reported in the insert of **Figure 5.4**. From the chromatogram of $P3HT_{N_2}$, it is possible to extrapolate the molar mass of 1785

g.mol^{-1}, which corresponds to ≈10 units of 3HT per polymer chain. This molecular weight implies that the polymerization of 3HT under N_2 produces regiorandom P3HT polymers. This degree of polymerization was already reported in literature for regio-irregular poly(3-alkythiophenes) (HH and TT isomers shown in Figure 5.1).[27] In turn, the molar mass at M_p of $P3HT_{O_2}$ can be found at 3130 g.mol^{-1} and corresponds to about 18 units of 3HT per polymer chain. As it will be demonstrated by ATR-FTIR, $P3HT_{O_2}$ polymers are functionalized with carbonyl and hydroxyl groups. However, those groups are not taken into account in SEC calculations since the number of groups and their exact position on 3HT monomers is not known at the present study. However, it is clearly to note from SEC analysis that $P3HT_{O_2}$ has higher molecular weight than $P3HT_{N_2}$. In this regards, SEC's findings demonstrate that γ-induced oxidative polymerization of 3HT in dichloromethane under O_2 atmosphere not only reduce the needed irradiation dose but also relatively increases the molecular weight. The likelihood of this slight increase is the halogenated alkyl peroxy radicals, which affords high oxidation potential and makes 3HT polymerization feasible with lower irradiation doses. In addition, the polymerization of 3HT under O_2 seemingly induces production of P3HT polymers with regioregular pattern. In our previous work, it has been shown that there is no concrete influence of used solvent on the molecular weight. However, this study on 3HT

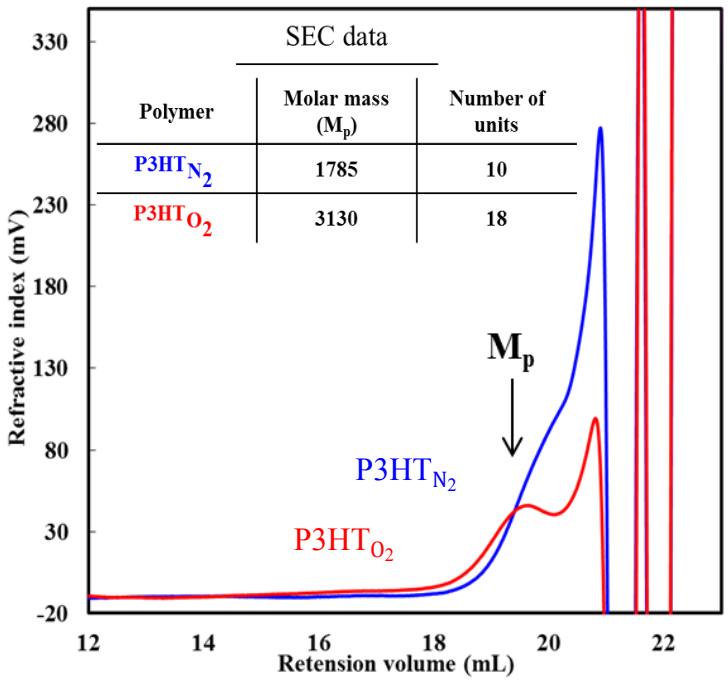

Figure 5.4 SEC chromatograms of THF solution containing 10 mg.mL^{-1}of P3HTs polymers which were synthesized by γ-induced polymerization in DCM under N_2 or O_2 atmospheres at irradiation dose of 75 and 35 kGy, respectively. The initial concentration of 3HT was 10 mM.

manifests that the oxidizing power of chloromethyl peroxyl radicals gives rise to elongation of P3HT polymer chain.

5.2.3. Chemical characterization of $P3HT_{N_2}$ and $P3HT_{O_2}$ polymers:

ATR-FTIR was used to assert the successful formation of $P3HT_{N_2}$ and $P3HT_{O_2}$ polymers and also to verify the oxidative polymerization in dichloromethane solutions under different atmospheres: N_2 or O_2. The irradiated solutions were first dried naturally under hood. After solvent removal, the remaining dark solid part in case of $P3HT_{O_2}$(synthesized at 35 kGy under O_2) and $P3HT_{N_2}$ (synthesized at 75 kGy under N_2) which look like glutinous, were characterized after deposition and squeezed on the ATR support of the FTIR spectrophotometer by ATR-FTIR spectroscopy. The spectra were recorded for both $P3HT_{N_2}$ and $P3HT_{O_2}$ polymers together with 3HT monomers within a wavenumber region from 600 to 4000 cm^{-1} as shown in **Figure 5.5**.

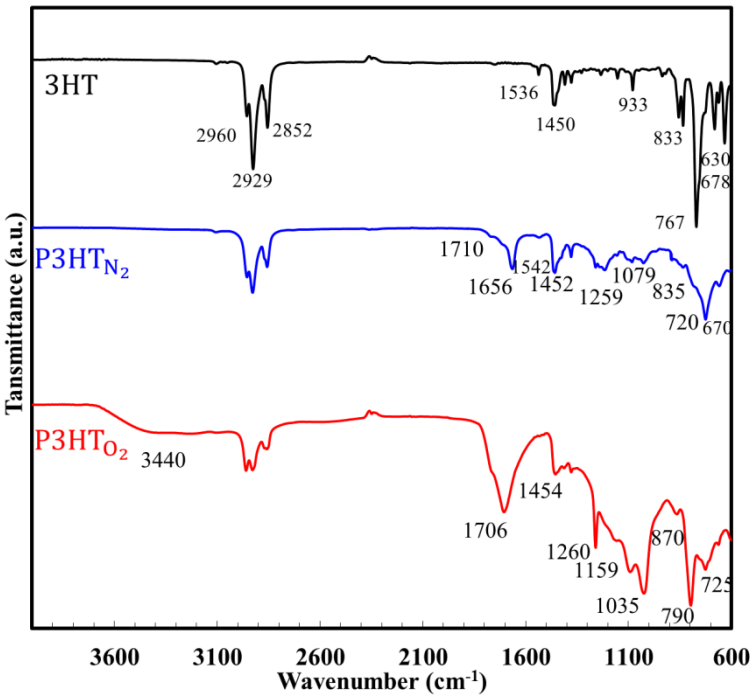

Figure 5.5 ATR-FTIR spectra of pure 3HT monomers, $P3HT_{N_2}$ and $P3HT_{O_2}$ polymers. The polymers were synthesized by γ-induced polymerization of 3HT in DCM under N_2 or O_2 atmospheres at an irradiation dose of 75 or 35 kGy. The initial concentration was 10 mM in 3HT.

Table 5.1 displays the absorption modes and the positions of the representative peaks of 3HT monomers, $P3HT_{N_2}$ and $P3HT_{O_2}$polymers. The bands at 767 and 833 cm^{-1} are attributed to the =C-H out-of-plane stretching vibrations of pure 3HT.[28-29] These peaks are remarkable

in the monomer spectrum and barely noticeable in the polymers spectrum confirming the quantitative polymerization of 3HT monomers. Of major importance, the vibration modes of the aliphatic moieties of hexyl side chain of 3HT units are observed for all samples. The asymmetric stretching vibration mode for -CH_3 and –CH_2- are detected at 2960 cm^{-1} and 2929 cm^{-1}, respectively, and the symmetric -C-H stretching vibration in -CH_2- is detected at 2852 cm^{-1}.[29] In addition, the symmetric C=C ring stretching vibration mode is observable for all recorded spectra around 1452 cm^{-1}.[28-29] The peaks that are assigned to asymmetrical stretching vibrations mode of quinoid configuration in thiophene ring are noticeable around 1542 and 1656 cm^{-1}.The peaks at 633, 678 790, and 933 cm^{-1} are associated with the absorption of C-S-C bonds of the thiophene ring.[29] The peak at 723 cm^{-1} is the characteristic absorption on the in-planeand out-of-plane rocking vibration of -$(CH2)_n$-..[29-31] The peak at 835 cm^{-1} is the bending vibration of the Cβ-H bond.[30] In the spectrum of $P3HT_{N_2}$, the peak at 1710 cm^{-1} is the signature of carbonyl group (C=O)[28], which is presumably formed due to the presence of traces of oxygen.

Functional group	Position (cm^{-1})
C=C (symmetric stretching mode)	≈1450
C=C (asymmetrical stretching vibrations mode of quinoid configuration in thiophene ring)	≈1656 and 1542
C-O (bending vibration)	≈ 870, 1079, 1160 and 1260
C-S-C (stretching vibrations)	633, 678, 790, and 933
=Cα-H (in-plane and out-of-plane deformation vibrations)	767
C=O (stretching vibrations)	≈1706
O-H stretching vibration mode	≈ 3100 to 3600
=Cβ-H (out-of-plane deformation vibration)	≈833
-$(CH_2)_n$- (in-planeand and out-of-plane rocking vibration)	≈ 720

Table 5.1 ATR-FTIR absorption peaks of 3HT and P3HT polymers

It is worthy to note that the recorded IR spectra do not show any peak associated to C-Cl bond. This proves that no chlorine atom is covalently bonded onto the $P3HT_{N_2}$and $P3HT_{O_2}$ polymer chains. The observed peaks in the IR spectra of 3HT monomers and $P3HT_{N_2}$ polymers are in good agreement with the literature.[29, 31] However, compared to the spectrum of $P3HT_{N_2}$, the spectrum of $P3HT_{O_2}$, highlights other characteristic peaks. The remarkable peak at 1706 cm^{-1} is ascribed to C=O stretching mode of the carboxylic acid group moieties.[28] The broad band at 3440 cm^{-1} is the vibration mode of –O-H group. The prominent peaks at 870, 1079, 1160 and 1260 cm^{-1} are attributed to –C-O stretching mode.[28] Other than those peaks that are associated with –O-H and C=O groups, all the other peaks in

the spectrum of $P3HT_{O_2}$ are matching the observed peaks in the spectrum of $P3HT_{N_2}$. This noticeable difference between $P3HT_{N_2}$and $P3HT_{O_2}$ polymers is explained by the difference that exists between generated oxidizing species: $CH_2Cl^{\bullet}$/ $CHCl_2^{\bullet}$ on one hand and $CH_2ClO_2^{\bullet}$/$CHCl_2O_2^{\bullet}$ on the other hand. These data imply that chloromethyl peroxyl radicals have not only an influence on the increase in the molecular weight and in the facilitating the polymerization mechanism but also have a clear influence on the chemical structure of the polymers. All in all, ATR-FTIR observations reveal the successful synthesis of P3HT polymers by both applied environmental conditions and besides chloromethyl peroxyl radicals lead to the functionalization of P3HT polymers with carboxylic groups. The synthesis of functionalized P3HT polymers with carboxylic acid groups was reported already in literature by chemical route.[28]

5.2.4. Structural Characterization of $P3HT_{N_2}$ and $P3HT_{O_2}$polymers:

Earlier in previous studies, we reported the influence of using different oxidizing species ($HO^{\bullet}$/$N_3^{\bullet}$/ $SO4^{\bullet-}$) on PEDOTs morphology through our radiolytic methodology in aqueous solutions.[17] The influence of the generated couple of oxidizing species: $CH_2Cl^{\bullet}$/ $CHCl_2^{\bullet}$ and $CH_2ClO_2^{\bullet}$/$CHCl_2O_2^{\bullet}$ on the morphology of P3HT polymers will be here. In the current study, morphology of the $P3HT_{N_2}$ and $P3HT_{O_2}$ which were produced by dichloromethane radiolysis under N_2 or O_2 at the appropriate irradiation dose, were analyzed by SEM, AFM and Cryo-TEM microscopies.

5.2.4.1.Cryo-TEM observations

After the post-treatment and solvent removal, Cryo-TEM microscope was used to check the morphology of $P3HT_{N_2}$ and $P3HT_{O_2}$ polymers in solution prepared in dichloromethane. As done before in SEC experiment (see scheme 5.2), the remaining dark solid part in case of $P3HT_{O_2}$(synthesized at 35 kGy under O_2) and $P3HT_{N_2}$ (synthesized at 75 kGy under N_2) which look like glutinous, that were obtained after solvent evaporation from $P3HT_{N_2}$ and $P3HT_{O_2}$ were dissolved in 10 mL DCM. The recorded cryo-TEM images of $P3HT_{N_2}$ and $P3HT_{O_2}$ are displayed in **Figure 5.6a** and **Figure 5.6b**, respectively.

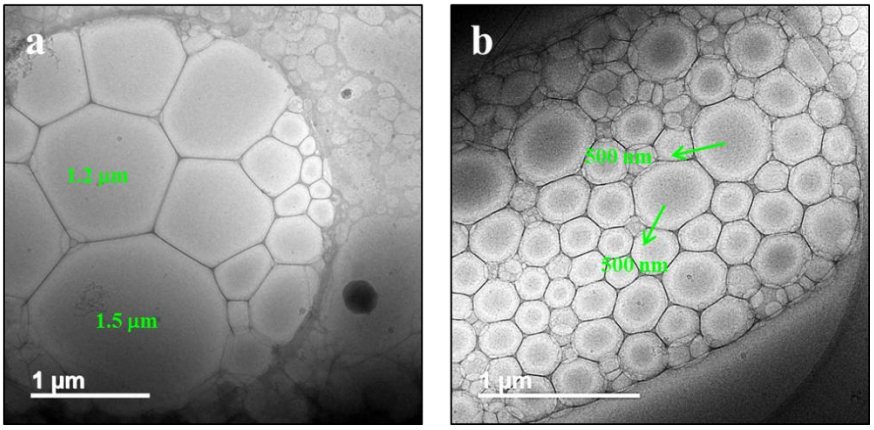

Figure 5.6 Cryo-TEM images of : (a) $P3HT_{N_2}$ polymers self-assembled in aggregated blocks in DCM solvent under N_2 atmosphere after γ-irradiation at 75 kGy (b) $P3HT_{O_2}$ polymers self-assembled in aggregated nano-spheres in DCM solvent under O_2 atmosphere after γ-irradiation at 35 kGy . The initial concentration in 3HT was 10 mM.

Thanks to sample freezing, this technique enables *in situ* observation, into dichloromethane solution, of radiosynthesized polymers, avoiding any phase transition and any aggregation which could result from drying procedures. **Figure 5.6a** and **b** display a zoom of one of the circular holes of the holey-carbon grid coated with $P3HT_{N_2}$ and $P3HT_{O_2}$ polymers in the DCM solvent. As seen in cryo-TEM image in **Figure 5.6a**, the hole is fully coated with $P3HT_{N_2}$ compacted blocks contrasting objects. The $P3HT_{N_2}$ close aggregated blocks are heterogeneous in size with diameters comprised between 100 nm and 1.5 µm. These compact blocks correspond to self-assemblies of independent amorphous $P3HT_{N_2}$ chain polymers. Such polymeric structure should be originated from the fact that P3HT polymers are hydrophobic and aggregate thanks to vander waals and π-stacking interactions. In **Figure 5.6b** is possible to see the cryo-TEM image of $P3HT_{O_2}$ in which the carbon hole is fully coated with aggregated clusters of nano-spheres. The $P3HT_{O_2}$ aggregated nano-spheres are heterogeneous in size with diameters comprised between 100 nm and 500 nm. Apparently, $P3HT_{O_2}$ polymers chains interact with each other and form hydrogen-bond. These hydrogen-bonds should come from the carboxylic acids groups formed during DCM radiolysis under O_2 atmosphere.

5.2.4.2. SEM observations and EDX analysis

SEM images recorded after deposition of dried $P3HT_{N_2}$ and $P3HT_{O_2}$ polymers powders onto carbon tape adhered to aluminum mounts and after gold coating are displayed on **Figure 5.7**. The representative SEM image of $P3HT_{N_2}$ is exhibited in **Figure 5.7a**. The image shows

compacted blocks and large aggregation of $P3HT_{N_2}$. These aggregations are ascribed to the fact that P3HT polymers are hydrophobic and self-assemble thanks to vander waals and π-stacking interactions. By contrast, SEM image of $P3HT_{O_2}$is presented in **Figure 5.7c** which shows markedly aggregated clusters of spheres of several hundreds of nanometers. This aggregation behavior seems to be the consequence of hydrogen-bond interactions between $P3HT_{O_2}$ polymers which are in case of O_2 atmosphere functionalized with carboxylic acids groups. The elemental composition of the compacted blocks of $P3HT_{N_2}$ and the aggregated spheres of $P3HT_{O_2}$ were also analyzed by energy dispersive X-Ray (EDX) within selected regions without gold coating. EDX analysis for $P3HT_{N_2}$ and $P3HT_{O_2}$ shows substantially presence of sulfur and carbon atoms (result not shown) in the whole samples, demonstrating that our materials are effectively made of P3HT polymers. Evidently, EDX data highlighted as well the presence of oxygen atoms in $P3HT_{O_2}$. In addition, EDX enabled the detection of chlorine atoms dispersed in $P3HT_{N_2}$and $P3HT_{O_2}$. This observation definitely proves that radiosynthesized P3HT are both doped with chloride ions, in total agreement with our results obtained by UV-Vis absorption spectrophotometry (absorption at 900 nm) and by ATR-FTIR spectroscopy.

5.2.4.3. AFM observations

AFM microscopy was used to check the topographical morphology of $P3HT_{N_2}$ and $P3HT_{O_2}$ polymers and to verify that they constitute respectively compacted blocks and aggregated spheres. In order to do so, few drops of ethanolic solution of $P3HT_{N_2}$ and $P3HT_{O_2}$(3 $mg.mL^{-1}$) were dropped on mica sheet and dried naturally. Later on, they were characterized by typical atomic force microscope (AFM). According to the AFM images of the samples recorded in tapping mode (**Figure 5.7**), the bottom dark areas having no thickness correspond to the substrate, while, the bright areas, correspond to the topography of the samples. The topography of $P3HT_{N_2}$shown in **Figure 5.7b** displayed as the bright area corresponds to the thicker regions made up of close aggregated blocks in total agreement with cryo-TEM and SEM results (Figure 5.6a and Figure 5.7a). The topography images nevertheless reveal here the presence of big particles with average size 1 to 5 µm. The AFM topography of $P3HT_{O_2}$, presented in **Figure 5.7d**, shows markedly spheroidal nanoparticles of several hundreds of nanometers. This observation is also consistent with the recorded cryo-TEM and SEM (Figure 5.6b and Figure 5.7b) images and it matches the observed size and shape.

According to the microscopic observations (Cryo-TEM, SEM and AFM), γ–radiation induced polymerization of 3HT in dichloromethane under N_2 or O_2 leads successfully up to two different structures: aggregated blocks and spheroidal nanoparticles. These dissimilarities are indeed originated from existing different oxidizing species: $CH_2Cl^{\bullet}$/ $CHCl_2^{\bullet}$ and $CH_2ClO_2^{\bullet}$/$CHCl_2O_2^{\bullet}$. As a consequence of presence of oxygen, carboxylic groups are formed and infixed along the polymer chains forming so-called $P3HT_{O_2}$. This was confirmed by ATR-FTIR spectroscopy. Subsequently, carboxylic groups evidently enable hydrogen bonds interactions between the polymer chains. This definitely leads to $P3HT_{O_2}$ globular nanostructures with possessing hydrophilic properties. By contrast, $P3HT_{N_2}$ polymers are free from any functional group and for that reason they get together to form aggregated blocks by Vander Waals and π-stacking interactions.

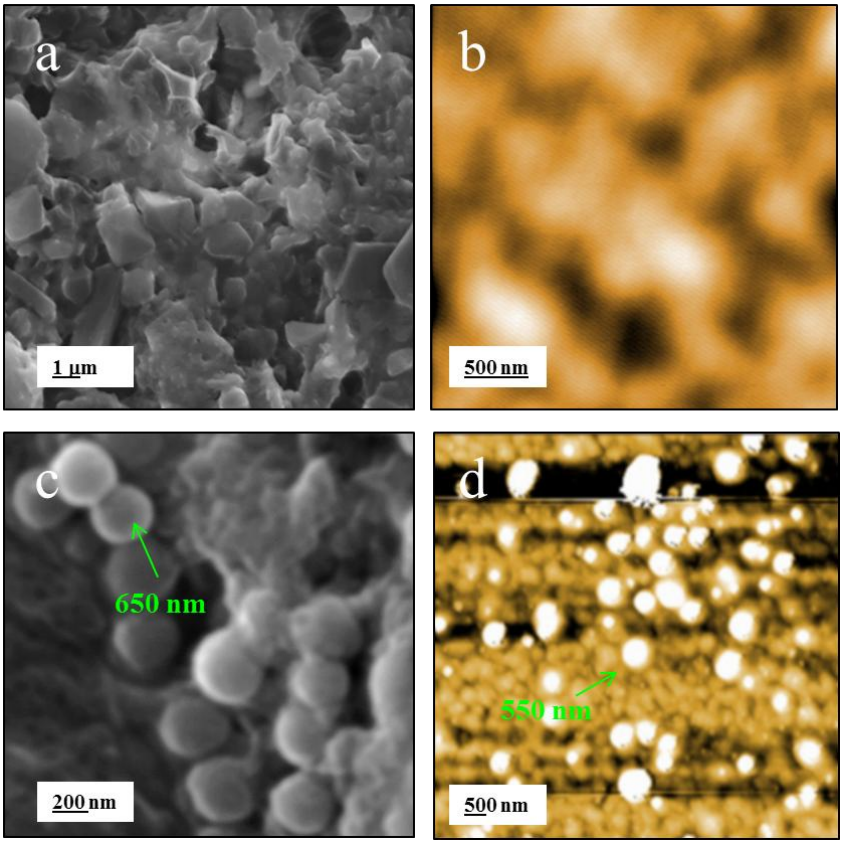

Figure 5.7 Morphological characterizations of $P3HT_{N_2}$ and $P3HT_{O_2}$ by SEM and AFM microscopies. a) and c) are SEM images of dried $P3HT_{N_2}$and $P3HT_{O_2}$ polymers powder after deposition onto carbon tape adhered to aluminum mounts and after gold coating. b) and d) AFM topographic images of $P3HT_{N_2}$and $P3HT_{O_2}$ polymers after deposition onto the CaF_2 disk. The AFM is used in tapping mode. The polymers were synthesized by γ-induced polymerization in DCM under under N_2 or O_2 atmospheres at irradiation doses of 75 or 35 kGy. The initial concentration was 10 mM in 3HT.

5.2.5. Physico-chemical properties of $P3HT_{N_2}$ and $P3HT_{O_2}$ polymers:

Thermogravimetric analysis (TGA) was used in order to check and to compare the physico-chemical properties and thermo-degradability of the two different radio-synthesized P3HT polymers. The TGA thermograms for $P3HT_{N_2}$ and $P3HT_{O_2}$ are shown in **Figure 5.8**. TGA thermosgram of $P3HT_{N_2}$ exhibits two continuous decompositions. The first decomposition is observed up to 110 °C and corresponding to 10 % of initial weight loss. This weight loss can be attributed to evaporation of some unreacted 3HT monomers and dimers. The second decomposition is observed from 110 °C until a complete degradation at 700 °C. This weight loss is caused by loss of $P3HT_{N_2}$ oligomers characterized by relatively low molecular weight.

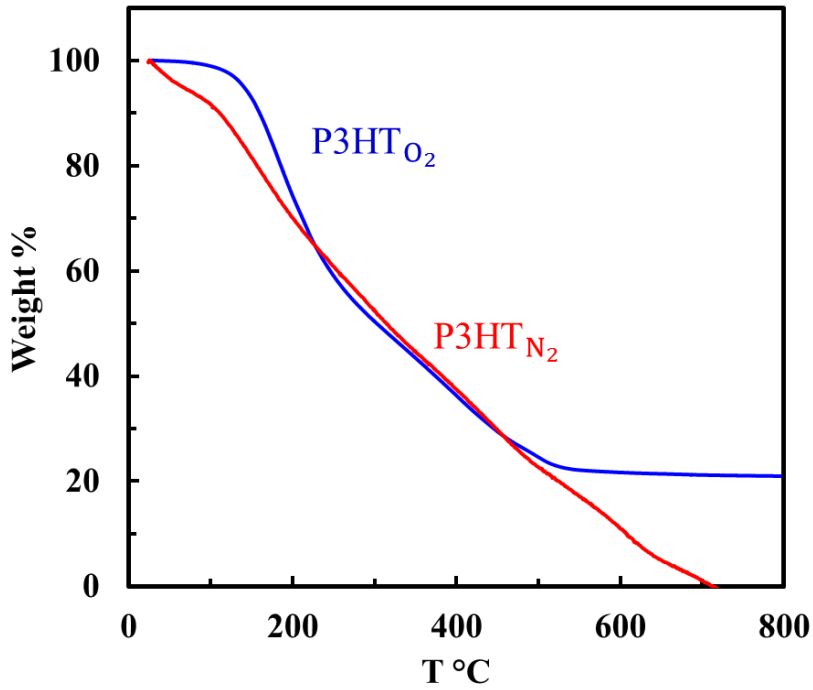

Figure 5.8 Thermogravimetric (TGA) graph of dried $P3HT_{N_2}$ and $P3HT_{O_2}$ polymers powder. The polymers were synthesized by γ-induced polymerization of 3HT in DCM under N_2 or O_2 atmospheres at an irradiation dose of 75 or 35 kGy. The initial concentration was 10 mM in 3HT.

In case of $P3HT_{O_2}$, the weight loss exhibits three stages of decomposition. From 30 to 155 °C, $P3HT_{O_2}$ is quite stable. Up to that temperature, $P3HT_{O_2}$ shows only 8% of initial weight loss which is attributed to evaporation of solvent residual and some unreacted 3HT monomers. The second decomposition is observed from 155 °C to 255 °C, which may be caused by the degradation of the oligomers of low molecular weight of $P3HT_{O_2}$. The third

decomposition stage is observed in the range 270-520 °C; this weight loss may be caused by the loss of $P3HT_{O_2}$ polymers characterized by relatively high molecular weight.

The TGA findings indicate that $P3HT_{O_2}$ has generally better thermal stability and particularly at the initial stage of weight loss when comparing to $P3HT_{N_2}$. This is evidently due to the higher molecular weight and presence of longer polymer chains possessed by $P3HT_{O_2}$ as shown by SEC analysis earlier.

However, this TGA analysis is different in comparison with what have already been reported in the literature concerning P3HT polymers synthesized by conventional methodologies.[32] This substandard behavior in comparison with P3HT polymers produced by conventional methodologies is due to the relatively low molecular weight of the radiosynthesized P3HT.

5.2.6. Examination of electrochemical electrical properties of P3HT polymers:

In order to investigate the electronic properties of $P3HT_{N_2}$ and $P3HT_{O_2}$ polymers for future application opportunity in organic solar cells, it is of great importance to perform conductivity test, optical band gaps calculations via Tauc's plot and cyclic voltammetry.

5.2.6.1.Conductivity measurements:

To measure the electrical conductivity, $P3HT_{N_2}$ and $P3HT_{O_2}$ polymers obtained after γ-irradiation and solvent evaporation were dissolved in DCM at a concentration of 10 $mg.mL^{-1}$. Then, 100 µL of the solutions were spin-coated on clean glass substrate and the obtained films were both doped with $NOBF_4$ (20 mM) in acetonitrile. After measuring the thickness of the films by a surface profiler, their conductivity was determined by four-point probe technique. The average electrical conductivity was calculated for $P3HT_{N_2}$ and $P3HT_{O_2}$ and found as 0.2×10^{-3} $S\cdot cm^{-1}$ and 0.7×10^{-3} $S\cdot cm^{-1}$, respectively. In comparison, $P3HT_{O_2}$ possesses higher conductivity than $P3HT_{N_2}$ pretty much 3 times more. The results are consistent with SEC data since $P3HT_{O_2}$ has higher molecular weight and thus higher conductivity. However, the calculated electrical conductivity which has been reported for P3HT polymers chemically synthesized by $FeCl_3$ and doped with I_2 and possessing high molecular weight (M_w = 111200 $g.mole^{-1}$), is 0.34 $S\cdot cm^{-1}$.[33] Although the measurements are inconsistent with the reported one in literature, $P3HT_{N_2}$ and $P3HT_{O_2}$ possessing high conductivity when comparing to their molecular weights.

5.2.6.2.Cyclic voltammetry analysis and electrical band gap calculations:

In order to further check the electronic properties of radio-synthesized $P3HT_{N_2}$ and $P3HT_{O_2}$ polymers with a view to incorporate these polymers into organic photovoltaics cells (OPVs), it is necessary to estimate the energy level of the highest occupied molecular orbital (HOMO) from the ionization potential, the energy level of the lowest unoccupied molecular orbital (LUMO) from the electronic affinity, as well as the electronic band gap by cyclic voltammetry (CV). The electrochemical behavior of P3HT polymers and their characteristic oxidation and reduction peaks are presented in **Figure 5.9**.

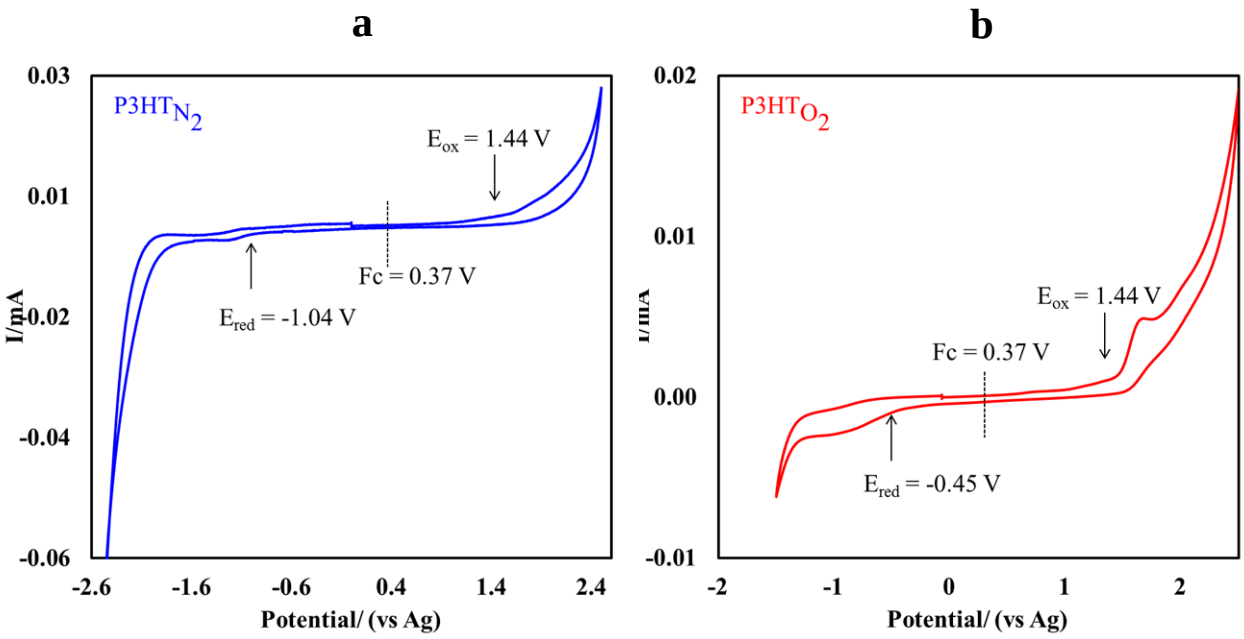

Figure 5.9. Cyclic voltammetry of 3 $mg.L^{-1}$ of $P3HT_{N_2}$ and $P3HT_{O_2}$ recorded in acetonitrile containing 0.1 M of $TBAPF_6$ at a scan rate of 100 $mV.s^{-1}$. The polymers were synthesized in DCM at dose 75 kGy for $P3HT_{N_2}$ or 35 kGy for $P3HT_{O_2}$. Ferrocenium/ferrocene (Fc^+/Fc) redox potential was measured in order to calibrate the pseud reference electrode (0.37 V vs SCE in the present study).

The CV profiles show the main p-doping (oxidation) process occurring at onset potential of +1.44 V for both $P3HT_{N_2}$ and $P3HT_{O_2}$ while n-doping starts at −1.05 V for $P3HT_{N_2}$ and at −0.45 V for $P3HT_{O_2}$. Knowing these potential values, one can calculate, from the equations given in **Scheme 5.3**, the HOMO/LUMO energy levels of radio-synthesized $P3HT_{N_2}$ and $P3HT_{O_2}$: E_{HOMO} amounts to −5.87 eV for both while E_{LUMO} amounts respectively to −3.38 eV for $P3HT_{N_2}$ and −3.98 eV for $P3HT_{O_2}$.These energy values lead to an electrochemical band gap of 2.49 V for $P3HT_{N_2}$ and of 1.89 V for $P3HT_{O_2}$ as illustrated in

scheme 6.3. The HOMO/LUMO energy levels of the material are calculated by using the ferrocene ionization potential value as the standard. The corrected value of 4.8 eV vs vacuum of ferrocene is widely adopted. This value is based on the calculation obtained by Pommerehne *et al.*[34] The calculations demonstrate that $P3HT_{O_2}$ affords higher E_{gap} than $P3HT_{N_2}$. Nevertheless, the obtained energy band gaps are relatively matching with earlier reported works are related to P3HT synthesis by conventional methods.[35]

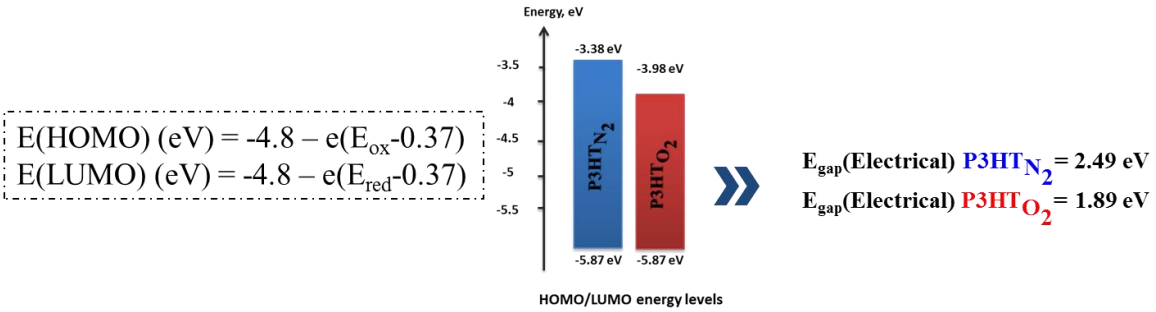

Scheme 5.3 The calculated HOMO/LUMO energetic levels of $P3HT_{N_2}$ and $P3HT_{O_2}$ by using the indicated empirical equations and their electronic band gaps (E_{gap} (electrical)) that are obtained from the energy difference of E(HOMO) and E(LUMO)

5.2.6.3.Optical band gaps calculations:

Optical band gap is one more parameter which is important for applications such as in solar cells. We therefore used Tauc's plot, which can be directly obtained from the recorded absorption spectra. Here, we considered the UV-Vis absorption spectra earlier obtained at the appropriate irradiation dose for quantitative polymerization: 75 kGy for $P3HT_{N_2}$ and 35 kGy for $P3HT_{O_2}$ (see **Figure 5.2a and Figure 5.3b).** Both $P3HT_{N_2}$ and $P3HT_{O_2}$ have amorphous structures. Accordingly, the indirect optical band gap E_{gap} was determined by extrapolating the straight-line portion of the plot of $(\alpha h\upsilon)^{1/2}$ versus $(h\upsilon)$ to the energy axis from UV-Vis absorption spectra as shown in **Figures 5.10 (a and b)**. The optical band gap energies of $P3HT_{N_2}$ and $P3HT_{O_2}$ were estimated to be 2.30 eV and 1.68 eV, respectively. As already explained, the electronic band gap is larger than the optical band gap, as well known that the measurement by electrochemistry requires additional energy because of Coulomb interactions.

The calculations show that E_{gap}(optical) of $P3HT_{O_2}$ exhibits a considerable difference (0.62) in comparison with E_{gap} (optical) of $P3HT_{N_2}$. Notably, this value is consistent with the difference that was obtained by electrical band gaps. This difference can be understood since

$P3HT_{O_2}$ possess higher molecular weight and distinct optical properties as demonstrated earlier. The obtained results from electrical conductivity measurements, cyclic voltammetry and optical band gaps calculations are promising and favorable for practical applications. In particular, they can presumably be used in solar cells due to their appropriate and pertinent E_{gap} values in the field.

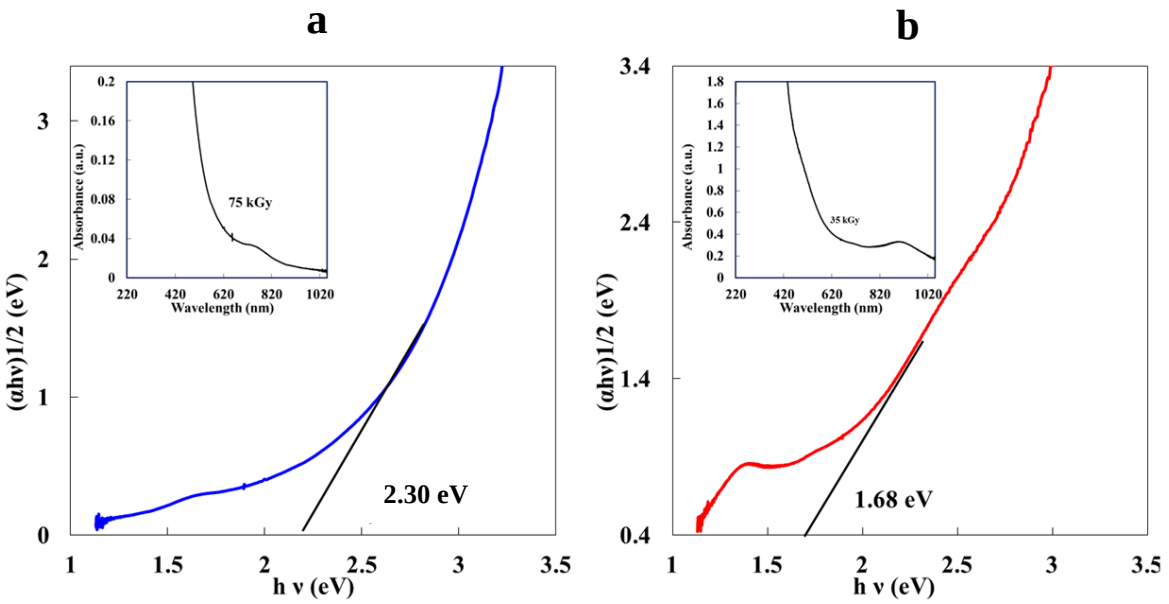

Figure 5.10 Tauc's-plot analysis of UV-Vis absorption spectra $P3HT_{N_2}$ and $P3HT_{O_2}$ synthesized in DCM solvent under N2 at 75 kGy or under O2 at 35 kGy for optical band gap assessment indicating the indirect transitions for a) $P3HT_{N_2}$ and b) $P3HT_{O_2}$. The UV-Vis absorption spectra are given in insert

5.3. Conclusion

In this chapter, starting from hydrophobic 3HT monomers, the aim was to prepare P3HT conducting polymers by radiation induced polymerization method. In this context, recently new strategy has been elaborated by taking into account the fact that dichloromethane is able to dissolve a wide range of organic compounds as well as irradiated dichloromethane is a good oxidizing system. In previous chapters, γ-induced oxidative polymerization in dichloromethane was successfully employed to polymerize EDOT into PEDOT polymers and TAA into PTAA. This methodology enabled us to overcome issues such as low processability and insolubility in aqueous solutions of monomers such as 3HT. For this purpose, the polymerization was controlled and optimized under different environmental conditions by varying the: atmosphere (N_2 or O_2) in order to estimate the appropriate irradiation dose for quantitative polymerization of 3HT.

In case of EDOT and TAA monomers, it was evident that the oxidative polymerization in deaerated solutions of dichloromethane proceeds favourably with the generated primary radicals and the two neutral chloromethyl and dichloromethyl radicals at irradiation dose of 35 kGy. That was possible since solvent radical cations possess high ionizing potential and enable feasibly the initiation of oxidative polymerization of EDOT and TAA. The neutral chloromethyl radicals can behave as oxidizing agents, but their redox potentials are too low to initiate the oxidative polymerization since 3HT possesses higher oxidation potential than EDOT and TAA. Nevertheless, it is well known that the chlorosubstituted methyl radicals react at diffusional rate with O_2 to produce the corresponding peroxyl radicals making the oxidizing power of which is higher with respect to the original carbon centred radicals feasible the oxidation of oligothiophenes such as 3HT.[20]

With this in mind, starting from 3HT monomers dissolved in dichloromethane solution, the oxidative polymerization of P3HT was successfully induced by gamma irradiation under three environments: air, oxygen and nitrogen saturated solutions of dichloromethane. Under these conditions, three polymers were formed and so-called: "$P3HT_{N_2}$", "$P3HT_{air}$" and "$P3HT_{O_2}$". The formation of these polymers was confirmed by UV-Vis and ATR-FTIR absorption spectroscopies. Dose effect study was carried out for all polymers. $P3HT_{N_2}$ needs approximately an irradiation dose of 75 kGy to proceed with the quantitative oxidative polymerization in dichloromethane, while $P3HT_{air}$ and $P3HT_{O_2}$ need irradiation doses of 55 kGy and 35 kGy, respectively. The case of air-saturated solution represents the intermediate case between nitrogen and oxygen saturated solutions. For that reason we focused on the two extreme conditions: N_2 and O_2 atmospheres. Eventually, we can say that introducing oxygen in the irradiated dichloromethane was evident approach to boost up the oxidative polymerization through the production of $CH_2ClO_2^{\bullet}$/$CHCl_2O_2^{\bullet}$.

Detailed comparative studies for the electrical and optical properties were carried out between the two radio-synthesized $P3HT_{N_2}$ and $P3HT_{O_2}$ polymers. UV-Vis absorption spectra reveal that $P3HT_{O_2}$ has distinct optical properties than $P3HT_{N_2}$. Dopeding of $P3HT_{N_2}$ and $P3HT_{O_2}$with chloride ions was also detected. The spectral behaviors were explained by SEC analysis which demonstrated that $P3HT_{O_2}$ polymers have higher molecular weight. ATR-FTIR spectra and EDX highlighted the presence of –COOH groups in $P3HT_{O_2}$polymers. TGA analysis demonstrated that $P3HT_{O_2}$ polymers have better thermal stability than $P3HT_{N_2}$ polymers

Morphological analysis of $P3HT_{N_2}$and $P3HT_{O_2}$ was carried out in dichloromethane solution and after deposition onto substrate by cryo-TEM, SEM and AFM. The microscopic observations demonstrated that γ-synthesized P3HT polymers have two different structures: aggregated blocks in case of $P3HT_{N_2}$ and spheroidal nanoparticles in case of $P3HT_{O_2}$.

The cyclic voltammetry (CV) analysis was used to evaluate HOMO and LUMO energy levels and then to calculate the electronic band gap. A lower electronic band gap was found for $P3HT_{O_2}$ (~1.89 eV) in comparison with that of $P3HT_{N_2}$ (~2.49 eV). Tauc's plots were also used to determine the optical band gap. Consistently to the findings of electronic band gaps, the optical band gap for $P3HT_{O_2}$ (1.68 eV) is lower than the optical band gap for $P3HT_{N_2}$ (2.30 eV). Definitely, $P3HT_{O_2}$ shows higher optical band gap than that of $P3HT_{N_2}$. Finally, the electrical conductivity records are quite remarkable and somewhat comparable with those are already reported in literature. Thus, we can claim that we succeeded in the synthesis of promising and usable P3HT polymers for practical applications.

Interestingly, radiation-induced polymerization in dichloromethane under O_2 offers producing polymers functionalized with carboxylic groups. This would improve the adhesion properties of radio-synthesized P3HT and therefore this gives P3HT polymers the advantage to be fixed onto certain materials such as TiO_2 or certain surfaces such as ITO substrates.

According to obtained findings, controlling the morphology and increasing the molecular weight of radio-synthesized polymers could enhance their optical and electrical properties. Additionally, using a small subset of building blocks and resort to co-polymerization will be immensely helpful to achieve the desired properties. The fact that dichloromethane and water are immiscible solvents, offers the possibility to use of microemulsion polymerization through gamma radiolysis with the view of having a controlled morphology.

Lastly, the use of radiation induced polymerization offers production of different types of conducting polymers, different nanostructurations and different optical and electrical properties. In the previous 4 chapters, all the synthesized CPs possess very interesting features, no matter if they are synthesized in aqueous or in dichloromethane solutions. Therefore in the next chapter we will incorporate our radiosynthesized CPs in photovoltaics, we will test their power conversion efficiency and we will compare their performances with some standard materials.

References

1. Wei, Y.; Chan, C. C.; Tian, J.; Jang, G. W.; Hsueh, K. F., Electrochemical polymerization of thiophenes in the presence of bithiophene or terthiophene: kinetics and mechanism of the polymerization. *Chemistry of Materials* **1991,** *3* (5), 888-897.

2. Cutler, C. Electrochemical and photoelectrochemical studies of functionalised polythiophenes. University of Wollongong, University of Wollongong, Department of chemistry, 2000.

3. Ferraris, J. P.; Newton, M. D., Electrochemical and optical properties of thiophene-alkylheteroaromatic copolymers. *Polymer* **1992,** *33* (2), 391-397.

4. Roncali, J.; Garreau, R.; Yassar, A.; Marque, P.; Garnier, F.; Lemaire, M., Effects of steric factors on the electrosynthesis and properties of conducting poly(3-alkylthiophenes). *The Journal of Physical Chemistry* **1987,** *91* (27), 6706-6714.

5. Lattach, Y.; Deniset-Besseau, A.; Guigner, J.-M.; Remita, S., Radiation chemistry as an alternative way for the synthesis of PEDOT conducting Polymers under "soft" Conditions. *Radiation Physics and Chemistry* **2013,** *82*, 44-53.

6. Murali, M. G.; Rao, A. D.; Yadav, S.; Ramamurthy, P. C., Narrow band gap conjugated polymer for improving the photovoltaic performance of P3HT:PCBM ternary blend bulk heterojunction solar cells. *Polymer Chemistry* **2015,** *6* (6), 962-972.

7. Tremel, K.; Ludwigs, S., Morphology of P3HT in Thin Films in Relation to Optical and Electrical Properties. In *P3HT Revisited – From Molecular Scale to Solar Cell Devices*, Ludwigs, S., Ed. Springer Berlin Heidelberg: Berlin, Heidelberg, 2014; pp 39-82.

8. Marrocchi, A.; Lanari, D.; Facchetti, A.; Vaccaro, L., Poly(3-hexylthiophene): synthetic methodologies and properties in bulk heterojunction solar cells. *Energy & Environmental Science* **2012,** *5* (9), 8457-8474.

9. Pappenfus, T. M.; Hermanson, D. L.; Kohl, S. G.; Melby, J. H.; Thoma, L. M.; Carpenter, N. E.; da Silva Filho, D. A.; Bredas, J.-L., Regiochemistry of Poly(3-hexylthiophene): Synthesis and Investigation of a Conducting Polymer. *Journal of Chemical Education* **2010,** *87* (5), 522-525.

10. Klauk, H., Organic thin-film transistors. *Chemical Society Reviews* **2010,** *39* (7), 2643-2666.

11. Mccullough, R. D.; Tristramnagle, S.; Williams, S. P.; Lowe, R. D.; Jayaraman, M., Self-Orienting Head-to-Tail Poly(3-Alkylthiophenes) - New Insights on Structure-Property Relationships in Conducting Polymers. *J Am Chem Soc* **1993,** *115* (11), 4910-4911.

12. Jiang, C.; Chen, G.; Wang, X., High-conversion synthesis of poly(3,4-ethylenedioxythiophene) by chemical oxidative polymerization. *Synthetic Metals* **2012,** *162* (21), 1968-1971.

13. Ishigaki, A.; Koizumi, H., Radiation-induced polymerization of 3-octylthiophene. *Radiation Physics and Chemistry* **2012,** *81* (7), 803-806.

14. Emmi, S. S.; Beggiato, G.; Casalbore-Miceli, G., Transient species in the pulse radiolysis of methylene chloride and the self-reaction of chloromethyl radicals. *International Journal of Radiation Applications and Instrumentation. Part C. Radiation Physics and Chemistry* **1989,** *33* (1), 29-37.

15. Alfassi, Z. B.; Mosseri, S.; Neta, P., Reactivities of Chlorine Atoms and Peroxyl Radicals Formed in the Radiolysis of Dichloromethane. *J Phys Chem-Us* **1989,** *93* (4), 1380-1385.

16. Emmi, S. S.; Poggi, G.; D'Angelantonio, M.; Russo, M.; Favaretto, L., The solvatochromic effect on some oligothiophene radical cations: a pulse radiolysis and semiempirical investigation. *Radiation Physics and Chemistry* **2003,** *67* (3), 251-256.

17. Lattach, Y.; Coletta, C.; Ghosh, S.; Remita, S., Radiation-Induced Synthesis of Nanostructured Conjugated Polymers in Aqueous Solution: Fundamental Effect of Oxidizing Species. *ChemPhysChem* **2014,** *15* (1), 208-218.

18. Coletta, C.; Cui, Z.; Dazzi, A.; Guigner, J.-M.; Néron, S.; Marignier, J.-L.; Remita, S., A pulsed electron beam synthesis of PEDOT conducting polymers by using sulfate radicals as oxidizing species. *Radiation Physics and Chemistry* **2016,** *126*, 21-31.

19. Cui, Z.; Coletta, C.; Rebois, R.; Baiz, S.; Gervais, M.; Goubard, F.; Aubert, P.-H.; Dazzi, A.; Remita, S., Radiation-induced reduction–polymerization route for the synthesis of PEDOT conducting polymers. *Radiation Physics and Chemistry* **2016,** *119*, 157-166.

20. Emmi, S. S.; D'Angelantonio, M.; Beggiato, G.; Poggi, G.; Geri, A.; Pietropaolo, D.; Zotti, G., The generation and spectral characterization of oligothiophenes radical cations. A pulse radiolysis investigation11This paper was presented at the 10th International Meeting on Radiation Processing, 11–16 May 1997, Anaheim, California, U.S.A. *Radiation Physics and Chemistry* **1999,** *54* (3), 263-270.

21. Ushida, K.; Yoshida, Y.; Kozawa, T.; Tagawa, S.; Kira, A., Evidence of Oxidation of Aromatic Hydrocarbons by Chloromethyl Radicals: Reinvestigation of Intersolute Hole Transfer Using Pulse Radiolysis. *The Journal of Physical Chemistry A* **1999,** *103* (24), 4680-4689.

22. Beiting, E. J.; Zeringue, K. J.; Stickel, R. E., Absorption spectra of thiophene between 225 and 246 nm at elevated temperatures. *Spectrochimica Acta Part A: Molecular Spectroscopy* **1985,** *41* (12), 1413-1418.

23. Truszkowski, S.; Szymański, W., Stable products and radicals in the radiolysis of dichloromethane and 1,1,-dichloroethane gamma-irradiated in an oxygen-free atmosphere. *Journal of Radioanalytical and Nuclear Chemistry* **1994,** *177*, 415-423.

24. Bahry, T.; Cui, Z.; Deniset-Besseau, A.; Gervais, M.; Sollogoub, C.; Bui, T.-T.; Remita, S., An alternative radiolytic route for synthesizing conducting polymers in an organic solvent. *New Journal of Chemistry* **2018,** *42* (11), 8704-8716.

25. Kim, T.; Kim, J.; Kim, Y.; Lee, T.; Kim, W.; Suh, K. S., Preparation and characterization of poly(3,4-ethylenedioxythiophene) (PEDOT) using partially sulfonated poly(styrene-butadiene-styrene) triblock copolymer as a polyelectrolyte. *Current Applied Physics* **2009,** *9* (1), 120-125.

26. Isse, A. A.; Lin, C. Y.; Coote, M. L.; Gennaro, A., Estimation of Standard Reduction Potentials of Halogen Atoms and Alkyl Halides. *The Journal of Physical Chemistry B* **2011,** *115* (4), 678-684.

27. Barta, P.; Cacialli, F.; Friend, R. H.; Salaneck, W. R.; Zagorska, M.; Pron, A., On the influence of regioregularity on electronic and optical properties of poly(alkylthiophenes). *Synthetic Metals* **1999,** *101* (1-3), 296-297.

28. Lohwasser, R. H.; Bandara, J.; Thelakkat, M., Tailor-made synthesis of poly(3-hexylthiophene) with carboxylic end groups and its application as a polymer sensitizer in solid-state dye-sensitized solar cells. *Journal of Materials Chemistry* **2009,** *19* (24), 4126-4130.

29. Floresyona, D.; Goubard, F.; Aubert, P.-H.; Lampre, I.; Mathurin, J.; Dazzi, A.; Ghosh, S.; Beaunier, P.; Brisset, F.; Remita, S.; Ramos, L.; Remita, H., Highly active poly(3-hexylthiophene) nanostructures for photocatalysis under solar light. *Applied Catalysis B: Environmental* **2017,** *209*, 23-32.

30. Singh, B.; Kaur, A., Photoelectrical, optical, and transport properties of poly (3-hexylthiophene)-zinc sulfide hybrid nanocomposites. *Journal of Applied Physics* **2014,** *116* (6), 063709.

31. Kalonga, G.; Chinyama, K.; Munyati, O.; Maaza, M., *Characterization and Optimization of P3HT and PCBM blends for Photo-absorption*. 2013; p 93-102.

32. Xia, H.; Ye, Z.; Liu, X.; Peng, J.; Qiu, F., Synthesis, characterization, and solution structure of all-conjugated polyelectrolyte diblock copoly(3-hexylthiophene)s. *RSC Advances* **2014,** *4* (38), 19646-19653.

33. Kuila, B. K.; Nandi, A. K., Physical, Mechanical, and Conductivity Properties of Poly(3-hexylthiophene)−Montmorillonite Clay Nanocomposites Produced by the Solvent Casting Method. *Macromolecules* **2004,** *37* (23), 8577-8584.

34. Pommerehne, J.; Vestweber, H.; Guss, W.; Mahrt, R. F.; Bässler, H.; Porsch, M.; Daub, J., Efficient two layer leds on a polymer blend basis. *Advanced Materials* **1995,** *7* (6), 551-554.

35. Wu, I. C.; Lai, C.-H.; Chen, D.-Y.; Shih, C.-W.; Wei, C.-Y.; Ko, B.-T.; Ting, C.; Chou, P.-T., Cu(i) chelated poly-alkoxythiophene enhancing photovoltaic device composed of a P3HT/PCBM heterojunction system. *Journal of Materials Chemistry* **2008,** *18* (36), 4297-4303.

Chapter 6 application opportunity in photovoltaics

Photovoltaics cells have met a board interest among the people and have become widely distributed and desirable. This sophisticated technology is clean, silent and is considered as a green source of energy because it is a friend of the environment. In addition, the solar cells can be constructed to any size depending on energy requirements. The solar cells require materials which first absorb the sunlight, and secondly materials which assure the electrons movement. These materials are represented by semiconductors in forms of donor- acceptor (p-n) types. Thus, based on the materials, photovoltaic cells can be found in several forms: organic, inorganic and hybrid organic-inorganic (perovskite) cells. The principle of working is generally that when the sunlight hits the surface of the solar penal, the outermost electrons of the atoms of particular semiconductor such as silicon get excitation. That process will be followed by electron-hole pair generation, then charge separation and as a consequence, occurrence of an electric current. [1-2]

In industry, manufacturing of inorganic photovoltaic cells (IPVs) (**Figure 6.1a**)[3] is predominant compared with organic photovoltaics cells (OPVs) (**Figure 6.1b**), due to the chemical and thermal stability of IPVs, their long life time and importantly, their high Power Conversion Efficiencies (PCEs). However, IPVs are costly and consume energy through many steps of purification. Organic solar cells based on semiconductor polymers have attracted a great attention as a potential and promising source of renewable energy due to their low cost production, flexibility and easy to commercialize.[4] This type of photovoltaics has some issues such as their inefficiency and low stability that is represented by photochemical degradation. However, intensive researches have been made in order to increase their power conversion efficiencies (PCEs). The in-between those two types, the hybrid organic-inorganic metal halide perovskite solar cells (PSCs) emerge to be promising due to their remarkable efficiency (**Figure 6.1c**).[5-6] PSCs have become a research "hot spot" for many solar cell researchers. The perovskite materials show various advantages such as long carrier diffusion lengths, widely-tunable band gap with great light absorption potential. The low-cost fabrication techniques together with the high efficiency make PSCs comparable with Si-based solar cells.[5, 7] But the drawbacks such as device instability, *J-V* hysteresis and lead toxicity reduce the further improvement and the future commercialization of PSCs.[6]

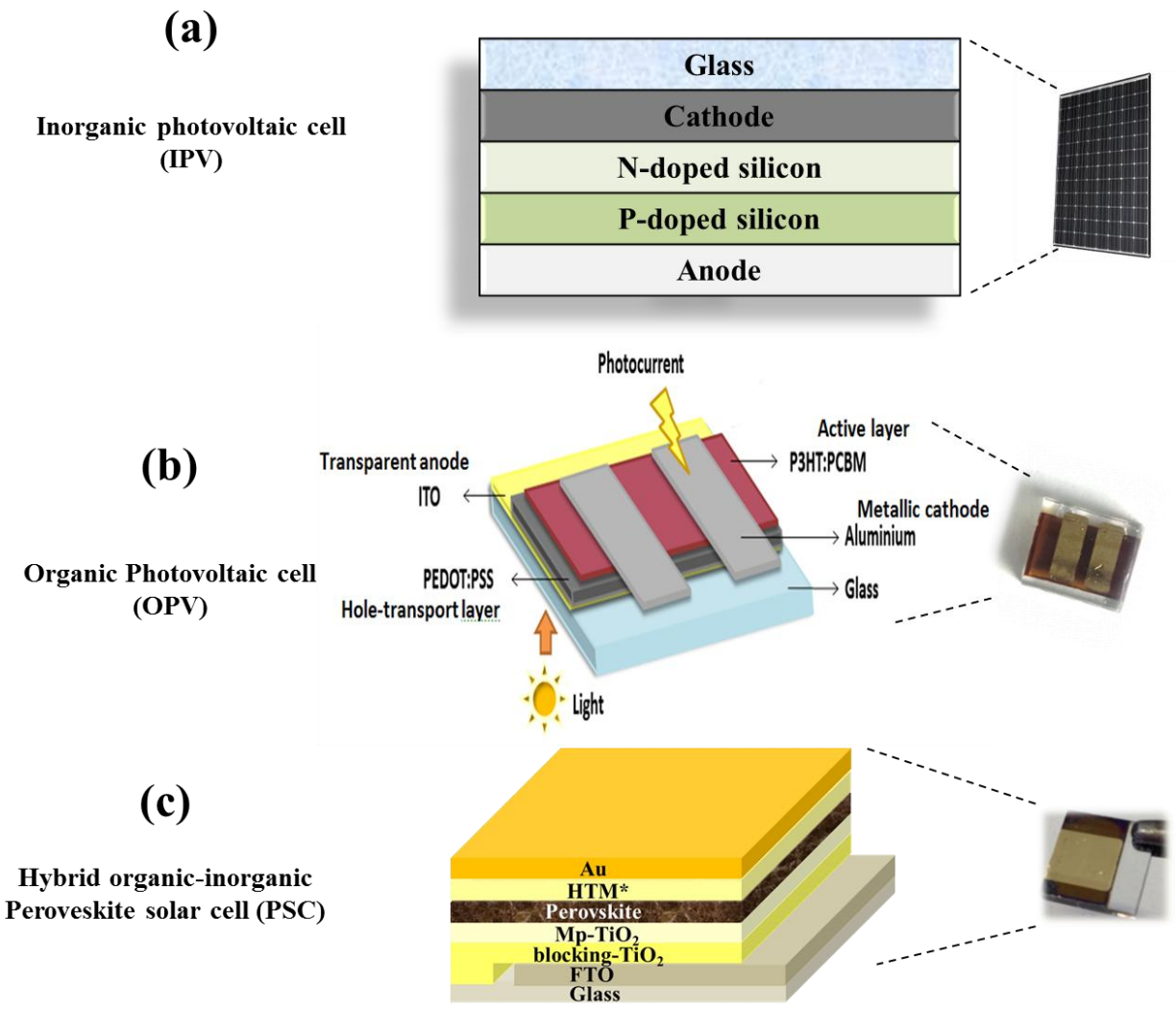

Figure 6.1 Displays of some schematic types of solar cells showing the main components which are involved in their structure: a) Inorganic photovoltaic cell model (IPV) , b) Organic photovoltaic cell (OPV) fabricated in previous work, c) Hybrid organic-inorganic perovskite cell (PSC) fabricated in this work.

PSCs usually consist of: transparent anode, metallic cathode, conducting layer or hole-transport layer (HTL) and light-absorbing layer or active layer.[6] Generally, a thin layer of ITO (Indium tin oxide) or FTO (Fluorine-doped tin oxide) coated on the top of small piece of glass is used as anode while a film of gold or aluminum placed on the top of the device is used as cathode. ITO/FTO is transparent and resistant to many different types of common solvents, so almost any type of materials of the upcoming layer can be used to deposit on ITO/FTO substrate. The light-absorbing layer in PSCs is a perovskite structured compound. The perovskite materials have been demonstrated with largely tunable band gap (e.g., $CH_3NH_3PbX_3$ has a band gap from 1.5 eV to 2.3 eV)[8] and great light absorption coefficient (higher than 10^4 cm^{-1})[9-10], which is similar to other thin film solar cell materials such as

CdTe[11] and copper zinc tin sulfide (CZTS).[12] Its low-cost and convenient fabrication techniques also serve as the possible advantages over silicon-based devices that require complicated and costly high-vacuum deposition methods.[6] Besides perovskite materials which are used for light harvesting, the hole-transport materials (HTM) are very important.[7, 13] HTM are used as contacts and for electron and hole extraction. An ideal hole-transport material (HTM) must fulfil some general requirements for efficient operation in PSCs.[7] First, the HOMO energy level of the HTM must be compatible with the valence band energy of the perovskite to provide a suitable driving force for the charge transfer. Furthermore, the LUMO level of the HTM must be significantly higher than that of the perovskite absorber to exhibit electron-blocking properties. The HTM should also have sufficient hole mobility, as well as excellent thermal, morphological, and photochemical stabilities, and good hydrophobic properties to protect the perovskite material from moisture deposit on the ITO layer.[13] HTM layer helps the active layer by inducing crystallization of the p-type semiconducting phase and refines the surface of the anode so that there is a flatter contact between the semiconducting layer and the substrate. Consequently, the hole-transport layer improves the fill factor (FF) which, in conjunction with open circuit voltage (V_{OC}) and short-circuit current density (J_{SC}), determines the maximum power from a solar cell. The HTM layer also increases the short-circuit current density (J_{SC}). The most common HTM material for PSCs is Spiro-OMeTAD. This compound has been successfully adapted to PSCs, with power conversion efficiencies of over 22%.[7] However, its complicated steps of synthesis are an obstacle to its large-scale production. Therefore, finding an alternative HTM that can offer high efficiency performance in PSCs and synthesis simplicity will be immensely substantial.[5, 7, 13]

Polymeric HTMs have paramount importance in the field due to their extraordinary properties. Besides the polymeric materials can be easily synthesized, they have important advantages in terms of processability, thermal and mechanical stability, and higher intrinsic hole mobility.[14-16] Among the different types of conducting polymers, thiophene and its derivatives are effectively advantageous to be used as HTMs in PSCs.[7] This is originated from the fact that the presence of sulfur atoms in S-containing heterocyclic building blocks might give better HTM/perovskite interactions.[17-18]

The objective of the use of radiation chemistry in the field of synthesis of conducting polymers is the fabrication innovating conductive material applicable in photovoltaics. In this context, the radio-produced conducting polymers appear to be suitable as HTM and fulfil the requirements. Based on the outcomes of cyclic voltammetry analysis and optical band gaps

estimations, few tests have been carried out toward our endeavors to incorporate the radio-synthesized polymers in photovoltaics.

Thus in this chapter, some of radio-synthesized polymers will be used as new HTM layers to fabricate PSCs. Later the fabricated devices will be evaluated through *J-V* characteristic curves and then their fill factor and power conversion efficiency will be estimated. Lastly, the obtained values will be compared with Spiro-OMeTAD and with similar materials that are reported in literature.

4.4. **Experimental**

4.4.1. **Samples preparation for PSCs fabrication**

For this experiment, the following radio-synthesized conducting polymers were selected for PSCs devices fabrication to be used as HTM:

- $PEDOT_{CH_2Cl_2}$ polymers synthesized by dichloromethane radiolysis under N_2 atmosphere at irradiation dose of 35 kGy
- $PTAA_{H_2O}$ polymers synthesized in aqueous solution under N_2O atmosphere and irradiated at irradiation dose of 35 kGy
- $PTAA_{CH_2Cl_2}$ polymers synthesized by dichloromethane radiolysis under N_2 atmosphere at irradiation dose of 35 kGy
- $P3HT_{N_2}$ polymers synthesized by dichloromethane radiolysis under N_2 atmosphere at irradiation dose of 75 kGy
- $P3HT_{O_2}$ polymers synthesized by dichloromethane radiolysis under N_2 atmosphere at irradiation dose of 35 kGy

In all experiments, Spiro-OMeTAD is used as standard HTM for comparison

These radio-synthesized CPs were directly incorporated in PSCs devices after drying procedure. To test the radio-synthesized conducting polymers and to check their performance as HTM materials, the corresponding polymers were dissolved in an adequate solvent that was selected according to a solubility test (see chapter1, table 1.5).

The radio-synthesized conducting polymers solutions were prepared at concentration of 10 $mg.mL^{-1}$. A solution of Spiro-OMeTAD was prepared by dissolving 72 mg in 1 mL in DCM or in THF. Then all the HTMs were doped under identical conditions in the PSC devices. In this purpose, 17.5 µL of bis(tri-fluoro-methyl- sulfonyl) imide lithium salt solution (Li-TFSI) solution (520 mg in 1 mL ACN) were added to HTMs solutions. Later the

components of PSCs were spin coated layer by layer. **Figure 6.2** displays the physical appearance of some of PSCs devices after spin coating of HTM layer. The procedure of the elaboration of the PSCs is described in details in chapter 1.

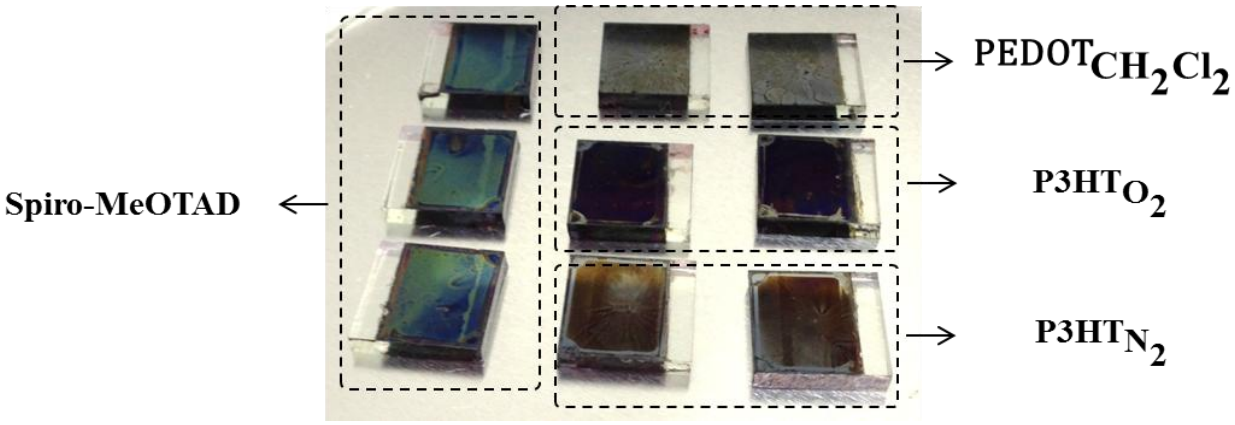

Figure 6.2 Photographical images for some of fabricated PSCs by utilizing the radiosynthesized conducting polymers and Spiro-MeOTAD as HTM layers. The device components are FTO/TiO2cp/TiO2pr/Perovskite/Spiro-MeOTAD or radiosynthesized conducting polymers. The Perovskite layer is $CH_3NH_3PbI_3$.

4.4.2. **Current-Voltage (*J-V*) characteristic curves**

The *J-V* characteristic curves represent the relation between the current flowing through an electronic device and the applied voltage across its terminals. This curve is used to determine the important parameters which enable us to calculate the fill factor and the efficiency of the device. **Figure 6.3** shows the typical *J-V* and all the parameters which are needed to perform the device calculation.

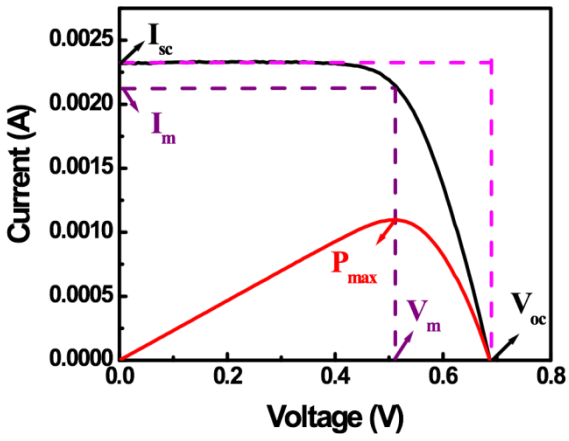

Figure 6.3 *J-V* Characteristic curve of a solar cell showing all the characteristic parameters under illumination and in the dark

Where Isc is the short circuit current which is defined as the current through the solar cell when the voltage across the solar cell is zero (I = J_{SC} at V=0). While V_{OC} is the open circuit voltage, which is the voltage when the current equals to zero (V (at J=0) = V_{OC}). P_{max} is the maximum power from the solar cell. J_m and V_m are the current and the voltage at P_{max}. From the previous parameters, the fill factor (FF) which is considered as a measure of the quality of the solar cell, being calculated by comparing the maximum power to the theoretical power (P_T) as following:

$$FF = \frac{P_{MAX}}{P_T} = \frac{J_m \times V_m}{Jsc \times Voc} \times 100\% \quad (6.1)$$

The efficiency (η) of the devices is commonly used as a parameter to examine the performance and compare it with other devices. The efficiency is defined by the ratio of energy output from the solar cell to input energy (P_{in}) from the sun. In fact there are many factors which can affect the efficiency of the device such as the temperature of the solar cell, preparation conditions and the spectrum and intensity of the incident sunlight.

$$\text{Efficiency } (\eta) = \frac{P_{MAX}}{P_{in}} = \frac{Jsc \times Voc}{P_{in}} \times FF\% \quad (6.2)$$

4.5. Results and discussion

4.5.1. Preliminary test for checking the efficiency and photo-activity of radio-synthesized polymers in hybrid PSCs:

Before to begin with PSCs fabrication and then to record *J-V* characteristic curves, the solubility of our radiosynthesized polymers was verified in several solvents. The solubility and processability of PSCs components has key role in PSCs performance.[6] Accordingly, it is important to comment on the findings that were obtained from these experiments.

6.2.1.1.Solubility test:

In general, due to the poor processability and low solubility of conducting polymers in common solvent, their numbers of applications are limited. This lack of processability is

related to the rigidity of the polymer chain, which is a direct consequence of the high level of conjugation of the polymer that in turn affects the molecular conductivity.[19] Having high solubility and good processability is important parameter in the construction of photovoltaics, most notably to prepare homogeneous film at fixed thickness. It is worthy to mention, to obtain good film with desired thickness; the concentration of polymer solution should be prepared more than 10 $mg.mL^{-1}$. In this regard, it is well known that chlorinated solvents are commonly used to solubilize conducting polymers and thereafter, to prepare thin film. Therefore, to proceed with the fabrication of photovoltaic cells, a solubility test for $PEDOT_{CH_2Cl_2}$, $PTAA_{CH_2Cl_2}$, $PTAA_{H_2O}$, $P3HT_{N_2}$ and $P3HT_{O_2}$ was performed at the corresponding concentration in several chlorinated organic solvent and besides THF and DMSO, as depicted in solubility's table in chapter 1 (Table 1.5)

Figure 6.4 displays few photographical images of the radio-synthesized conducting polymers at a concentration of 10 $mg.mL^{-1}$ in the adequate solvents. The findings show that both $PTAA_{CH_2Cl_2}$, $PTAA_{H_2O}$ and $PEDOT_{CH_2Cl_2}$ polymers possess very poor processability in most of the chlorinated solvents. However, $PTAA_{CH_2Cl_2}$, $PTAA_{H_2O}$ have very good solubility in DMSO and THF. Interestingly, $P3HT_{N_2}$, $P3HT_{O_2}$ evidently show the best processability among the radiosynthesized polymers. As can be seen in table 1.5 $P3HT_{N_2}$, $P3HT_{O_2}$are soluble in almost all of the tested solvents.

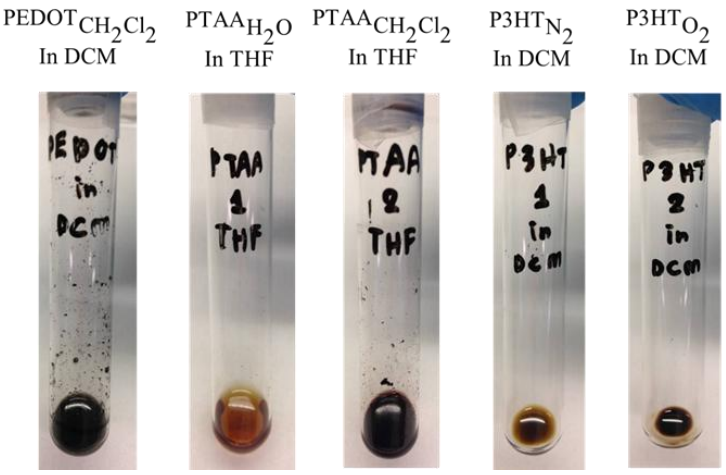

Figure 6.4 photographical images of the of radio-synthesized conducting polymers dessolved in an adequate solvents (DCM or THF.

The findings suggest that solubility of our radio-synthesized polymers show poor processability in common organic solvents and consequently restricted applications. The poor

processability could be ascribed to som aggregations and some cross linkings in some cases during polymerization. As a consequence, the photo-activity measurements proceeded throughout fabrication of two sets of PSCs devices. The first set, $PEDOT_{CH_2Cl_2}$, $P3HT_{N_2}$, $P3HT_{O_2}$ and Spiro-OMeTAD in DCM. The second set $PTAA_{CH_2Cl_2}$, $PTAA_{H_2O}$ and Spiro-OMeTAD in THF.

6.2.1.2.Photo-activity measurements of hybrid PSCs:

The as-prepared radio-synthesized conducting polymers were tested as HTMs in PSC devices, by using $CH_3NH_3PbI_3$ as the absorber material. **Figure 6.5** presents a schematic view for the fabricated device and shows all the incorporated components in the elaboration process. Our devices were composed of a thin compact TiO_2 layer, a mesoporous TiO_2 layer filled and capped with the $CH_3NH_3PbI_3$ perovskite, a HTM layer and finally a thermally evaporated Au layer. According to our electrochemistry results that are represented by electrical conductivity, electronic and optical band gaps estimations, the radio-synthesized conducting polymers were usable as HTMs. Thus, the current-voltage (*J-V*) curves were plotted to characterize the fabricated OPVs devices. The fill factors (FF) and the power conversion efficiencies (PCEs) were calculated based on the equations (6.1) and (6.2).

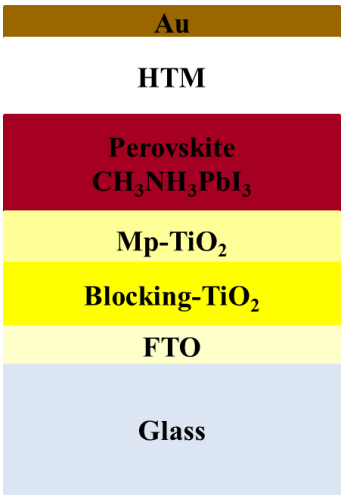

Figure 6.5 PSC device structure incorporating different components.

4.5.1.1. J-V characteristic curves of PEDOT, $P3HT_{N_2}$, $P3HT_{O_2}$ and Spiro-OMeTAD in DCM:

The best current density–voltage (*J–V*) curves for the various HTMs are shown in **Figure 6.6**. Best and average *J–V* curve parameters under one sun illumination, as well as their standard deviations, are shown in **Table 6.1**.

Devices		J_{SC}	V_{OC}	FF	PCE (%)	Average	SD
Spiro-OMeTAD	1	11.649	0.910	0.661	7.010	5.99	0.97
	2	11.814	0.930	0.463	5.084		
	3	13.406	0.920	0.477	5.883		
PEDOT in DCM	1	2.9527	0.510	0.207	0.312	0.21	0.15
	2	7.748	0.050	0.261	0.101		
$P3HT_{N_2}$ in DCM	1	-	-	-	-	-	-
	2	-	-	-	-		
$P3HT_{O_2}$ in DCM	1	3.697	0.220	0.240	0.195	0.14	0.07
	2	2.091	0.180	0.244	0.092		

Table 6.1 Photovoltaic characteristics of PSCs that contain radio-synthesized conducting polymers or Spiro-OMeTAD in DCM as HTMs

Figure 6.6 shows the *J–V* characteristics of PSCs on glass substrates that utilized PEDOT, $P3HT_{N_2}$, $P3HT_{O_2}$ as well as Spiro-OMeTAD as the HTM layer under AM 1.5 G illumination at an intensity of 100 $mW.cm^{-2}$.

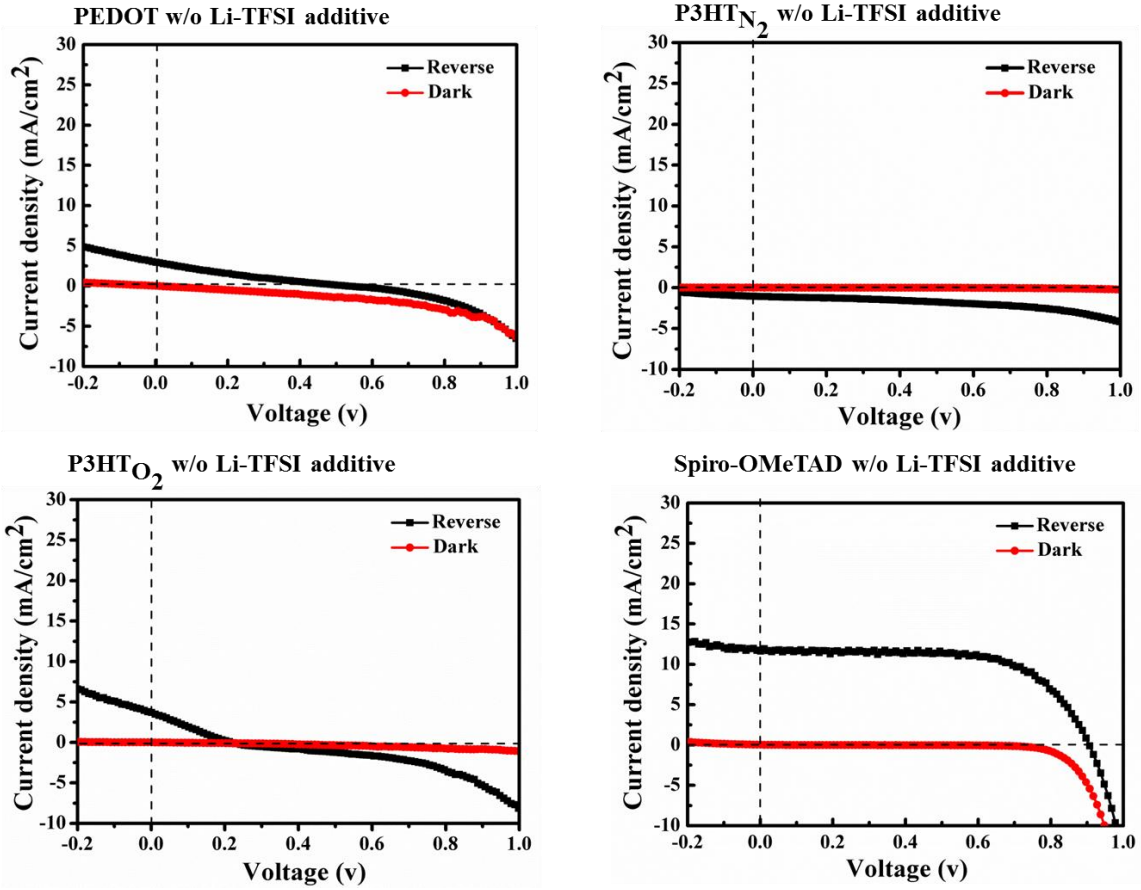

Figure 6.6 *J–V* characteristics of PSCs that contain PEDOT, $P3HT_{N_2}$, $P3HT_{O_2}$ or Spiro-OMeTAD in DCM as HTM layers under forward or reverse bias

The statistical data for the PSCs are summarized in **Table 6.1**. The *J-V* curves corresponding to $P3HT_{N_2}$ polymers did not show any photo-activity. This can be attributed to their low electrical conductivity and poor optical properties. However, the PSC containing PEDOT, $P3HT_{O_2}$ as a HTM layers exhibited poor photovoltaic performance with an average efficiency of 0.2% and 0.14%, respectively. The low efficiency of these PSCs resulte from their low J_{SC} (PEDOT: 5.35 $mA.cm^{-2}$/ $P3HT_{O_2}$:2.89 $mA.cm^{-2}$) and FF (PEDOT: 0.23/$P3HT_{O_2}$:0.242) values. By utilizing Spiro-OMeTAD as the HTM layer, the J_{SC} and FF values are improved and consequently, a relatively high efficiency of 5.99% was obtained when comparing with PEDOT and $P3HT_{O_2}$.

When comparing the measured parameters from the Spiro-OMeTAD and the radiosynthesized polymers (PEDOT, $P3HT_{N_2}$ and $P3HT_{O_2}$) we can note that the fabricated devices have very low performances, which can be ascribed to the preparation conditions, cleaning steps and the incident light intensity. Moreover, the photo-activity is very sensitive to the photovoltaics (PVs) temperature. In another hand, the performance is also affected by the used materials (hole-transport layer, solvents, FTO/ITO substrates, etc.). In addition, there are many factor effects on the performance like the molecular weight of radio-synthesized polymers, the configuration pattern, morphologies, physical state, etc.

4.5.1.2. J-V characteristic curves of $PTAA_{CH_2Cl_2}$, $PTAA_{H_2O}$ and Spiro-OMeTAD in THF:

In the same way as before, the two polymeric HTMs ($PTAA_{CH_2Cl_2}$, $PTAA_{H_2O}$) as well as Spiro-OMeTAD have been implemented in PSCs after doping with Li-TFSI. The I-V curves recorded under dark and simulated sunlight. The curves parameters are gathered in **Table 6.2** and the best *J-V* curves of the record cells are disclosed in **Figure 6.7**. The fill factors (FF) and the power conversion efficiencies (PCEs) were calculated based on the equations (6.1) and (6.2).

The best Spiro-OMeTAD cell delivered 0.59 %. In case of radio-synthesized PTAA polymers, the efficiency was found lower. The $PTAA_{CH_2Cl_2}$ cell delivered a PCE of 0.2 % while $PTAA_{H_2O}$ cell delivered only 0.03 %. As can be observed for the obtained data, the PSCs based on $PTAA_{CH_2Cl_2}$ has better performance and higher PCE in comparison to PSCs based on $PTAA_{H_2O}$. Indeed, as we could see in chapter 4, $PTAA_{CH_2Cl_2}$showed better optical and electrical properties that are represented by relatively higher conductivity and lower

optical and electrical band gaps. These properties altogether make $PTAA_{CH_2Cl_2}$ as HTM better than $PTAA_{H_2O}$.

Devices		J_{SC}	V_{OC}	FF	PCE (%)	Average	SD
Spiro-OMeTAD	1	4.297	0.490	0.232	0.489	0.59	0.14
	2	-	-	-	-		
	3	3.867	0.590	0.302	0.690		
$PTAA_{H_2O}$ in THF	1	-	-	-	-	0.03	0.03
	2	1.400	0.140	0.255	0.050		
	3	1.589	0.030	0.234	0.011		
$PTAA_{CH_2Cl_2}$ in THF	1	1.224	0.580	0.401	0.285	0.20	0.07
	2	0.599	0.530	0.482	0.153		
	3	1.001	0.440	0.366	0.161		

Table 6.2 Photovoltaic characteristics of PSCs that contain radio-synthesized conducting polymers or Spiro-OMeTAD in THF as HTMs

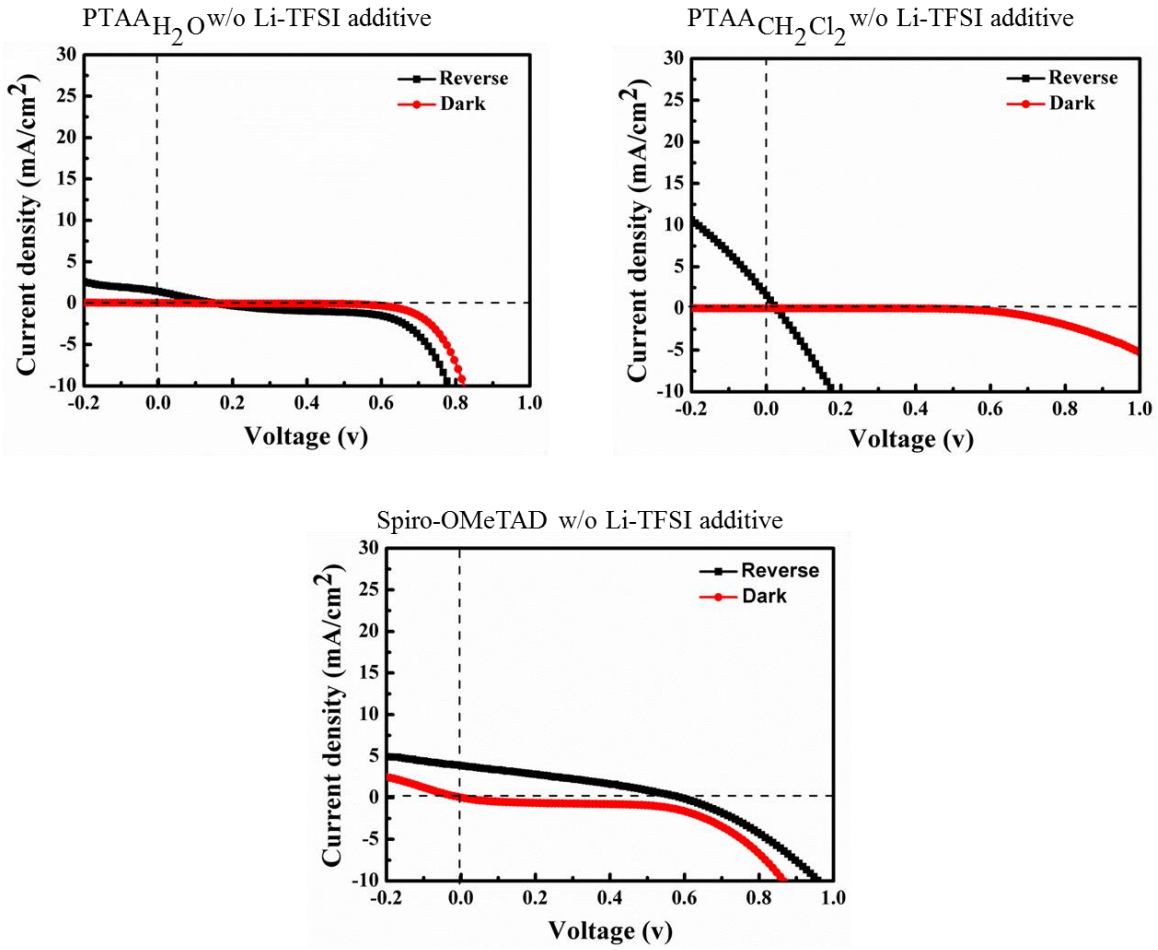

Figure 6.7 J–V characteristics of PSCs that contain $PTAA_{CH_2Cl_2}$, $PTAA_{H_2O}$ or Spiro-OMeTAD in THF as HTM layers under forward or reverse bias

By contrast, it has been reported in literature the fabrication of PSCs that incorporates components similar to our CPs for the fabricated PSCs.[20] The fabricated PSCs devices incorporated two polymeric HTMs: PTAA and P3HT polymers. Those polymers were chemically synthesized with high degree of polymerization and high yield of regioregularity. The PTAA cell delivered a PCE of 7.38% while P3HT cell delivered 5.85 %.[20] We can note that all the fabricated devices have very low performances including those containing spiro-OMeTAD. This low performance can be ascribed to the preparation conditions, cleaning steps and the incident light intensity and therefore, it is needed to control and optimize the fabrication condition. However, the low molecular weight and the low yield of regioregularity of the radio-sythesized polymers affect the performance of PSCs.

4.6. **Conclusions**

Conducting polymers have potential applications in many fields and one of the most promising applications is photovoltaics. Our endeavor to radio-synthesized conducting polymers for highly efficient solar cells has been made through in this chapter. To proceed with this endeavor, the radio-synthesized conducting polymers have been well characterized in terms of physical, optical and electrical properties. The obtained results revealed that the radio-synthesized polymers possess remarkable electrical and optical properties. Moreover, they are promisingly usable for practical applications.

Thus, in a further step of this work, the radio-synthesized polymers were used as novel HTMs for elaboration of some hybrid organic-inorganic solar cells, namely, perovskite solar cells (PSCs). For comparison purpose, Spiro-OMeTAD was used as standard HTM. Before beginning the elaboration procedure, the solubility of powder of radio-synthesized conducting polymers was studied in several organic solvents. The PSCs devices were subsequently fabricated by using the adequate solvent. After PSCs fabrication, we measured the produced photocurrent and voltage from the PSCs devices which were fabricated by radio-synthesized conducting polymers and Spiro-OMeTAD. *J-V* curves were plotted to determine the characteristic parameters. The fill factor (FF) and PCEs were calculated. The measurements showed that the photovoltaic effects are very small, even for Spiro-OMeTAD. The obtained conversion efficiencies are negligible for $PTAA_{H_2O}$ and $P3HT_{N_2}$, since the yield is lower than 0.1%. The low performance of these radio-synthesized polymers could be ascribed to the poor absorption in the visible region of the UV-Vis spectrum, low molecular weight and small electronic band gap and due to the fabricated device itself.

Although, the studied Photovoltaic properties in this chapter are not enough satisfactory, this experiment highlighted the distinct performance between the radio-synthesized polymers. For example, as shown in chapter 5, the use of water radiolysis leads to $PTAA_{H_2O}$ while the use of dichloromethane radiolysis leads to $PTAA_{CH_2Cl_2}$. Evidently, these two polymers exhibited different optical and electrical properties. Thus, the higher PCE value that obtained in case of $PTAA_{CH_2Cl_2}$was construed in accordance to their better properties in comparison with those of $PTAA_{H_2O}$. Similar findings have been observed in case of $P3HT_{N_2}$ and $P3HT_{O_2}$. The PSCs devices that were fabricated in presence of $P3HT_{O_2}$ polymers led to 0.242 % PCE while $P3HT_{N_2}$ polymers did not show any photoactivity. As demonstrated in chapter 6, $P3HT_{O_2}$ in comparison with $P3HT_{N_2}$, has better electrical conductivity, higher molecular weight and smaller electronic and optical band gaps and therefore $P3HT_{O_2}$ presents positive results in photoactivity tests.

Finally, the findings suggest proceeding with further investigations to improve the performance of the radiosyntheiszed conducting polymers in the PVs devices through optimizing the synthesis conditions. In particular, controlling the morphology and increasing the molecular weight of the radio-synthesized polymers could enhance their optical and electrical properties. In addition, optimizing fabrication of PSCs will definitely enhance the performance (thickness of the component layer, using different architectures, etc.)

References

1. Sharma, S.; Jain, K. K.; Sharma, A., Solar Cells: In Research and Applications¡ªA Review. *Materials Sciences and Applications* **2015,** *Vol.06No.12*, 12.

2. Miles, R. W.; Hynes, K. M.; Forbes, I., Photovoltaic solar cells: An overview of state-of-the-art cell development and environmental issues. *Progress in Crystal Growth and Characterization of Materials* **2005,** *51* (1), 1-42.

3. Mrinalini, M.; Islavath, N.; Prasanthkumar, S.; Giribabu, L., Stipulating Low Production Cost Solar Cells All Set to Retail…! *The Chemical Record* **2019,** *19* (2-3), 661-674.

4. Lu, L.; Zheng, T.; Wu, Q.; Schneider, A. M.; Zhao, D.; Yu, L., Recent Advances in Bulk Heterojunction Polymer Solar Cells. *Chemical Reviews* **2015,** *115* (23), 12666-12731.

5. Bui, T.-T.; Ulfa, M.; Maschietto, F.; Ottochian, A.; Nghiêm, M.-P.; Ciofini, I.; Goubard, F.; Pauporté, T., Design of dendritic core carbazole-based hole transporting materials for efficient and stable hybrid perovskite solar cells. *Organic Electronics* **2018,** *60*, 22-30.

6. Shi, Z.; Jayatissa, A. H., Perovskites-Based Solar Cells: A Review of Recent Progress, Materials and Processing Methods. *Materials (Basel)* **2018,** *11* (5), 729.

7. Le, T. H.; Dao, Q.-D.; Nghiêm, M.-P.; Péralta, S.; Guillot, R.; Pham, Q. N.; Fujii, A.; Ozaki, M.; Goubard, F.; Bui, T.-T., Triphenylamine–Thienothiophene Organic Charge-Transport Molecular Materials: Effect of Substitution Pattern on their Thermal, Photoelectrochemical, and Photovoltaic Properties. *Chemistry – An Asian Journal* **2018,** *13* (10), 1302-1311.

8. Jeon, N. J.; Noh, J. H.; Yang, W. S.; Kim, Y. C.; Ryu, S.; Seo, J.; Seok, S. I., Compositional engineering of perovskite materials for high-performance solar cells. *Nature* **2015,** *517*, 476.

9. Park, N.-G., Perovskite solar cells: an emerging photovoltaic technology. *Materials Today* **2015,** *18* (2), 65-72.

10. Green, M. A.; Ho-Baillie, A.; Snaith, H. J., The emergence of perovskite solar cells. *Nat Photonics* **2014,** *8* (7), 506-514.

11. Rangel-Cárdenas, J.; Sobral, H., Optical Absorption Enhancement in CdTe Thin Films by Microstructuration of the Silicon Substrate. *Materials (Basel)* **2017,** *10* (6), 607.

12. Shi, Z.; Jayatissa, A. H., One-pot hydrothermal synthesis and fabrication of kesterite Cu2ZnSn(S,Se)4 thin films. *Progress in Natural Science: Materials International* **2017,** *27* (5), 550-555.

13. Ulfa, M.; Pauporté, T.; Bui, T.-T.; Goubard, F., Impact of Organic Hole Transporting Material and Doping on the Electrical Response of Perovskite Solar Cells. *The Journal of Physical Chemistry C* **2018,** *122* (22), 11651-11658.

14. Hsu, C.-Y.; Chen, Y.-C.; Lin, R. Y.-Y.; Ho, K.-C.; Lin, J. T., Solid-state dye-sensitized solar cells based on spirofluorene (spiro-OMeTAD) and arylamines as hole transporting materials. *Physical Chemistry Chemical Physics* **2012,** *14* (41), 14099-14109.

15. Holliday, S.; Donaghey, J. E.; McCulloch, I., Advances in Charge Carrier Mobilities of Semiconducting Polymers Used in Organic Transistors. *Chemistry of Materials* **2014,** *26* (1), 647-663.

16. Arias, A. C.; MacKenzie, J. D.; McCulloch, I.; Rivnay, J.; Salleo, A., Materials and Applications for Large Area Electronics: Solution-Based Approaches. *Chemical Reviews* **2010,** *110* (1), 3-24.

17. Liu, X.; Kong, F.; Guo, F.; Cheng, T.; Chen, W.; Yu, T.; Chen, J.; Tan, Z. a.; Dai, S., Influence of π-linker on triphenylamine-based hole transporting materials in perovskite solar cells. *Dyes and Pigments* **2017,** *139*, 129-135.

18. Saliba, M.; Orlandi, S.; Matsui, T.; Aghazada, S.; Cavazzini, M.; Correa-Baena, J.-P.; Gao, P.; Scopelliti, R.; Mosconi, E.; Dahmen, K.-H.; De Angelis, F.; Abate, A.; Hagfeldt, A.; Pozzi, G.; Graetzel, M.; Nazeeruddin, M. K., A molecularly engineered hole-transporting material for efficient perovskite solar cells. *Nature Energy* **2016,** *1*, 15017.

19. Ruiz, J.; Gonzalo, B.; Dios, J. R.; Laza, J. M.; Vilas, J. L.; León, L. M., Improving the Processability of Conductive Polymers: The Case of Polyaniline. *Advances in Polymer Technology* **2013,** *32* (S1), E180-E188.

20. Shit, A.; Nandi, A. K., Interface engineering of hybrid perovskite solar cells with poly(3-thiophene acetic acid) under ambient conditions. *Physical Chemistry Chemical Physics* **2016,** *18* (15), 10182-10190.

Conclusions and perspectives

Current research aims to develop new conducting polymers (CPs) and new synthesis strategies with the aim to control and improve the optical and electrical properties of these materials. In this context, our auspicious endeavor to develop a promising methodology based on radiation chemistry to synthesize conducting polymers for highly efficient solar cells and other practical applications is being developing and evolving. The merit of radiation methodology is that the polymerization can be performed at ambient temperature and pressure. Also, the oxidation takes places thanks to solvent radiolysis products, in the absence of my external chemical initiators.

The radiolytic method was developed by Samy Remita‘s team (Laboratoire de Chimie Physique, LCP) and this new method opens a novel approach for the synthesis of CPs. Based on the radiolytic method, synthesis of different kinds of CPs has been carried out by the way of γ-rays as well as accelerated electrons and the effect of synthetic conditions on the polymerization has been investigated. Moreover, with pulse radiolysis study, a step-by-step mechanism has been demonstrated for the polymerization of organic conjugated monomers. Furthermore, the synthetic conditions have been varied by using different atmospheres (N_2O, N_2, O_2 or air) or by using additive reagents and chemicals (NaN_3, $K_2S_2O_8$, isopropanol or *tert*-butanol) or by simply adjusting the pH of the medium. Indeed, all the new synthetic routes based on oxidation or reduction of organic monomers have been successfully led to production of CPs and CPs nanocomposites. Thus, the versatility of radiolytic methodology has been proved to be a potential alternative method.

It is worth noting that upon my arrival to Samy Remita‘s team, I involved and participated in the ongoing studies, in particular the works which were related to the synthesis of CPs in very acidic medium and synthesis of CPs nanocomposites. Nevertheless, the radio-synthesized conducting polymers produced in the previous works had some limitations which restrict their applications due to the poor processability which is attributed to the rigidity and inter-chain interactions of the polymer chains or to the crosslinking that may occur during γ-irradiation. Moreover, the optical and electrical properties of the radio-synthesized conducting polymers that were obtained in aqueous media under different experimental conditions needed to be improved. In addition, their molecular weight was low. On the other hand, radiation-induced polymerization in aqueous solution cannot always be used due to poor processability, low solubility and even sometimes insolubility of some of organic monomers.

In this thesis, in order to develop a new synthetic and processable method for conducting polymers production, to control the optical properties of radio-synthesized materials, to tune polymers morphology, to increase their molecular weight and to overcome the low solubility and low processability issues, we extended our methodology based on radiation chemistry through a new synthetic approach in order to polymerize the organic monomers in organic solvents by exploiting the oxidizing species *in situ* produced from γ-radiolysis of the used solvent.

In the very beginning of the present work, we looked for solvents which enable the good solubilization of organic monomers in general and 3HT in particular. Water in presence of conjugated SDS surfactants, ethanol, CCl_4, $CHCl_3$ and CH_2Cl_2 solvents were used. In order to synthesize P3HT polymers, different solutions were prepared with all these solvents at different concentrations in 3HT monomers. These solutions were irradiated under different atmospheres, at different doses and dose rates. While radiolysis of water (with SDS) and ethanol did not lead to polymers, irradiation of CCl_4, $CHCl_3$ and CH_2Cl_2 solutions enabled the preparation of P3HT polymers which were characterized in solution by UV-Vis absorption spectroscopy and cyro-TEM microscopy, and after deposition by ATR-FTIR spectroscopy and SEM microscopy. Although, the good results obtained thanks to CCl_4 radiolysis, we did not proceed with further investigations due to its toxicity. Thus, the investigations have been procceded with $CHCl_3$ and CH_2Cl_2. However, the results and data that came out from CH_2Cl_2 were more encouraging and promising than those obtained with $CHCl_3$. As a consequence, the development of new synthetic and processable radiolytic route for conducting polymers production in CH_2Cl_2 has been proceeded.

As seen in chapter 2, our strategy based on radiation chemistry was extended to the preparation of conducting polymers into organic solvents. In particular, starting from EDOT monomers dissolved in dichloromethane solvent and under N_2 atmosphere, we elaborated and optimized the synthesis by gamma-rays of PEDOT polymers. The polymers were found (by ATR-FTIR and EDX) naturally doped with chloride anions generated in the medium through dichloromethane radiolysis. As demonstrated by dose effect study, the dose of 36 kGy is the optimal irradiation dose which enables quantitative polymerization of 10 mM in EDOT and as a consequence, the yield of EDOT oxidation in dichloromethane, under N_2 atmosphere, was found to be 4.12×10^{-7} mol.J^{-1}. Above this irradiation dose, an overoxidation was systematically was observed by ATR-FTIR and SEC analysis, which leads to the degradation of PEDOT polymer chains. Radiation induced oxidative polymerization of EDOT monomers

in dichloromethane was studied under other atmospheres (air and O_2). Additionally, several attempts were tried out to increase the molecular weight of PEDOT polymers synthesized in dichloromethane under N_2 atmosphere at 36 kGy.

The morphology of PEDOT polymers synthesized in dichloromethane under N_2 atmosphere and at an irradiation dose of 36 kGy was checked in solution and after deposition. All used characterizations techniques indicated the production of amorphous PEDOT polymers doped with chloride ions and highlighted the self-assembly of these polymers into polydisperse globular particles (size comprised between 100 nm and 1.5 µm). PEDOT polymers synthesized in dichloromethane under N_2 atmosphere and at an irradiation dose of 36 kGy were found to be characterized by good thermal stability and by interesting electronic properties.

The versatility, reliability and simplicity of our original synthetic method based on γ-irradiation of dichloromethane and aqueous solutions were successfully exhibited in chapter 4. Starting from TAA monomers dissolved either in dichloromethane or in aqueous solution, the oxidative polymerization of PTAA was successfully induced by gamma irradiation at doses of 36 kGy. Depending on the solvent, two different PTAA polymers were formed successfully (namely $PTAA_{CH_2Cl_2}$ and $PTAA_{H_2O}$). It is important to note that normally, by using chemical method PTAA is synthesized only after carrying out an esterification reaction to protect the carboxylic acid moiety of the monomers from the oxidative decomposition. On another hand, the electro-polymerization of PTAA is not realizable since TAA has limited solubility in conventional aqueous media and also its oxidation potential is higher than that of water decomposition. The merit of our work based on radiation chemistry is that PTAA polymers have been formed directly without using oxidizing agents or any prior esterification thanks to both radiolytic routes: dichloromethane and water radiolysis. All the characterization techniques as well as data analysis manifested forming distinct chemical and optical properties for $PTAA_{CH_2Cl_2}$ and $PTAA_{H_2O}$ polymers. Nevertheless, SEC analysis highlighted the absence of solvent influence on the molecular weight. Also TGA analysis highlighted good and convergent thermal stabilities. Notably, the electrochemistry experiments showed that $PTAA_{CH_2Cl_2}$ and $PTAA_{H_2O}$ polymers are both favorable for practical use.

Ultimately, the development of radition induced synthesis of conducting polymers in dichloromethane moved forward to the synthesis of P3HT polymers. The aim was to generate oxidizing species that insure the oxidative polymerization of 3HT monomers. Thus, in chapter

5 the synthesis of P3HT has been made possible through dichloromethane radiolysis by means of dichloromethyl, chloromethyl and their corresponding peroxyl radicals. The neutral chloromethyl radicals can behave as oxidizing agents, but their redox potentials are too low to ensure quantitative oxidative polymerization since 3HT possess higher oxidation potential. By contrast, dichloromethyl and chloromethyl peroxyl radicals are possessing oxidizing power higher than the original carbon centred radicals. Those radicals enabled us to easily form conducting polymers of P3HT. Dichloromethyl, chloromethyl and their corresponding peroxyl radicals were secured by preparing dichloromethane solutions and then irradiating them under N_2, air or O_2 atmospheres. Under these atmospheres, three different polymers were produced and so-called "$P3HT_{N_2}$", "$P3HT_{air}$" and "$P3HT_{O_2}$". The formation of these polymers was confirmed by UV-Vis and ATR-FTIR absorption spectroscopies. Dose effect study was carried out for all polymers. $P3HT_{N_2}$ needs approximately irradiation dose of 75 kGy to proceed with the oxidative polymerization in dichloromethane, while $P3HT_{air}$ and $P3HT_{O_2}$ need irradiation dose of 55 kGy and 35 kGy, respectively. The case of air saturated solution represents the intermediate case between nitrogen and oxygen saturated solutions. For that reason we focused on two conditions: N_2 and O_2 atmospheres.

UV-Vis and ATR-FTIR absorption spectroscopies revealed that $P3HT_{O_2}$ has distinct optical properties than $P3HT_{N_2}$. The spectral behaviors were explained by SEC analysis that showed the higher molecular weight of $P3HT_{O_2}$. Interestingly, carboxylic acid groups were detected in ATR-FTIR spectrum of $P3HT_{O_2}$ polymers. Furthermore, EDX analysis confirmed the presence of oxygen in $P3HT_{O_2}$. Morphological analysis of $P3HT_{N_2}$ and $P3HT_{O_2}$ was carried out after deposition onto substrate by SEM and AFM. The microscopic observations demonstrated that γ-synthesized P3HT have two different nano-structures: aggregated blocks ($P3HT_{N_2}$) and spheroidal nanoparticles ($P3HT_{O_2}$). P3HT polymers were also characterized by interesting electrical properties. $P3HT_{O_2}$ showed higher energy band gap (optical and electronic) than that of $P3HT_{N_2}$. Finally, the electrical conductivity records were quite remarkable and somewhat comparable with those already reported in literature.

Due to the remarkable electrical and optical properties that were obtained for all radio-synthesized conducting polymers, we lastly and most importantly decided to incorporate these materials in hybrid organic and inorganic perovskite solar cells (PSCs). According to our cyclic voltammetry analysis and optical and electronic band gaps, the radio-synthesized conducting polymers were suitable for application as HTMs. Thus, chapter 6 was dedicated to

the use of radio-synthesized conducting polymers in practical application, namely PSCs fabrication. For this purpose, we studied the solubility of our radio-synthesized polymers in some common organic solvents that are usually used in preparation of PSCs. After finding an adequate solvent, we elaborated PSCs. After PSCs fabrication, we measured the produced photocurrent and voltage. *J-V* curves were plotted to determine the characteristic parameters. The measurements showed that the photovoltaic effects are very small, even for Spiro-OMeTAD used as standard. The low performance of the radio-synthesized polymers could be ascribed to their low molecular weight, electrical conductivity and also due to the fabricated device itself.

In the end, the present study bears witness to the potential of such a new radiation-based methodology and gives us a glimpse of future promising industrial applications in the field of conducting polymers synthesis. The versatility of this methodology has been proved to be a potential alternative method. However, there are also few questions that worth further investigations to improve the performance of the radio-synthesized polymers in photovoltaics.

In order to control the morphology and producing conducting polymers with different nanostructures possessing high molecular weight, micro-emulsion polymerization would be immensely helpful for that purpose. The fact that dichloromethane and water are immiscible solvents, offers the use of micro-emulsion polymerization through gamma radiolysis with the view of having a controlled morphology. This is an ongoing project in which I took part and I participated in. Indeed, radiation-induced polymerization was used for the first time to polymerize 3-hexylthiophene (3HT) and 3,4-ethylenedioxythiophene (EDOT) into micro-emulsions in order to control the morphology of these polymers. Two kinds of micro-emulsions (water in DCM (w/o) and DCM in water (o/w)) were used. The idea of using micro-emulsions is to polymerize a water soluble monomer (i.e. PEDOT) in the aqueous phase of micro-emulsions and water insoluble monomer (i.e. 3HT) in the organic phase. We successfully studied the preparation conditions of both micro-emulsions and revere micro-emulsions. **Figure 1** shows one example of an observation made in the case of reverse micro-emulsions (w/o) by using Cryo-TEM.

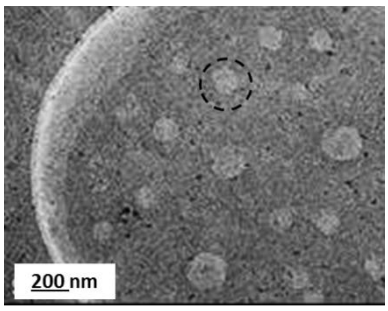

Figure 1 Cryo-TEM image of a reverse microemulsion before irradiation

As can be seen, the less contrasted spherical particles represents the reverse micelles that contain water. These spherical particles are dispersed in a more contrasting medium that represents the oil phase (DCM). The ongoing work is aiming to find the proper conditions to control the shape and the size of the micelles (i.e. tubes, spheres, rods, etc) and thus synthesizing nanostructured conducting polymers with controlled morphology and enhanced chain length. The use of radiation induced synthesis of conducting polymers within micro-emulsions will be immensely helpful to improve the optical and electrical properties of conducting polymers and consequently enhance the photo conversion yields in organic photovoltaic devices

Furthermore, in order to improve the processability and the solubility, to adjust the hydrophilicity, to enhance the electronic properties, the use of copolymerization will be advantageous to our radiation based methodology.

This project has been recently launched and I took a part of it. Therefore we decided to extend our methodology to the preparation in water or in organic solvents of new conducting materials by the way of radiation induced copolymerization. **Figure 2** shows some copolymers of pyrrole with other organic monomers which we already radio-synthesized in water and dichloromethane.

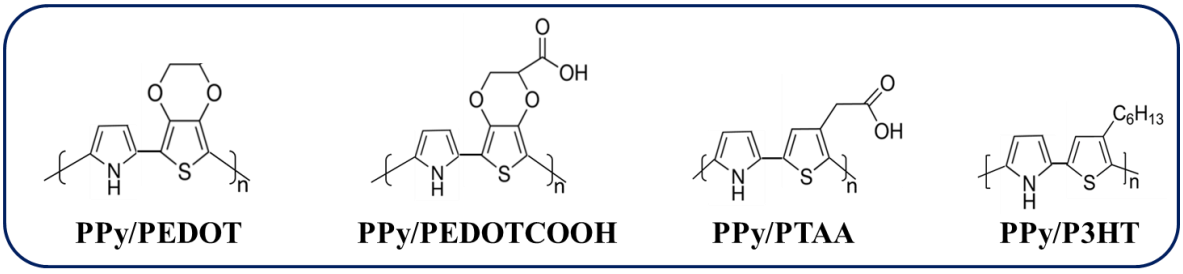

Figure 2 Chemical structures of several copolymers that are made of pyrrole with other monomers we recently synthesized by γ-radiolysis

Radiation induced copolymerization would be promising approach for tuning PPy physicochemical properties and also improving of PPy processability and stability. This was evident in case of copolymerization of PPy/PTAA in aqueous solution under N_2O atmosphere. Indeed, radiation induced copolymerization of Py:TAA enabled us to gain better optical properties than the individual homo polymers as can be seen in **Figure 3**.

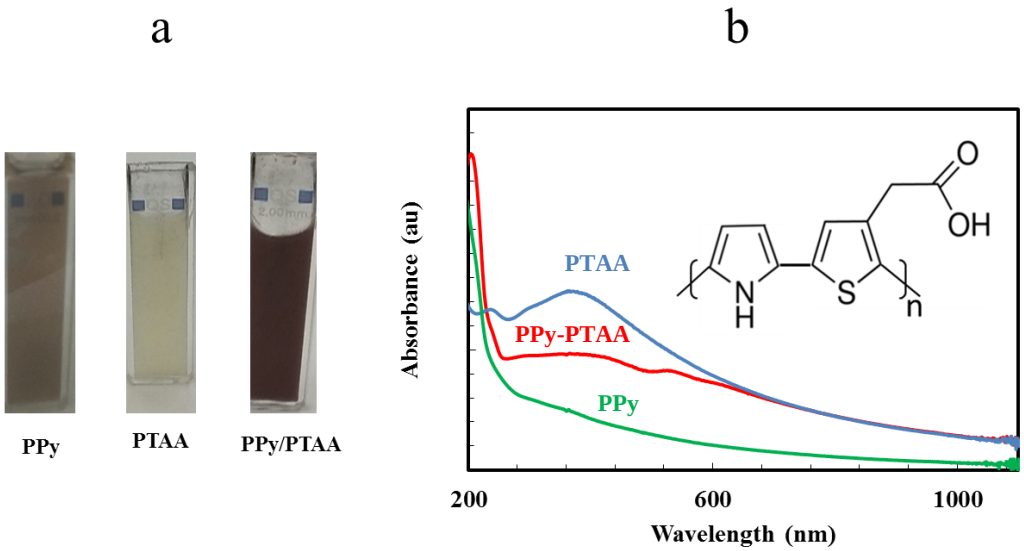

Figure 3 Radiation induced polymerization of Py and TAA in presence of 10 mM of each and copolymerization of Py:TAA in presence of (5mM:5mM) in aqueous solutions under N_2O at irradiation dose 36 kGy: a) photographical images of polymers and copolymers after g-irradiation, b) UV-Vis absorption spectra of polymers and copolymers after g-irradiation. Path length 2 mm. Reference: water.

As can be seen in **Figure 3a** the color of copolymer is quite different from those of homo-polymers. Furthermore, it is possible to observe a red-shift in the absorption of coplymer with new transition at higher wavelength as exhibited in **Figure 3b**. From these preliminary data and findings, we can say that the radio-synthesized copolymers seems to be promising for an application opportunity in electrochromic devices.

Further investigations for development and implementation of radiation based methodology are proceeded with preparation of radio-synthesized conducting copolymers for electrochromic applications. In fact, using a small subset of building blocks and resort to co-polymerization is immensely helpful in order to achieve the desired electrochromic features. The purpose of the work is to adjust and enhance the electrochromic features of the copolymers by varying the chemical nature of organic monomers.

Appendix

Synthèse de thèse de doctorat

Discipline: Chimie

Extension de la procédure radiolytique à la préparation de polymères conducteurs dans des solvants organiques: synthèse, caractérisation et applications

Le travail porte sur l'étude de nouvelles voies de synthèse radioinduite de polymères conducteurs en vue de l'optimisation des méthodes d'obtention aux regards des propriétés optiques et conductrices recherchées. L'étude est construite autour de deux objectifs principaux : initialement, comprendre, d'un point de vue fondamental, l'ensemble des mécanismes physico-chimiques et chimiques conduisant aux propriétés attendues ; Deuxièmement, parvenir à une parfaite maîtrise de l'ensemble des procédés, de la préparation des échantillons aux méthodes de caractérisation, en passant par les irradiations.

Le manuscrit présenté comporte 236 pages, divisées en six chapitres enrichis de 350 références bibliographiques; et il pourrait être résumé dans le **Schéma 1**.

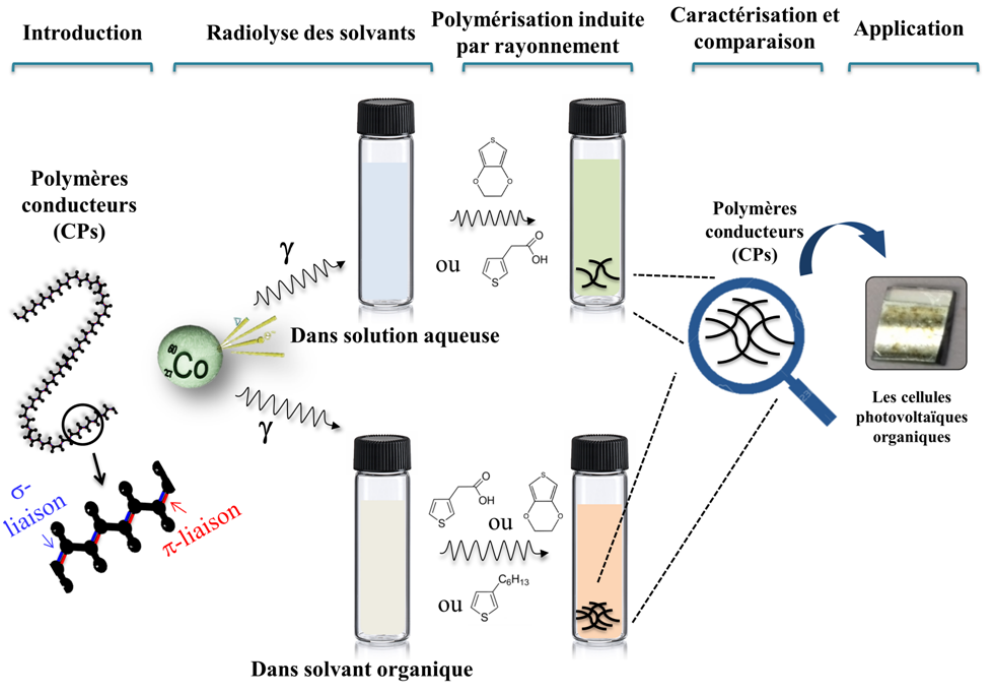

Schéma 1. les grandes lignes de la thèse

L'introduction rappelle les caractéristiques physiques principales des polymères conducteurs, ainsi que les principes de la conductivité électrique et du dopage de matériaux caractérisés par une structure de bande bien définie. Les applications et les principales approches de synthèse sont évoquées, avant une présentation structurée des différents chapitres.

Le chapitre 1 est consacré aux matériels, instruments et méthodes de synthèse. Il commence par une description détaillée des solvants et réactifs qui seront utilisés plus tard dans l'étude. Une partie importante concerne la description des moyens et protocoles d'irradiation gamma. Elle est suivie par la description des méthodes de préparation des échantillons obtenus en vue des mesures de conductivité électrique. Pour terminer, sont détaillées plus d'une dizaine de méthodes de caractérisation.

Le chapitre 2 est consacré à une description exhaustive des travaux et résultats antérieurs obtenus par l'équipe, sur lesquels se fonde cette nouvelle étude. Ces travaux concernaient la synthèse du poly (3,4- éthylènedioxythiophène) (PEDOT) en solutions aqueuses, par faisceaux d'électrons et gamma, et du 3,4- éthylènedioxythiophène (EDOT) en radiolyse gamma. Il est rappelé que les composés obtenus sous irradiation possèdent des propriétés optiques et électriques semblables à celle des mêmes milieux obtenus par des méthodes industrielles, mais avec l'avantage d'un contrôle bien meilleur de la synthèse.

Le chapitre 3 est consacré à la présentation d'une nouvelle voie de synthèse du PEDOT, faisant appel au dichlorométhane, dans lequel les monomères EDOT sont davantage solubles. Les résultats et la discussion portent sur de nombreux paramètres : effets de doses sous atmosphères variées (N_2, air, O_2). Cette nouvelle stratégie de synthèse donne d'excellents résultats, attestés par de nombreuses caractérisations faites au laboratoire. Ce chapitre, et les méthodes qui y sont développées, ouvre une voie particulièrement originale à de nouvelles études, telles qu'elles seront décrites dans la suite.

Le chapitre 4 porte sur la synthèse induite par le rayonnement gamma à 36 kGy du poly (3-thiophene acetic acid) (PTAA) dont les monomères sont solubles dans l'eau et le dichlorométhane. Selon le solvant choisi, deux types de polymères amorphes, de poids moléculaires semblables, sont obtenus, aux propriétés chimiques et optiques distinctes, résultant de nanostructures distinctes et de tailles différentes d'un ordre de grandeur. Les mesures conductimétriques font apparaître des propriétés électriques supérieures à celle mentionnées jusqu'à présent dans les travaux d'autres équipes. Au-delà de ces points, un

important résultat de ce chapitre concerne la mise en évidence de l'effet du solvant sur le contrôle de la morphologie du produit obtenu, à l'échelle de la dizaine à la centaine de nanomètres.

Le chapitre 5 est consacré à l'étude de la synthèse radioinduite du poly (3-hexylthiophène) (P3HT) dans le dichlorométhane, sous différentes atmosphères. Dans ce chapitre, l'auteur tire avantage des nombreux résultats déjà obtenus afin de pouvoir effectuer une polymérisation maitrisée du 3HT, insoluble dans l'eau, dans le dichlorométhane. La polymérisation fonctionne bien sous irradiation gamma et sous atmosphères O_2 et N_2, donnant naissance à deux types de structures bien distinctes, selon la nature du gaz présent et la quantité de dose déposée. Les propriétés optiques et conductrices sont différentes et, là encore, les morphologies des structures nanométriques sont impliquées. Les données physiques mesurées, relatives aux gaps et aux conductivités, sont semblables à celles connues dans les matériaux obtenus par méthodes non radiolytique, ce qui, une fois de plus, valide les méthodes choisies.

Le sixième et dernier chapitre constitue une analyse comparative des nombreuses propriétés optiques et physiques mises en évidence sur tous les polymères étudiés dans ce travail, au regard d'applications industrielles possibles, notamment pour la production d'énergie photovoltaïque. Il s'avère que les futures études devront s'attacher à mieux contrôler les morphologies, d'où découlent les propriétés de production (gap) et de transport de charges (conductivité) au sein du matériau. Mais ceci est mieux réalisable bien mieux par voie de synthèse radiolytique que par toute autre méthode.

Une conclusion synthétise les principaux résultats originaux obtenus et propose de nouvelles perspectives de recherche en insistant sur la nécessité d'étendre les études à davantage de matériaux

université PARIS-SACLAY
ÉCOLE DOCTORALE
Sciences chimiques : molécules, matériaux, instrumentation et biosystèmes

Titre : Extension de la procédure radiolytique à la préparation de polymères conducteurs dans des solvants organiques: synthèse, caractérisation et applications

Mots clés : polymères conducteurs, procédure radiolytique, solvants organiques, synthèse

Résumé : Dans le présent travail, nous avons étendu aux solvants organiques notre méthodologie radiolytique de synthèse de polymères conducteurs (PCs), initialement développée en solutions aqueuses. Dans ce contexte, la polymérisation des PCs a été étudiée par radiolyse gamma dans différents solvants organiques et sous différentes conditions expérimentales. La synthèse radio-induite a, en particulier, été optimisée dans le dichlorométhane grâce à la variation et à l'ajustement de différents paramètres : atmosphère, dose, débit de dose, concentration des monomères, etc. Cette synthèse a ainsi pu mener à la préparation de différents types de polymères conducteurs : poly (3,4-éthylènedioxythiophène) (PEDOT), poly (3-thiophène acétique acide) (PTAA) et poly (3-hexylthiophène) (P3HT). Ces derniers ont été totalement caractérises en solutions ou après dépôt par des techniques analytiques, spectroscopiques et microscopiques complémentaires. Nous avons en particulier démontré la simplicité et la versatilité de la polymérisation radio-induite de TAA que ce soit dans le dichlorométhane ou dans l'eau, et avons mis en évidence quelques différences notables entre ces deux voies de synthèse. Nous avons, par ailleurs, évalué l'influence de la nature des espèces radiolytiques oxydantes générées dans le dichlorométhane, via la variation de l'atmosphère de travail (N_2, air ou O_2), sur les propriétés des polymères conducteurs radio-synthétises, en particulier dans le cas de P3HT. Parmi les nombreuses propriétés physiques chimiques que nous avons sondées dans le cas de tous nos polymères conducteurs radio- synthétises les propriétés électroniques et électrochimiques ont fait l'objet d'une attention particulière. Nos matériaux ont alors été incorporés au sien de cellules solaires à pérovskite hybrides organiques-inorganique (PSCs) et y ont été utilisés comme matériaux de transport de trous (HTMs). Notre nouvelle stratégie radiolytique de synthèse décrite et étende dans le présent manuscrit, ouvre sans aucun doute la voie à la préparation de nouveaux PCs nanostructurés, de morphologie contrôlée et aux propriétés augmentées : par exemple grâce à l'utilisation d'une polymérisation en microémulsions ou par le développement d'une copolymérisation raisonnée.

Université Paris-Saclay
Espace Technologique / Immeuble Discovery
Route de l'Orme aux Merisiers RD 128 / 91190 Saint-Aubin, France

université PARIS-SACLAY
ÉCOLE DOCTORALE
Sciences chimiques : molécules, matériaux, instrumentation et biosystèmes

Title : Extension of radiolytic procedure to the preparation of conducting polymers in organic solvents: synthesis, characterization and applications

Keywords : conducting polymers, radiolytic procedure, organic solvents, synthesis

Abstract: The extension of our original radiolytic methodology to the use of organic solvents was an important alternative approach to radiation-induced polymerization of conducting polymers (CPs) in aqueous solutions. The polymerization of CPs was studied by using γ -radiolysis of several organic solvents under different environmental conditions. The optimization of the synthesis conditions of CPs was then conducted into dichloromethane solvent. After optimization of the synthesis conditions (atmosphere, dose, dose rate, concentration of organic monomers, etc.), the use of dichloromethane radiolysis was successfully employed to synthesize various types of conducting polymers: Poly (3,4-ethylenedioxythiophene) (PEDOT), Poly (3-thiophene acetic acid) (PTAA) and Poly (3-hexylthiophene) (P3HT). The radio-synthesized polymers were fully characterized in solution and after deposition by complementary analytical, spectroscopic and microscopic techniques. Also, the simplicity and versatility of radiation induced polymerization of 3-thiophene acetic acid in dichloromethane and in aqueous solutions was demonstrated. The differences between the two radiolysis routes were highlighted. Furthermore, the influence of generating different oxidizing species under different atmospheres (N_2, air or O_2) upon γ-irradiation of dichloromethane solutions containing organic monomers was also studied in particular in case of P3HT. The electronic and electrochemical properties were checked for all radio-synthesized CPs. Accordingly, these polymers were then incorporated in hybrid organic and inorganic perovskite solar cells (PSCs) and used as hole transport materials (HTMs). Our new radiolytic strategy described and extended in this manuscript opens the way for the preparation of new nanostructured CPs with controlled morphology and enhanced properties by using microemulsion polymerization and also for the preparation of processable conjugated materials through copolymerization.

Université Paris-Saclay
Espace Technologique / Immeuble Discovery
Route de l'Orme aux Merisiers RD 128 / 91190 Saint-Aubin, France